WAPD-TM-1336
DOE RESEARCH AND
DEVELOPMENT REPORT

RESULTS OF INITIAL NUCLEAR TESTS ON LWBR

(LWBR Development Program)

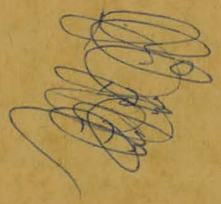

JUNE 1979

CONTRACT DE-AC11-76PN00014

BETTIS ATOMIC POWER LABORATORY
WEST MIFFLIN, PENNSYLVANIA

Operated for the U. S. Department of Energy by
WESTINGHOUSE ELECTRIC CORPORATION

DISCLAIMER

WAPD-TM-1336

RESULTS OF INITIAL NUCLEAR TESTS ON LWBR

(LWBR Development Program)

Editor: W.K. Sarber

Contributors

W.B. Doub
R.J. Eckert
L.B. Freeman
G.L. Hartfield
H.C. Hecker
W.K. Sarber

June 1979

Contract No. DE-AC11-76PN00014

Printed in the United States of America
Available from the
National Technical Information Service
U.S. Department of Commerce
5285 Port Royal Road
Springfield, Virginia 22151

NOTE

This document is an interim memorandum prepared primarily for internal reference and does not represent a final expression of the opinion of Westinghouse. When this memorandum is distributed externally, it is with the express understanding that Westinghouse makes no repesentation as to completeness, accuracy, or usability of information contained therein.

BETTIS ATOMIC POWER LABORATORY WEST MIFFLIN, PENNSYLVANIA

Operated for the U.S. Department of Energy
by
WESTINGHOUSE ELECTRIC CORPORATION

79-741/0149

FOREWORD

The Shippingport Atomic Power Station located in Shippingport, Pennsylvania was the first large-scale, central-station nuclear power plant in the United States and the first plant of such size in the world operated solely to produce electric power. This program was started in 1953 to confirm the practical application of nuclear power for large-scale electric power generation. It has provided much of the technology being used for design and operation of the commercial, central-station nuclear power plants now in use.

Subsequent to development and successful operation of the Pressurized Water Reactor in the DOE-owned reactor plant at the Shippingport Atomic Power Station, the Atomic Energy Commission in 1965 undertook a research and development program to design and build a Light Water Breeder Reactor core for operation in the Shippingport Station.

The objective of the Light Water Breeder Reactor (LWBR) program has been to develop a technology that would significantly improve the utilization of the nation's nuclear fuel resources employing the well-established water reactor technology. To achieve this objective, work has been directed toward analysis, design, component tests, and fabrication of a water-cooled, thorium oxide fuel cycle breeder reactor for installation and operation at the Shippingport Station. The LWBR core started operation in the Shippingport Station in the Fall of 1977 and is expected to be operated for about 3 to 4 years. At the end of this period, the core will be removed and the spent fuel shipped to the Naval Reactors Expended Core Facility for a detailed examination to verify core performance including an evaluation of breeding characteristics.

In 1976, with fabrication of the Shippingport LWBR core nearing completion, the Energy Research and Development Administration established the Advanced Water Breeder Applications (AWBA) program to develop and disseminate technical information which would assist U.S. industry in evaluating the LWBR concept for commercial-scale applications. The program will explore some of the problems that would be faced by industry in adapting technology confirmed in the LWBR program. Information to be developed includes concepts for commercial-scale prebreeder cores which would produce uranium-233 for light water breeder cores while producing electric power, improvements for breeder cores based on the technology developed to fabricate and operate the Shippingport LWBR core, and other information and technology to aid in evaluating commercial-scale application of the LWBR concept.

All three development programs (Pressurized Water Reactor, Light Water Breeder Reactor, and Advanced Water Breeder Applications) have been administered by the Division of Naval Reactors with the goal of developing practical improvements in the utilization of nuclear fuel resources for generation of electrical energy using water-cooled nuclear reactors.

Technical information developed under the Shippingport, LWBR, and AWBA programs has been and will continue to be published in technical memoranda, one of which is this present report.

INTENTIONALLY BLANK

TABLE OF CONTENTS

TABLE OF CONTENTS (cont'd)

This report presents and discusses the results of physics tests performed at beginning of life on the Light Water Breeder Reactor (LWBR). These tests have confirmed that movable seed assembly critical positions and reactivity worths, temperature coefficients, xenon transient characteristics, core symmetry, and core shutdown are within the range of values used in the design of the LWBR and its reactor protection analysis. Measured core physics parameters were found to be in good agreement with the calculated values.

RESULTS OF INITIAL NUCLEAR TESTS ON LWBR
(LWBR Development Program)

Editor: W.K. Sarber

I. INTRODUCTION AND SUMMARY

This report presents the results of the initial nuclear tests on the light water breeder reactor (LWBR) installed in the Shippingport Atomic Power Station, which is operated by Duquesne Light Company. The light water breeder reactor was developed and designed by the Bettis Atomic Power Laboratory under the technical direction of the Division of Naval Reactors of the U.S. Department of Energy. The results of the initial nuclear tests are important to confirm the adequacy of the LWBR design and to qualify the nuclear design model used in the analysis of LWBR nuclear performance.

Following core installation, fill of the LWBR core with water was completed on April 20, 1977. Initial criticality at ambient temperature (about 150°F) was achieved on August 26, 1977. Zero power physics testing was initiated immediately following criticality and was completed on September 3, 1977. The station startup test was performed to raise the power level gradually from near zero power to full power. Full power operation of LWBR

was achieved on September 21, 1977. In conjunction with the station startup test, flux wire activations were performed at near zero power and at full power conditions. Subsequently, additional physics tests were performed at high power conditions.

Sections II through VI of this report provide more details about the LWBR core, the methods for performing physics tests at Shippingport, the test procedures, the results obtained during physics testing, and comparisons with predicted performance using analytical methods which are also described. A summary of the topics covered by each section follows.

Section II presents a description of the LWBR core.

Section III describes the basic methods used in obtaining physics data at Shippingport.

Section IV presents a detailed discussion of each of the physics tests which were performed.

Section V presents the measured test results, along with a somewhat detailed description of the analytical models employed to calculate LWBR core nuclear characteristics. Two types of calculations are described. The RCP computer code (Reference 7), a three-dimensional, explicit, full energy range Monte Carlo code, was used to estimate source range count rates as a function of water level during initial fill. Movable seed assembly bank critical positions, bank worths, temperature coefficients, and xenon worths were calculated using an explicit, three-dimensional, symmetric one-sixth core PDQ (Reference 4) model. Details of the calculation models and the nuclear design of LWBR are presented in References 2 and 3.

Section VI presents the detailed conclusions drawn from the results of initial physics tests of the LWBR core in the Shippingport Plant. In general, agreement is good between measured test results and calculations of the as-built core. All nuclear parameters are within the range of values used in core protection analysis and the LWBR Safety Analysis Report. The cold

critical core was 0.35% $\Delta\rho$ less reactive than predicted, and at low power under normal operating conditions the core was 0.05%$\Delta\rho$ more reactive than predicted. Cold shutdown was 1/2 to 1%$\Delta\rho$ more than predicted and movable seed assembly reactivity worth was about 10% more than predicted. Core power is symmetric within 1% and axial power and flux shapes agree almost exactly with prediction. The measured temperature coefficient is lower than the best estimate prediction but within the range of expected uncertainty. The pressure coefficient was also somewhat lower than predicted. At full power the core was 0.18%$\Delta\rho$ more reactive than predicted. The reactivity worth of xenon is about 1.05 times the predicted value.

The results above indicate that LWBR core is performing well within the design range of nuclear parameters. A more detailed discussion of the conclusions is given in Section VI.

The physics tests performed at beginning of life consisted of the following types of measurements:

A. Precritical Test

Source range count rates as a function of water level during initial fill of the reactor vessel.

B. Zero Power Tests

1. Critical height and differential reactivity worth of 12 movable seed assembly bank near ambient temperature.

2. Temperature coefficient of reactivity near ambient temperature.

3. Azimuthal reactivity symmetry measurements near ambient temperature.

4. Single seed out of bank critical height and differential reactivity worth near ambient temperature.

5. Critical height and differential reactivity worth of 12 movable seed assembly bank near normal operating temperature and pressure conditions.

6. Temperature coefficient of reactivity near normal operating temperature.

7. Partial bank differential reactivity worths at normal operating temperature and pressure.

8. Pressure coefficient of reactivity at normal operating temperature and pressure.

9. Flow coefficient of reactivity at normal operating temperature and pressure.

10. Flux wire activations.

C. Station Startup (initial approach to full power operation).

D. High Power Tests

1. Flux wire activations.

2. Moderator coefficient of reactivity near full power.

3. Power coefficient of reactivity near full power.

4. Differential reactivity worth of 12 movable seed assembly bank near full power.

5. Xenon reactivity measurement (equilibrium and peak xenon worths).

The inverse kinetics simulator (IKS) was used to measure reactivity during the performance of the above measurements. The IKS is described in Reference 1.

II. CORE DESCRIPTION

The light water breeder reactor (LWBR) core is a pressurized, light-water-moderated and -cooled, thermal breeder which has been designed and installed into the existing reactor vessel at the Shippingport Atomic Power Station (SAPS). At full rated power the LWBR core produces 236.6 thermal megawatts (MWt) which is converted to about 72 gross electrical megawatts (MWe). The core is operated at an average primary coolant temperature of 531°F and a beginning-of-life pressure of 1985 pounds per square inch (gauge). The core is designed to breed using the uranium-233/thorium fuel cycle in a pressurized light water reactor plant. To achieve this objective, the core has been designed to minimize parasitic neutron losses in core and structural materials, and core reactivity is controlled with minimum parasitic neutron loss using movable fuel control.

A. Fuel Modules and Fuel Assemblies

Figure II-1 presents a cross-sectional view of the LWBR core showing the orientation of the types of modules which comprise the core configuration. As shown, the core contains the following types of fuel modules and fuel assemblies:

1. Twelve identical hexagonal movable seed assemblies.

2. Twelve stationary annular hexagonal blanket fuel assemblies, which combine with movable seed assembllies to form seed-and-blanket modules. Of the 12 stationary blanket fuel assemblies, nine are composed of two blanket regions denoted as regular blanket and power-flattening blanket regions, as shown on Figure II-1.

3. Fifteen reflector blanket fuel modules.

The seed-and-blanket modules contain both fissile uranium-233 and fertile thorium-232, while the reflector blanket fuel modules initially contain only thorium.

The three central seed-and-blanket modules (Type I modules), shown in Figure II-2, are designed to be typical of those which could be utilized in a large light water breeder reactor plant. The surrounding nine seed-and-blanket modules (Type II and III modules) have a slightly larger outer (power flattening) blanket region that is fueled with a somewhat higher uranium-233 content and larger water volume fraction than the blanket region of the inner modules. Use of this more highly loaded wetter blanket region which is nuclearly more active than the inner blanket region produces a relatively uniform power distribution within the interior of the core, thereby better simulating the breeding environment of a typical large core. The 15 reflector blanket fuel modules surround the interior 12 seed-and-blanket modules and serve to reduce neutron leakage from the relatively small Shippingport core. Surrounding the reflector blanket fuel modules are 15 stainless steel, non-fuel filler units whose purpose is to limit flow leakage by filling the space between the reflector modules and the lower barrel.

B. Reactivity Control

To eliminate the parasitic loss of neutrons in conventional control rod poison materials and enhance breeding in a light water, uranium-233/thorium environment, core reactivity control is achieved entirely by varying the geometric relationship between the movable seed assemblies and the associated stationary annular blanket assemblies which surround each seed assembly. For LWBR operation, this reactivity control is achieved by uniformly positioning the 12 movable seed assemblies in a bank by means of individual control drive mechanisms. Each movable seed assembly is positioned axially within its associated annular blanket assembly to achieve core reactivity control. This control scheme is analogous in concept and operation to that of conventional poison rod control in that negative rectivity addition and core shutdown are achieved by lowering the control elements and positive reactivity addition is achieved by raising the control elements.

Figure II-3 shows an axial elevation sketch of a seed-and-blanket module. At the shutdown position with all movable seed assemblies unlatched and at zero inches, the bottoms of the movable seed assemblies are 60 inches below the bottoms of the blanket assemblies. To achieve criticality and bring the core to power, the movable seed assemblies are lifted so that they are more nearly in axial alignment with the blanket fuel assemblies. Figure II-4 presents a curve showing the 12 movable seed assembly bank position as a function of time in life for full power operation.

For purposes of this report, a movable seed assembly will be referred to as a "seed", and the 12 movable seed assembly bank will be referred to as the "12 seed bank" or simply "bank".

C. Instrumentation

The nuclear operation and characteristics of the LWBR core are monitored by nuclear instrumentation which indicates neutron leakage flux from source level to 150 percent of reactor design power. The nuclear instrumentation consists of four neutron flux level monitoring channels. Each channel includes (1) a pair of instrument wells in the neutron shield tank, (2) a BF_3 proportional counter assembly for source range flux monitoring, (3) a compensated ion chamber (CIC) for intermediate range and power range flux monitoring, and (4) associated circuitry, data recorders, meters, test equipment, and power supplies.

Figure II-5 shows the radial location of the power and intermediate range nuclear instrument wells with respect to the orientation of the LWBR core. The instrument wells for the Channels A and D power and intermediate range nuclear instruments each contain an additional CIC which is available for physics testing in conjunction with the inverse kinetics simulator (IKS); the IKS will be discussed in Section III. As shown in Figure II-5, the outer edge of the core is farther from the channel B and D CIC's than is the case for the channel A and C CIC's. To minimize the variations in detector current among the detectors for a given power level, it is necessary to reduce the sensitivity of the channel A and C CIC's relative to the channel

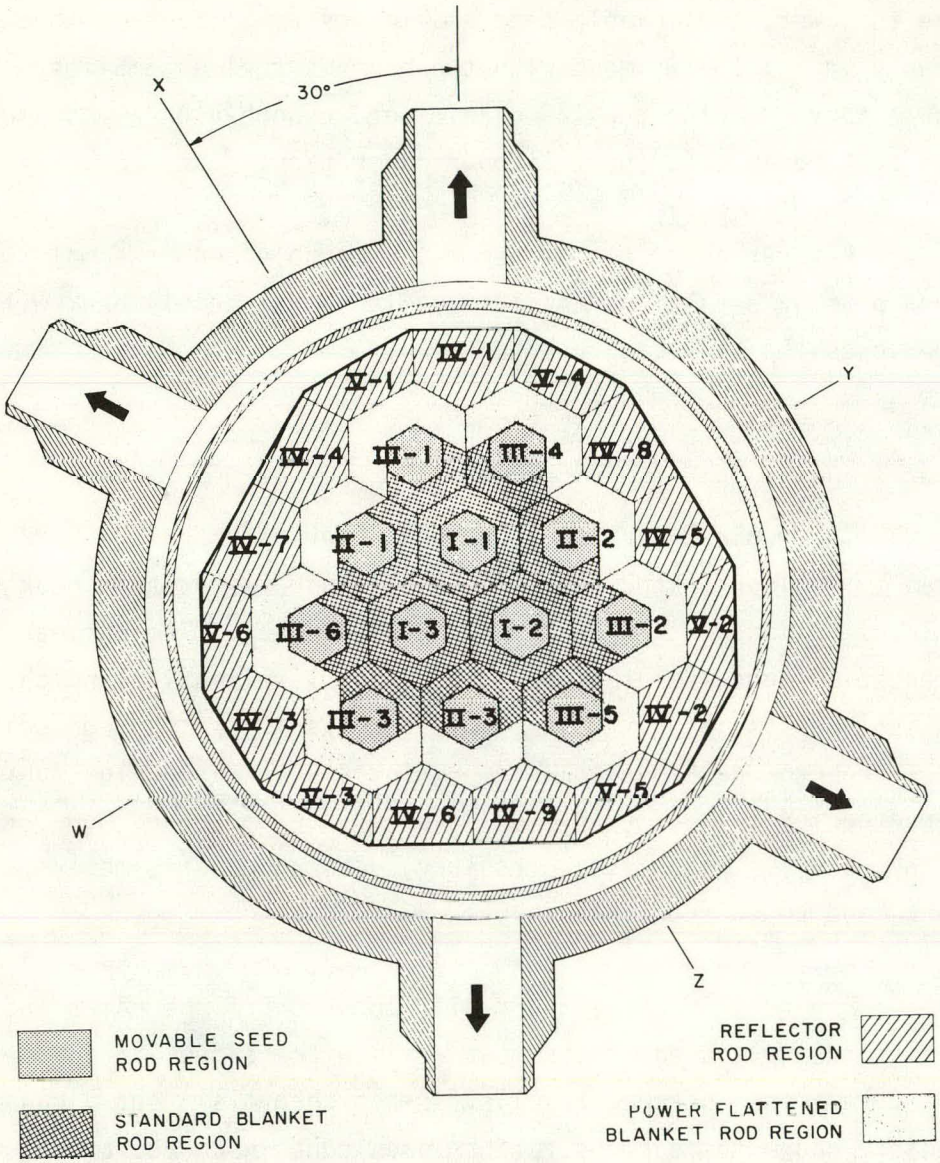

FIGURE II-1 - LWBR CROSS SECTION MODULE IDENTIFICATION

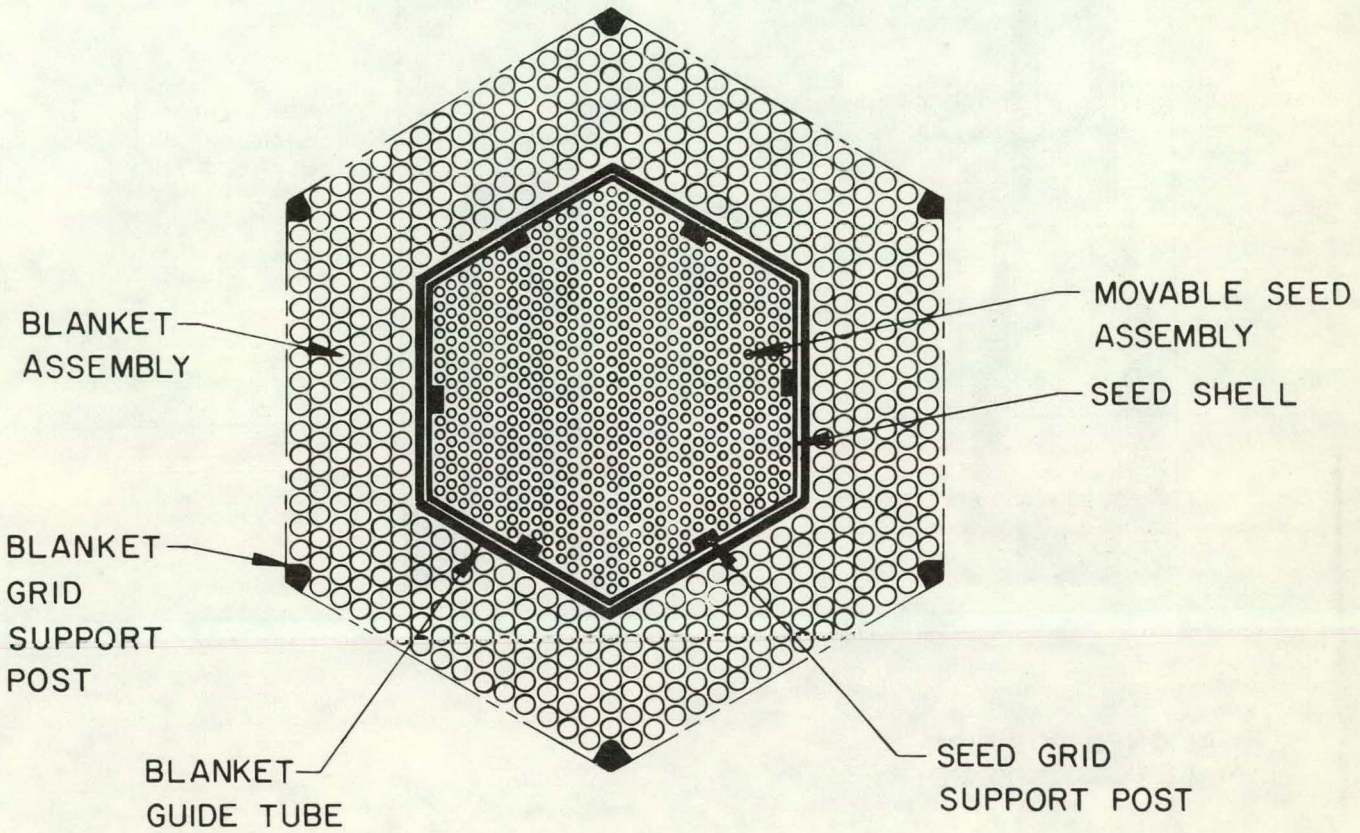

FIGURE II-2 - TYPICAL SEED-AND-BLANKET MODULE CROSS SECTION

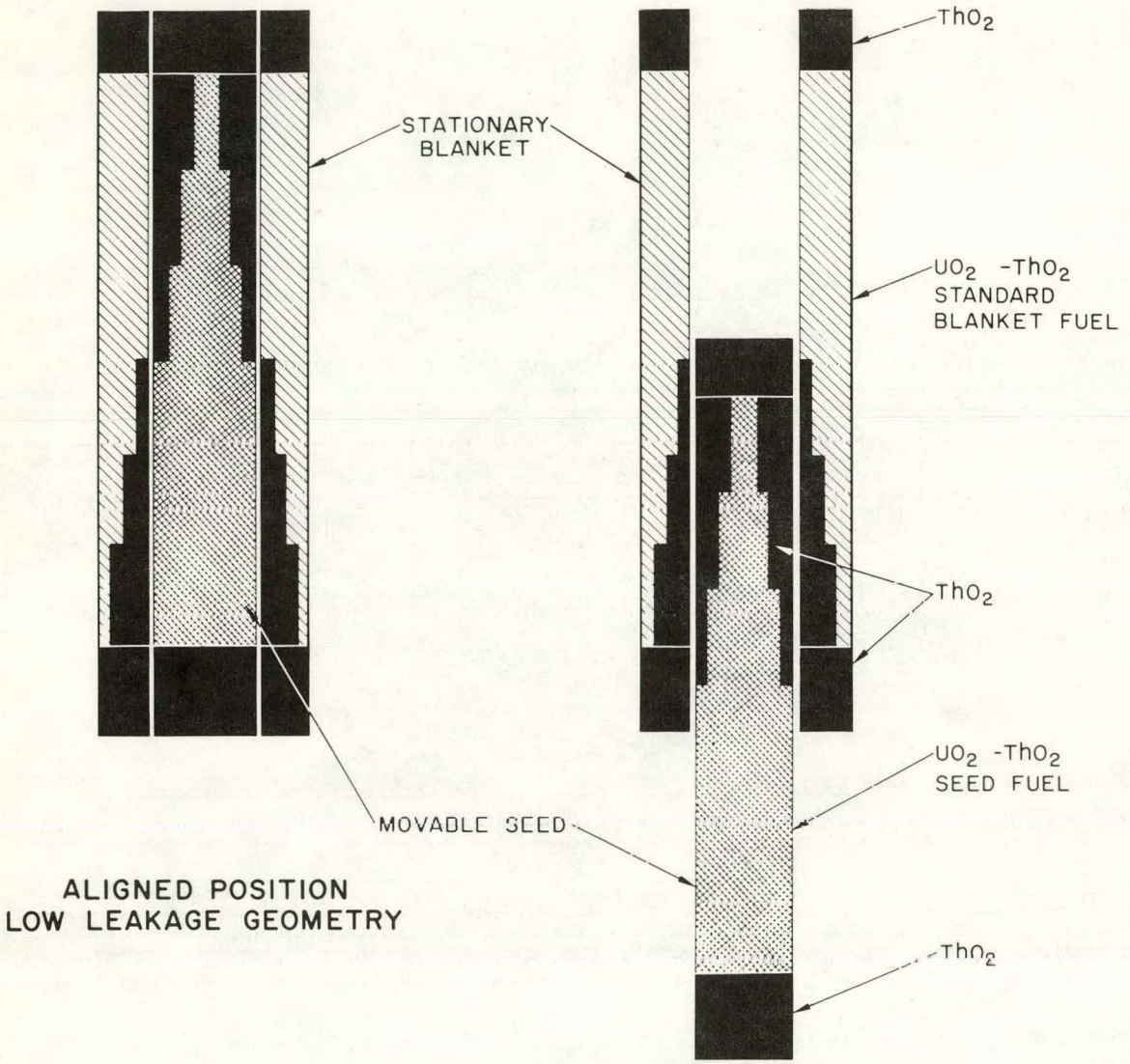

FIGURE II-3 - MOVABLE FUEL CONTROL

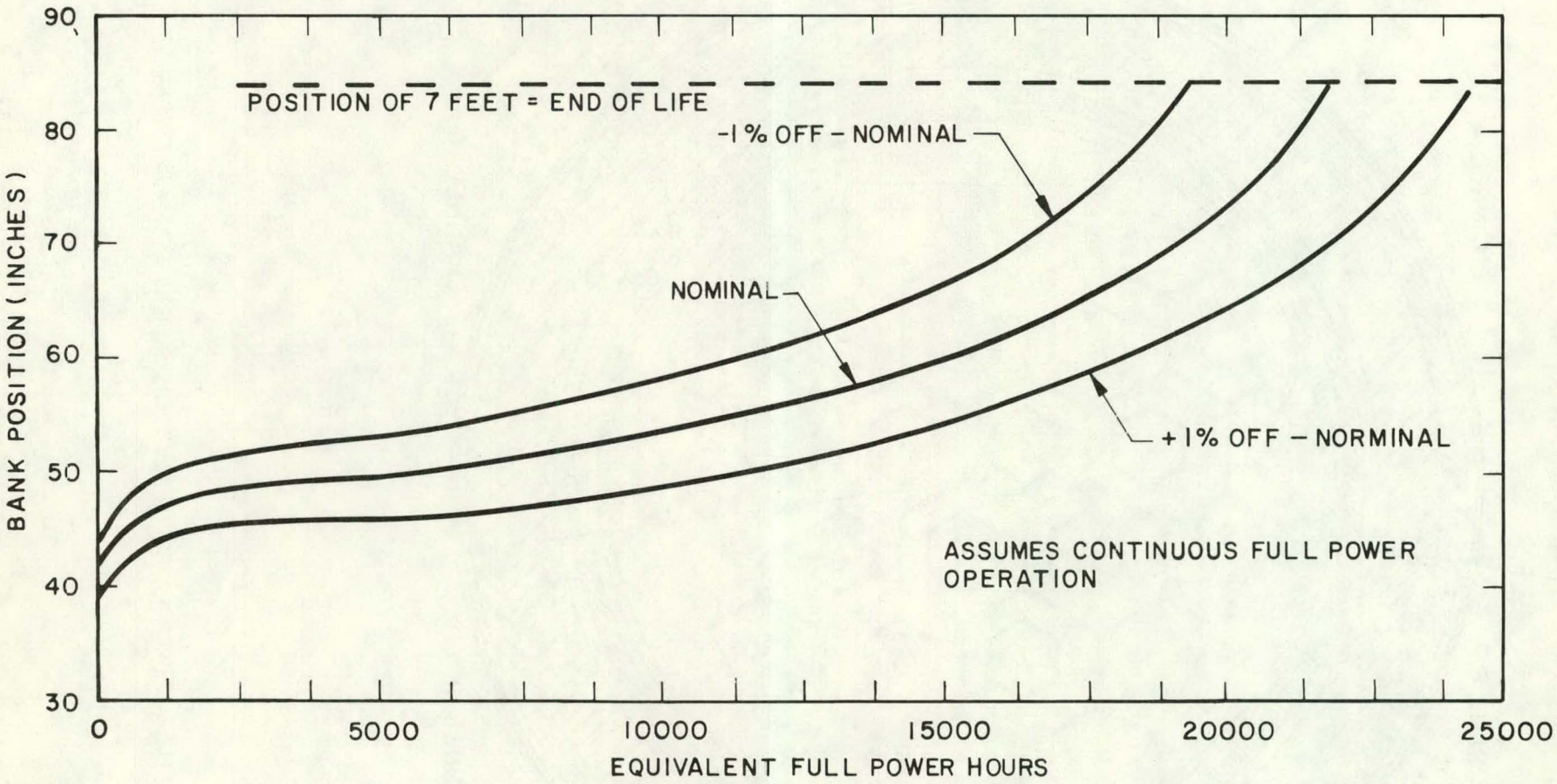

FIGURE II-4 - PREDICTED 12 MOVABLE SEED ASSEMBLY BANK POSITION OVER LIFETIME, AS-BUILT LWBR CORE

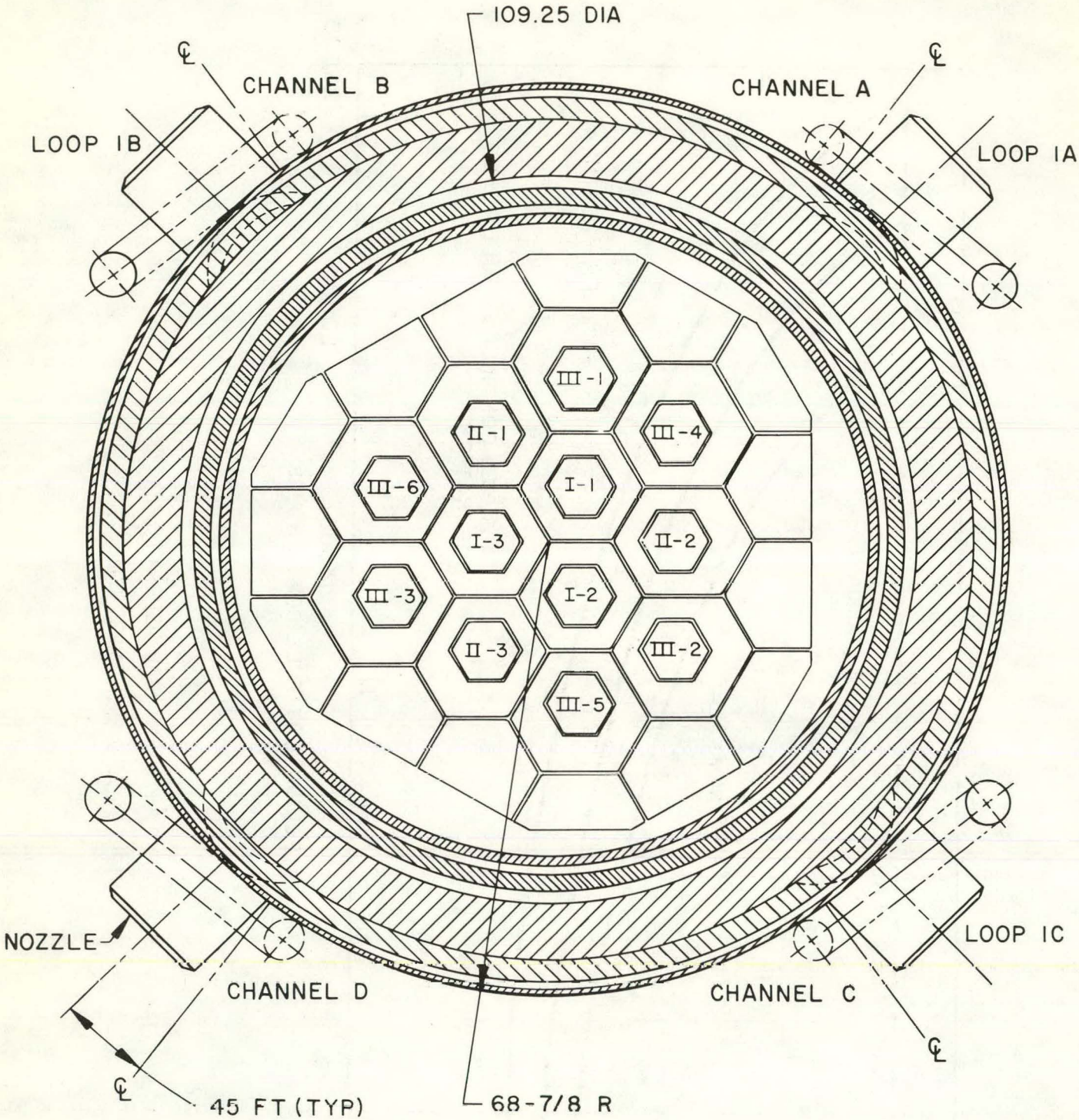

FIGURE II-5 - POWER RANGE NUCLEAR INSTRUMENT WELL LOCATIONS

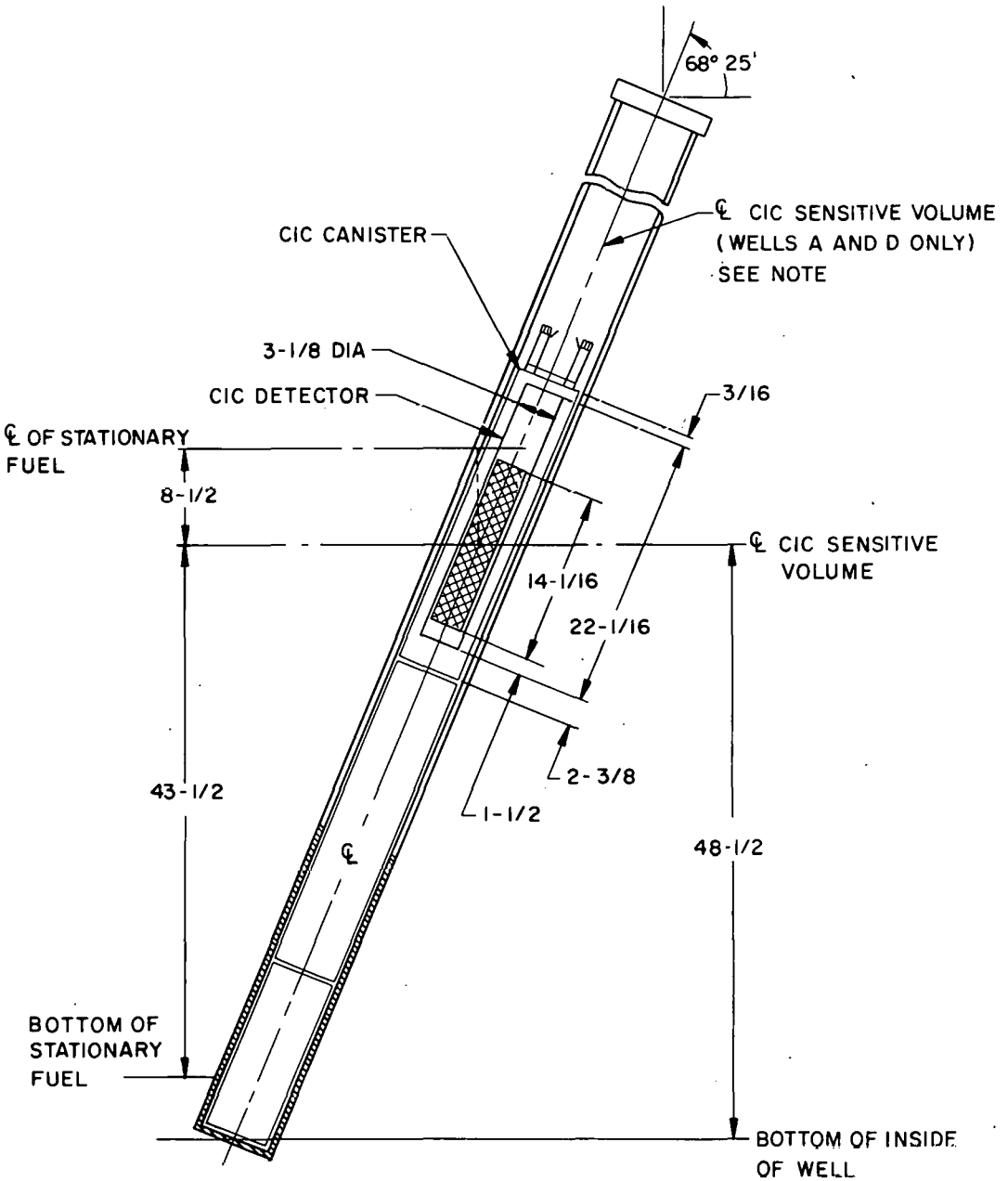

NOTE: INSTRUMENT WELLS A AND D EACH CONTAIN TWO CIC'S
THE ADDITIONAL CIC'S ARE USED FOR PHYSICS TESTING

FIGURE II-6 - AXIAL ELEVATION OF COMPENSATED ION CHAMBERS

B and D CIC's. This is accomplished by adding Boral strips around the channel A and C CIC's to reduce the thermal neutron flux and adjusting the thickness of polyethelene sleeves to thermalize the fast neutron flux. The polyethelene sleeves around the channel B and D CIC's are 26/32 inch thick compared to 22/32 inch sleeves around the channel A and C CIC's.

The source range instruments are located adjacent to the power range nuclear instrument wells. The axial location of the source range nuclear instrument wells is presented in Figure V-1.

The axial location of the compensated ion chambers used for normal core operation is shown in Figure II-6. The CIC's used for physics testing are located immediately above the CIC's used for normal operation in power range nuclear instrument wells A and D.

III. DATA REDUCTION METHODS

A. Reactivity Worth and Critical Position Measurements

The reactivity worth and critical position of a seed or group of seeds were measured by lifting and lowering the controlling seeds to obtain a series of positive and negative reactivity insertions near criticality. Reactivity insertions were measured using the inverse kinetics simulator (IKS). The IKS is a small analog computer which supplies time-dependent reactivity data from an input signal directly proportional to reactor power (i.e., ion chamber current). The time-dependent reactivity is generated directly and instantaneously by solving the six delayed neutron group, space-independent reactor kinetics equations:

$$\frac{dN}{dt} = \frac{\Delta k}{l^*} N - \sum_{j=1}^{j=6} \frac{dCj}{dt}$$

$$\frac{dCj}{dt} = \frac{\beta j}{l^*} N - \lambda j Cj$$

where N = neutron density in the reactor

Δk = reactivity

l^* = effective neutron lifetime, seconds

C_j = concentration of neutrons in delayed neutron group j

βj = Number of delayed neutrons appearing in group j per prompt neutron produced.

λj = decay constant associated with group j

t = time

The LWBR six group delayed neutron data are based on weighted averages of U^{233} and Th^{232} fission fractions at beginning of life. Corrections to the IKS reactivity data based on lifetime variations of the U^{233} and Th^{232} fission fractions and corrections for $\bar{\beta}/\beta$ are discussed in Section III.B.

The advantage of the IKS over other reactivity measurements, such as measuring the stable period with a stopwatch, is the fast reponse and direct reading of the IKS. A detailed discussion of the construction and operation of the IKS is presented in Reference 1.

The step by step procedure for reactivity worth and critical position measurement was performed as follows:

1. With the core near critical, the position (h_0) and reactivity of the controlling seed(s) were recorded.. Reactivity was read from the IKS.

2. The controlling seed(s) were lifted to a height designated as h_1 above the critical position (h_0) to attain a fast startup rate in the range of 0.5 decades per minute (DPM) to 0.9 DPM, and the reactivity from the IKS was recorded.

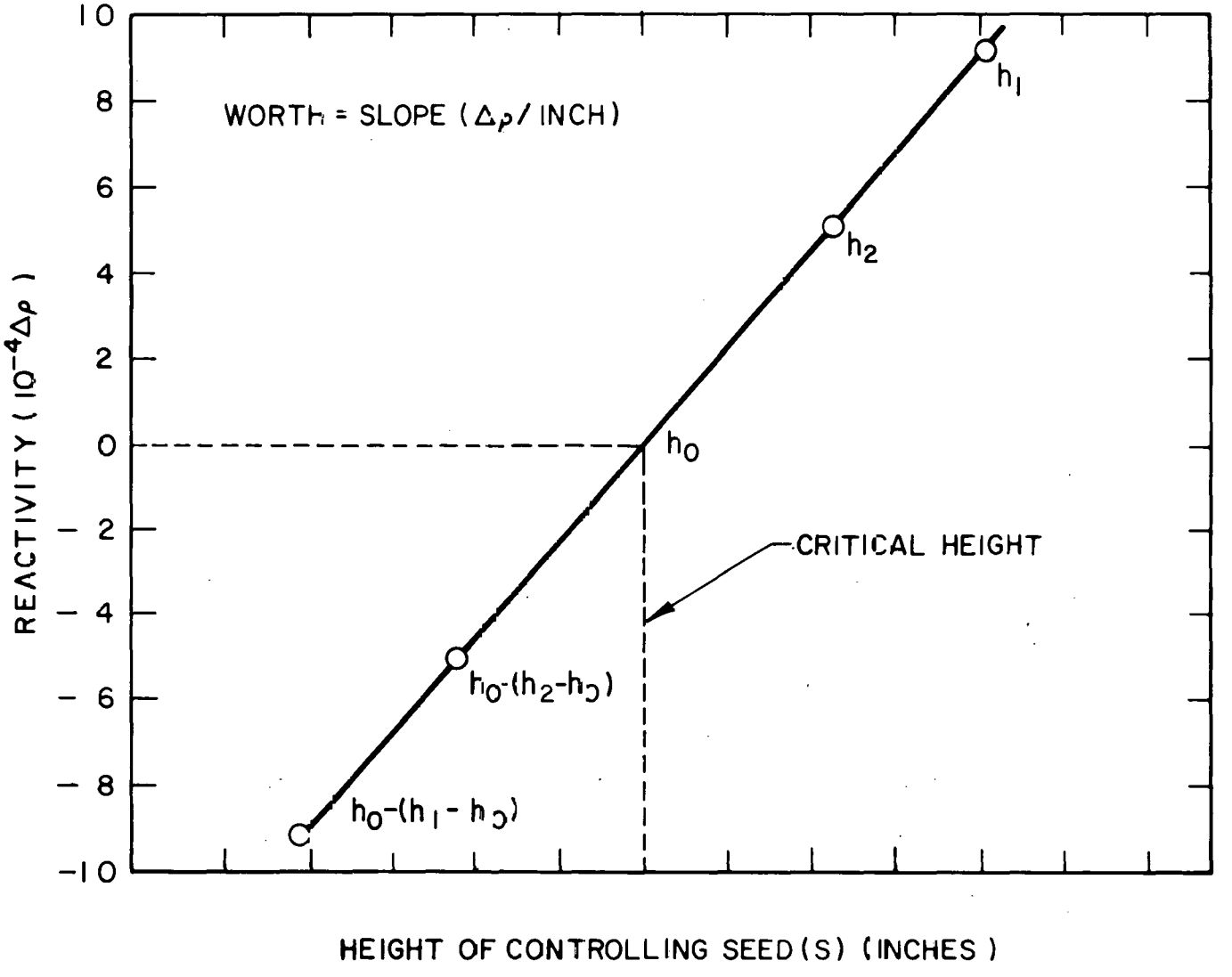

FIGURE III-1 - WORTH AND CRITICAL POSITION MEASUREMENT

3. The controlling seed(s) were then lowered an increment of height corresponding to h_1-h_0 below the critical position, and the reactivity was measured using the IKS.

4. The controlling seed(s) were then lifted to a height designated as h_2 to attain a slow startup rate in the range of 0.2 DPM to 0.4 DPM, and the reactivity was measured using the IKS.

5. The controlling seed(s) were lowered an increment of height corresponding to h_2-h_0 below the critical position, and the reactivity was measured using the IKS.

6. The controlling seed(s) were lifted to remeasure the reactivity at h_1 as a check on the repeatability of the measurement.

The reactivity worth and critical position measurement are shown graphically on Figure III-1. The slope of the curve determined by reactivity versus height of controlling seed(s) gives the worth in units of 10^{-4} $\Delta\rho$/inch and the height corresponding to zero reactivity gives the critical position.

B. Corrections to Data

The value of $\bar{\beta}$ = 0.00332 initially used to program the inverse kinetics simulator for LWBR was based on early nuclear design calculations. More recent calculations with the as-built nuclear design model, described in detail in References 2 and 3, show that the early value of $\bar{\beta}$ used to program the IKS was too large by a factor of 1.02 cold and 1.01 hot due to a reduced thorium fission fraction. Therefore, the reactivity values determined by the IKS at beginning of life were multiplied by a factor of 0.98 cold and 0.99 hot. In addition, the IKS reactivity values were multiplied by a factor of 1.02 to account for a $\bar{\beta}/\beta$ correction based on Monte Carlo calculations using the explicit, three-dimensional program RCP01 (Reference 2). This $\bar{\beta}/\beta$

correction accounts for differences in energy spectra of delayed and prompt neutrons. The net result of the two corrections is that the reactivity values as determined from the IKS at beginning of life were multiplied by 1.00 for cold measurements and 1.01 for hot measurements.

Additional corrections to the reactivity data were made for temperature and pressure variations when required. The corrections were made according to the following equation:

$$\rho' = \rho^{IKS} - \alpha_m (\bar{T}_m - \bar{T}_o) - \alpha_p (P_m - P_o)$$

where:

ρ' = corrected reactivity

ρ^{IKS} = IKS measured reactivity (multiplied by 1.00 cold and 1.01 hot)

α_m = measured temperature coefficient of reactivity

$\bar{T}_m$ = average of 4 Mueller Bridge cold leg temperature measurements at the time ^{IKS} was measured

$\bar{T}_o$ = average of 4 Mueller Bridge cold leg temperature measurements at reference temperature

α_p = pressure coefficient of reactivity

P_m = primary system pressure at the time ^{IKS} was measured

P_o = primary system pressure at the reference pressure

IV. DESCRIPTION OF TESTING METHODS

This section presents a discussion of the methods used for performing the initial physics tests for LWBR.

A. Initial Reactor Fill With Water

The purpose of this test was to fill the reactor vessel with demineralized water to a height which covers the core in a safe and controlled manner.

The initial fill test procedure was based on the use of the source multiplication method of monitoring the core reactivity behavior during the fill operations. Three 100 microgram californium-252 neutron sources (2.34 x 10^8 neutrons/sec each) were inserted into the core, one in each Type I module flux well, prior to initial fill. The sources were located in the 2-foot overlap region between the seed and blanket U233 bearing fuel with the seeds in the fully lowered position, see Figure V-1. Count rates were monitored with the four source range nuclear instrument channels. When the count rate was reduced to 5 counts per second or less, special physics test equipment (scalers and buffer amplifier), connected to source range nuclear instrument channels B and C, was used to provide accurate count rate data.

The initial fill was performed by gravity feed from the reactor plant water storage tank through the reactor plant charging system. The flow rate was initially adjusted to 5.0/+0/-1.0 gpm using a throttle valve, and the valve was locked at that position. A dewatering pump provided capability for removing water from the reactor vessel in the event of an approach to criticality. Manual and automatic trips for dewatering were set at count rates based on a calculated count rate versus water height curve.

B. Cold Zero Power Tests

1. Initial Approach to Criticality

The purpose of this test was to approach and achieve initial criticality of the LWBR core in a safe controlled manner and to determine the overlap between the source and intermediate nuclear instrumentation ranges at cold plant conditions.

The initial approach to criticality of the LWBR core was performed by a controlled lifting of the 12 seed bank at a primary coolant temperature and pressure of 150 ± 5°F and 325 ± 50 psig, respectively. The test was conducted using the three 100-microgram californium-252 neutron sources, each placed in the flux well of a Type I module at the same elevation as for the initial fill, to monitor the core neutron level. The approach

began by latching all control drive mechanisms and lifting the 12 seed bank continuously to the position where the bottom indicator lights went off (approximately 6 inches from the bottom). Reactivity insertion rates were reduced by using a procedure which consisted of lifting the 12 seed bank for 7 seconds and then waiting for 23 seconds. The critical bank height was estimated periodically by plotting inverse count rate versus height and extrapolating to the critical position.

Following initial criticality, the overlap between the source and intermediate range nuclear instrument readings was confirmed by recording the readings of the individual intermediate range log level meters at first indication and again when the corresponding source range meters reached full scale.

2. Cold Twelve Seed Bank Measurements

The purpose of this test was to determine the 12 seed bank differential reactivity worths and core temperature coefficient of reactivity for cold plant conditions.

a. Twelve Seed Bank Cold Critical Position and Bank Worth

The 12 seed bank worth and critical position were determined at approximately 150°F and 170°F with pressure in the range of 325 ± 25 psig. The worth at the above temperatures and pressure was measured using the method described in Section III.A.

b. Cold Temperature Coefficient of Reactivity

After the 12 seed bank worth at 150°F was measured (see Section III.A), the bank heights associated with the faster positive startup rate and the slower negative startup rate were used as reference positions to which the bank was periodically positioned as the coolant temperature was increased approximately 10°F, using the main coolant pumps as a heat source. The reactivity was measured at these positions, and the temperature

coefficient of reactivity was determined from the slope of the line determining by plotting reactivity at constant seed position versus temperature, as shown in Figure IV-1.

The above procedure was repeated following the bank worth measurement at approximately 170°F.

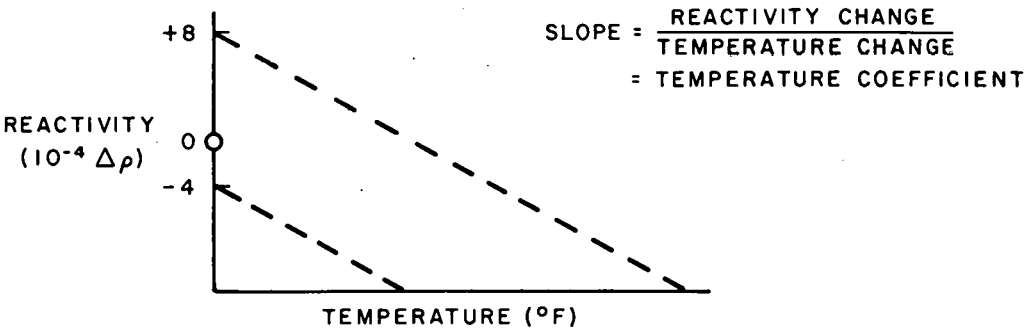

FIGURE IV-1 - TEMPERATURE COEFFICIENT MEASUREMENT

3. Azimuthal Symmetry Measurements

The purpose of this test was to obtain data to verify that no significant asymmetries initially existed among the various seed/blanket modules.

Core symmetry measurements were made at a coolant temperature of approximately 150°F with pressure in the range of 325 ± 25 psig. The 12 seed bank was lowered approximately 0.2 inch below the critical position. A single Type I seed was transferred to auxiliary control and lifted above the bank of 11 remaining seeds until criticality was re-established. The worth and critical position of the single seed was determined using the method described in Section III.A. The single seed was then lowered to the bank position and transferred to normal control. This procedure was repeated for each of the three Type I seeds, then for each of the three Type II's, and then for each of the six Type III seeds. At the completion of the symmetry measurements, the 12 seed bank was lifted to establish criticality.

4. Single Seed Out of Bank Measurements

The purpose of this test was to obtain data to be used in determining the shutdown characteristics of the LWBR core.

Single lifted seed measurements were made as follows at a coolant temperature of approximately 150°F with pressure in the range of 325 ± 25 psig. A single Type I seed (I-1) was transferred to auxiliary control and lifted while the bank of 11 remaining seeds was lowered, maintaining a near critical condition until the 11 seed bank had been lowered to the 11.5-inch position. The worths and critical positions of the withdrawn single seed and the 11 seed bank were measured. The 12 seed bank was re-established by lowering the single seed and lifting the 11 seed bank. The above procedure was repeated for a Type II seed (II-2) and then for a Type III seed (III-4).

C. Hot Zero Power Tests

1. Hot 12 Seed Bank Measurements

The purpose of this test was to determine 12 seed bank differential worths and temperature coefficients of reactivity for hot plant conditions. Also during this test, the overlap between the source and intermediate range nuclear instruments at hot plant conditions was determined.

a. 12 Seed Bank Hot Critical Position and Bank Worth

The 12 seed bank worth and critical position were determined at approximately 490°F, 510°F, and 532°F, with pressure in the range of 1985 ± 20 psig.

b. Hot Temperature Coefficient of Reactivity

The temperature coefficient of reactivity was measured for coolant temperature ranges of 490.5°F to 494°F, 510°F to 512.5°F, and 533°F to 535.5°F using the same procedure discussed in Section IV.B.2.b for the cold temperature coefficient of reactivity.

c. Source to Intermediate Range Overlap

Source to intermediate range nuclear instrumentation overlap was determined at 531 ± 3°F and 1985 ± 20 psig. The overlap was measured by increasing reactor power level from midway in the source range and recording the reading of the individual intermediate range log level meters at first indication and again when the corresponding source range log level meters reached full scale.

2. Partial Bank Worths

The purpose of this test was to determine the degree of nuclear coupling between the seeds and to confirm the adequacy of the predicted intermodule coupling effect in LWBR performance calculations. Partial bank worths and critical positions were determined as follows at a coolant temperature of 531 ± 3°F and a pressure of 1985 ± 20 psig. First the three Type I seeds were transferred to auxiliary control, and the worth and critical position were measured for these three seeds. The three Type I seeds were returned to normal control; then a single Type I seed (I-1) was transferred back to auxiliary control, and the worth and critical position for the single seed were measured. Finally the single seed was returned to normal control. A similar set of measurements was performed for the three Type II seeds followed by a single Type II seed (II-1), and then for the six Type III seeds followed by two Type III seeds (III-1 and III-4). The Type III measurements were performed with 2 seeds out of bank to represent calculations involving half core symmetry. (see Section V.B.5).

3. Pressure Coefficient of Reactivity

The purpose of this test was to obtain data for use in determining the effects of changes in coolant pressure on core reactivity at zero power and constant coolant temperature. The resulting reactivity coefficient represents primarily the sum of the water density and fuel clad flexibility effects on reactivity.

The pressure coefficient of reactivity was determined at a coolant temperature of 531 ± 3°F. With the primary pressure at 1775 ± 10 psig, a critical position was established for the 12 seed bank. The three Type I seeds were transferred to auxiliary control. A slow negative startup rate (0.1 to 0.2 DPM) was established by lowering the three Type I seeds to establish a reference position h_1, and the reactivity was measured using the IKS. Next the three Type I seeds were lifted to establish and maintain criticality as the coolant pressure was increased approximately 150 psig to 1925 ± 10 psig. The three Type I seeds were then lowered back to the reference position h_1, and the reactivity measured using the IKS. The change in reactivity at the constant partial bank height h_1 for the corresponding change in pressure was then used to calculate the pressure coefficient of reactivity.

For a second measurement of the pressure coefficient of reactivity, a critical position was established for the 12 seed bank at a primary pressure of 1925 ± 10 psig. The above procedure was then repeated for a coolant pressure increase to 2025 ± 10 psig.

4. Flow Coefficient of Reactivity

The purpose of this test was to obtain data for use in determining the effects of changes in coolant flow on core reactivity at zero power and constant coolant temperature and pressure.

The flow coefficient of reactivity was determined at a coolant temperature of 531 ± 3°F and a pressure of 1985 ± 20 psig. By lifting the 12 seed bank, a slow positive startup rate (0.1 to 0.2 DPM) was established with the 4 main coolant pumps operating on FAST speed. One pump was turned off. Reactivity was measured with the IKS for both pump configurations. The change in reactivity resulting from turning off one pump determined the flow coefficient of reactivity for the change in flow when switching from 4 pumps at FAST speed to 3 pumps at FAST speed.

5. Flux Wire Activations

The purpose of this test was to activate neutron flux wires to obtain axial activation profiles at low power, hot, xenon free conditions. The flux wire activation data were used to evaluate core symmetry and radial and axial neutron flux distributions.

The flux wires were irradiated at a coolant temperature of 531 ± 3°F and a pressure of 1985 ± 20 psig prior to the first ascension to power. Using the axial flux measurement system (AFMS), six encapsulated thorium flux wires were inserted into the core, specifically in modules I-1, I-2, I-3, II-1, III-1, and IV-7. See Figure 1 of Appendix A for the flux wire locations. The wires were irradiated for 150 minutes at approximately 1% core power and then withdrawn to a cocked position out of the core for a decay or cooling period. The wires were then removed and transported to the Bettis Atomic Power Laboratory for determination of activation profiles. Thorium irradiations were then performed in a second set of module locations consisting of the remaining two flux wells in modules II-3 and III-2 and their symmetrically located counterparts in modules II-1 and III-1. The counting of thorium activity senses protactinium-233 gamma emissions, which when corrected for decay time are proportional to neutron capture rate in thorium. The small diameter wires experience relatively little resonance self-shielding, so the capture rate in the wires is predominantly epithermal. The two sets of irradiations for thorium provide 10 wires whose activations can be related to each other to determine core symmetry and flux distributions.

D. Station Startup Test

The purpose of this test was to determine reactor core characteristics during station startup and initial full power operation and to determine the operating characteristics of the nuclear instrumentation while reactor power is increased from the intermediate range to the full power rating of the reactor.

At hot plant conditions, the reactor power level was gradually increased (by increasing steam demand) from an initial level in the intermediate range until calorimetric indication of full power (236.6 MW_t) was obtained. The plant electric load was increased from zero to full load (72 MWe) in prescribed steps. The critical height of the 12 seed bank increased to add positive reactivity to compensate for the negative reactivity from the power induced fuel temperature rise and from the increased amount of xenon and other poisons in the core resulting from the accumulated time at power.

During the power ascension, measurements and tests were performed at "key levels" that correspond approximately to 0%, 20%, 25%, 50%, 60%, 75%, 87%, and 97% of indicated reactor power. The key levels were established based on fuel element considerations and requirements for chemistry testing. For each key level, the 12 seed bank height was required to be within a specified range at the end of the period of power operation at that level. Also, power/flow setpoints were adjusted and tested prior to raising the power to the next key level. The power was held constant at each of the above levels for the minimum time necessary to satisfy fuel clad irradiation requirements and to accomplish other testing which was performed concurrent with station startup.

Also determined during the station startup test were relationship between compensated ion chamber detector current and reactor power level and the intermediate-to-power range nuclear instrument overlap.

E. Hot High Power Tests

1. Flux Wire Activations

The purpose of this test was to activate flux wires to obtain axial activation profiles at high power, equilibrium xenon conditions. The activations were performed on copper-nickel alloy (15% Cu, 85% Ni) wires. The flux wire activation data were used to evaluate core symmetry and radial and axial flux distributions.

During the ascension to power (station startup), before equilibrium xenon was established, copper-nickel wires were irradiated with the core near 70% of full power to provide additional checks of core power distribution. The copper-nickel wires were inserted in modules I-1, I-2, I-3, II-1 and III-1 (see figure 1 of Appendix A) and irradiated for 15 minutes.

Following the establishment of equilibrium xenon at full power, copper-nickel wires were irradiated for 10 minutes in modules I-1, I-2, I-3, II-1 and III-1. A second set of copper-nickel wires was irradiated for 10 minutes in modules II-3, III-2, II-1, and III-1. Following irradiation, the wires were cooled, removed and transported to Bettis for counting.

In the Counting Facility at Bettis, the copper-nickel wires were counted at two times. About 24 hours after removal from the core, the wires were β-counted for Cu^{64}, using a proportional counter. Then, 10 to 14 days after removal from the core, γ's from Co^{58} were counted using a "through the head", NaI crystal, γ counter with a discrimination window. At this same time, additional β-counting was done to measure the Co^{58} β's and the Compton scattered electrons produced by the Co^{58} γ's; this was done to correct the β -counting for Cu^{64}.

The count rates were corrected for the effective "dead time" of the counter, for background with no wire present, for the decay time since removal from the core, and where necessary, for drift effects on the electronics which may have been due to temperature change. A correction was also made for the effect on the activation shape due to activation during transit into and out of the core. The copper-nickel count rates for Cu^{64} were corrected for Co^{58} β's and β's produced by Co^{58} γ rays, as discussed above. The resulting profiles represent the measured thermal and epithermal (copper) and fast (nickel) flux activations at the time of removal from the core.

2. Bank Reactivity Worth; Moderator and Power Coefficients of Reactivity at Power

The purpose of this test was to obtain relationships between reactivity, power level, moderator temperature, and fuel position. The data were used to predict the seed motion required to compensate for fission product poison behavior and core depletion and to control load demand changes.

The test was performed at a coolant temperature of 531 ± 3°F and pressure of 1985 ± 20 psig with the 12 seed bank. The test consisted of three phases.

The first phase of the test determined the relationship between power level and fuel position. Starting with the reactor power level at 97 ± 3% and equilibrium xenon conditions, two power decreases of 6 ± 1% each were performed, and changes in fuel position were observed and recorded. During power decreases, T_{avg} was maintained within ± 1°F of its initial value.

The second phase of the test perturbed (raised) the 12 seed bank and allowed T_{avg} to stabilize at an increased temperature while maintaining the steam power constant (approximately 85%). These data were used to determine the relationship between average moderator temperature (T_{avg}) and fuel position. The temperature range was limited to 531 ± 3°F. To effectively utilize the available temperature range, T_{avg} was lowered to approximately 528.5°F prior to the start of this measurement.

The third phase of the test lifted the 12 seed bank a known distance, measured the reactivity, power, and temperature, and used these data to determine the 12 seed bank reactivity worth at approximately 85% power. The excess core reactivity was recorded by the IKS. The data logger was programmed to record the bank height, the nuclear instrumentation average power, and T_{avg} at a frequency of approximately once every second during the transient. After completion of the transient, 12 seed bank was lowered, power and T_{avg} were returned to their initial values, and the transient was repeated.

3. Xenon Reactivity Transient

The purpose of this test was to determine the reactivity variation with time during the xenon transient following a rapid plant shutdown from full power, equilibrium xenon conditions.

Following operation at 97% ± 3% power to establish equilibrium xenon, the turbine plant power was reduced to zero in a period of 70 minutes. Following turbine plant shutdown, reactor power was established in the intermediate range at 8×10^{-10} to 1×10^{-9} amperes with all 12 seeds in a level bank at the primary system temperature and pressure of 531 ± 3°F and 1985 ± 20 psig.

Immediately following shutdown, reactivity measurements were made during the xenon transient by lifting the 12 seed bank from the critical position to a reference height to obtain a stable startup rate between 0.7 to 0.8 DPM. Following the reactivity measurement with the 12 seed bank at the reference height the bank was lowered a corresponding increment below the critical position to obtain a negative reactivity insertion. Reactivity was measured with the bank at this position. The bank was then lifted to repeat the positive reactivity measurement at the reference position, and finally returned to the critical position. This type series of measurements was repeated every 30 minutes for 2.5 hours following shutdown, every 15 minutes for 2.5 to 4.5 hours following shutdown, and every 60 minutes for 4.5 to 20 hours following shutdown.

V. PRESENTATION AND INTERPRETATION OF TEST RESULTS

A. Calculational Models

1. Monte Carlo Calculation of Neutron Count Rates for Initial Fill

Calculations of total detector count rate (neutrons absorbed in boron-10 per second) were carried out for source range detector C. The

calculations were performed using the RCP01 computer code (Reference 7). The core, plus BF_3 source range neutron detectors, was represented by a symmetric one-third core RCP01 laydown, which included core barrel, baffle shield and pressure vessel. Periodic boundary conditions were established on the radial faces of the one-third core to provide an exact representation of the full core geometry and source and detector placements.

2. LWBR Nuclear Design Model

Performance characteristics for the LWBR core were calculated using four group diffusion theory in explicit two- and three-dimensional PDQ (Reference 4) calculations with few-group constants obtained from the energy spectrum program PAX (References 5 and 6). These included RZ calculations for a central (Type I) module, and explicit three-dimensional calculations with reflecting boundary conditions for both one-sixth and one-half of the core. Calculational biases, obtained from experimental results and from Monte Carlo neutron transport theory calculations (RCP01 program, Reference 7), were used to correct LWBR core calculational results.

Features of the calculational model, described in detail in Reference 2 include:

1. An automated system of processing manufacturing data for direct input to the PAX and PDQ analysis programs.

2. An extensive analysis of nuclear data for a Th-U^{233} system.

3. An accurate resonance integral calculation which makes externally generated resonance correction factors unnecessary.

4. Space Energy corrections to infinite medium cross sections based on one-dimensional multi-group transport theory calculations.

5. An explicit three-dimensional diffusion-burnup calculation which includes the capability of axially positioning movable seed fuel regions prior to a spatial flux calculation.

6. A modified P-3 transport calculation for the high energy group of neutrons.

7. Fuel and coolant temperature feedback to the three-dimensional neutron distribution. The feedback includes the effects of clad diameter shrinkage and fuel pellet radial growth.

8. Xenon feedback to compute the spatial flux distribution associated with equilibrium nuclide concentrations of iodine and xenon.

Various PDQ calculations were done with different three-dimensional geometric models. Mesh spacings used depended on the degree of detail required and the computer space available. Most calculations for the LWBR core were done with a symmetric one-sixth core geometry. A one-half core model, with larger transverse and axial mesh spacings than in the one-sixth core geometry, was used for a few one-half core symmetric configurations, such as where one seed was misaligned from the bank position.

B. Presentation and Discussion of Test Results

1. Initial Fill Count Rates

The count rates from the four source range instrument channels with the three californium sources installed are presented in Table V-1 at four water fill conditions (see Figure V-1):

Table V-1

Measured Count Rates During the Initial Fill

	Count Rate			
Fill Condition	Ch.A	Ch.B	Ch.C	Ch.D
Case 1	670	400	398	794
Case 2	414	233	304	521
Case 3	131	58	92	104
Case 4	4.6	1.8	6.5	2.9

Case 1 - Core completely dry

Case 2 - Core partially filled, with water level at the bottom of the detector sensitive region

Case 3 - Core partially filled, with water level barely covering the neutron source and above the detector sensitive region

Case 4 - Core completely filled

RCP01 calculations of count rate versus water level for the fill heights described in Table V-1 were performed prior to initial fill. Results of these calculations are presented in TAble V-2 for source range channel C, and the calculated count rates are compared with the corresponding measured count rates.

Table V-2

Calculated Count Rates At Channel C During the Initial Fill

Fill Condition	Calculated Count Rate at Channel C (cps)	Measured Count Rate at Channel C (cps)
Case 1	428 ± 41	398
Case 2	490 ± 52	304
Case 3	122 ± 11	92
Case 4	6.0 ± 0.8	6.5

The agreement between the RCP01 predicted absolute count rates, with their associated uncertainty, and the measured count rate is very good. The measured count rates for the core completely dry and the core completely filled (cases 1 and 4) are within the probable error bands presented in Table V-2. The measured count rates in the intermediate locations (Cases 2 and 3) are more difficult to relate to the calculated count rate due to uncertainty in the water level (±2 inches) and the fact that the count rate is rapidly dropping as a function of water level in this region.

2. Initial Criticaliy

Initial criticality was achieved at a 12 seed bank position of 27.34 inches, with a primary coolant temperature of 149.25°F and pressure of 310 psig. Inverse source range count rates were monitored to anticipate the approach to criticality.

Subsequent to initial criticality, measurements of source range and intermediate range nuclear instrument overlap yielded the results given in Table V-3.

Table V-3
Intermediate Range Readings (amperes)

Channel	N_1	N_2	Decades of Overlap
A	2×10^{-11}	3×10^{-10}	1.18
B	3×10^{-11}	5×10^{-10}	1.22
C	2×10^{-11}	4×10^{-10}	1.30
D	2×10^{-11}	6×10^{-10}	1.48

Values in "Decades of Overlap" column were calculated as follows:

$$\text{Decades of overlap} = \log_{10} (N_2/N_1)$$

where N_1 = initial intermediate range log level meter reading (that is, detectable increase in meter indication)

N_2 = highest reading on the intermediate range log level meter when the corresponding source range log level meter reads full scale.

The readings satisfy the requirement of a source to intermediate nuclear instrument range overlap of at least 0.25 decades to raise the power level into the intermediate range.

3. Zero Power Critical Positions, 12 Seed Bank Worths, and Temperature Coefficients of Reactivity

Results of the differential reactivity worth and critical position measurements are shown graphically on Figures V-2, -3, -4, and -5 for the 12 seed bank worth determinations at cold and hot temperature conditions. The figures also provide 12 seed bank critical positions, where $\Delta\rho = 0.00$. The measured values of bank worth and critical position are summarized in Table V-4 for two cold core temperatures and three hot core temperatures.

Table V-4

Measured 12 Seed Bank Critical Positions and Reactivity Worths

Temperature (°F)	Pressure (psig)	Critical Bank Height h_c (inches)	12 Seed Bank Worth ($10^{-4}\Delta\rho$/inch)
152.06	325	27.38	62.99
169.18	320	27.46	63.08
490.09	1988	31.38	52.28
509.44	1994	31.96	52.99
532.33	1988	32.70	51.03

Results of the temperature coefficient of reactivity measurements are presented graphically in Figures V-6, -7, -8, and -9 for cold and hot temperature conditions. Slopes of $\Delta\rho$/°F, calculated by the method of least squares, are presented in Table V-5 for five ranges of temperatures. Note that the measured data shown in Figures V-6 through -9 were corrected for 12 seed bank position differences in addition to pressure and $\bar{\beta}/\beta$ corrections described in Section III.B.

Table V-5

Measured Temperature Coefficients of Reactivity

Temperature Range (°F)	Temperature Coefficient ($10^{-4}\ \Delta\rho$/°F)		
	$+\ \Delta\rho$	$-\ \Delta\rho$	Average
152-160	-0.331	-0.289	-0.310
170-180	-0.285	-0.369*	-0.327
490.5-494	-1.336	-1.366	-1.351
510-512.5	-1.466	-1.651	-1.559
533-535.5	-1.747	-1.680	-1.714

*Least square fit for six points, where point at 173.6°F is not included (Curve 4 of Figure V-6).

Calculaed values for critical 12 seed bank positions, 12 seed bank reactivity worths, and temperature coefficients of reactivity are presented in Table V-6 along with measured values which have been corrected to the same temperature as used in the calculations.

Table V-6

Calculated Values for Critical Bank Position, Bank Worths and Temperature Coefficients of Reactivity at Zero Power

Parameter	Temperature (°F)	Calculated Value	Measured Value
Cold Critical Height	150	26.82 inches	27.37 inches
Cold Bank Worth	150	60.1 x $10^{-4}\Delta\rho$/inch	63.0x10^{-4} $\Delta\rho$/inch
Cold Temperature Coefficient	155	-0.66 x $10^{-4}\Delta\rho$/°F)	-0.31x$10^{-4}\Delta\rho$/°F
Hot Critical Height	531	32.55 inches	32.65 inches
Hot Bank Worth	531	46.1 x $10^{-4}\Delta\rho$/inch	51.1x$10^{-4}\Delta\rho$/inch
Hot Temperature Coefficient	535	-2.22 x 10^{-4} $\Delta\rho$/°F	-1.71x$10^{-4}\Delta\rho$/°F

The measured cold critical bank height for the 12 seed bank was higher than the calculated height by 0.55 inch. Using the measured cold bank worth to calculate core reactivity, this difference in critical heights indicates that the core was 0.35 percent less reactive than as-built calculations, well within the design allowance band of ±1.0 percent. The cold bank measured worth was larger than the calculated worth by 7.0 percent.

The measured hot critical bank height for the 12 seed bank was higher than the calculated height by 0.10 inches. Using the measured hot bank worth to calculate core reactivity, this difference in critical heights indicates that the core was slightly (0.05 percent, well within the ±1.0 percent allowance band) less reactive than as-built calculations at normal operating temperature. The hot bank worth was 11.9 percent larger than the calculated worth; the hot measured bank worth is within the band of bank worths used for specifying seed movement speeds.

4. Cold Zero Power Symmetry Characteristics

Results of the differential worth and critical position measurements for each of the single seeds during the symmetry measurements are shown graphically in Figures V-10 through -21. From each of the curves in Figures V-10 through 21, a critical height and a worth for the single seed were obtained. These results are tabulated in Table V-7.

a. Single Seed Worths

The worths calculated by using all the reactivity data (as plotted in Figures V-10 through -21) could be interpreted as indicating a slight asymmetry in the core power distribution, with the power being higher on the side of the core toward the III-3 and III-6 modules. However, this interpretation is not consistent with the critical positions: for the higher worth modules criticality should occur with the seeds at lower positions, but such is not the case. The apparently asymmetrical distribution of worths is probably coincidental and due to measurement uncertainties.

The individual seed worths calculated using all reactivity data show a somewhat high variability within each module type. To pursue the source of this variability, the worth and critical position were obtained for each seed using the positive reactivity data only. These are tabulated in Table V-7.

The positive reactivity data yield single seed worths which are much more uniform within a given module type than the worths from the curves (Figures V-10 through V-21), even though fewer data points are being included for each seed. No uneven distribution of reactivity worth toward one side of the core is present. From these data, or by looking at the negative reactivity data alone, it is concluded that the negative reactivity data are the cause of the variable worth distribution obtained from the curves. It was also verified that inaccuracy of drawing curves did not itself introduce the worth asymmetry, since a least-squares linear fit to the same data used for the curves showed a similar worth asymmetry.

It is not known why the negative reactivity data in this set of measurements cause non-uniform worths. Flux wire activtion data discussed later in this report confirm that there is very little asymmetry in the LWBR core. It is concluded that the more reliable estimates of symmetry results from single rod worth measuring come from the positive reactivity data.

Table V-7
Critical Positions and Single Seed Worths From
Cold Symmetry Test

	All Reactivity Data		Positive Reactivity Data	
Module	Critical Seed Position (inches)	Seed Worth ($10^{-4}\Delta\rho$/inch)	Critical Seed Position (inches)	Seed Worth ($10^{-4}\Delta\rho$/inch)
I-1	28.89	6.93	28.93	7.62
I-2	28.86	7.49	28.88	7.62
I-3	28.93	7.49	28.93	7.48
II-1	29.26	6.44	29.29	7.03
II-2	29.12	6.55	29.14	7.17
II-3	29.14	7.19	29.17	7.38
III-1	29.86	5.32	29.87	5.94
III-2	29.80	5.32	29.84	6.13
III-3	29.77	5.73	29.75	6.02
III-4	29.75	5.39	29.79	6.01
III-5	29.72	5.48	29.75	6.00
III-6	29.84	5.64	29.84	5.93

b. Single Seed Critical Positions

Core symmetry requirements demand that the critical positions for single seeds within a given module type fall within certain allowance bands. The acceptance criterion for cold symmetry testing, based on variations in seed positioning, temperature variations, and other possible measurement errors, is a 0.2-inch variation between seeds of a given type. Using the critical positions from positive reactivity data (see Table V-7), the maximum variations $(\Delta h_c)_{max}$ in critical position between seeds of a given type module are as follows:

Module Type	$(\Delta h_c)_{max}$
I	0.05
II	0.15
III	0.12

Thus the variations in single seed critical positions satisfy the acceptance criterion.

c. Determination of Power Symmetry Using Single Seed Worth and Critical Position Data

An approximate relationship may be derived (see Reference 9) to indicate the significance of the measured worths with respect to power symmetry. This derived relationship states that with one effective energy group, if the fuel material in a core is perturbed by $\Delta\nu\sigma_f$ and $\Delta\sigma_a$ from critical, the reactivity is:

$$\Delta\rho \approx \frac{\int \left[\Delta\nu\sigma_f - \Delta\sigma_a\right] \phi^2 \, dV}{\int \nu\sigma_f \phi^2 \, dV}$$

For two parts of the core V_1 and V_2 having similar, uniform materials, if the same uniform perturbation is made in both parts,

$$\frac{\Delta\rho_1}{\Delta\rho_2} \quad \frac{\int_{V_1} \phi^2\, dV}{\int_{V_2} \phi^2\, dV} \approx \frac{\int_{V_1} p^2\, dV}{\int_{V_2} p^2\, dV}$$

where P is the power density. Thus the power in two almost-symmetric modules of the same type should be in the approximate ratio of

$$\frac{\sqrt{(\Delta\rho/\Delta h)_1}}{\sqrt{(\Delta\rho/\Delta h)_2}}$$

Table V-8 shows ratios of the parameter $\sqrt{\Delta\rho/\Delta h}$ for each module from Table V-7 to the average value of the same parameter for each of the 3 types of module. Another way to compare the worths is to compare the size of the "bumps" $h_c - h_B$ from the uniform bank to critical; that is, the distance the individual seed had to be lifted to achieve criticality (during the single seed critical position tests). Thus, Table V-8 also shows the ratio of the parameter $\frac{1}{\sqrt{h_c - h_B}}$ to the average value of the same parameter for each of the 3 types of module. Table V-8 also shows the averages of the two ratios for each module.

Table V-8
Use of Reactivity Worth Measurements to Test Power Symmetry

Module	$\frac{\sqrt{\Delta\rho/\Delta h}}{\langle \sqrt{\Delta\rho/\Delta h} \rangle_{\text{Type}}}$	$\frac{\frac{1}{\sqrt{h_c - h_B}}}{\langle \frac{1}{\sqrt{h_c - h_B}} \rangle_{\text{Type}}}$	Average
I-1	1.003	0.996	1.000
I-2	1.003	1.011	1.007
I-3	0.994	0.993	0.994
II-1	0.988	0.983	0.986
II-2	0.999	1.007	1.003
II-3	1.013	1.010	1.012
III-1	0.995	0.985	0.990
III-2	1.011	1.003	1.007
III-3	1.001	1.007	1.004
III-4	1.000	1.000	1.000
III-5	0.999	1.011	1.005
III-6	0.994	0.994	0.994

Figure V-22 presents an LWBR core map showing the average value of the two ratios for each module. Based on the data shown in Figure V-22, an apparent asymmetry of approximately ±1% existed across the LWBR core at beginning of life. It is noted that the high side of the core is adjacent to the Channel D compensated ion chamber (CIC) to which the IKS is connected; this could be a possible explanation of the worth gradient across the core. However, the $\frac{1}{\sqrt{h_c - h_B}}$ ratios, which should be independent of the IKS, also exhibit the same type of gradient. So, although an apparent asymmetry existed, its magnitude is small, much smaller than was assumed in the core safety analysis.

5. Cold Zero Power Shutdown Characteristics

Results of the determination of differential worth and critical position for out-of-bank seeds (I-1, II-2, and III-4) and the 11 seed bank are presented in Table V-9. Linear fits to the data using the method of least squares were done.

Table V-9
Critical Positions and Reactivity Worths
From Cold Shutdown Testing at BOL

All data have been corrected to uniform temperature (152°F) and pressure (330 psig). Data are critical height h_c (inches) and worth $\Delta\rho/\Delta h$ ($10^{-4}\Delta\rho$/inch).

Module with Seed - Out of Bank	Single Seed h_c	Single Seed $\Delta\rho/\Delta h$	Bank h_c	Bank $\Delta\rho/\Delta h$
I-1	55.73	25.85	11.50	11.55
II-2	47.50	28.14	11.50	6.78
III-4	45.89	31.33	11.50	4.78

PDQ calculations were done with seeds from two Type III modules on opposite sides of the core withdrawn a few feet from the seed bank. The bank was near the 11-inch position. This calculation was made possible by using one-half core geometry. Since in the actual core the two modules are widely separated and previous calculations have shown that they are almost decoupled, a comparison can be made to an experiment with the seed from a single Type III module withdrawn, based on the assumption that the worth of one or two such seeds should be about the same. The resulting calculated critical seed position for a Type III module is 41.3 inches for a nominal core. The cold beginning of life core is underreactive by 0.35% (see Section V.B.3) relative to a best estimate nominal core, so to correct the critical position estimate for the off-nominal reactivity a reactivity worth is needed.

Four calculations were done for beginning of life, cold conditions with the seeds from the pair of Type III modules withdrawn. These calculations covered a wide range of seed positions, and a curve of eigenvalue versus position was drawn. In the vicinity of 46 inches, the calculated reactivity worth is

$$\frac{\Delta \rho}{\Delta h} = 0.0032\, \Delta\rho/\text{inch}.$$

Using the worth, the estimated critical bank position is

41.3 inches + 1.1 inches = 42.4 inches

(The 1.1-inch addition is the correction for the core being underreactive).

Although the Type III module is the most important because it is the most reactive, a calculation was also done with the seed from a Type I module withdrawn from the lowered bank. Similar corrections were made to the PDQ calculation of the core eigenvalue as were necessary in the case of the Type III seed withdrawn. The resulting critical position estimate for the Type I seed is 50./ inches for the 0.35%$\Delta\rho$ underreactive core.

The calculated critical position of a Type III seed withdrawn from the seed bank is 3.5 inches lower than the experimental (measured) position, when the calculated value is corrected using the experimental temperature coefficient. Using the measured worth, the 3.5-inch position difference represents a 1.1%$\Delta\rho$ conservatism in the calculated shutdown reactivity. About 1/3 of this difference is due to the use of the measured temperature coefficient to correct an available PDQ calculation to the test conditions. It is also likely that other corrections to PDQ cause part of the difference. Therefore, it is judged that the core is 1/2 to 1%$\Delta\rho$ more shutdown (conservative) than the calculation predicts with the seed from the most reactive module (Type III) withdrawn. Similar calculations for a seed from a Type I module gave a measured critical position 5 inches lower than the calculated position; the 5-inch difference is worth 1.3%$\Delta\rho$ less reactivity.

From the above, it is concluded that the calculation of the Type III module worth gave a result in satisfactory agreement with experiment.

The ordering of critical positions and worths among the three module types was to be expected because of the power-flattening blanket. That is, when the seed from one module is widely separated from the lowered seed bank, the reactivity of that module is much greater than the bank reactivity, and the module with the out-of-bank seed acts like a core-within-the-core. As such, the materials in the module with the out-of-bank seed determine its reactivity, rather than the geometric location of the module within the core. Since the Type III module has the largest volume of power-flattening blanket, it is the most reactive; then comes the Type II, and the Type I is least reactive since it has no power-flattening blanket. Thus the following relationships were expected:

$$(h_c)_{III} < (h_c)_{II} < (h_c)_I$$

$$\left(\frac{\Delta\rho}{\Delta h}\right)_{III} > \left(\frac{\Delta\rho}{\Delta h}\right)_{II} > \left(\frac{\Delta\rho}{\Delta h_I}\right)$$

The measurements discussed above have verified this ordering. (For a single seed only slightly displaced from a uniform bank, as in the symmetry measurements, the geometric location of the module is much more important and the ordering is reversed).

Since the most reactive module with a seed out-of-bank would have the greatest power fraction, the worth of the bank is lowest when seed from the most reactive module is out-of-bank:

$$\left(\frac{\Delta\rho}{\Delta h}\right)_{\text{Bank with a Type III seed up}} < \left(\frac{\Delta\rho}{\Delta h}\right)_{\text{Bank with a Type II seed up}} < \left(\frac{\Delta\rho}{\Delta h}\right)_{\text{Bank with a Type I seed up}}$$

In conclusion, the fact that a Type III module is the most reactive type in a single seed withdrawn configuration has been confirmed experimentally. In this configuration, the calculation is conservative in the sense that the core is 1/2 to 1% $\Delta\rho$ more shutdown than the calculation predicts.

6. Hot, Zero Power Partial Bank Worths

Reactivity measurements performed for the determination of differential worth for individual seeds and groups of seeds are shown graphically in Figures V-23 and 24. The measured worths are presented in Table V-10.

Type V-10
Measured Partial Bank Worths - Hot

Seeds	Measured Worth at 32.65 inches (10^{-4} $\Delta\rho$/inch)	Calculated Worth Between 31.85 and 35.37 inches (10^{-4} $\Delta\rho$/inch)
All 12	51.03*	45.51
3 Type I's	18.53	17.70
3 Type II's	13.56	12.64
6 Type III's	19.82	17.56
I-1	6.24	
II-1	4.48	
III-1, III-4	6.88	

*Measured in Hot Bank Worth Test

PDQ calculations approximating the test conditions (hot, clean, BOL) using the as-built model have been employed to analyze the measured results. This model describes one-sixth of the LWBR core radially in fine detail and contains movable fuel that is described axially on a uniform 3.52 inch mesh. For this analysis, the eigenvalue (K_{eff}) is computed for a reference case with the 12 seed bank placed at 31.85 inches, which is the mesh plane nearest to the hot measured critical bank position of 32.65 inches. Calculations have been performed by raising the 12 seed bank and each partial bank (partial bank is defined as the three Type I seeds, the three Type II seeds, or the six Type III seeds) one axial mesh interval (3.52 inches). The worths for the full bank and for each partial bank are then computed from

$$\frac{\Delta\rho}{\Delta h} = \frac{\lambda_2 - \lambda_1}{\lambda_2 \ \lambda_1 \ (h_2 - h_1)}$$

where λ_1 is the eigenvalue with all seeds banked at the reference position (h_1 = 31.85 inches) and λ_2 is the perturbed eigenvalue resulting from placing selected seeds at the next highest mesh point, h_2. The calculated worths are listed in Table V-10 along with the corresponding measured worths.

The results of this test can be analyzed to determine the degree of nuclear coupling between LWBR modules and to confirm the adequacy of the intermodule coupling effect in LWBR performance calculations. "Coupling" is thought of here in the following terms: In a tightly coupled core a local perturbation impacts the flux level everywhere in the core. If the perturbation is small, the space and energy distribution of the neutron flux throughout the core will not change significantly, only the overall level will change. It is this phenomenon which causes the worths of the control elements (seeds) of various modules to possess the additive properties described in the analysis below. If a core is loosely coupled, a small local perturbation will change both the space-energy distribution of the neutron flux and its level, and the worths of the control elements of various modules would not be additive.

The analysis is discussed in five parts as follows (worths are from Table V-10):

a. Objective - To demonstrate that the sum of the partial bank worths is greater than the worth of the 12 module bank.

Computations:

For measured values,

Σ(Partial Bank Worths)=(18.53 + 13.56 + 19.82) x $10^{-4}\Delta\rho$/in.

Types I, II, III =51.91 x $10^{-4}\Delta\rho$/inch

Measured Worth of 12 Seed Bank = 51.03 x $10^{-4}\Delta\rho$/inch.

Similarly, for the calculated values,

Σ(Partial Bank Worths)=(17.70 + 12.64 + 17.56)x$10^{-4}\Delta\rho$/inch

Types I, II, III =(47.90 x $10^{-4}\Delta\rho$/inch

Calculated Worth of 12 Seed Bank = 45.51$\Delta\rho$/inch (from Table V-10)

From the above, it can be seen that for the measured values, the sum of the partial bank worths is about 2% greater than the worth of the 12 seed bank, and for the calculated values the sum is about 5% greater. Thus the original hypothesis is confirmed for both the measured and calculated values.

The difference between the worth of the total bank and the sum of the worths of the partial banks, using calculated values, is greater than the difference found using measured values (5% versus 2%). This discrepancy is most likely due to the fact that, because of the spatial mesh limitations of the LWBR nuclear design model (a 3.5-inch axial mesh interval), the calculation of bank worth requires a much larger perturbation to the core than is actually made during a measurement. Thus the results found using measured worths are taken to be more accurately representative of true module characteristics.

b. Objective - For the members of the set of Type I modules, to demonstrate that each seed has the same individual worth. It is expected that each seed would have the same individual worth because of the core symmetry. Also, if the three seeds were added to the auxiliary drive one after the other, it is predicted that the second seed added would be worth slightly less than the first, and that the third seed added would be worth slightly less than the second. Hence, the following computation is performed to demonstrate that the measured worth of the seed from module I-1 is slightly more than 1/3 of the worth of Type I partial bank.

Computations:

$$\text{Average worth of type I seeds} = \frac{(18.53\times10^{-4}\Delta\rho/\text{in})}{3}$$

$$= 6.18 \times 10^{-4}\ \Delta\rho/\text{inch}$$

Measured Worth of I-1 = $6.24 \times 10^{-4}\ \Delta\rho$/inch.
(From Table V-10)

The worth of the seed from I-1 is approximately 1% greater than the average worth, thus supporting the original hypotheses.

c. Objective - For the members of the set of Type II modules, to demonstrate results similar to b. above.

Computations:

$$\text{Average worth of Type II} = \frac{13.56\times10^{-4}\ \Delta\rho/\text{inch}}{3} = 4.52\times10^{-4}\Delta\rho/\text{inch}$$

Measured worth of II-1 = $4.48 \times 10^{-4}\ \Delta\rho$/inch.
(from Table V-10)
The measured worth of the seed from I-1 is about 1% less than the average worth.

d. Objective - For the members of the Type III modules, to demonstrate results similar to b. above. (For purposes of the following computations, 6 Type III modules are treated as 3 pairs of near-neighbor modules).

Computations:

Average worth of a pair of Type III seeds = $\frac{19.82 \times 10^{-4} \Delta\rho/\text{inch}}{3}$

$= 6.61 \times 10^{-4} \Delta\rho/\text{inch}$

Measured Worth of III-1 and III-4 = $6.88 \times 10^{-4} \Delta\rho/\text{inch}$.
(From Table V-10)

The measured worth of the seeds from III-1 and III-4 is approximately 4% greater than the average worth.

e. Summary

The above results indicate that the LWBR core at operating temperature in a level bank configuration is tightly coupled. Using measured values, the sum of the Type I, Type II and Type III partial bank worths is only 2% greater than the worth of the 12 seed bank. The Type I single seed worth is measured to be approximately 1% greater than the average worth of a Type I seed; the Type II single seed worth is approximately 1% less than the average worth of a Type II, and the worth of the pair of Type III's is approximtely 4% greater than the average worth of a Type III pair. The result for Type II is consistent with the cold single seed worth results as seen in Table V-7, which indicated that the worth of seed II-1 is slightly lower than the worth of the other two Type II seeds.

7. Hot Zero Power Pressure Coefficient of Reactivity

Results of the reactivity measurements for the pressure coefficient of reactivity determination are presented in Table V-11.

Table V-11

Measurements of Pressure Coefficient of Reactivity

Pressure (psig)	Temperature (°F)	Reactivity ($10^{-4}\Delta\rho$)	Bank Height (inches)	Reactivity (corrected) for temperature and Bank Height ($10^{-4}\ \Delta\rho$)	Pressure Coefficient ($10^{-6}\Delta\rho$/psi)
1771	530.10	-1.90	32.627	-1.94	2.23
1926	530.275	-1.15	32.625	1.51	
1926	530.29	-1.33	32.608	-1.36	1.91
2023	530.16	0.69	32.608	0.49	

Using the pressure coefficient values from Table V-11, the average value of the pressure coefficient is 2.1 x $10^{-6}\Delta\rho$/psi.

Now the calculated value for pressure coefficient of reactivity will be determined and compared with the measured value. The calculated value is composed of contributions from both coolant density increase and fuel rod clad shrinkage during pressure increases. The coolant density coefficient component was obtained by determining the change in density per unit pressure at constant temperature and the change in density per unit temperatue at constant pressure, and then assuming that the ratio of the two quantities is equal to the ratio of the pressure coefficient to the temperature coefficient. This ratio is approximately -0.0103°F/psi. Using the calculated value of moderator coefficient of -1.85 x $10^{-4}\Delta\rho$/°F (3-dimensional PDQ calculation), the coolant density coefficient is

$$(-0.0103°F/psi)(-1.85 \times 10^{-4}\Delta\rho/°F) = 1.91 \times 10^{-6}\Delta\rho/psi.$$

The reactivity change due to clad shrinkage is calculated as follows. It is estimated that a 300 psi change in pressure from 1775 to 2075 psig will produce the following clad diametral shrinkage under hot, zero power, beginning of life conditions:

Seed	0.042 mils
Regular Blanket	0.120 mils
Power-flattening Blanket	0.108 mils

From PDQ studies of clad shrinkage, the following approximate reactivity effects of shrinkage were obtained. In the seed, shrinkage of 0.042 mils produces a $0.41 \times 10^{-4}\Delta\rho$ increase in reactivity. Shrinkage of 0.12 mils in the regular blanket and 0.108 mils in the power-flattening blanket produces $1.17 \times 10^{-4}\Delta\rho$ increase in reactivity. The total reactivity increase is thus $1.58 \times 10^{-4}\Delta\rho$. The pressure coefficient due to clad shrinkage is therefore $(1.58 \times 10^{-4}\Delta\rho) \div (300 \text{ psi}) = 0.53 \times 10^{-6}\Delta\rho/\text{psi}$.

Combining the coolant density and clad shrinkage components give the following calculated value for the pressure coefficient of reactivity:

$$(1.91 \times 10^{-6}\,\Delta\rho/\text{psi}) + (0.53 \times 10^{-6}\,\Delta\rho/\text{psi}) = 2.44 \times 10^{-6}\,\Delta\rho/\text{psi}.$$

Agreement between the calculated value of the pressure coefficient ($2.44 \times 10^{-6}\,\Delta\rho$/psi) and the measured value ($2.1 \times 10^{-6}\,\Delta\rho$/psi) is considered to be within the limits of experimental error due to uncertainties in pressure, temperature, and bank height determinations.

8. Hot Zero Power Flow Coefficient of Reactivity

Results of the reactivity measurements for the flow coefficient of reactivity determination are presented in Table V-12.

Table V-12

Measurement of Flow Coefficient of Reactivity

Flow Condition	Reactivity (10^{-4} $\Delta\rho$)	Temperature (°F)	Pressure (psig)	Bank Height (inches)	Reactivity (corrected for temperature, pressure) (10^{-4} $\Delta\rho$)
4 FAST	0	531.82	1985	32.68	0
4 FAST	2.73	531.00	1985	32.74	2.79
3 FAST	2.16	531.06	1983	32.74	2.36

From the above values for reactivity, it can be seen that

Flow coefficient = $(2.79 \times 10^{-4}\Delta\rho) - (2.36 \times 10^{-4}\Delta\rho)$

= $0.43 \times 10^{-4}\Delta\rho$ decrease in reactivity for 4 FAST to 3 FAST pump switch.

Now the calculated value of flow coefficient will be determined and compared with the measured value. During a flow transient resulting from switching from 4 pumps on FAST to three pumps on FAST, there will be a change in the spatial average of the absolute pressure in the core. During the transient, it is expected that the primary coolant pressure will remain essentially constant in the pressurizer, which is connected to the outlet main piping from the reactor vessel. The decrease in the pressure drop from the inlet of the core to the outlet of the reactor vessel will decrease the amount by which the absolute pressure in the fuel rod portion of the core exceeds the (measured) pressurizer pressure. This results in a negative reactivity insertion due to the pressure coefficient of reactivity. The average pressure in the core is expected to drop by 17.2 psi. Using the measured value ($2.1 \times 10^{-6}\Delta\rho$/psi) for the pressure coefficient (see Section V.B.7), the expected reactivity change when switching from the 4-FAST to 3-FAST pump configuration is

$$(2.1 \times 10^{-6}\Delta\rho/\text{psi})\ (17.2\ \text{psi}) = 0.36 \times 10^{-4}\Delta\rho.$$

Agreement between the calculated flow coefficient (0.36×10^{-4} $\Delta\rho$) and measured result (0.43×10^{-4} $\Delta\rho$) is good. Factors which could have affected the measured test results are (1) small dimensional changes in the core caused by flow-induced pressure drops and (2) temperature differences caused by turning off a loop. These effects were calculated to be very small (less than 0.1×10^{-4} $\Delta\rho$) and the results of this test confirm this conclusion.

9. Flux Wire Activations

The axial flux wire activation profiles are presented in Appendix A. A summary of the wire activations is presented in Table 1 of Appendix A. Sequence number 1 is the standard two activation, 10 wire irradiation set for thorium wires at low power. Sequence number 5 is the irradiation set for copper-nickel wires near full power. Sequence numbers 3 and 4 are the copper-nickel irradiations performed at near 70% of full power to provide additional checks of core symmetry.

As indicated, each profile is normalized to have an average value of unity. Figures referred to in the following discussion are the figures of Appendix A.

a. Thorium Activation Profiles

Activation shapes for the thorium wires irradiated near zero power are shown in Figures 2 through 13. The first set of six wires is shown in Figures 2 through 7. In 3 cases (Figures 4, 6, and 10) the experimental data are known to be axially shifted a noticeable distance with respect to the core fuel; this is seen by the location of the measured flux dip locations, which are to the left of the location of the rod support grids that cause the flux dip. The amount of shift is about 1 inch and was due to positioning error of the wire in the core. Other smaller axial shifts are also present. The grid flux dips provide an excellent method for accurately establishing the axial position of flux wires.

The second set of four wires is shown in Figures 8 through 11. Modules II-1 and III-1 are common to the two sets of wire locations, and the data for these two modules show close agreement, the peak in the II-1 module being about 1% lower in the first wire set. The experimental point near 41 inches in the III-1 plot for the second wire set is about 2 1/2% lower than in the first wire set, and this is either a statistical fluctuation or bad experimental data.

Figure 12 is a second counting of the same wire as in Figure 2. The repeatability is very good. Figure 13 is a counting of the same wire as in Figure 5, also showing good repeatability.

b. Copper-Nickel Profiles at Full Power, Equilibrium Xenon

Copper-nickel alloy wires were irradiated at full power, equilibrium xenon, at the end of the station startup test (after about 200 effective full power hours of operation). The copper activations are shown in Figures 14 through 24. The first set is in Figures 14 through 18 (there is no wire available for module IV-7). The profiles of the second set of wires (Figures 19 through 22) are similar to those of the first set, with 3% being the largest peak-to-peak variation. Figure 23 is a second counting (in the same channel) of the same wire as in Figure 14; comparison of Figures 23 and 14 shows about 1 1/2% variation in the peak. Figure 24 is a counting of the same wire as in Figure 19, but in the other channel; comparison of Figures 24 and 19 show a 1% variation in the peak. Thus, the channel-to-channel variation is no more than the variation in reproducibility of a given channel.

The nickel activations are shown in Figures 25 through 35, with the first set in Figures 25 through 29. The nickel experimental profiles are from the same wires as the copper profiles. The second set of activations (Figures 30 through 33) agrees with the first set. Figures 29 and 34 show good reproducibility for a given counting channel; Figures 25 and 35 show about 1% difference near the peak from one channel to another.

In addition to the dips in the experimental points due to the grids, it is possible to see other heterogeneities in the axial profiles. In particular, in the Type I modules, the rod row adjacent to the row with the flux well has a 70 inch binary length instead of an 84 inch length. At the 14-inch position, there is a small bump in the experimental profile (Figures 14, 15, and 16) due to this fuel zone change. The calculational profile does not show the bump because of the 3.5 inch axial mesh size. The bump does not appear in Types II and III modules because there is no zone change in the rod row adjacent to the flux well.

c. Copper-Nickel Profiles Near 70% Power

Copper-nickel wires also were irradiated near 70% power. By comparing the experimental activation shapes at different power levels, it is possible to see the effect of 12 seed bank position, power level, and poison buildup on power shape. Table 1 of Appendix A shows that between the 1% and 68% power irradiations, the 12 seed bank position moved about 4 inches due to the power reactivity. Between the 68% and 71% power irradiations, the bank power irradiations, the bank moved about 3 inches due to both power reactivity and poison increase. By comparing experimental activations at 68% and 71% power (where the power level change is small and its effect on power shape is negligible), it is possible to separate the bank position plus poison effects from the power level effect. Figure 48 for copper activation of wires in module II-1 shows that the 2-inch bank position change and poison increase has a small effect on the axial shape and causes about a 3% decrease in the peak to average activation. Figure 49 shows a similar comparison for nickel; a 3% decrease occurs in this case also.

Figures 36 through 41 show the copper activation shapes at 3 power levels, and Figures 42 through 47 show the nickel activation shapes at 2 power levels. Table V-13 gives the approximate peak-to-peak decrease in activation from the figures. In going from 68% to 97% power, or 71% to 97% power, the peak-to-average activation changes less for copper than for nickel.

The measured peak to average activation changes can be summarized as follows. The power change from 1% to 68% with the accompanying 4-inch bank position change reduced the activation peak to average in copper by about 6%. The poison buildup with the associated 2-inch bank position change reduced the activation peak to average in copper by 3%. The 3-inch bank position change required to compensate for a power increase from 71% to 97% with associated poison buildup reduced the peak to average roughly 4% for copper, 7% for nickel. The total effect from bank position movement of 9 inches, xenon poison increase from zero to full power equilibrium, and power increase from zero to full power is a reduction of roughly 13% in copper peak to average activation.

Table V-13
Change in Normalized Peak Activation
From One Irradiation to Another

	Copper Activation		Nickel Activation	
Module	Figure (Appendix A)	Power Range 68% to 97%	Figure	Power Range 68% to 97%
I-1	36	-7%	42	-8%
I-2	37	-9%	43	-11%
III-1	40	-7%	46	-9%
III-2	41	-7%	47	-9%
		68% to 71%		68% to 71%
II-1	48	-3%	49	-3%
		71% to 97%		71% to 97%
II-1	38	-2%	44	-6%
II-3	39	-6%	45	-9%

d. Integral Axial Activations

The activation profiles from which the normalized plots were made were axially integrated to obtain average radial (or planar) activation values at the locations of the flux wells. The radial data are summarized in Tables V-14 and V-15: Table V-14 shows the results from the irradiation near zero power and Table V-15 shows the results from the irradiation at full power. The experimental integrals represent values of

$$\frac{N}{L_2 - L_1} \int_{L_1}^{L_2} \sum \sigma_g \phi_g \, dz,$$

which is an axial average of the activation $\sigma_g \phi_g$ (microscropic cross section times flux) summed over energy groups. The cross sections σ_g represent each of the reactions measured, and N is an arbitrary normalization constant. The integration range extends beyond the binary fuel by 4 or 5 inches at the top and 6 or 5 inches at the bottom.

The calculated integrals are of the same form as the experiment represents. The interval (L_1, L_2) is shifted about an inch, but this is of no consequence. To compare the experiment to the one-sixth core calculation, the experimental integrals were averaged for a given type of module. Both calculation and experiment were then normalized arbitrarily such that module Type II has the value unity. The numerical values thus represent a comparison of the shape from one module to another.

Table V-14 shows the discrepancy between experiment and calculation for the thorium activation. The E/C value is 1.0/0.9970 (0.3%) from one module type to another within the 12 module central core, and 1.0064/0.9970 (0.9%) when the reflector blanket is included.

Table V-15 shows an E/C value of 1.0/0.9772 (2.3%) for copper at full power, and an E/C value of 1.0147/1.0 (1.5%) for nickel. The estimated experimental error is 1 to 2% at the 1σ level due to repeatability and variability factors for wires and counters. All the discrepancies are essentially within the experimental error band.

Besides comparing calculation to experiment, it is of interest to compare experimental values from symmetrical locations within the core. This comparison is summarized in Table V-16. The special irradiations at 68% and 71% power are included. All the results indicated symmetric core operation within the experimental uncertainty of the measurement (1 to 2% at the 1σ level).

Table V-14

Radial Activation Distribution at the Flux Well Locations - Experiment versus Calculation, Low Power Flux Plots

Module Type	I	II	III	IV
Module #				
Thorium Flux Wire Results (pa-233 Activity)				
		Experiment*		
1	2.1146	0.9989	0.7416	
2	2.0832		0.7463	
3	2.1223	0.9941		
7				0.18854
Average (normalized to II)	2.1141	1.0	0.7465	0.18920
		Calculation*		
	2.1204	1.0	0.7467	0.1880
		Experiment/Calculation		
	0.9970	1.0	0.9997	1.0064

*The calculational results for thorium are quoted for an 8.07 mil diameter wire. Although the wires used in the experiment were of various diameters, the experimental values quoted above have been normalized to those for an 8.07 mil diameter wire.

Table V-15

Radial Activation Distribution at the Flux Well Locations - Experiment Versus Calculation, High Power Flux Plot (Approximately 100%) Copper-Nickel Flux Wire Results

Module Type	I	II	III	IV
Module #				
Cu-64 Activity				
		Experiment		
1	2.1801	1.0009	0.7675	
2	2.1781		0.7659	
3	2.1681	0.9991		
7				*
Average (normalized to II)	2.1754	1.0000	0.7667	--
		Calculation		
	2.2259	1.0000	0.7802	0.2767
		Experiment/Calculation		
	0.9772	1.0000	0.9827	--
Co-58 Activity				
		Experiment		
1	2.0051	0.9948	0.7796	
2	2.0296		0.7832	
3	2.0202	1.0052		
7				*
Average (normalized to II)	2.0183	1.0000	0.7814	--
		Calculation		
	1.9890	1.0000	0.7774	0.04775
		Experiment/Calculation		
	1.0147	1.0000	1.0051	--

*No experimental results were obtained for the flux well in module IV-7 since the flux wire "stuck" and did not insert into the reactor.

Table V-16

Summary of Experimental Symmetry Data

Ratios of Total Wire Activations

Activtor	1% Power	68% Power		71% Power		97% Power	
Module/Module	Th	Cu	Ni	Cu	Ni	Cu	Ni
I-2/I-1	0.985	1.003	1.010	--	--	0.999	1.012
I-3/I-1	1.004	--	--	--	--	0.994	1.008
II-3/II-1	0.995	--	--	1.006	0.978	0.998	1.011
III-2/III-1	1.006	1.002	1.008	1.001	1.003	0.998	1.005

e. Axial and Radial Peaking Factors

Calculation of relative wire activations in the LWBR flux well positions was based on few-group fluxes from LWBR design model three-dimensional PDQ08 calculations, coupled with activation cross sections and local flux perturbation factors from specific PAX03 calculations of the flux well geometries. The latter calculations were necessary since the flux wells are not represented in PDQ08. Each flux well replaces a single fuel rod and has different nuclear characteristics resulting from the different materials. The flux wires are in a perturbed environment because of these different characteristics. In addition, the flux wire geometries are such that special calculations are necessary to evaluate shielding effects on resonance cross sections of the flux wire materials.

The calculated activation of a flux wire at a specific height is the sum over four few-groups of the product of the following: the PDQ08 flux at that height, a flux perturbation factor from a Discrete Ordinate transport calculation (PAX03), and a material activation cross section as determined from PAX03 analyses. Calculated activation profiles, along with corresponding measured profiles as discussed previously, are shown in Figures 2 through 49 of Appendix A.

The results of the thorium activations at zero power and copper and nickel activations at full power were used as follows to obtain axial peaking factors. From each of the axial profiles a peak experimental activation and peak calculated activation were obtained. The peak experimental activation is the highest experimental point, unless that point was an anomalous jump in count rate which was clearly experimental error and could not fit on a smooth curve; then the next highest point was used. This happened in only 5 of the 44 experimental profiles examined. The experiment-to-calculation (E/C) ratio of peaks represents an "axial peaking factor" for that profile. A correction was made to account for the slightly different integration range (L_1, L_2) between calculation and experiment.

In cases where more than one pass was counted for a particular wire, the passes were averaged to get a single E/C for the wire. Then the wires were averaged for a given type of module. The results are axial factors for each material activated and for each type of module.

The E/C ratio results are shown in Table V-17. The mean value is shown together with an uncertainty. The mean represents the best estimate of the error in the calculational model. Because of the small number of profiles for a given activator and module type, the uncertainty given is the range of measured values rather than a standard deviation. Thus mean plus the positive uncertainty is the worst case E/C encountered among the profiles.

Table V-17
Experiment/Calculation Axial Factors from Flux Wires

Activator	Module Type	Number of Profiles Examined	E/C
Thorium, 1% Power	I	4	0.986 +0.009 -0.007
	II	6	0.991 +0.003 -0.006
	III	3	0.997 +0.005 -0.003
	IV	1	0.990
Copper, 97% Power	I	8	1.032 +0.012 -0.019
	II	5	1.017 +0.014 -0.020
	III	5	1.010 +0.008 -0.007
Nickel, 97% Power	I	4	0.995 +0.007 -0.009
	II	4	0.994 +0.003 -0.002
	III	4	0.996 +0.005 -0.007

NOTE: The E/C values represent the mean and the range.

The thorium activations at zero power and the copper and nickel activations at full power were also used to obtain radial peaking factors.

The radial results indicate that the module-to-module relative blanket power sharing is predicted within 2.3% (Table V-18), most of which is believed to be experimental error. Finally, the critical bank positions for zero and full power have been well predicted, which implies good seed-blanket power sharing predictions. These results taken collectively lead to the conclusion that the region-to-core factors (1.087 for regular blankets and 1.034 for seeds and power-flattening blankets) used in the as-built analysis of LWBR are adequate and, in the case of the regular blanket, conservative.

Table V-18
Summary of Experiment/Calculation for
Radial Activation Distributions

		E/C by Module Type			
Activator	Power Level	I	II	III	IV
Thorium	1%	0.9970	1.0	0.9997	1.0064
Copper	97%	0.9772	1.0	0.9827	--
Nickel	97%	1.0147	1.0	1.0051	--

f. Discussion of Results

Each wire activator provides a different spectrum averaged reaction. Calculations show that the copper is about 53% thermal in the Type I module, 59% thermal in Types II and III modules, and 78% thermal in the reflector. The thorium is abut 20% thermal and mostly epithermal, and the nickel responds to neutrons above 1 Mev. For comparison, the power in the limiting blanket rod of the Type I module is about 51% from thermal neutrons.

The fact that the experimental axial and radial flux profiles agreed well with calculations for all three activators as discussed in Sections V.B.9.a through e. provides assurance that the calculational model accurately describes the flux levels as a function of energy.

10. Station Startup Test

a. Ascension to Power

The ascension to full power was successfully carried out, meeting the acceptance criteria on 12 seed bank position at each key power level.

Figure V-25 shows the progress of station startup as recorded by the data logger. The figure shows measures of power by four methods: the generator, the nuclear instruments, and two calorimetric computers. The normal converter indication, which is a rough estimate of 12 seed bank position, is also shown.

Figures V-26 and V-27 show the two calorimetric computer outputs (percent) as a function of gross generator output (MW_e). Both computer outputs are normalized such that 97% indicated power corresponds to 236.6 MW_t reactor power. The ratio of the calorimetric power to the generator output is the plant efficiency ratio. It can be seen that the calorimetric power is linearly correlated with gross generator output, at least down to about 10 MW_e where the data have a lot of scatter. Two distinct sets of data are apparent, each one forming a linear relationship. This separation into two sets is due to "blowdowns," the removal of secondary water and replacement with clean water to control steam generator water chemistry.

The effect of a blowdown shows up as a sudden reduction in boiler drum level and a sudden increase in boiler feedwater flow. During a representative blowdown period, the secondary calorimetric indications based on feed flow rose about 3%, the nuclear instrument power rose about 1% and electrical output was essentially unchanged. Thus, the reactor power

increased, but the increase shown by the calorimetric indication conservatively exceeded the actual increase.

Hand calorimetric calculations were done at selected times and the generator output was recorded. No blowdowns occurred at these times. The results are listed in Table V-19, along with a least squares fitted line. The individual data point in Table V-19 farthest from the line is about 6% off at 50.5 MW_e. This line is drawn in Figure V-26 and -27 for comparison with the calorimetric computer data. In Figure V-26, the hand calorimetric line agrees very well with the lower set of calorimetric computer points (the set without blowdowns as expected). Although the data for the least squares fit only go to 35 MW_e, the line is drawn over the full range in Figure V-26 to show the degree of deviation at lower power levels. The line based on hand calorimetrics does not agree with the calorimetric computer 2 data in Figure V-27 as well as with the calorimetric computer 1 data. The plant produced 72 MW_e when the percent power is 93.6% from the hand calorimetric line and from calorimetric computer 1, and 94.5% from calorimetric computer 2. This indicates that overall plant efficiency was higher than had been assumed for LWBR analysis, which predicted 72 MW_e with calorimetric power of 97%.

During the power rise, the unloaded turbine reached its rated speed (1800 rmp) at a lower reactor power than expected, again indicating better than expected efficiency. This reactor power P at low generator loads has been calculated from the change in critical bank position as follows:

Table V-19

Hand Calorimetric Versus Generator Output

Date	Time	Hand Calculated Secondary Calorimetric Power Based on Total Boiler Feedwater Flow (Percent)	Generator Gross Output (MW_e)
9/14	0520	53.2	35.0
9/14	0825	64.66	47.5
9/14	0921	64.83	50.5
9/14	1920	68.82	50.5
9/16	0420	74.17	54.5
9/18	0551	82.92	62.5
9/18	2330	86.76	65.5
9/19	1702	89.90	69.0
9/20	1422	90.7	70.0
9/20	1600	93.3	71.0
9/20	1720	93.54	71.0
9/20	1800	93.44	71.0
9/21	0030	93.78	72.5
9/21	0256	93.2	72.5

Least Squares Line: Percent Power = (1.1514) (MW_e) + 10.6823

Correlation Coefficient = 0.9945

$$P = 0.97\,[h_p - h_o]\ \frac{(\Delta\rho)}{\Delta h}\ /\ (\Delta\rho/\Delta P)\ .$$

where

h_p is the bank position at power P (inches)

h_o is the bank position at zero power (inches)

$\frac{\Delta\rho}{\Delta h}$ is the bank worth ($10^{-4}\Delta\rho$/inch)

$\frac{\Delta\rho}{\Delta P}$ is the power coefficient ($10^{-4}\Delta\rho$/% power)

The bank worth $\Delta\rho/\Delta h$ and the power coefficient $\Delta\rho/\Delta P$ are taken from experimental data to be discussed later. The critical bank positions h_p and the resulting reactor powers are given in Table V-20.

Table V-20

Gross Generator Output (MW_e)	h_p (Inches)	T_{avg} (°F)	$h_p - h_o$ (Inches)	$\Delta\rho/\Delta h$ (10^{-4}/inch)	$\Delta\rho$(531°F) (10^{-4})	P(%)
0	32.85	531.43	0.20	51.42	9.54	4.2
5	33.28	532.0	0.63	51.19	30.52	13.3
10	33.58	531.4	0.93	51.02	46.76	20.3

The value of $\Delta\rho/\Delta P$ is 2.23×10^{-4}/%, and the 0.97 factor is to normalize the power to the calorimetric indication. The resulting power values are plotted as x marks in Figure V-26. It is seen how the calorimetric indication approaches the linear range between 10 and 15 MW_e.

The 12 seed bank position during the power ascension is plotted in Figure V-28. The fuel assembly synchronous position indicator (FASPI) for module II-2 was used for bank position. The measured positions as a function of time are shown as x marks. The rise in critical bank position is due both to power increases and to the increase in poison (xenon) content. For example, considering only the measured points, the bank position rise on September 14 from 01:45 to 07:30 is primarily due to power increases;

the bank position rise from 07:30 on September 14 to 04:00 on September 15 (28 hours) is primarily due to poison buildup.

Compensated ion chamber (CIC) currents were recorded during the power ascension, and are shown in Table V-21. They are plotted in Figures V-29 and lines are drawn as eye guides. Each channel shows a linear relationship, with the data at 63.7% power being farthest from linearity. The CIC currents for the four channels satisfied the acceptance criteria of (1) being sufficiently close to each other and (2) each individual current being between 30 and 318 microamperes (μa) at 100% power.

At the low power end of the power range instruments, with maximum gain, power range indication (about 1% power) was recorded with intermediate range currents between 0.8 and 2.5 x 10^{-7} amperes, confirming ample overlap between intermediate and power range nuclear instruments.

Table V-21

Compensated Ion Chamber Currents Versus Power Level

Calorimetric	Compensated Ion Chamber Current (Microamperes)			
Power (%)*	Channel A	Channel B	Channel C	Channel D
22.6	21.46	24.96	17.98	29.12
54.6	43.50	50.30	36.40	58.70
63.7	47.16	59.00	40.17	67.67
74.2	61.60	70.75	51.46	83.13
87.0	71.11	81.60	59.33	95.32
98.8	78.20	89.70	65.40	104.70

*97% means 236.6 MW_t reactor power. The data are hand calorimetric calculations except at 87% power where the calorimetric computer was used.

b. Bank Height Versus Power Calculations

Figure V-28 shows the calculated curve of 12 seed bank positions versus time during the ascension to power. The curve was started with the calculated hot, zero power critical position, corrected by a small amount of poison (3% of equilibrium protactinium) remaining from the previous power run. From this starting point, a power versus time history was constructed which approximated the measured power history. The approximate power history was used to obtain the calculated curve, and is written along the curve in Figure V-28. The power percentage numbers in Figure V-28 are normalized such that 100% corresponds to 236.6 MW_t reactor power.

From the starting point, the curve in Figure V-28 was built up from three components: power reactivity (the positive reactivity addition associated with a reduction in power from 100% to 0%), xenon, and other poisons. The following paragraphs examine each component.

(1) Power Reactivity - The power reactivity information was obtained from a curve of reactivity versus power level based on three-dimensional PDQ calculations run at 0%, 25%, 75%, and 100% power (Figure V-30). The calculated power reactivity addition from 100% to 0% power is 190 x 10^{-4} $\Delta\rho$ for xenon-free core conditions. From the curve given in Figure V-30, the reactivity change for each power change was obtained, and then the bank position change was computed from the reactivity change and the worth per inch of the 12 seed bank.

The reactivity worth of the 12 seed bank used to construct the calculated curve (Figure V-28) was calculated from PDQ. The worth varied from about 47 x 10^{-4} $\Delta\rho$/inch at the low power positions at the start of the test to 39 x 10^{-4} $\Delta\rho$/inch near 100% power.

(2) Xenon Content - To get the xenon content of the core during the startup, a computer code XENON was used to solve the iodine-xenon equations for a prescribed power history. This code provides the xenon concentration relative to equilibrium xenon, for which the reactivity worth has been obtained from PDQ calculations as 178 x 10^{-4} $\Delta\rho$.

(3) Other Poisons - The effect of other "poisons" includes protactinium, samarium, other fission products, and fuel burnup. This combination was treated as a single term worth 28 x 10^{-4} $\Delta\rho$ at 100 EFPH, and is well approximated as being linear with burnup (power x time).

As a check on the construction of the position versus time curve shown in Figure V-28, the equilibrium xenon position was compared to the 100 EFPH calculation from the as-built core depletion analysis. The depletion analysis predicts a critical position at full power of 41.70 inches for 100 EFPH. At the end of September 21 (192 hours in Figure V-28), there were 196.5 EFPH on the core. Correcting the PDQ position for the additional poison at this later time results in a 42.39-inch prediction at 196.5 EFPH, compared to 42.40 inches from Figure V-28. Thus, the PDQ result from the as-built depletion agrees with the time-dependent curve constructed from the zero power, clean position.

c. Power Range Nuclear Instrument Response Calculations

Monte Carlo (RCP) calculations were used to predict absolute detector response. The calculations were then corrected to reflect the actual as-built polyethylene thickness for each detector. (Earlier studies indicated that with Boral present the detector current would be approximately linear with polyethylene thickness. With no Boral present, the detector current is insensitive to polyethylene thickness). Taking the installed polyethylene thicknesses and presence or absence of Boral into account, Table V-22 lists the corrected values for predicted detector current and compares them with measured detector currents at 100% reactor power (236.6 MW_t). See Section II.C for a discussion of the power range detectors and arrangement of polyethylene sleeves and Boral strips.

The predicted values for detectors B and D show a range for the nominal value, as well as a confidence interval from the Monte Carlo statistics. The range for these cases without Boral accounts for the range of uncertainty in sensitivity of transmission to the polyethylene thickness. To estimate the error for detectors B and D, the midpoint (95 μa) is used as the predicted value. The error is stated as the difference between predicted and measured, in units of standard deviations.

Table V-22

Predicted and Measured Detector Current at 100% Reactor Power

Detector	Installed Polyethylene Thickness (Inches)	Predicted Detector Current (μa)*	Measured Detector Current(μa)	Error (In Units of Standard Deviation)
A	22/32	76 ± 27	76.8	-0.06
B	26/32	90 to 100 ± 48	88.1	+0.3
C	22/32	76 ± 26	64.2	+0.9
D	26/32	90 to 100 ± 48	102.8	-0.3

*95% confidence interval from Monte Carlo calculation; values corrected for polyethylene thickness and presence or absence of Boral (see Section V.B.10.c).

d. Discussion of Station Startup Test Results

The measured critical bank position at full power, equilibrium xenon at the end of the station startup test was 0.41 inch lower than the nominal calculated position. This indicates that the core at full power is 0.18% $\Delta\rho$ more reactive than predicted (based on measured bank worths). The calculated change in bank position from hot, zero power conditions to full power, equilibrium xenon is greater than the measured change by 0.59 inch (1.06 times the measured value). Given the calculated bank worth (about 0.88 of the measured value), the calculated poison plus power reactivity is determined to be less than measurement by 0.27% $\Delta\rho$ (the calculation is 0.93 of the measured total reactivity change).

The Shippingport Plant was found to be more efficient than had been predicted. At beginning of LWBR core life, it produced between 76 and 78 MW_e gross generator output at 100% indicated core power (243.9 MW_t) rather than the predicted 74.2 MW_e gross. In addition, the unloaded turbine reached its rated speed at approximately 4% of core power, half of that which was expected to be required. The higher plant efficiency appears to be due to the clean conditions of the A and D steam generators and improved feedwater temperature and vacuum conditions.

Finally, power range detector response (measured detector current) was found to be in excellent agreement with RCP Monte Carlo calculational results. The measured currents at full power were within one standard deviation of the RCP (Monte Carlo) calculations.

11. Temperature and Power Coefficients of Reactivity at Power; Bank Worth at Power

This test was initially performed at approximately 200 EFPH, immediately following the high power flux wire irradiation which took place at the end of the station startup test. The power coefficient was measured first, followed by the temperature coefficient and finally the bank worth.

a. Data and Measured Values for Temperature and Power Coefficients

Measured data for the power coefficient and temperature coefficient are presented in Table V-23. Data were taken shortly after the first power reduction, after a 15-minute wait, and after a 30-minute wait; only data from the last of these three sets of measurements is listed in Table V-23. Similarly, only the last set of measurements taken after the second power reduction is listed in Table V-23. Hence, all of the tabulated data record plant parameters during steady-state conditions.

Table V-24 shows the changes in the parameters that occurred between each set of runs listed in Table V-23. Each row in Table V-24 is used to infer the coefficient value shown in a box. When determining the power coefficients, the bank height change (Δh) was corrected for temperature changes by using the predicted best estimate value of the temperature coefficient from the test procedure. Similarly, when determining the temperature coefficient, Δh was corrected for power changes by using the previously determined value of power coefficient. Finally, the power coefficient calculations were repeated using the same measured values but employing the previously calculated temperature coefficient to correct for temperature variations. In all calculations, the bank height has been corrected for pressure changes using the measured pressure coefficient of $2.1 \times 10^{-6} \Delta\rho$/psig and an estimated bank worth of $46 \times 10^{-4} \Delta\rho$/inch.

The value (based on measurements) of the power coefficient is 33.3% (ΔP)/inch for both runs; the value (based on measurements) of the temperature coefficient is 22.3°F/inch based on the differences between Runs 8 and 9. The value between Runs 7 and 8 is about 2% smaller, but this is based on a temperature change which is only half as large as that from Runs 8 and 9, producing a less accurate result.

Table V-23

Measured Data for Power and Temperature Coefficients at Power

Run #	Measurement	Power Level in % Calorimetric (Ch2)	Power Level in % NIS**(Avg)	T_{avg} °F	Pressure psig	Bank Height*, in (inches)
1	Initial Condition	96.5	97.0	531.0	1970	41.98
4	1st Power Reduction	90.0	90.5	531.1	1990	41.78
7	2nd Power Reduction	84.6	84.9	531.0	1986	41.615
8	T_{avg} Reduction	84.5	83.3	528.75	1997	41.51
9	T_{avg} Increase	84.5	84.5	534.0	1988	41.75

*Fuel assembly synchronous position indicator (FASPI) III-2 used for bank positions

**Nuclear Instrument System

Table V-24

Data Reduction for Power and Temperature Coefficients at Power

Differences Between Runs	ΔP(%) Calorimetric (Ch 2)	ΔT_{avg} (°F)	Δp (psig)	Δh (measured) (inches)	Δh (corrected) (inches)	$\frac{\Delta P}{\Delta h}$	$\frac{\Delta T_{avg}}{\Delta h}$
1 and 4	+6.5	-0.1	-20	+0.20	+0.1947	33.38	26.6[a]
4 and 7	+5.4	+0.1	+ 4	+0.165	+0.1630	33.13	26.6[a]
7 and 8	+0.1	+2.25	-11	+0.105	+0.1030	33.25[b]	21.84
8 and 9	0.0	-5.25	+ 9	-0.24	-0.2359	33.25[b]	22.26
1 and 4 (repeat)	+6.5	-0.1	-20	+0.20	+0.1953	33.28	22.26[c]
4 and 7 (repeat)	+5.4	+0.1	+ 4	+0.165	+0.1624	33.25	22.26[c]

[ ] Indicates value based on measurements

a = Value of $\Delta T_{avg}/\Delta h$ from expected results (best estimate)

b = Value of $\Delta P/\Delta h$ from average of two previous measurements

c = Value of $\Delta T_{avg}/\Delta h$ from previous measurement (runs 8 and 9)

b. Data for Bank Worth

During the transient the 12 seed bank was lifted 0.10 inch (from 41.51 to 41.61 inches as measured on the fuel assembly seed position indicator for seed III-2). This was based on the desire to limit the power increase magnitude to about 3.5% power. Measured data for the bank worth portion of the test are shown on Figures V-31 and V-32.

(1) Power and T_{avg}

Figure V-31 shows the nuclear instrument indicated power and core T_{avg} as a function of time during the first transient. Both of these data have been derived from the data logger which was set to record inferred data about every second. The actual interval between data points is 0.87 second, inferred from the elapsed time of 100 points. The fine divisions on the base axis of Figure V-31 represent the interval between data points.

The nuclear instrument plot shows that the power rises while the bank is being lifted, the peak is attained when the bank is held at the elevated position, and the power then falls to an almost constant steady-state value until the bank is lowered to end the transient, at which time the power falls rapidly. Note that the power falls below its initial value because the bank is lowered below the initial value. The terminal position desired for this transient is the initial value, but during physics tests all bank motions are terminated by a lift of at least 0.060 inch to eliminate any hysteresis effects. After final lift of the bank, the power returns to its initial value and is ready for the repeat measurement.

The T_{avg} plot shows a reasonably smooth increase of 0.41°F after an initial delay of approximately 18 seconds; part of the delay is the time required to initiate the transient by lifting the bank, but the major portion is the time required to transport the coolant through the primary plant. At the end of the transient, the coolant in transport continues to raise the T_{avg} indication until the bank reaches its minimum position.

(2) Reactivity - Figure V-32 is a copy of the strip chart showing the net reactivity versus time as measured by the IKS (inverse kinetics simulator). The ordinate is the time scale, increasing from bottom to top with one division representing 10 seconds. The base is the reactivity scale with 0, 50, 100 scale divisions nominally representing - 10 x 10^{-4}, 0, and + 10 x 10^{-4} $\Delta\rho$ respectively. From bottom to top is shown the first positive reactivity insertion caused by lifting the bank, the lowering of the bank through the initial position, and the immediate return to the initial position. Then follows a period of time at a slower chart speed with the IKS turned off (in STANDBY); this interval is characterized by a perfectly straight line at the 50 unit position. This is followed by a period of approximately 35 seconds with the IKS turned on (in OPERATE) at the 49+ unit position prior to the repeat measurement.

The second transient is very similar to the first except that the bank was held fixed at the elevated position for approximately 50 seconds following the first transient and for approximately 30 seconds following the second. Hence, only the first will be analyzed. The zero reactivity position appears to be slightly biased below 50 units (approximately 49.3 units) because the reactivity during the 15-second period prior to the initiation of the transient is constant. In addition, during this period the nuclear instrument indicated power and T_{avg} were also constant as shown on Figure V-31. The peak reactivity observed during the initial transient was 0.76 x 10^{-4} $\Delta\rho$. The inferred zero reactivity value and the peak reactivity value were used in replotting the measured data to compare with calculations.

c. Calculated Values for Power Coefficient, Temperature Coefficient, and Bank Worth

The calculated values are based on one-sixth core PDQ calculations of the as-built core.

(1) Power and Temperature Coefficients - The power coefficient was determined by computing the reactivity difference between two

PDQ calculations, one at 100% power and one at 75% power, and dividing by the power difference to obtain $-1.30 \times 10^{-4} \Delta\rho/\%$ power. This includes a slight correction for variations in the moderator temperature in the core due to power level changes.

The Doppler portion of the calculated temperature coefficient for the high power range is $-0.617 \times 10^{-4} \Delta\rho/°F$, and the water density portion is $-1.56 \times 10^{-4} \Delta\rho/°F$ for transients slow enough to allow the metal-water channels to be heated. The calculated combined temperature coefficient is thus $-2.177 \times 10^{-4} \Delta\rho/°F$.

The calculated bank worth at 100 EFPH between 38.9 inches and 42.4 inches was $39.5 \times 10^{-4} \Delta\rho$/inch. The bank heights during this test were between 41.5 and 42.0 inches. For purposes of calculating the power and temperature coefficients, a bank height change (Δh) is used to generate a reactivity change ($\Delta\rho$) that is just sufficient to counteract the $\Delta\rho$ change produced as a result of a power change (ΔP), a temperature change (ΔT_{avg}), or a pressure change (Δp). In equation form this relationship is expressed as

$$\Delta\rho = 0 = \left(\frac{\partial\rho}{\partial h}\right) \Delta h + \left(\frac{\partial\rho}{\partial P}\right) \Delta P + \left(\frac{\partial\rho}{\partial T_{avg}}\right) \Delta T_{avg} + \left(\frac{\partial\rho}{\partial p}\right) \Delta p \quad .$$

Hence, the power coefficient can be expressed as

$$\frac{\Delta P}{\Delta h} = - \frac{(\partial\rho/\partial h)}{(\partial\rho/\partial P)} \quad \text{for constant } T_{avg} \text{ and constant pressure,}$$

and the temperature coefficient can be expressed as

$$\frac{\Delta T_{avg}}{\Delta h} = - \frac{(\partial\rho/\partial h)}{(\partial\rho/\partial T_{avg})} \quad \text{for constant power and constant pressure.}$$

For the above parameters

$$\frac{\Delta P}{\Delta h} = \frac{39.5 \times 10^{-4} \Delta\rho/\text{inch}}{1.30 \times 10^{-4} \Delta\rho/\%} = 30.4\%/\text{inch}$$

and $$\frac{\Delta T_{avg}}{\Delta h} = \frac{39.5 \times 10^{-4} \Delta\rho/\text{inch}}{2.177 \times 10^{-4} \Delta\rho/°F} = 18.1°F/\text{inch}$$

(2) 12 Seed Bank Worth - For the bank worth portion of the test, the transient was approximated by performing a transient plant analysis in which calculated Doppler and density coefficients were used to calculate the reactivity feedback. The initial power level was set at 83.7% of full power and the bank was withdrawn 0.1 inch, i.e., for 6 seconds at a rate of 1 inch per minute. The bank then remained at this elevation until the measured transient was complete. The bank worth was considered a parameter and calculations were performed for worths of 40, 46 and 52 x $10^{-4} \Delta\rho$/inch. The density coefficient is 25.4 x 10^{-4} x $\Delta\rho$/lb-ft^3, which is equivalent to -1.509 x $10^{-4} \Delta\rho/°F$ or essentially the same as the calculated value. The Doppler coefficient is -37.4 x $10^{-4} \Delta\rho/\sqrt{°R}$.

The calculated transients are displayed on Figure V-33 for the three choices of bank worth. Also shown are the measured results for the first measured transients that were previously presented on Figures V-31 and V-32. The three choices of bank worth produce satisfactory representation of the reactivity based on the results of Figure V-32. A bank worth of 46 x $10^{-4} \Delta\rho$/inch appears to give the best fit to the power transient.

As noted previously, the calculated bank worth at 100 EFPH between 38.9 and 42.4 inches was 39.5 x $10^{-4} \Delta\rho$/inch. The bank worth inferred from the above analysis of the transient represents the measured bank worth for this test.

The calculated values of bank worth, power coefficient, and temperature coefficient and the ratios of the coefficients are presented in Table V-25.

Table V-25

Calculated Values for Bank Worth and Temperature and Power Coefficients of Reactivity

Parameter	Units	Calculated Value	Measured Value
$\frac{\Delta P}{\Delta h}$	$\frac{\% \text{ Power}}{\text{inch}}$	30.4	33.3
$\frac{\Delta T_{avg}}{\Delta h}$	$\frac{°F}{\text{inch}}$	18.1	22.3
Bank Worth	$\Delta\rho$/inch	39.5×10^{-4}	46.0×10^{-4}
Power Coefficient	$\Delta\rho$/% Power	-1.30×10^{-4}	-1.38×10^{-4}
Temperature Coefficient	$\Delta\rho$/°F	-2.177×10^{-4}	-2.063×10^{-4}

d. Discussion

The measured coefficient is about 6% more negative than the calculated value, and the measured temperature coefficient is about 6% less negative than the calculated value. The bank worth as measured is significantly larger (approximtely 14%) than the calculated value. This result is very similar to that of the hot clean bank worth, which was measured to be 12% larger than calculated.

The hot core measured bank worth is within the band of 12 seed bank worths used for specifying fuel module speeds in the Safety Analysis Report. The difference between the measured and calculated hot power

coefficients is within the ±25 percent uncertainty assumed in the Safety Analysis Report. Similarly, the difference in the hot temperature coefficients at power is well within the ±25 percent uncertainty allowed for the moderator portion and the ±25 percent uncertainty allowed for the Doppler portion.

12. Xenon Reactivity

Table V-26 presents a tabulation of time, power level, and 12 seed bank height data during the shutdown from 97% power. Table V-27 presents a tabulation of temperature-and pressure-corrected (T = 528.5°F and P = 1980 psig) bank worth and critical position.

a. Measured Values

Figure V-34 presents a plot of bank height versus time during the xenon reactivity transient. Figure V-35 presents a plot of bank worth versus critical height during the transient with the line representing a least squares fit to the data.

The time to peak xenon, using 0408 as the time when the reactor neared zero power as indicated by the average linear level power meter, was 3 hours and 52 minutes (3.87 hours). The reactivity worth of peak xenon from equilibrium xenon, using an average measured bank worth of 45.69×10^{-4} $\Delta\rho$/inch and bank height increase of 0.54 inches (correcting the final shutdown bank position for temperature and pressure), is $24.7 \times 10^{-4} \Delta\rho$.

The power reactivity (the reactivity addition associated with a reduction in power from 100% to 0%) can be inferred using the data collected during the shutdown. The bank height at 97% power was 41.99 inches and the bank height at 0% power was 38.33 inches. Using a value of bank worth of $44.7 \times 10^{-4} \Delta\rho$/inch (obtained from Figure V-35) gives a power reactivity of 164×10^{-4} $\Delta\rho$ or 1.64% $\Delta\rho$.

The worth of equilibrium xenon can be inferred using the bank height at the time of shutdown for the xenon transient and the bank height for the startup which occurred at approximately 1600 on 9/28/77, following a 3.5-day shutdown. The poison conditions for each of these bank heights are summarized below.

12 Seed

Bank Height	Time	Day	Poison (Fraction of Equilibrium Concentration)	
38.33 inches	0413	9/23/77	Xe-135	1.000
			Sm-149	0.219
			Pa-233	0.200
34.49 inches	1000	9/28/77	Xe-135	0.015
			Sm-149	0.324
			Pa-233	0.194

In the above table, the xenon fraction was estimated using the XENON computer code; the samarium fraction was estimated using the XENON code with appropriate constants changed to represent samarium; and the protactinium fraction was estimated by hand calculations of buildup during power operation and decay during shutdown periods.

Using a value of $46.6 \times 10^{-4}\ \Delta\rho$/inch for bank worth between 34.49 inches and 38.33 inches (extrapolated from Figure V-35) gives a reactivity change of $1.79\%\ \Delta\rho$. Correcting this value for the changes in poison concentrations listed above gives a worth of equilibrium xenon of $1.88\%\ \Delta\rho$.

Due to the extended time required to shut down from full power to zero power, (70 minutes) a correction must be applied to the zero power, equilibrium xenon data. In reality, this position is not an equilibrium position because some xenon has been built in above equilibrium during the time expended while reducing power. The reactivity due to the xenon above the equilibrium value has been estimated using the computer code XENON. The calculations indicate that the xenon fraction of equilibrium is

1.025 at the end of the shutdown. Therefore, a reactivity correction of approximately 5 x 10^{-4} $\Delta\rho$ (0.025 x 190 x 10^{-4} $\Delta\rho$) should be applied to the power reactivity, worth of equilibrium xenon, and worth of peak xenon above equilibrium. The measured results tabulated in Table V-28 include this correction.

Table V-26
Shutdown Data

Time	Power Level Nuclear Instrument System Average (%)	12 Seed Bank Height (from Fuel Assembly Synchronous Position Indicator for Seed III-2) (inches)
0308	97	41.99
0313	93	41.85
0318	90.5	41.76
0323	84.1	41.51
0328	70.7	41.14
0333	63.5	40.87
0338	37	39.93
0343	35	39.85
0348	34	39.79
0353	24	39.42
0358	18	39.16
0403	11	38.33
0408	4	38.33
0413	2	38.33
0418	2 (1 x 10^{-9} amperes)	38.33

Table V-27
Xenon Reactivity Transient Results

12 Seed Bank Critical Height (inches)	12 Seed Bank Worth (10^{-4} $\Delta\rho$/in)
38.72	47.10
38.75	45.94
38.77	43.92
38.80	44.83
38.81	45.38
38.82	46.86
38.83	45.32
38.84	46.04
38.84	44.97
38.83	46.50
38.82	44.31
38.81	45.32
38.78	46.61
38.76	46.17
38.73	46.10
38.68	45.50
38.63	45.87
38.58	45.24
38.53	46.60
38.47	45.49
38.41	45.04
38.36	45.59
38.16	47.38
38.08	46.08
37.92	46.03
37.79	46.44
37.65	46.59
37.48	45.57
37.34	46.68
37.20	44.71
37.06	47.11
36.92	46.15

b. Calculated Values

Xenon reactivity worths were calculated using the explicit three-dimensional symmetric sixth-core PDQ as-built model. Calculations were performed at the following times.

	12 Seed Bank Height (in.)	λ(eigenvalue)
1. Full Power, 100 EFPH	38.9	0.9909
2. Zero Power, 100 EFPH	38.9	1.00923
3. Zero Power, 3.5 hours after calculation 2	38.9	1.00711
4. Zero Power 20 hours after calculation 2	38.9	1.01469

A value for the equilibrium to peak xenon worth can be calculated by comparing the eigenvalues (K_{eff} values) of calculations 2 and 3 and converting to reactivity. From Table V-28, the calculated equilibrium to peak xenon worth at 3.5 hours from shutdown is $18 \times 10^{-4} \Delta\rho$.

A value for power reactivity can be calculated by comparing calculations 1 and 2. The power reactivity is calculated to be 1.83% $\Delta\rho$. In addition, the worth from equilibrium xenon to 20 hours following shutdown, calculations 2 and 4, was $-56.0 \times 10^{-4} \Delta\rho$.

The worth of equilibrium xenon was determined using the PDQ as-built model calculations at 0 EFPH and 100 EFPH. Equilibrium xenon near beginning-of-life is worth 1.78% $\Delta\rho$. The bank worth calculated from PDQ, beginning-of-life Xenon Free Conditions is $42.0 \times 10^{-4} \Delta\rho$/inch at 37.13 inches. Calculated values are presented in Table V-28.

Table V-28
Measured Versus Calculated Reactivity Values During Xenon Transient

Parameter	Calculation	Measurement
Peak Xenon (from Equilibrium)	$18 \times 10^{-4} \Delta\rho$ at 3.5 hours	$30 \times 10^{-4} \Delta\rho$ at 3.87 hours
Xenon level 20 hours after shutdown (from Equilibrium)	$-56 \times 10^{-4} \Delta\rho$	$-62 \times 10^{-4} \Delta\rho$
Worth of Equilibrium Xenon	1.78% $\Delta\rho$	1.83% $\Delta\rho$
Worth of Peak Xenon	1.96% $\Delta\rho$	2.13% $\Delta\rho$
Worth of Xenon 20 hours after shutdown	1.22% $\Delta\rho$	1.21% $\Delta\rho$
Power Reactivity (100% to 0%)	1.83% $\Delta\rho$	1.69% $\Delta\rho$
12 Seed Bank Worth at 37.13 inches	42.0×10^{-4} $\Delta\rho$/inch	$46.30 \times 10^{-4} \Delta\rho$/inch

c. Discussion

The measured worths of equilibrium and peak xenon are higher than the calculated worths by approximately 1.03 and 1.09 times, respectively. The measured value of the power reactivity is approximately 0.92 of the calculated value. The total negative reactivity worth from zero power xenon free to full power equilibrium xenon due to power reactivity and xenon worth was measured as 3.52% $\Delta\rho$. Therefore, the total measured reactivity worth of power reactivity and equilibrium xenon worth is smaller than the calculated values by $9 \times 10^{-4} \Delta\rho$.

The measured 12 seed bank worth is approximately 1.102 times the calculated worth. This result is in good agreement with the measurement performed at hot, zero power, xenon free conditions which indicated the measured bank worth is approximately 1.12 times the calculated value.

An estimate of the worth of accumulated poisons can be made by comparing the measured change in bank height from the hot, zero power critical position measured immediately following the shutdown from full power to the critical position on 9/28/77. The change in bank height is 34.49 - 32.65 or 1.84 inches. Using an estimated bank worth of $50.2 \times 10^{-4} \Delta\rho$/inch at 33.57 inches, the reactivity difference is 92.4×10^{-4}; this difference is due to the buildup of poisons during operation for approximately 225 EFPH. The worth of the poisons, including other fission products, is calculated to be $73 \times 10^{-4} \Delta\rho$. Therefore, the measured worth of the accumulated poison in this case is about 1.27 times the calculated worth.

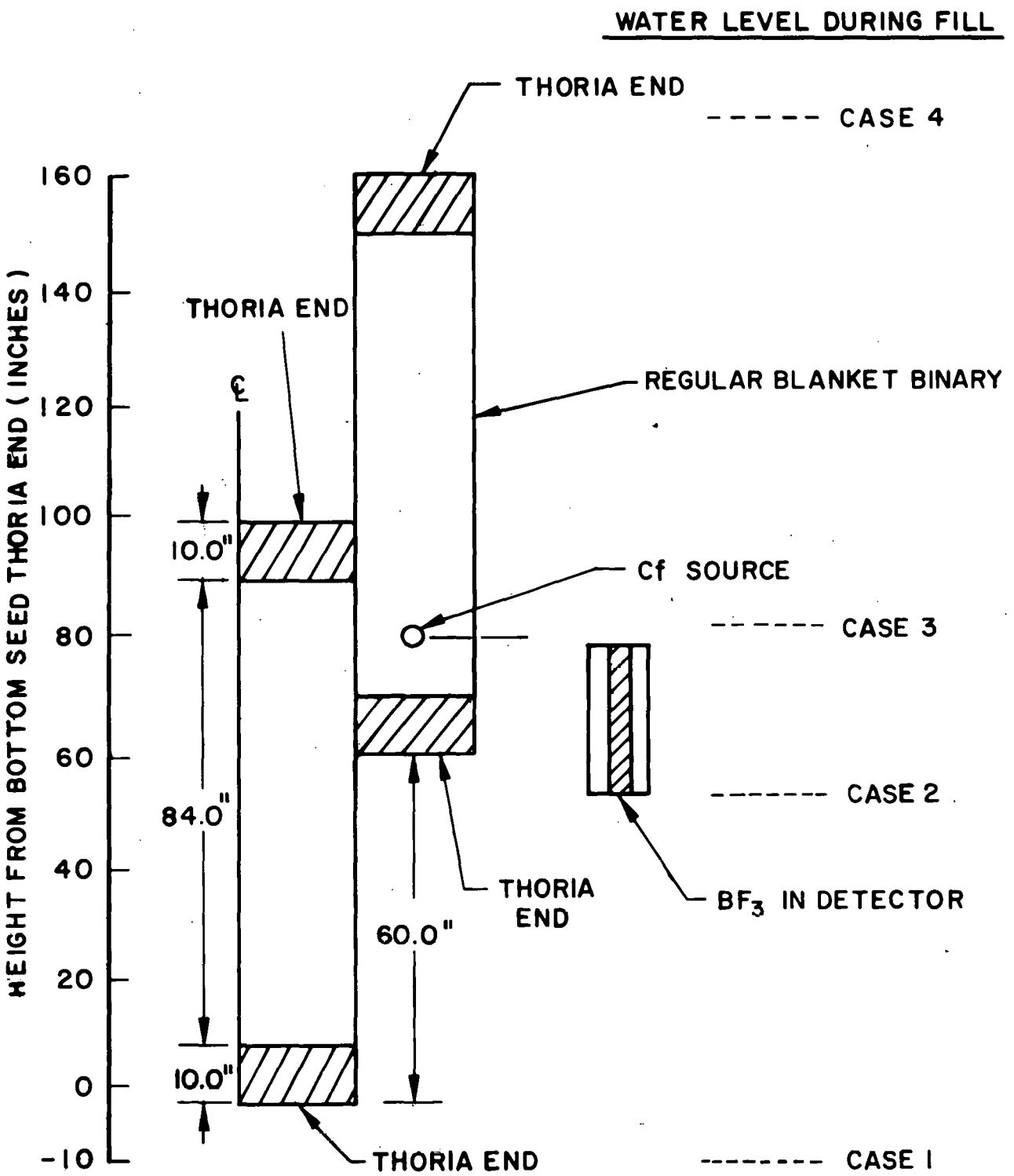

FIGURE V-1 - AXIAL POSITION OF SOURCE AND DETECTOR RELATIVE TO SEED AND REGULAR BLANKET DURING INITIAL FILL

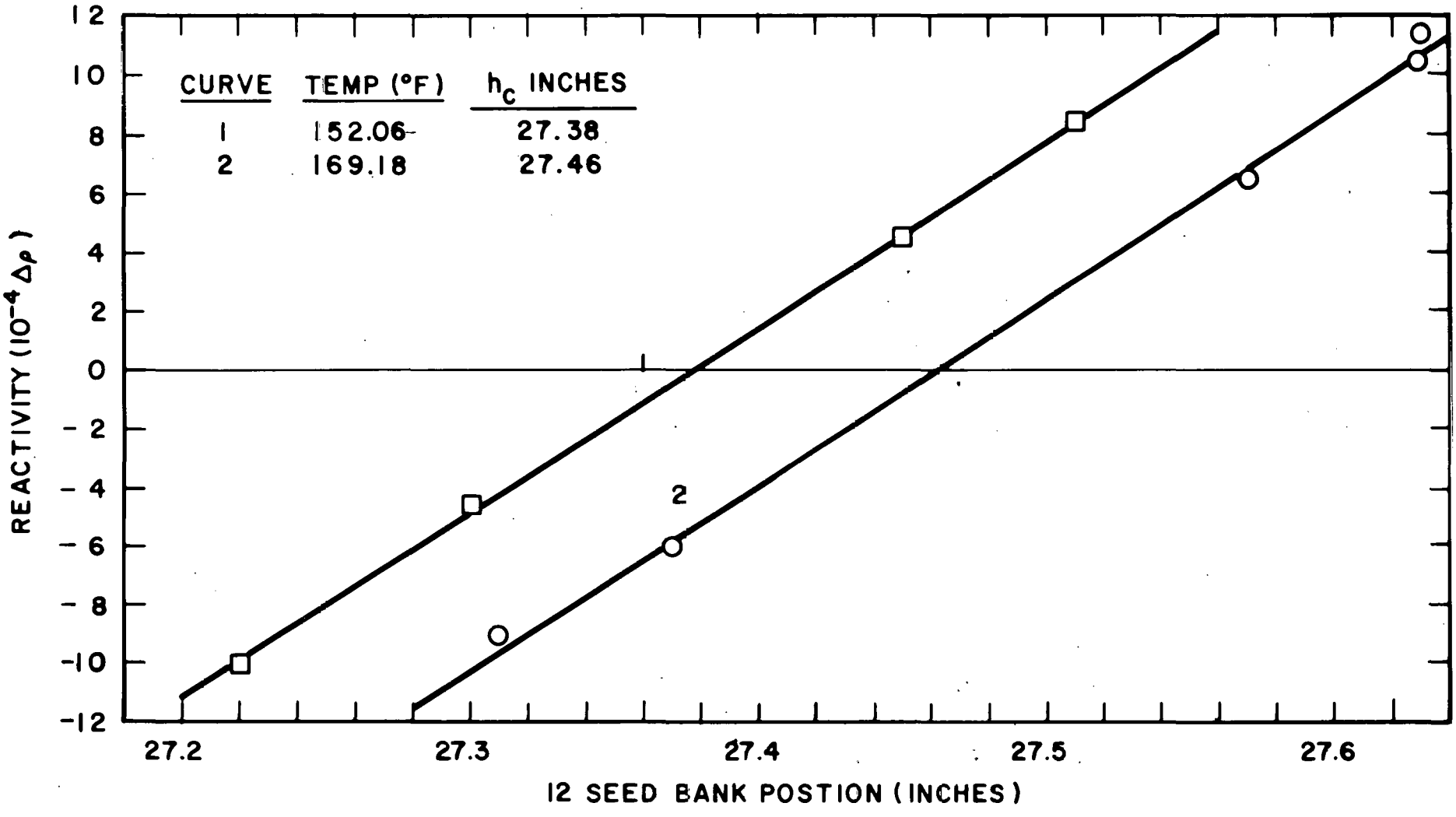

FIGURE V-2 - REACTIVITY VERSUS 12 SEED POSITION, COLD CORE

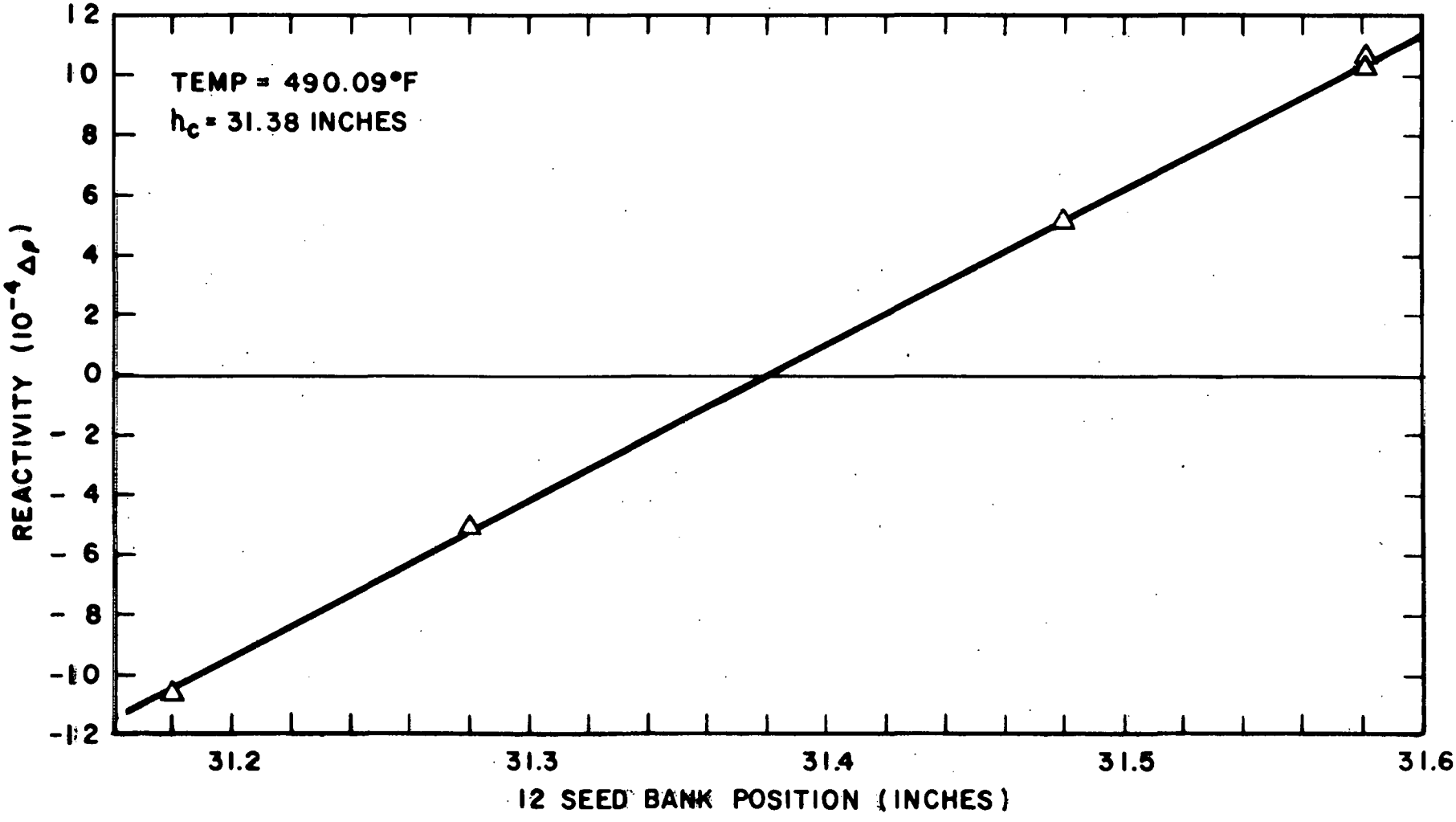

FIGURE V-3 - REACTIVITY VERSUS 12 SEED BANK POSITION, HOT ZERO POWER

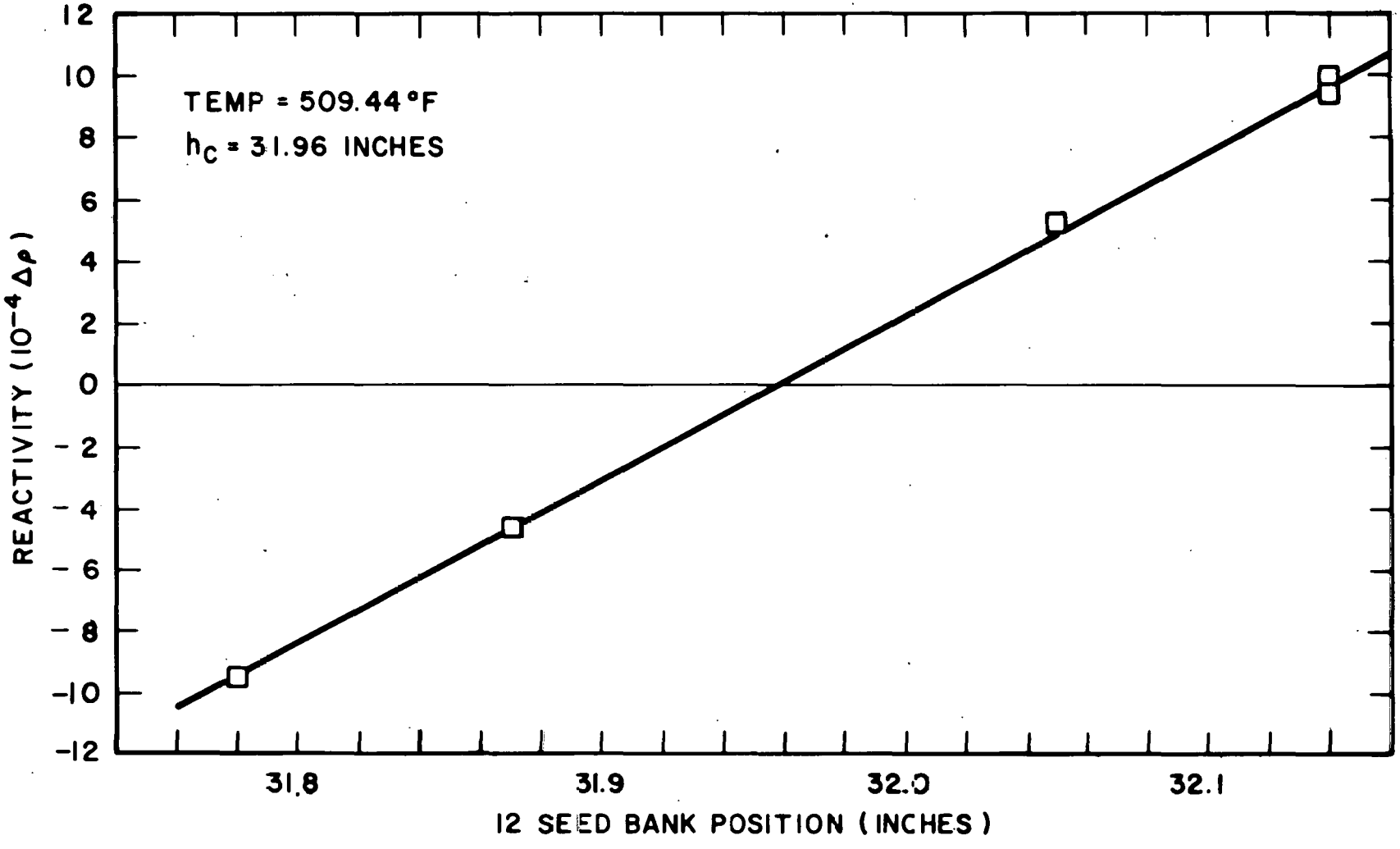

FIGURE V-4 - REACTIVITY VERSUS 12 SEED BANK POSITION, HOT ZERO POWER

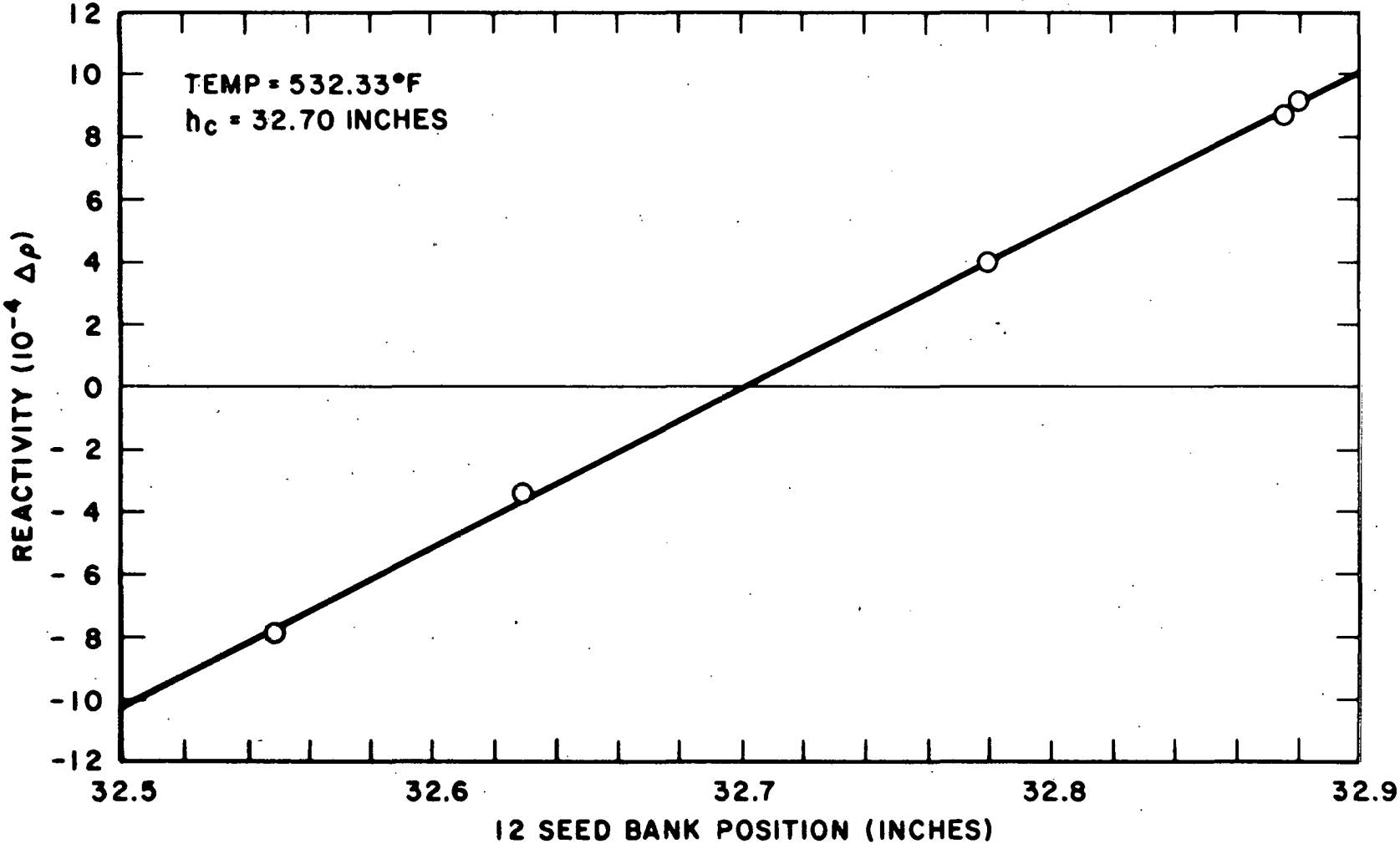

FIGURE V-5 - REACTIVITY VERSUS 12 SEED BANK POSITION, HOT ZERO POWER

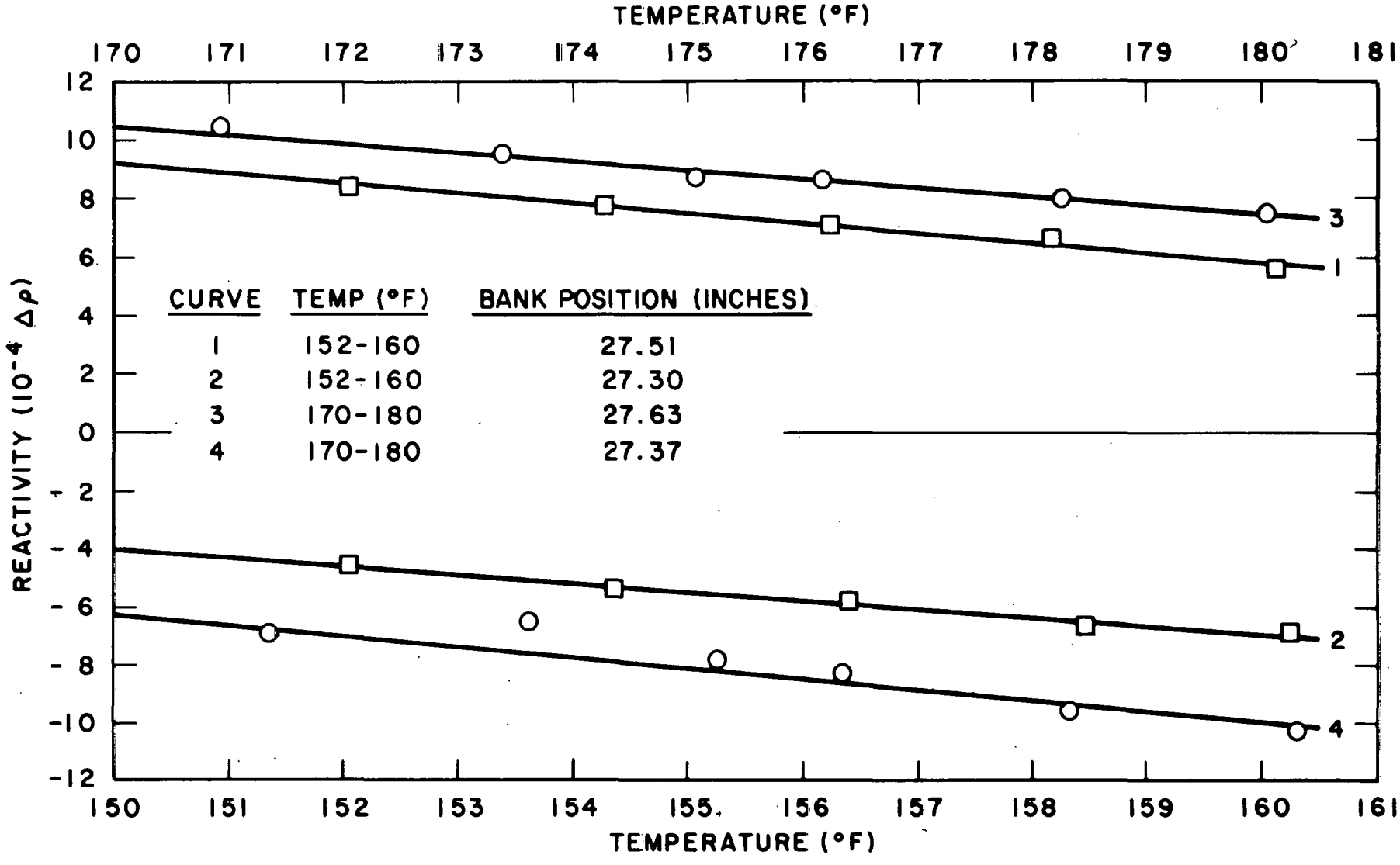

FIGURE V-6 - REACTIVITY VERSUS CORE TEMPERATURE, COLD CORE

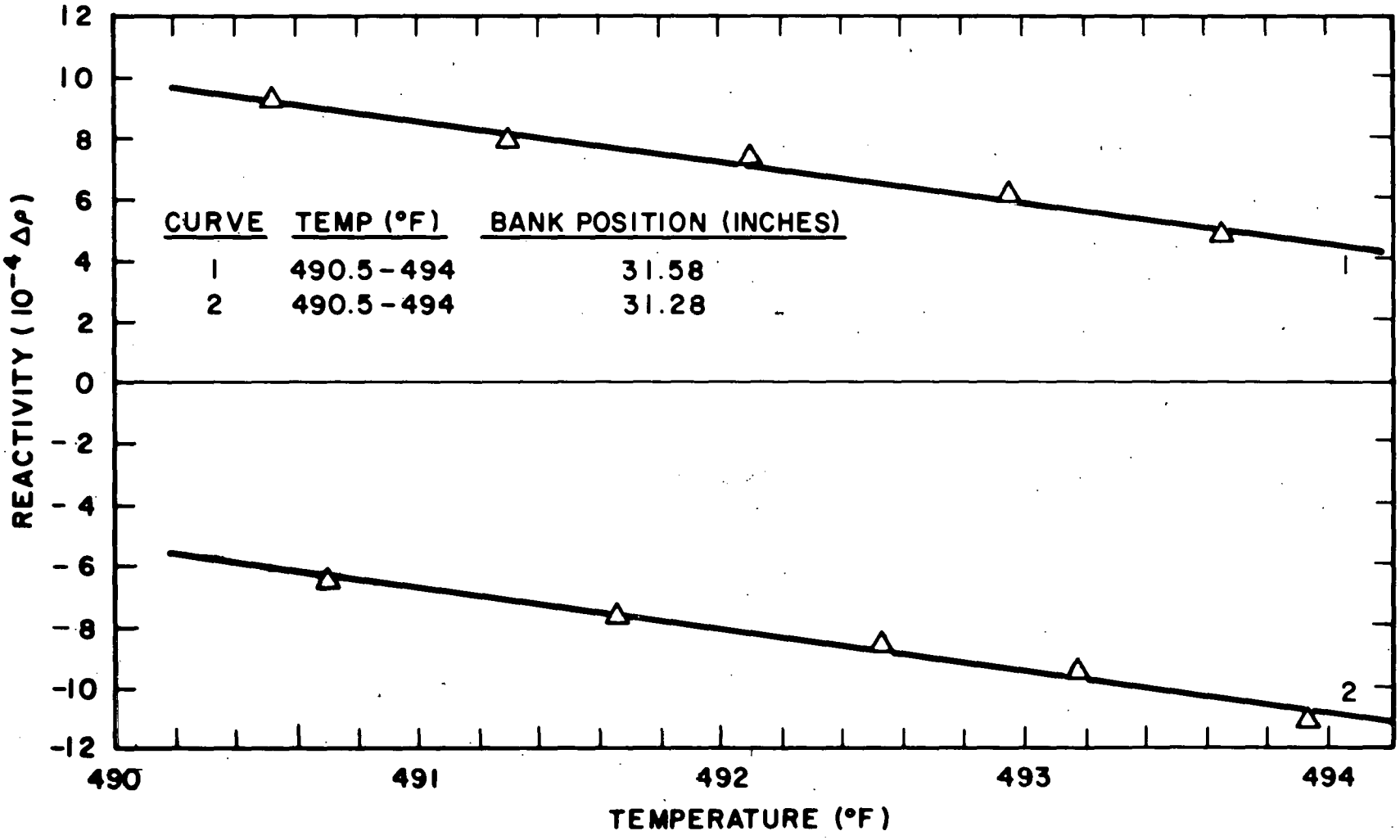

FIGURE V-7 - REACTIVITY VERSUS CORE TEMPERATURE, HOT ZERO POWER

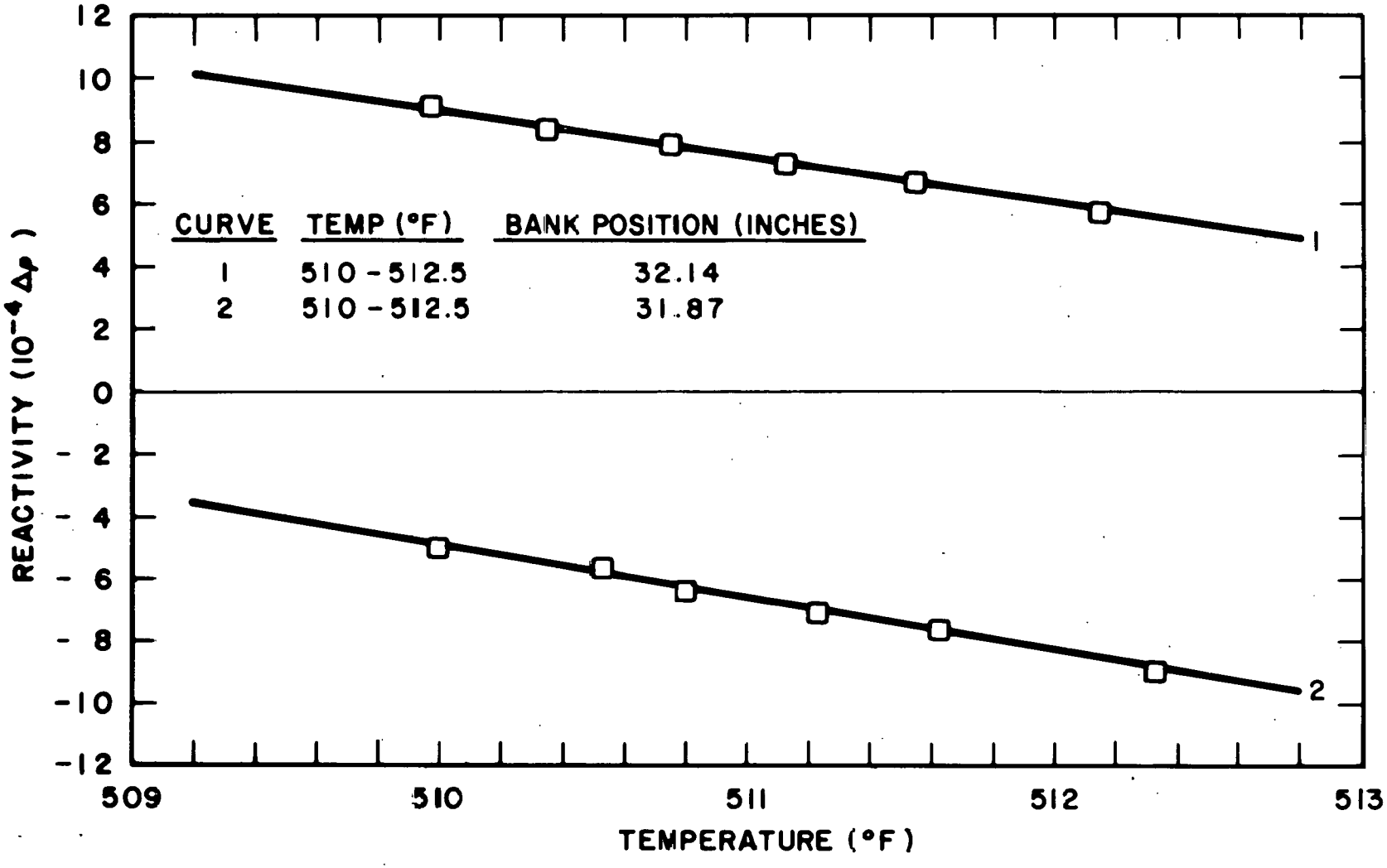

FIGURE V-8 - REACTIVITY VERSUS CORE TEMPERATURE, HOT ZERO POWER

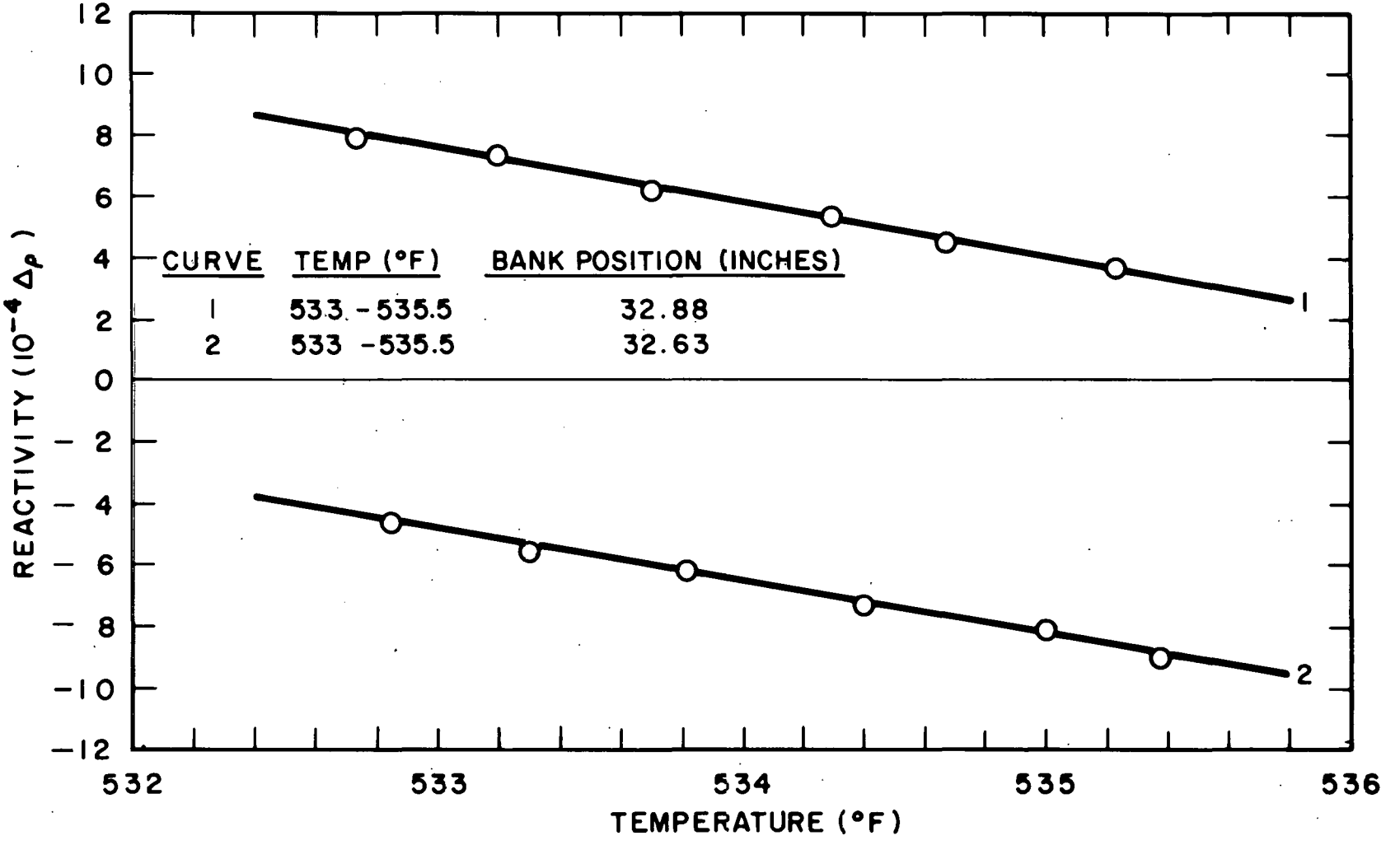

FIGURE V-9 - REACTIVITY VERSUS CORE TEMPERATURE, HOT ZERO POWER

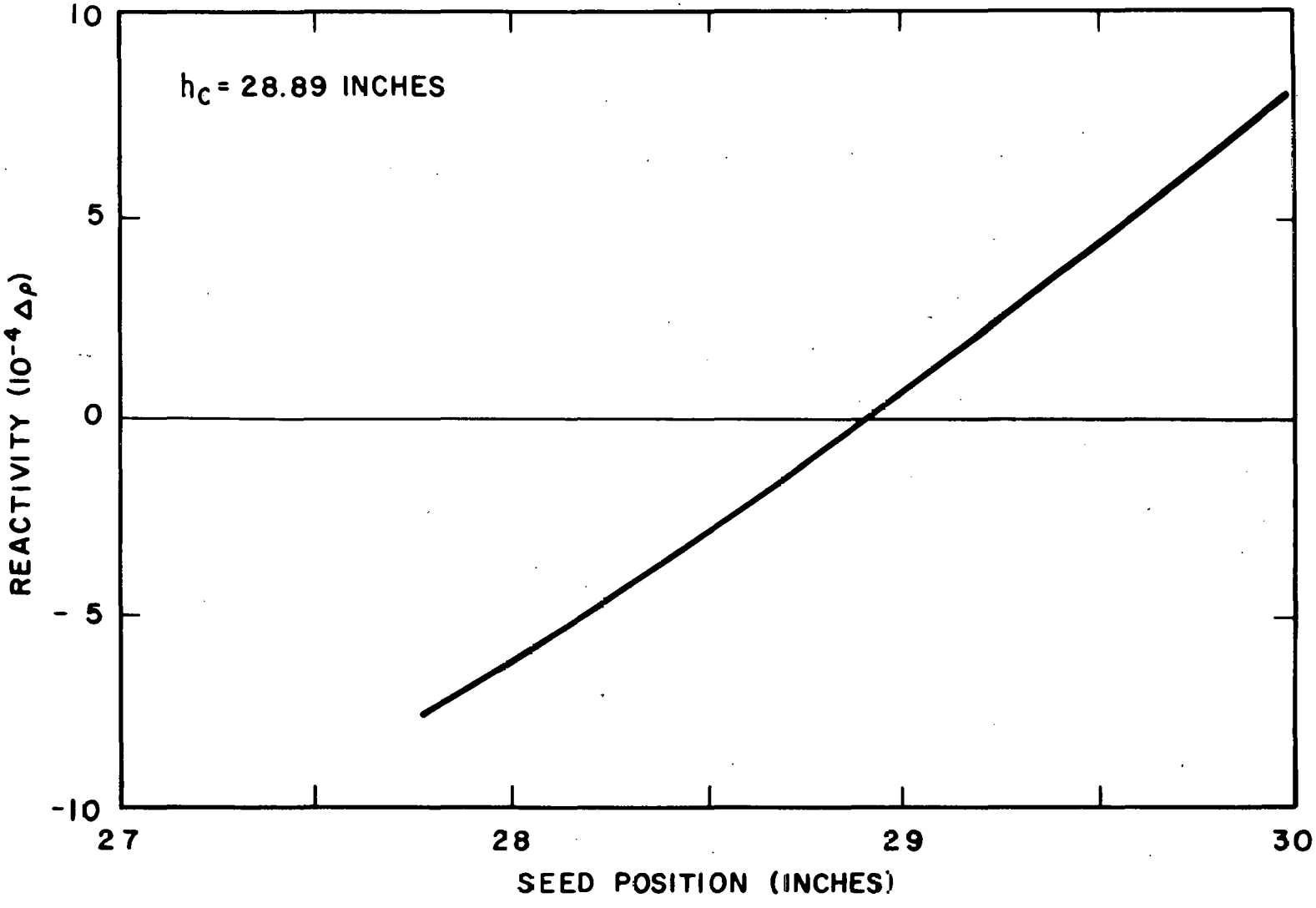

FIGURE V-10 - REACTIVITY VERSUS SEED POSITION FOR MODULE I-1

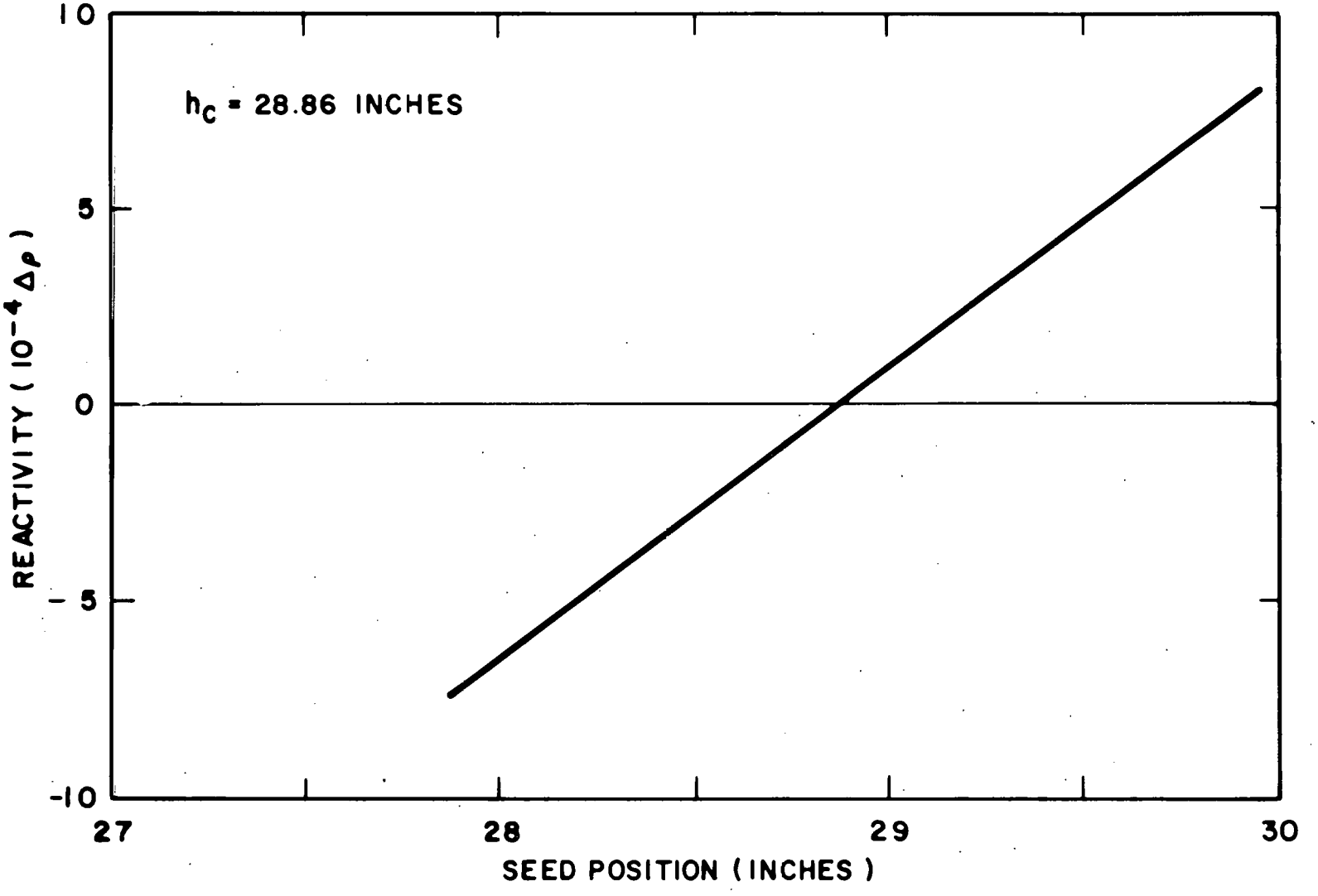

FIGURE V-11 - REACTIVITY VERSUS SEED POSITION FOR MODULE I-2

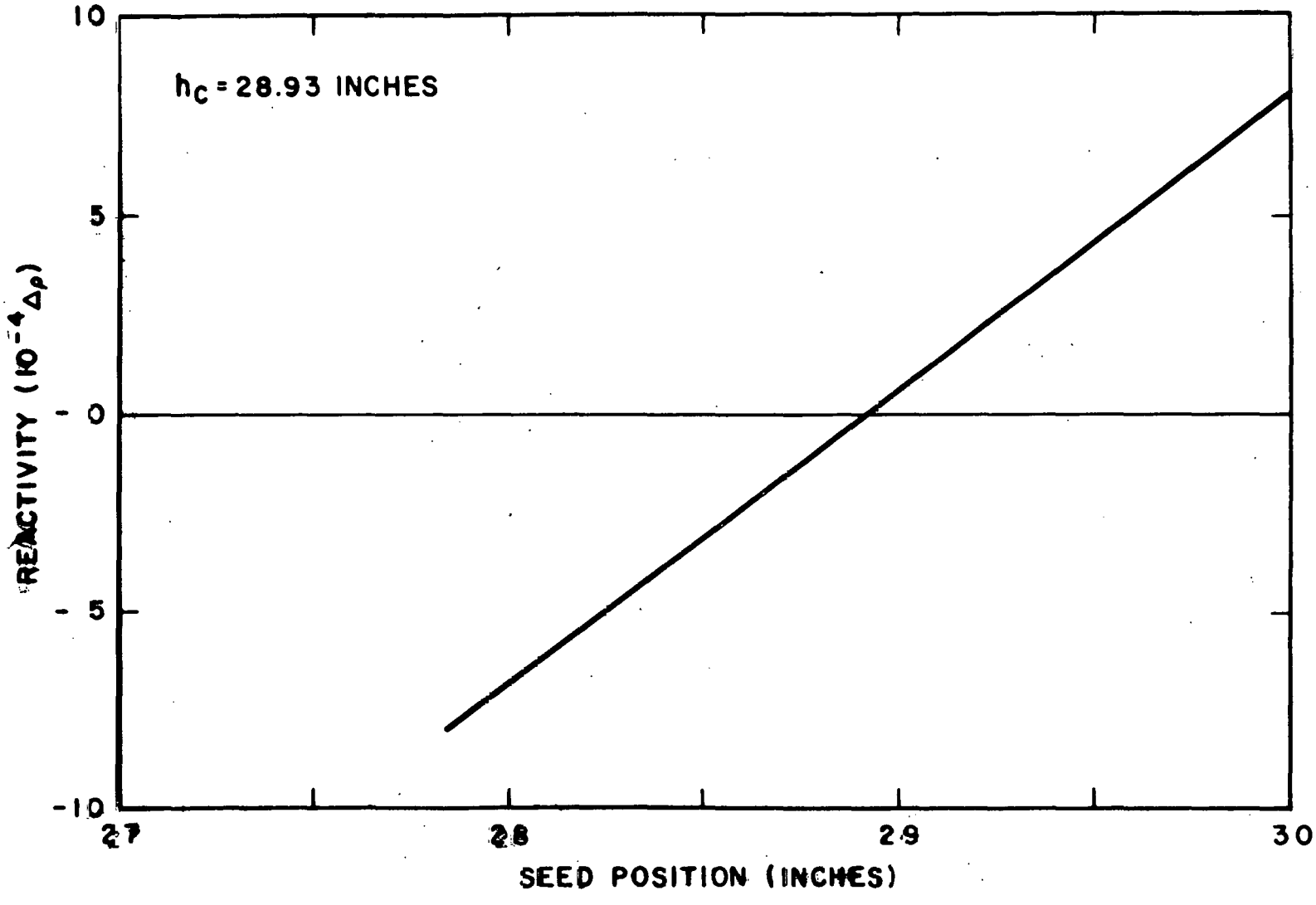

FIGURE V-12 - REACTIVITY VERSUS SEED POSITION FOR MODULE I-3

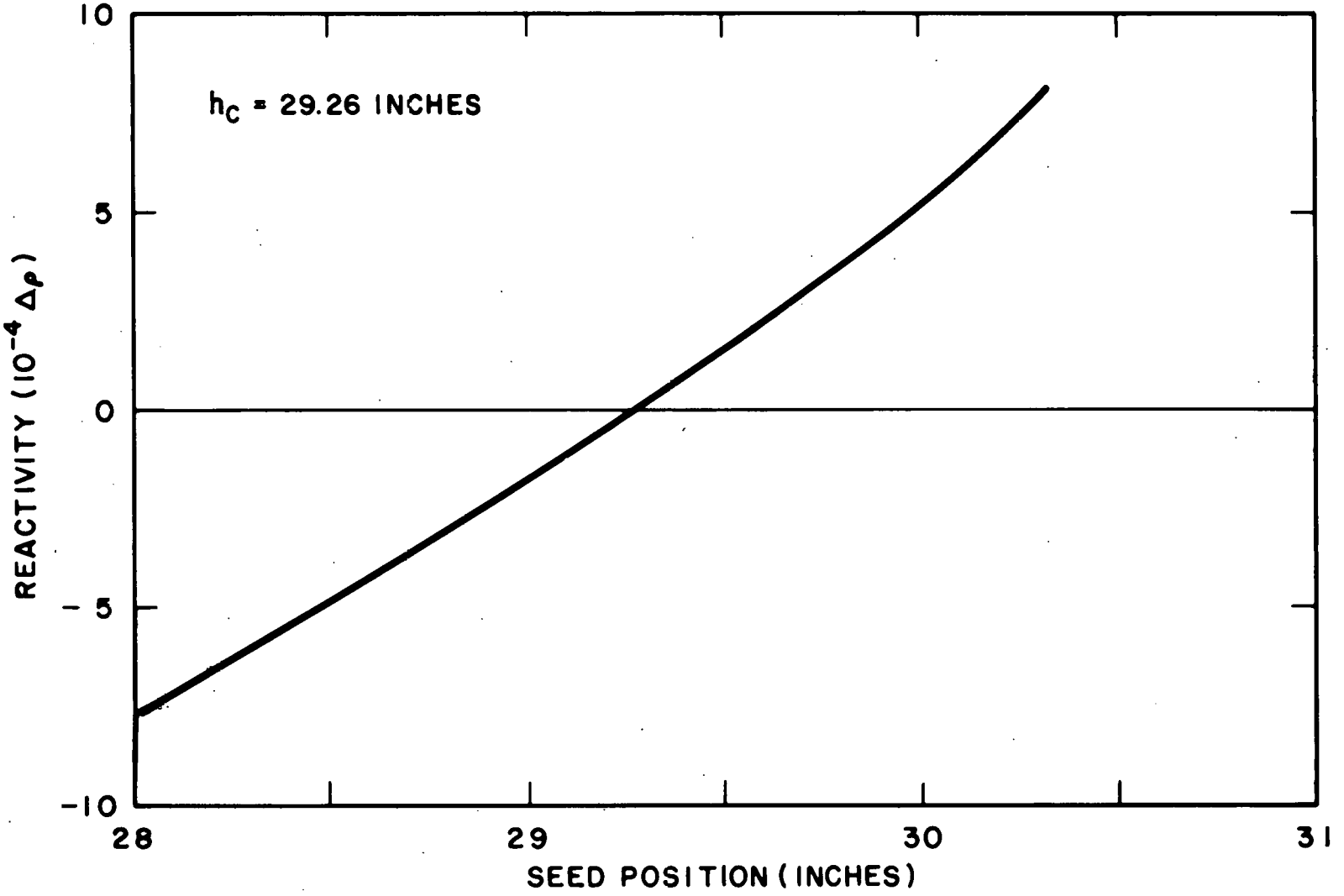

FIGURE V-13 - REACTIVITY VERSUS SEED POSITION FOR MODULE II-1

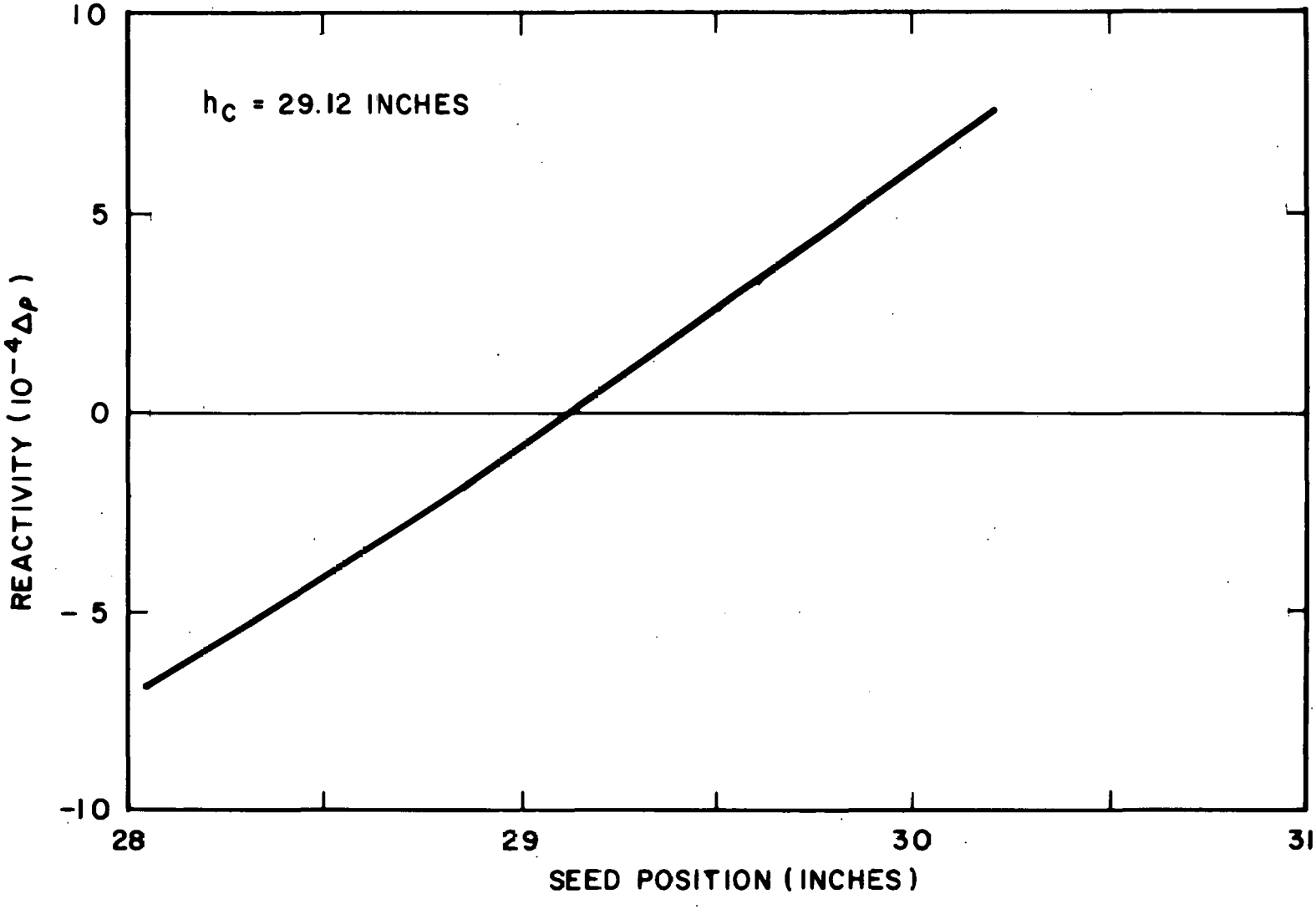

FIGURE V-14 - REACTIVITY VERSUS SEED POSITION FOR MODULE II-2

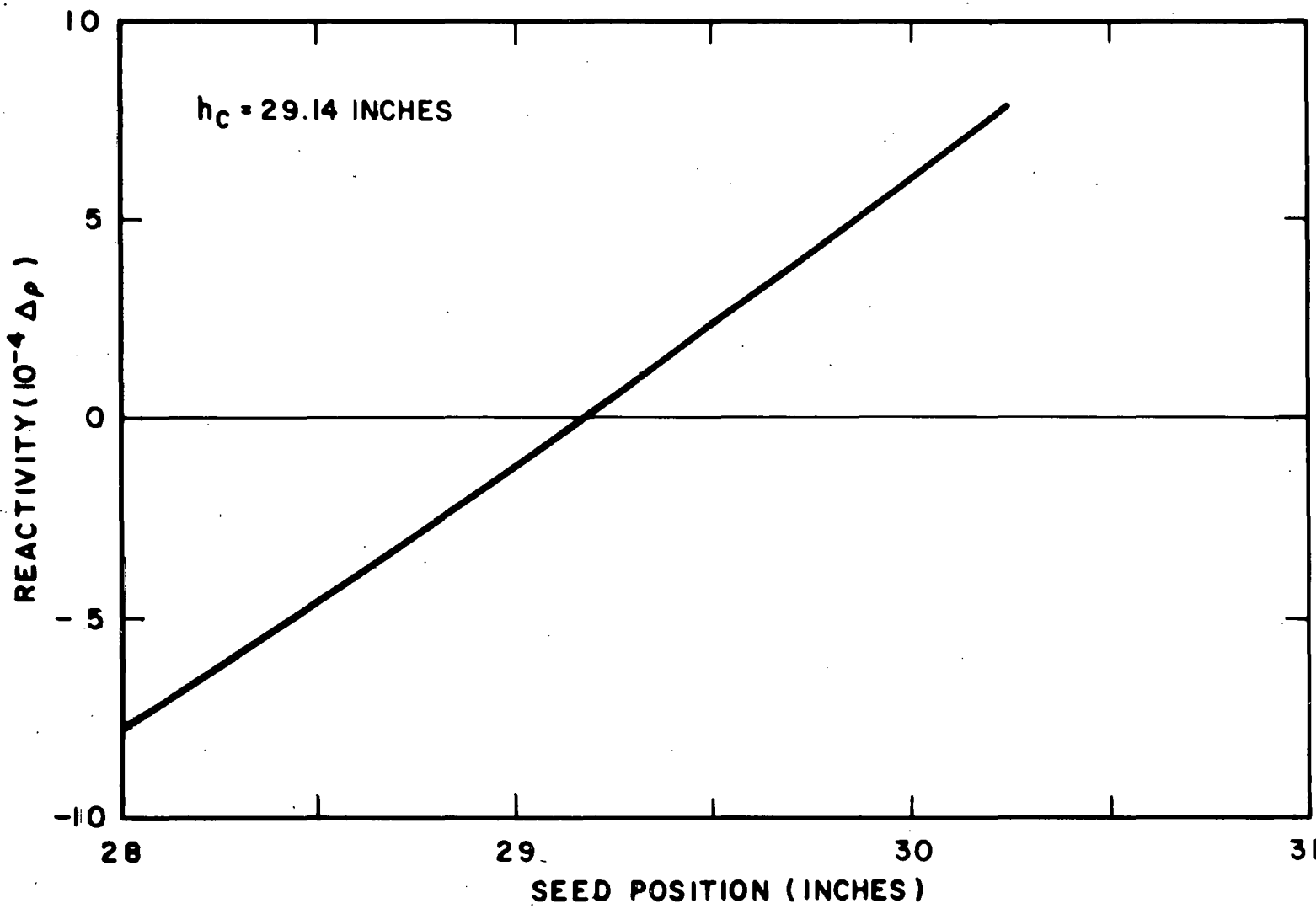

FIGURE V-15 - REACTIVITY VERSUS SEED POSITION FOR MODULE II-3

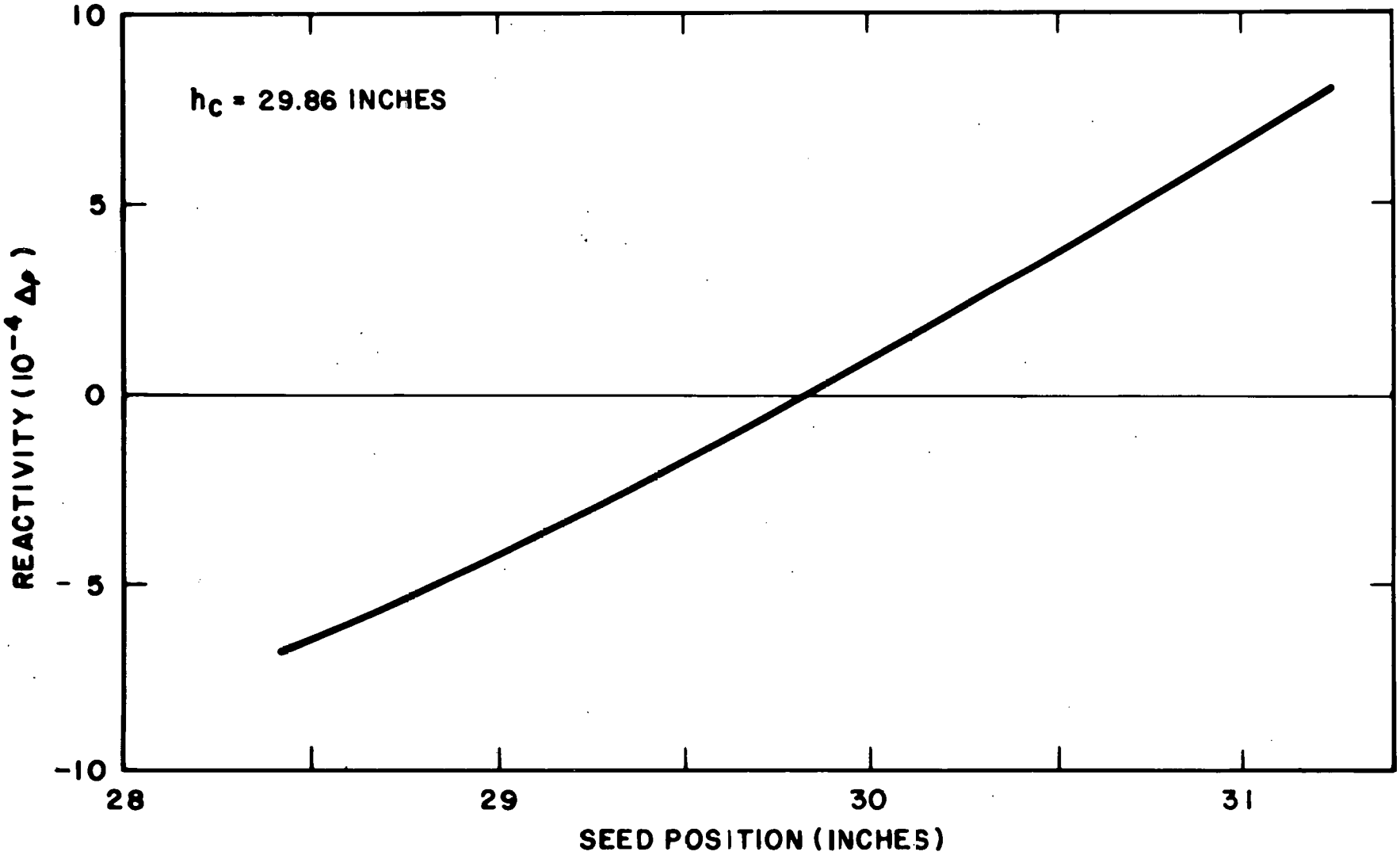

FIGURE V-16 - REACTIVITY VERSUS SEED POSITION FOR MODULE III-1

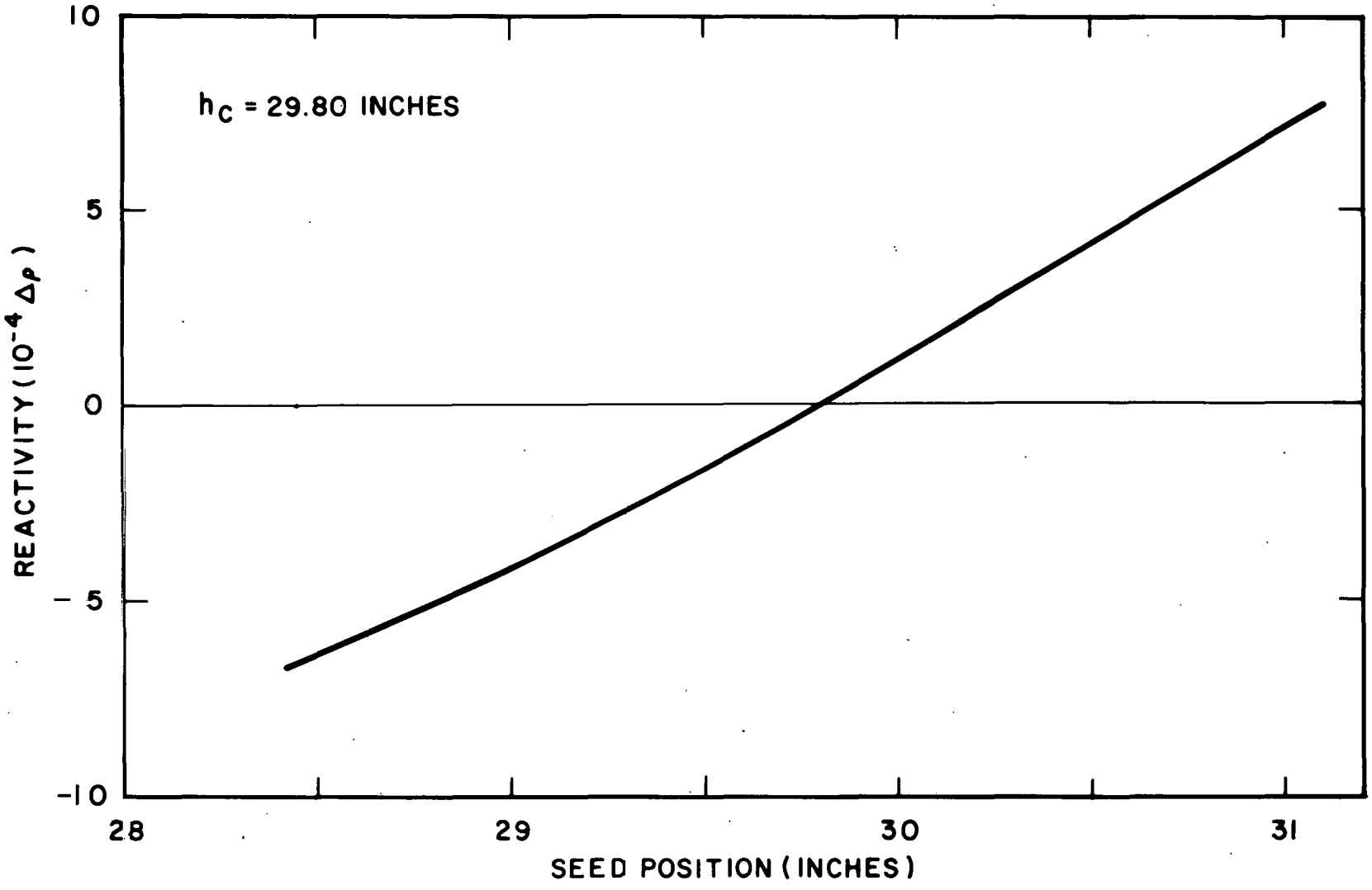

FIGURE V-17 - REACTIVITY VERSUS SEED POSITION FOR MODULE III-2

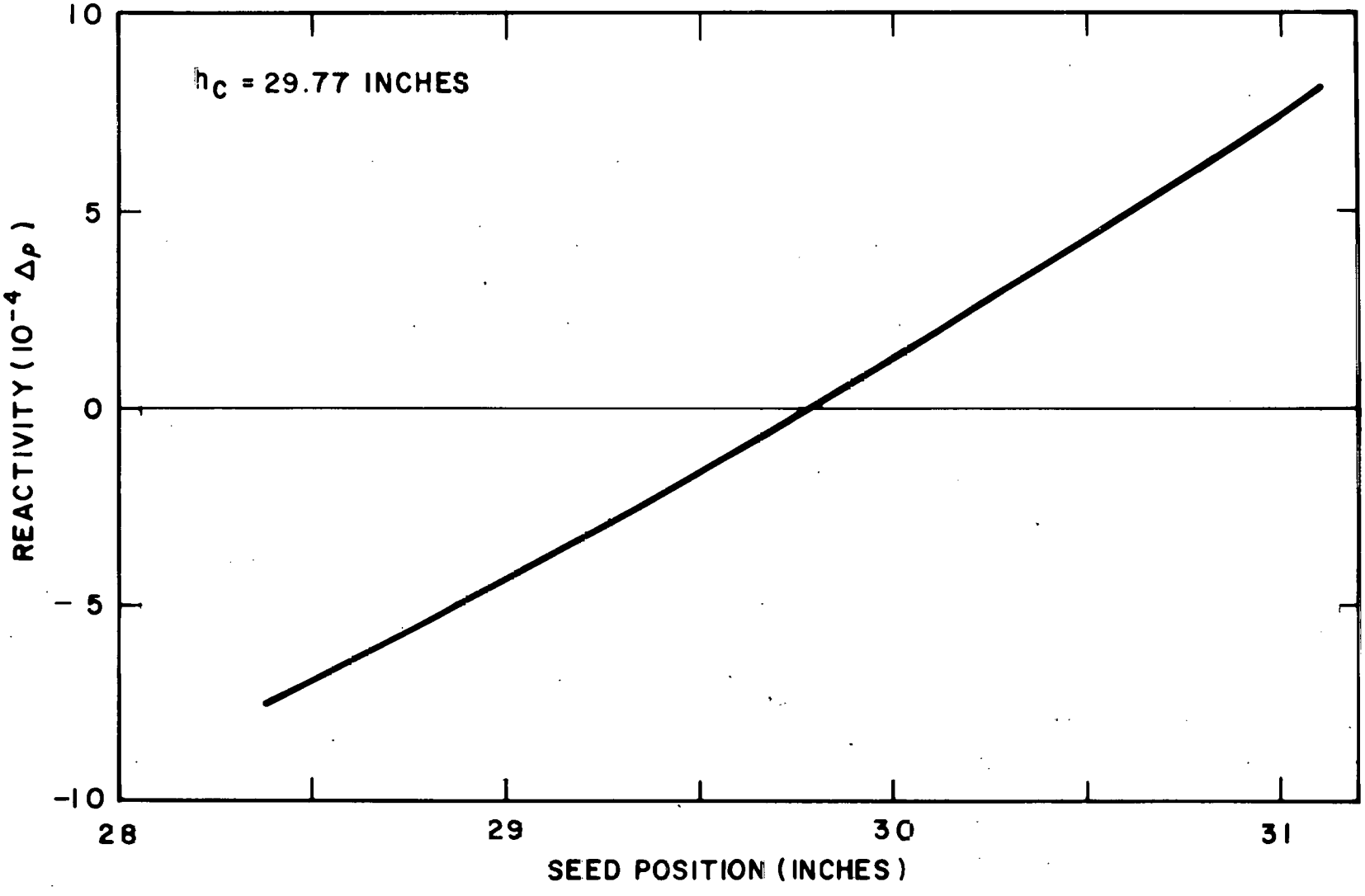

FIGURE V-18 - REACTIVITY VERSUS SEED POSITION FOR MODULE III-3

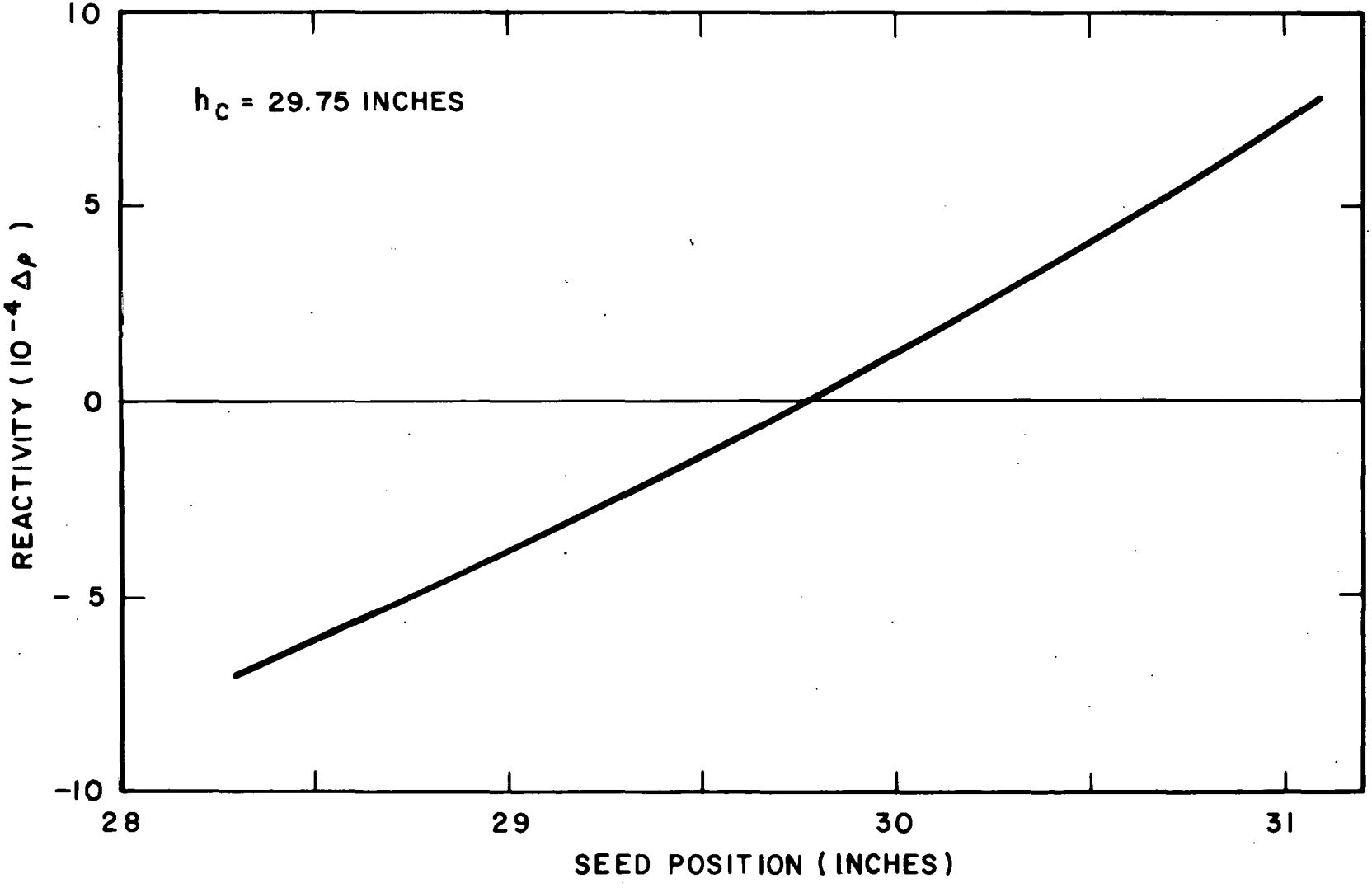

FIGURE V-19 - REACTIVITY VERSUS SEED POSITION FOR MODULE III-4

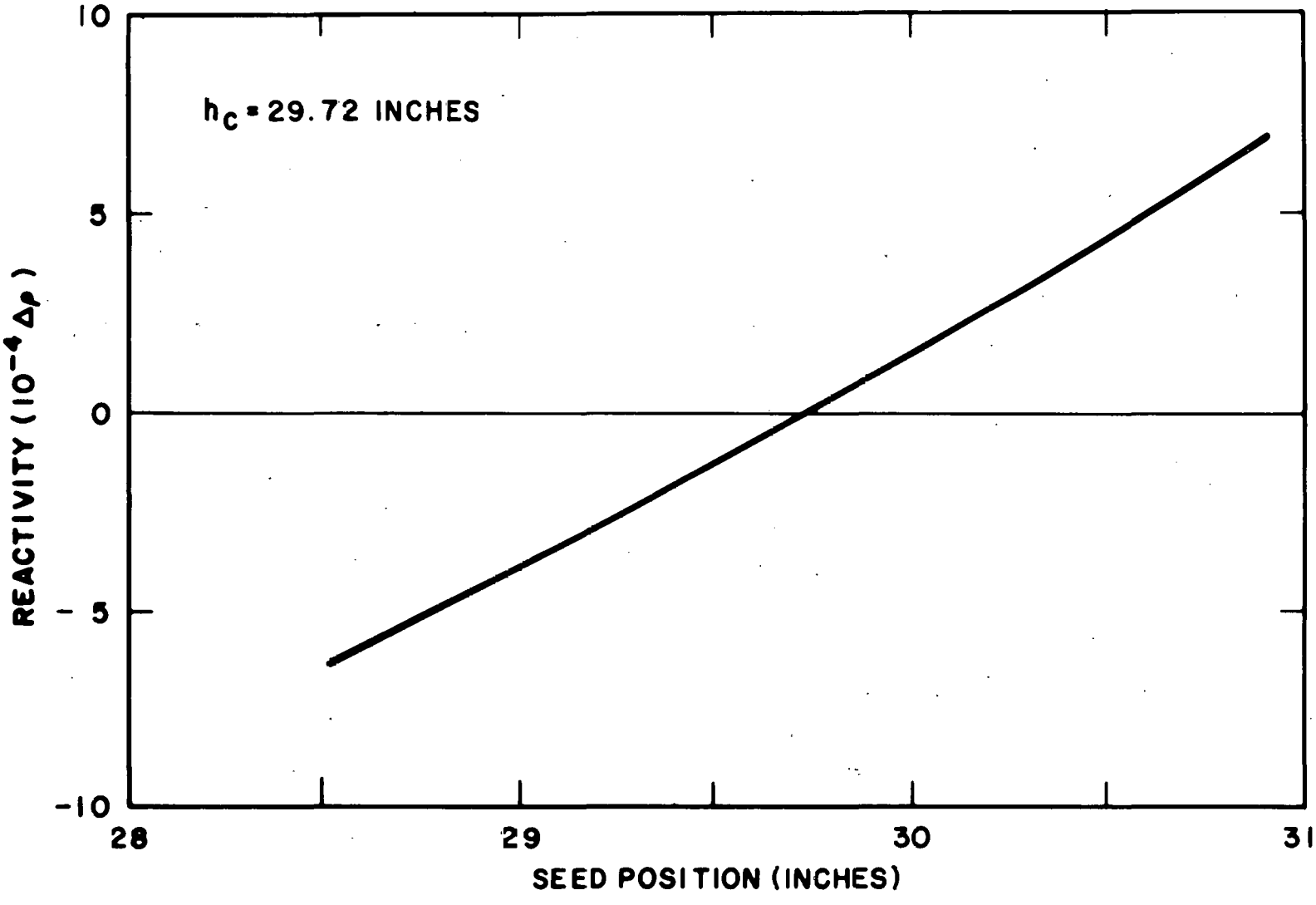

FIGURE V-2C - REACTIVITY VERSUS SEED POSITION FOR MODULE III-5

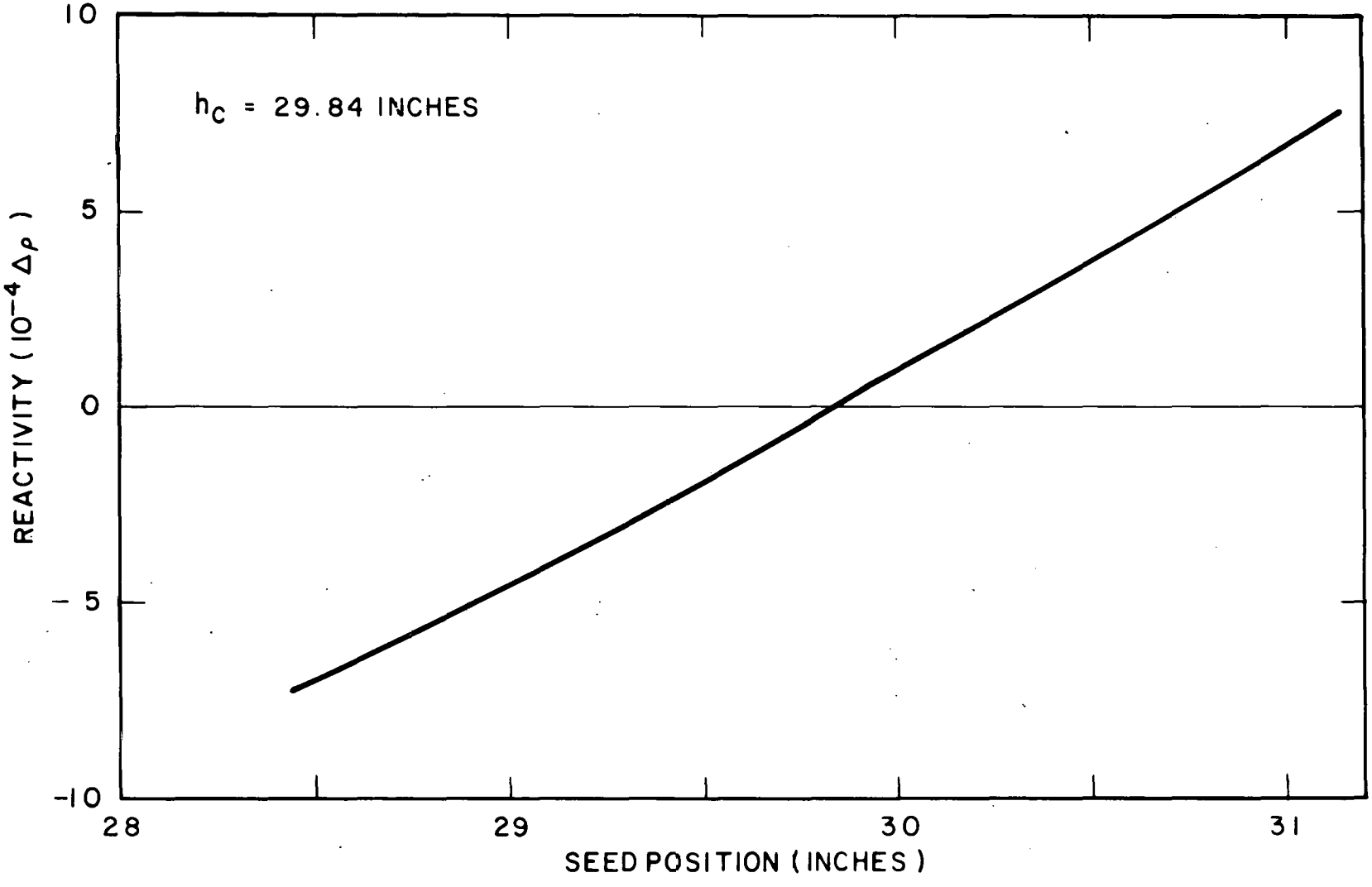

FIGURE V-21 - REACTIVITY VERSUS SEED POSITION FOR MODULE III-6

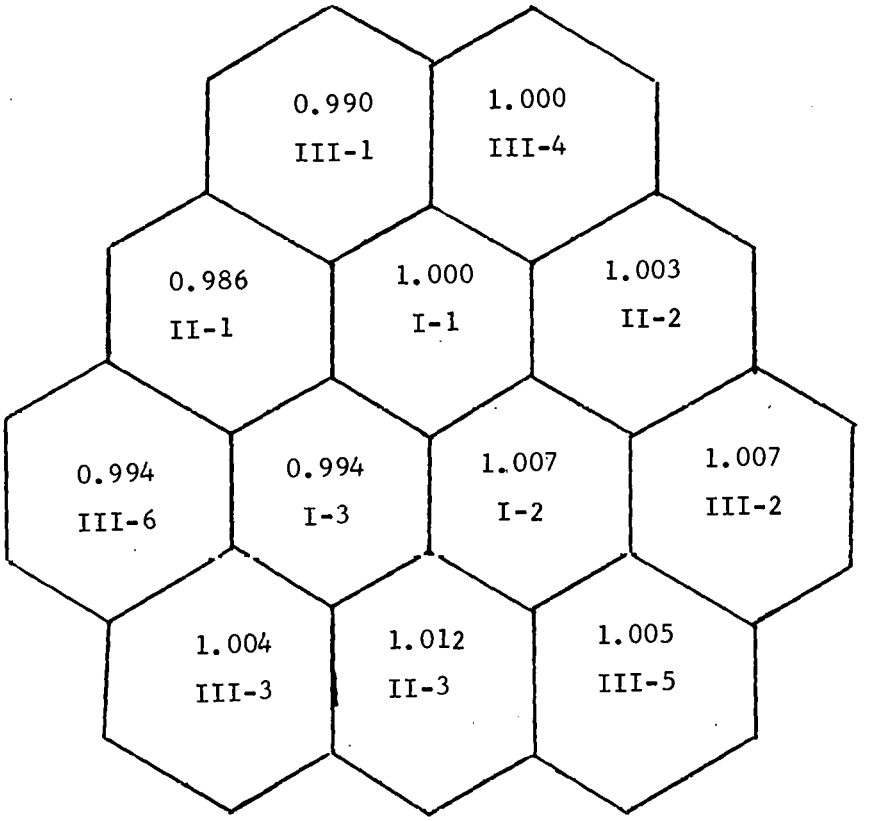

○ - CIC Channel D

LEGEND

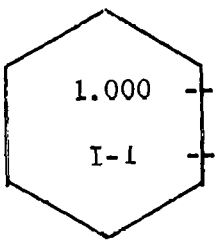

Average of two comparison of $\sqrt{\text{worth}}$

Module Type - Number

FIGURE V-22 - CORE MAP SHOWING $\sqrt{\text{WORTH}}$ COMPARISONS

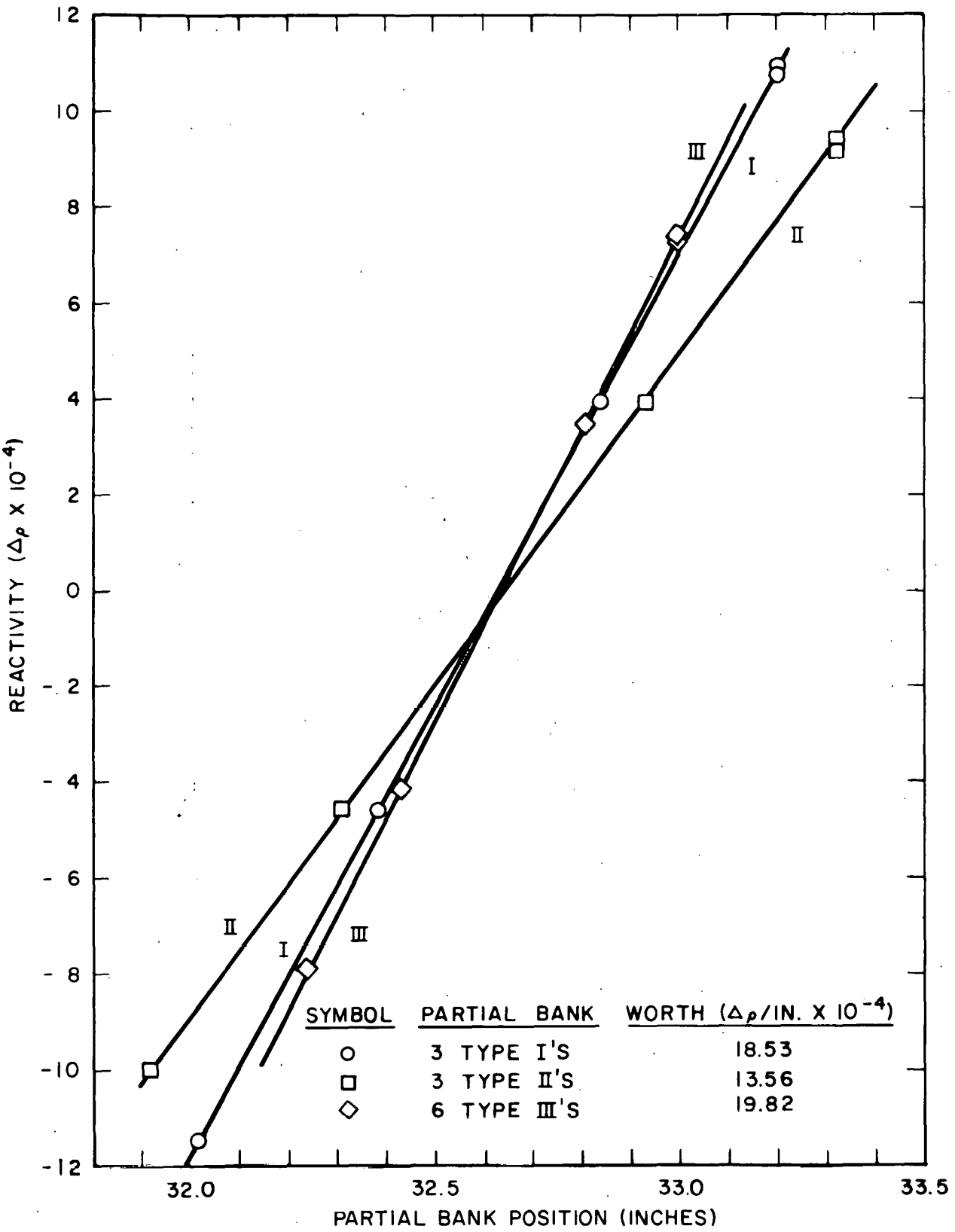

FIGURE V-23 - REACTIVITY VERSUS PARTIAL BANK SEED POSITION, HOT ZERO POWER

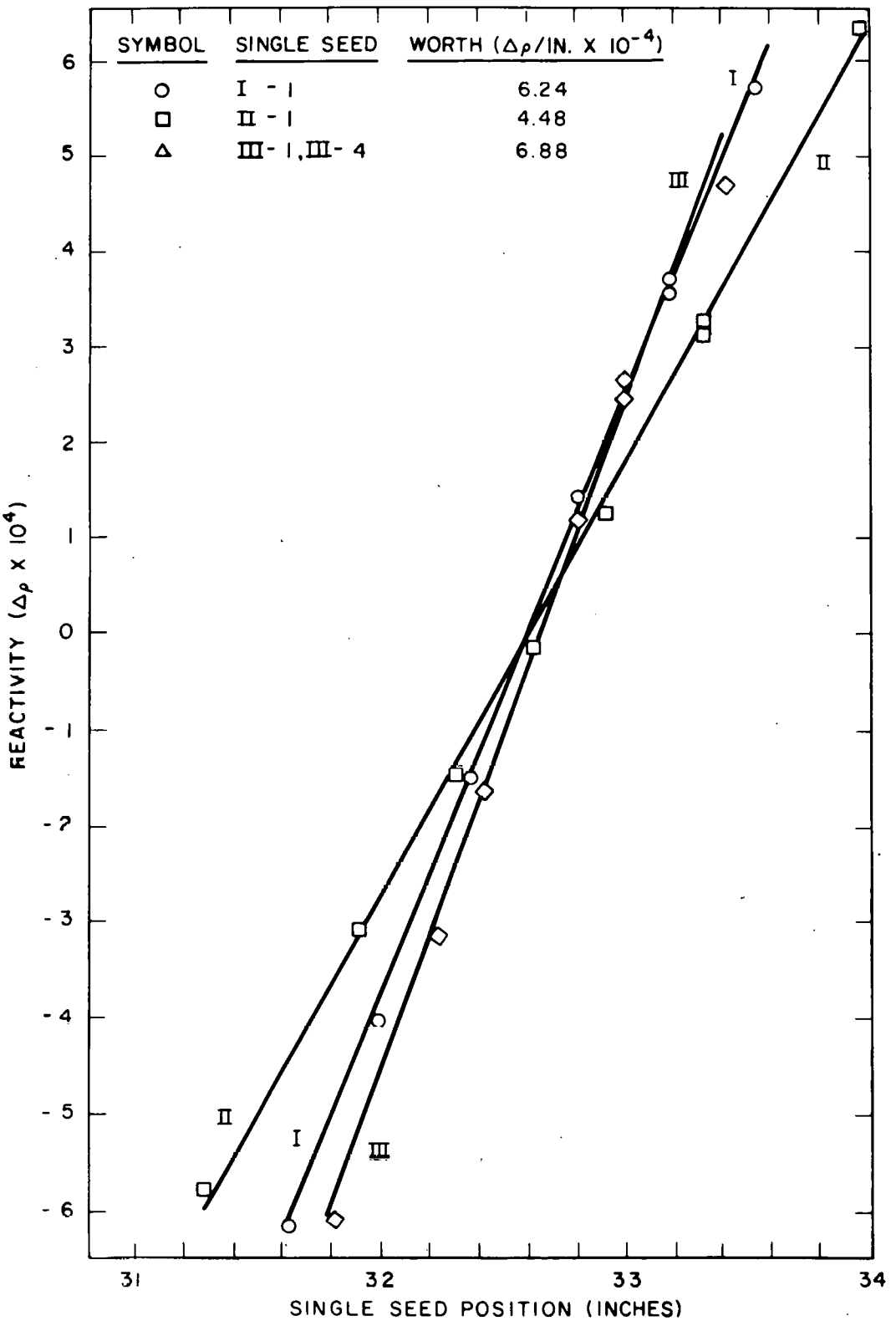

FIGURE V-24 - REACTIVITY VERSUS SEED POSITION, HOT ZERO POWER

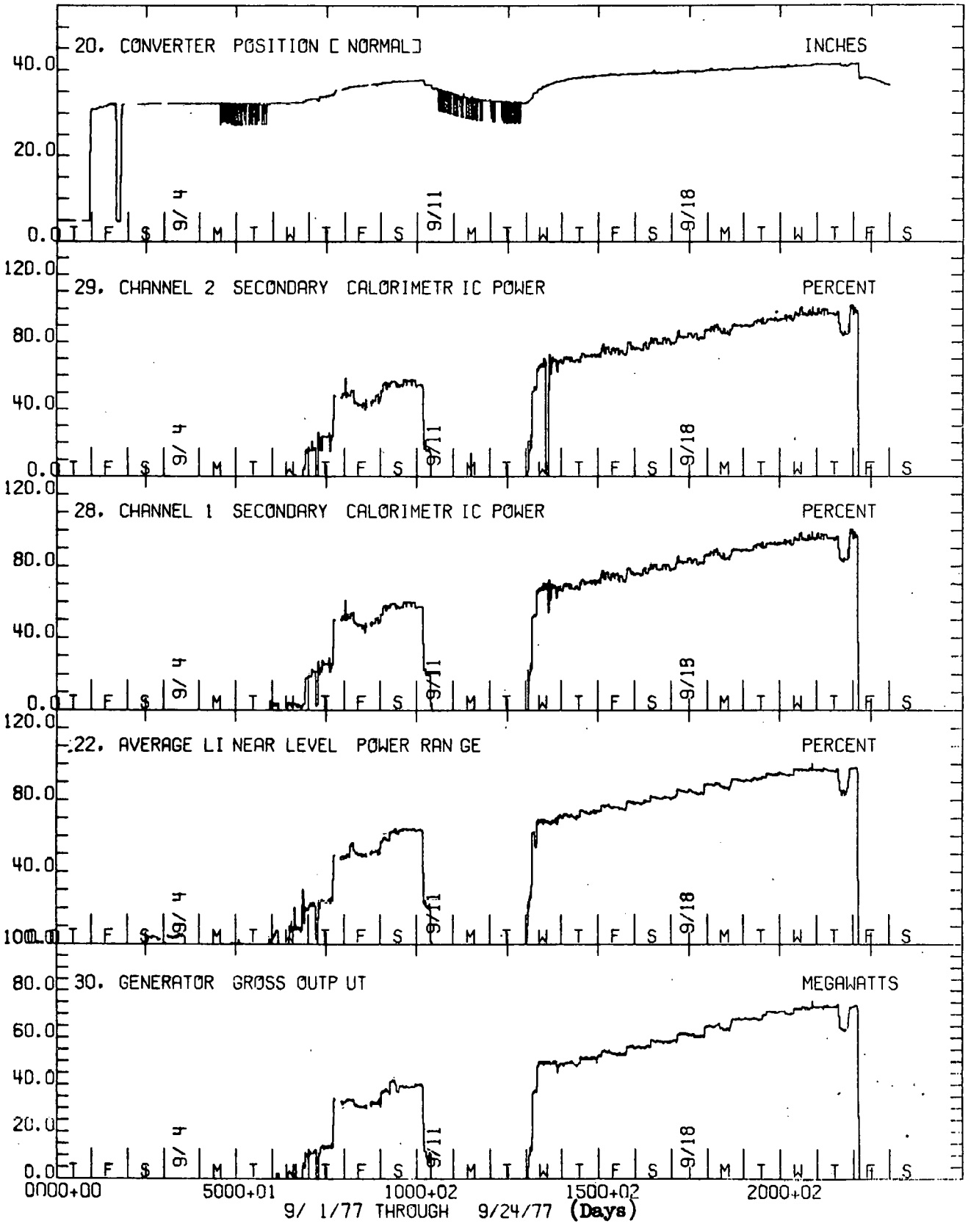

FIGURE V-25 - ASCENSION TO POWER

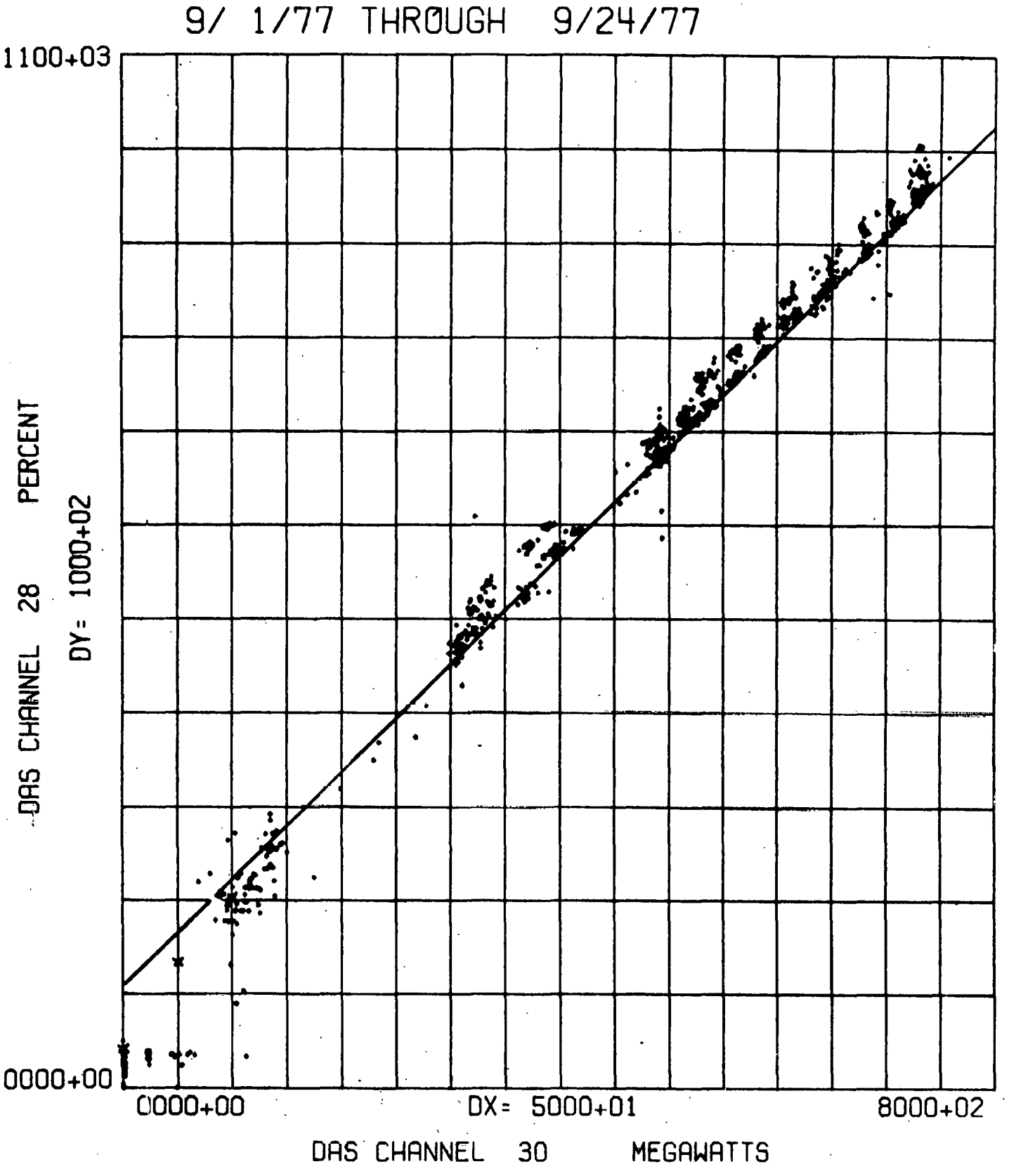

FIGURE V-26 - CALORIMETRIC COMPUTER 1 VERSUS GROSS GENERATOR OUTPUT

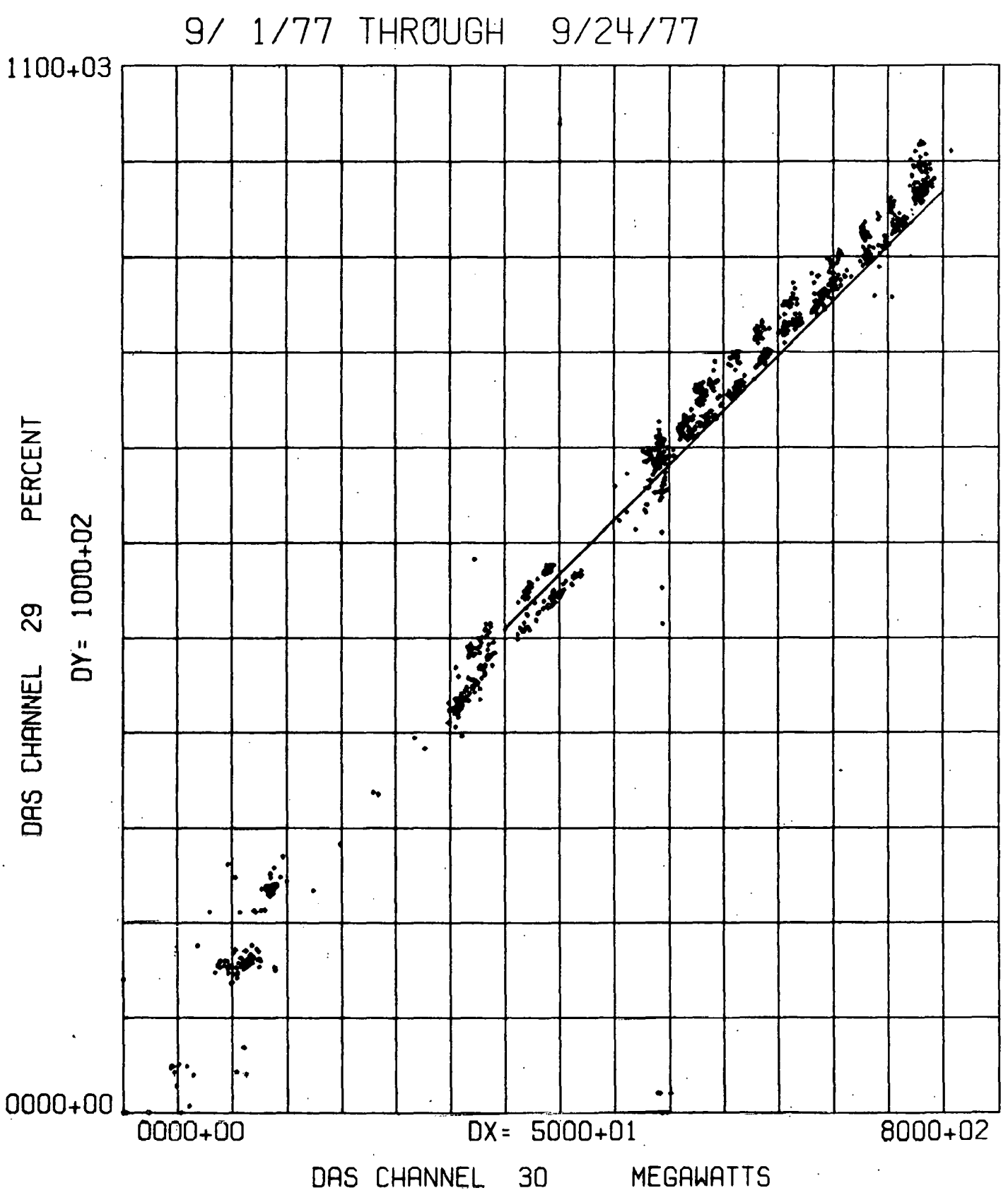

FIGURE V-27 - CALORIMETRIC COMPUTER 2 VERSUS GROSS GENERATOR OUTPUT

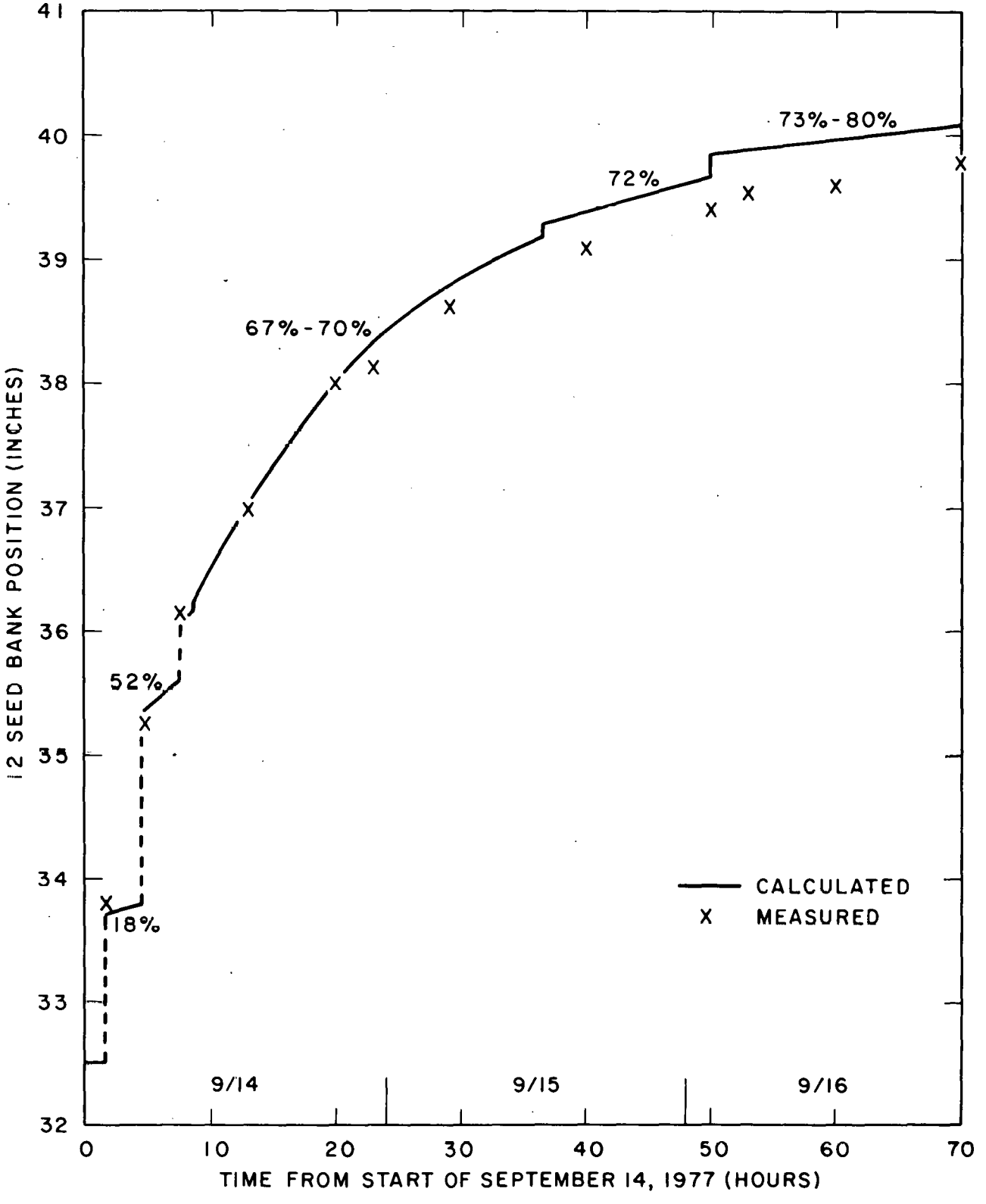

FIGURE V-28(a) - 12 SEED BANK POSITION VERSUS TIME

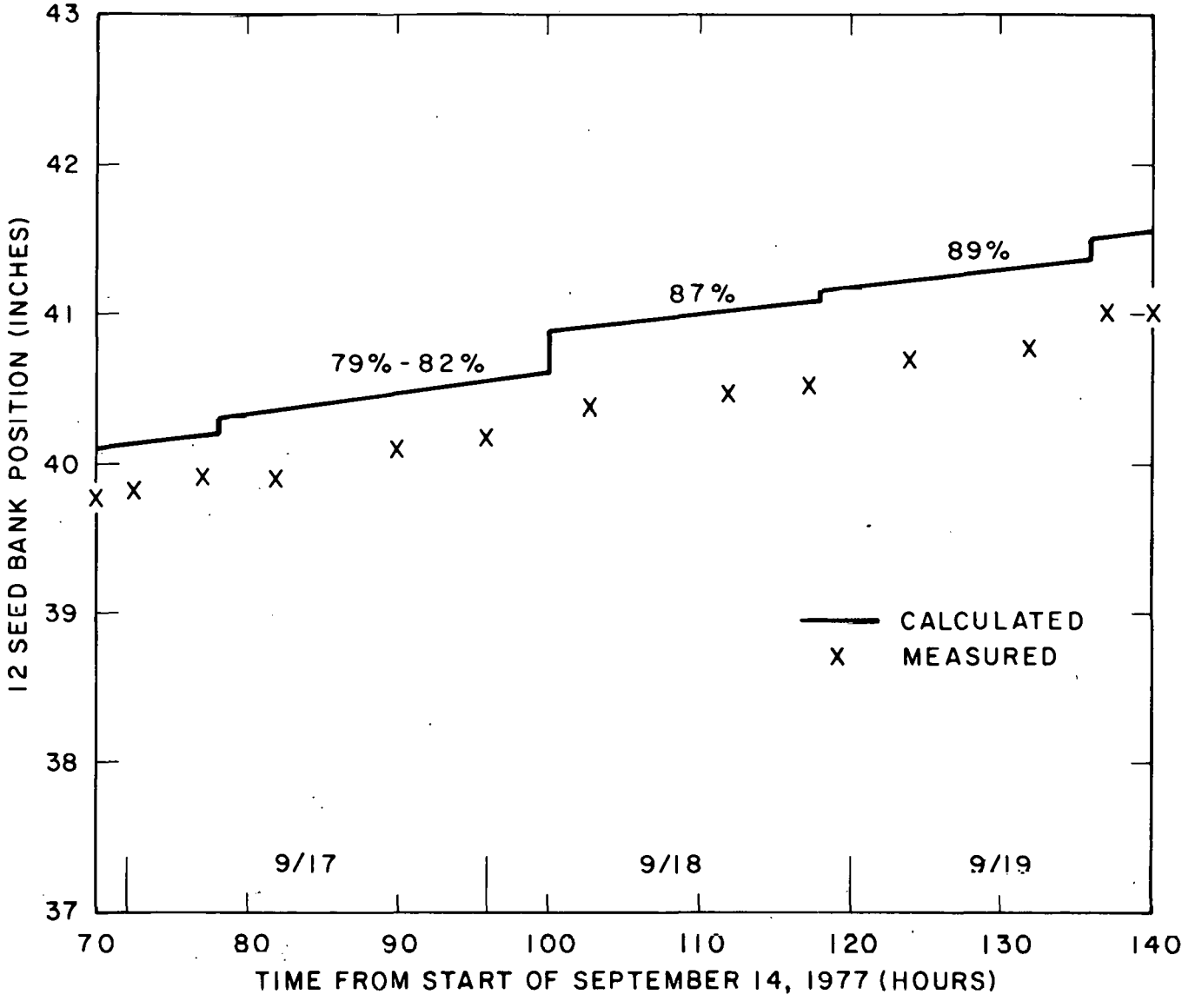

FIGURE V-28(b) - 12 SEED BANK POSITION VERSUS TIME

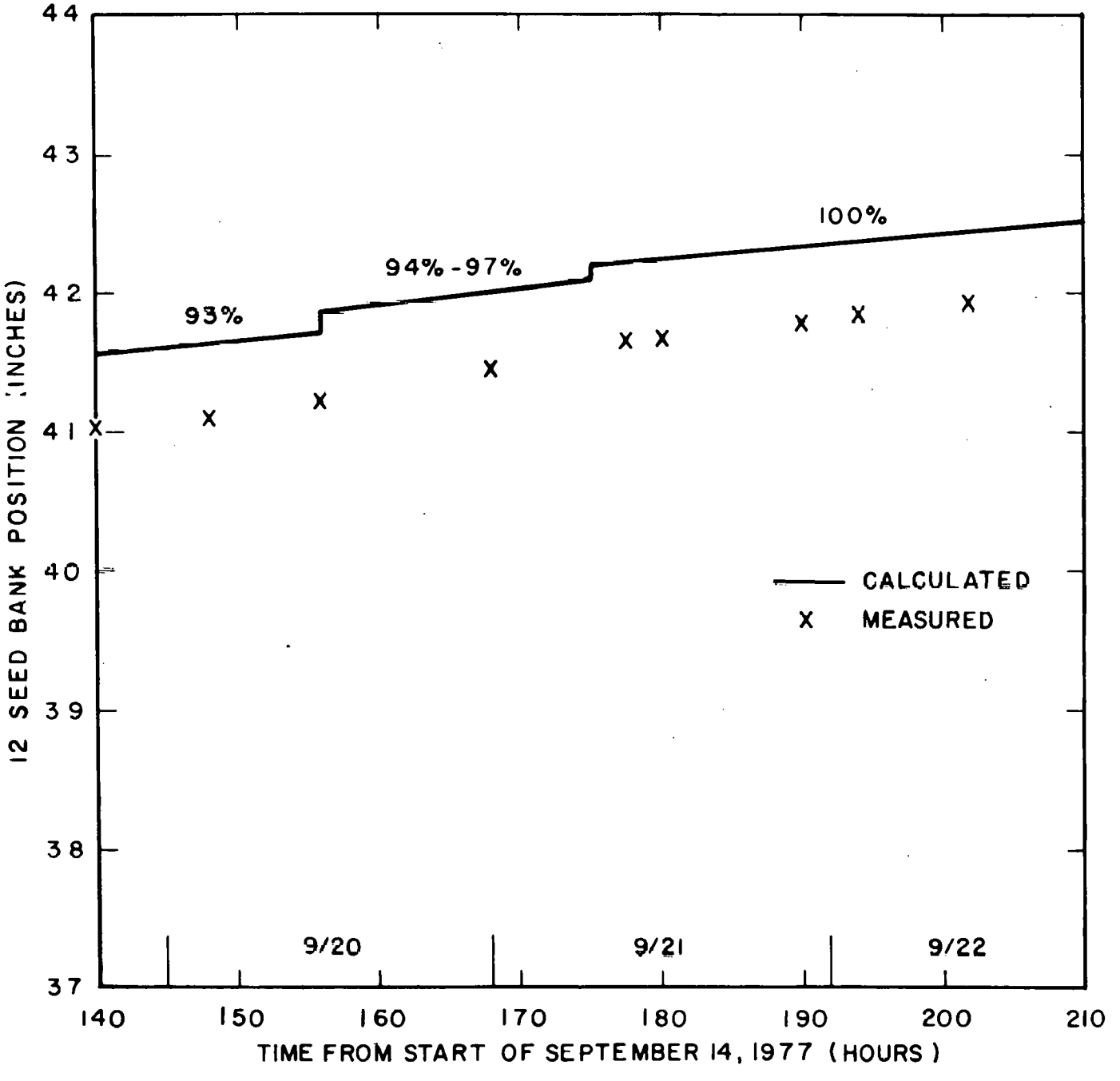

FIGURE V-28(c) - 12 SEED BANK POSITION VERSUS TIME

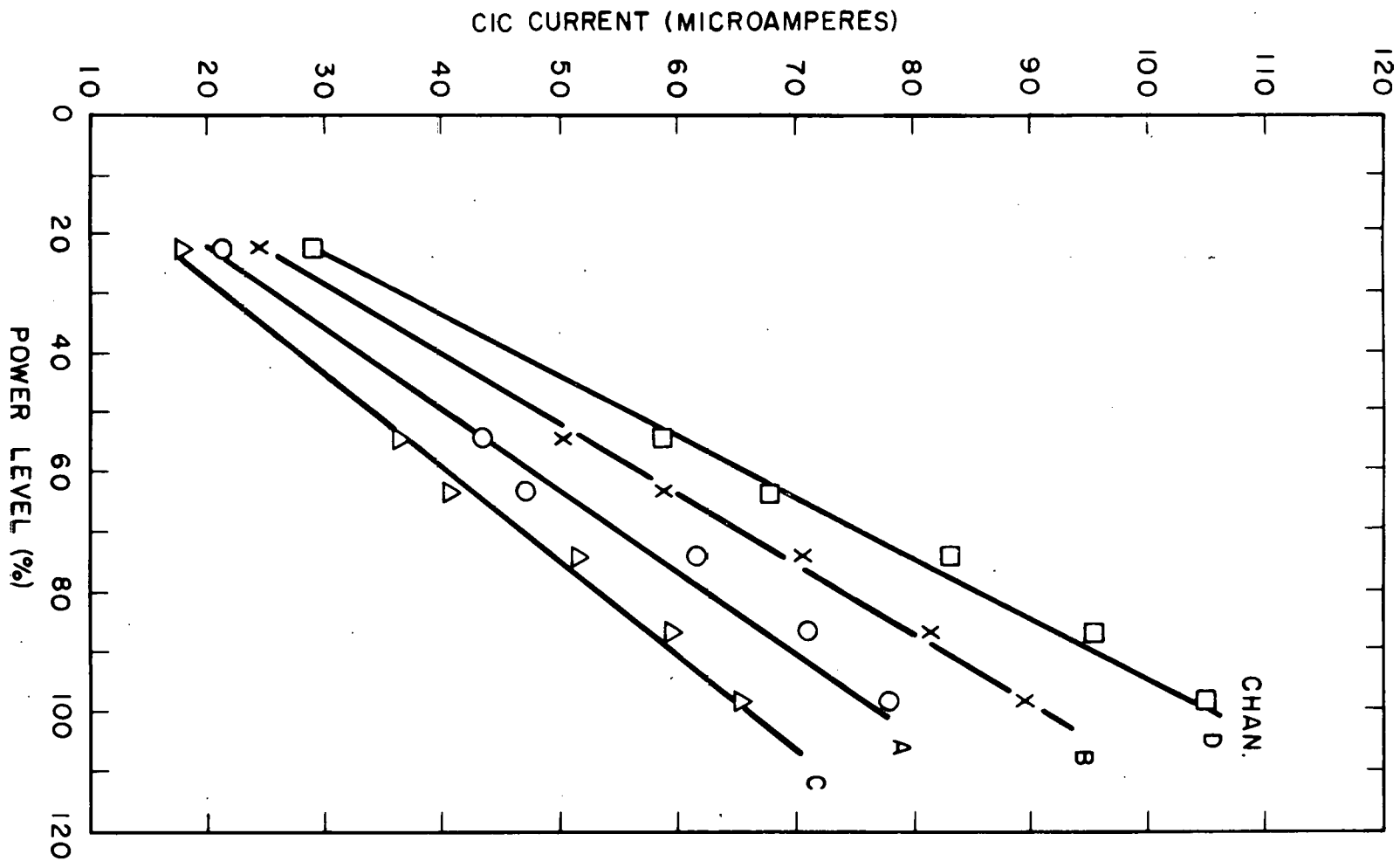

FIGURE V-29 - COMPENSATED ION CURRENT VERSUS CALORIMETRIC POWER LEVEL

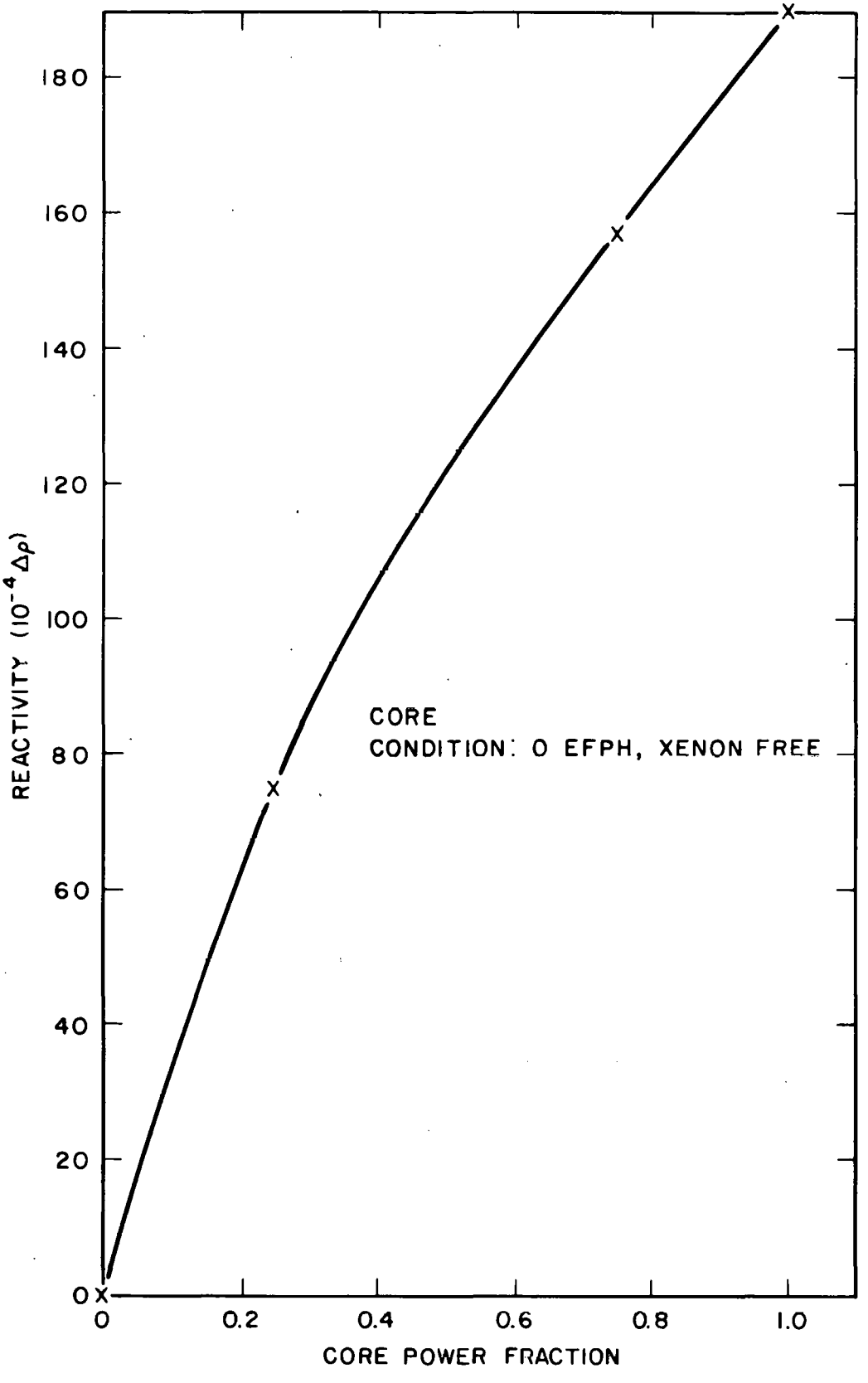

FIGURE V-30 - CALCULATED POWER REACTIVITY; CHANGE IN REACTIVITY VERSUS POWER LEVEL

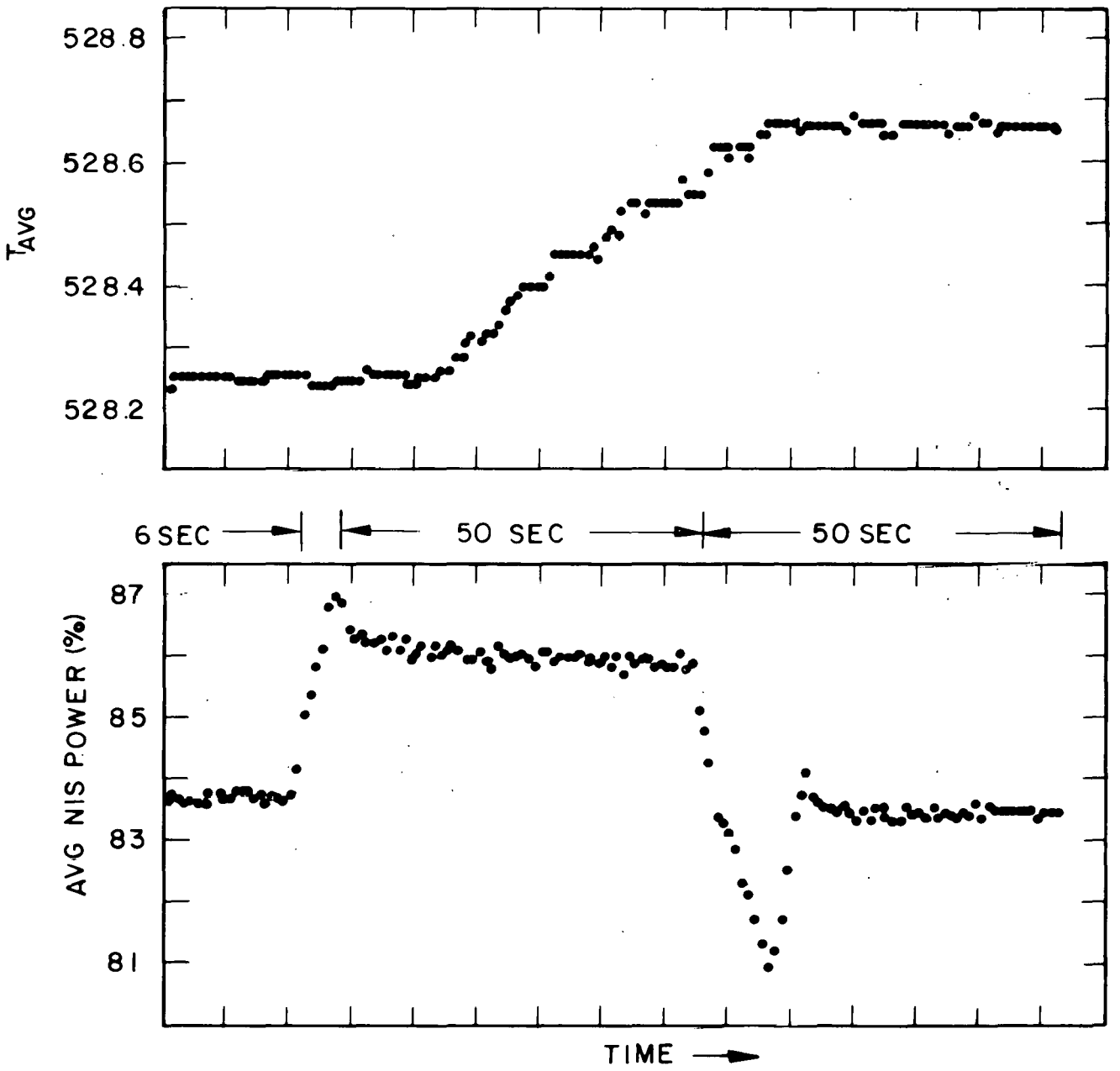

FIGURE V-31 - Tavg AND NIS POWER VERSUS TIME:
12 SEED BANK WORTH AT POWER

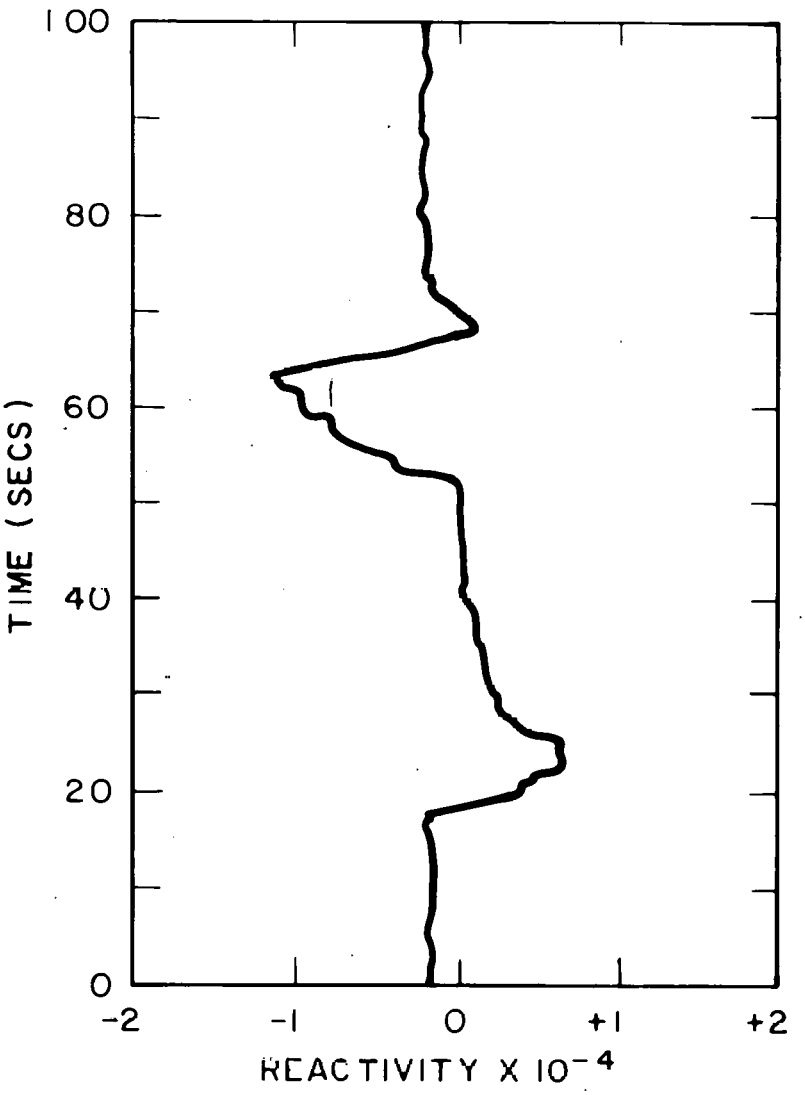

FIGURE V-32 - REACTIVITY VERSUS TIME:
12 SEED BANK WORTH AT POWER

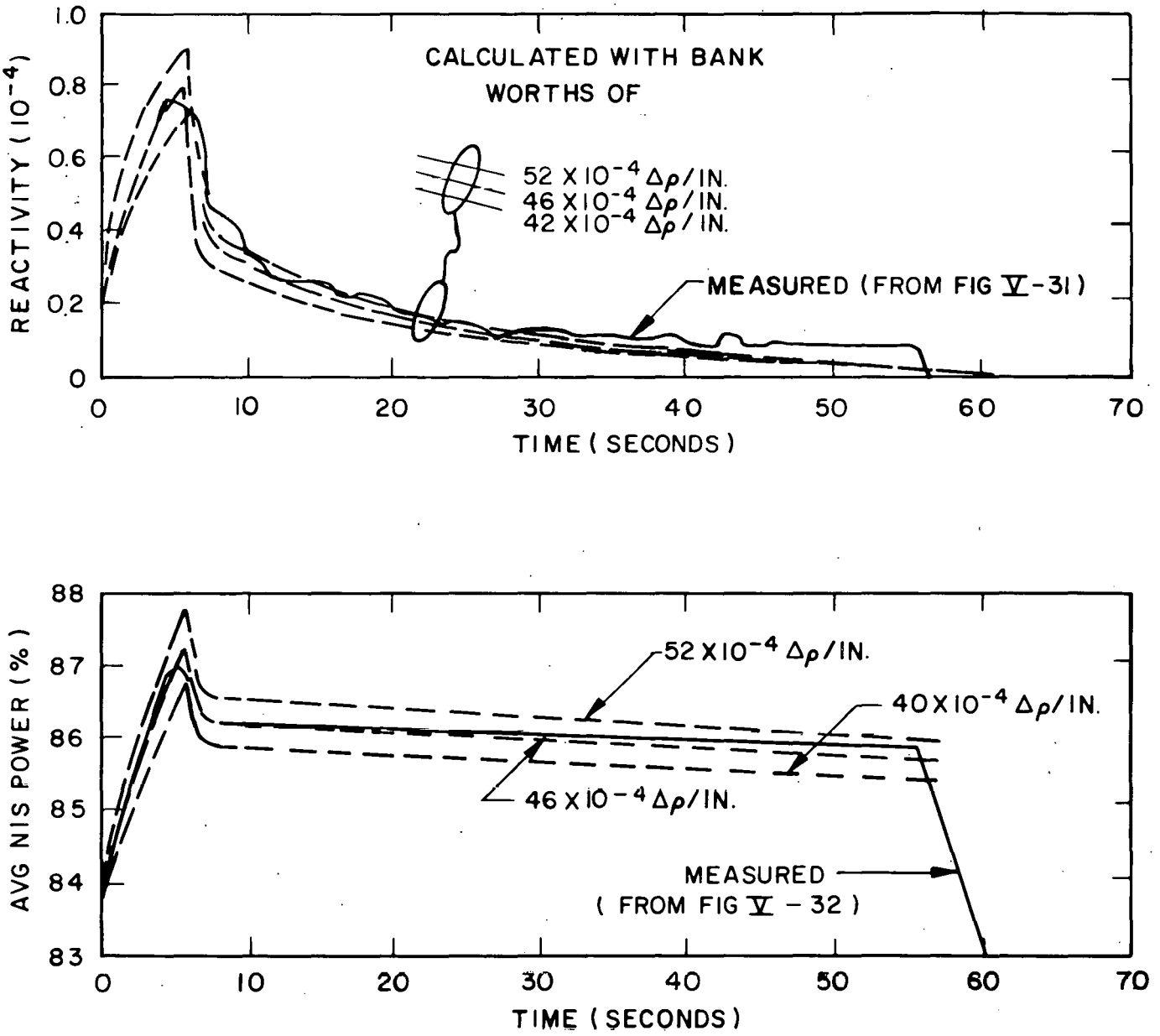

FIGURE V-33 - REACTIVITY AND NIS POWER VERSUS TIME

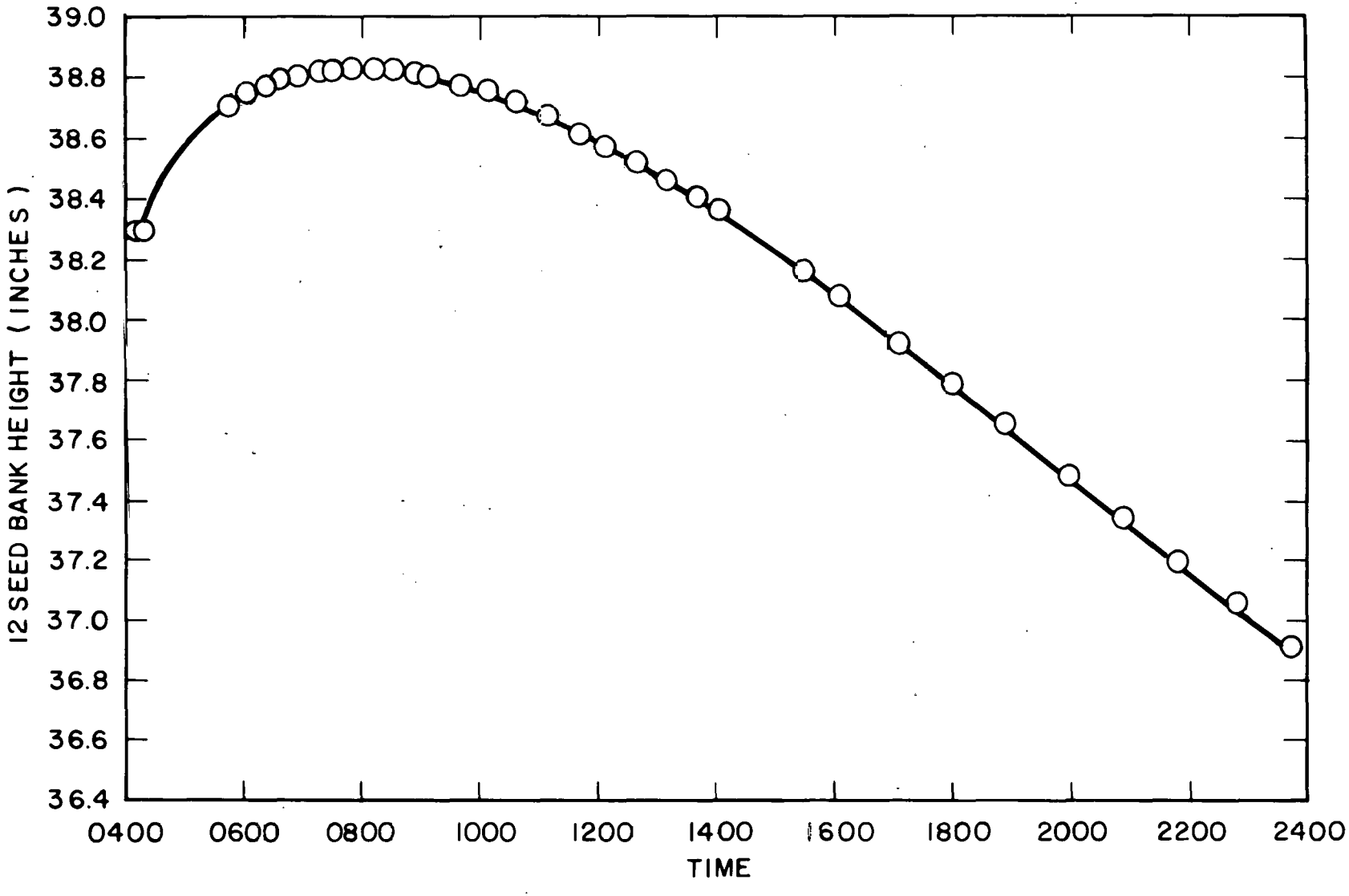

FIGURE V-34 - 12 SEED BANK HEIGHT VERSUS TIME DURING XENON TRANSIENT

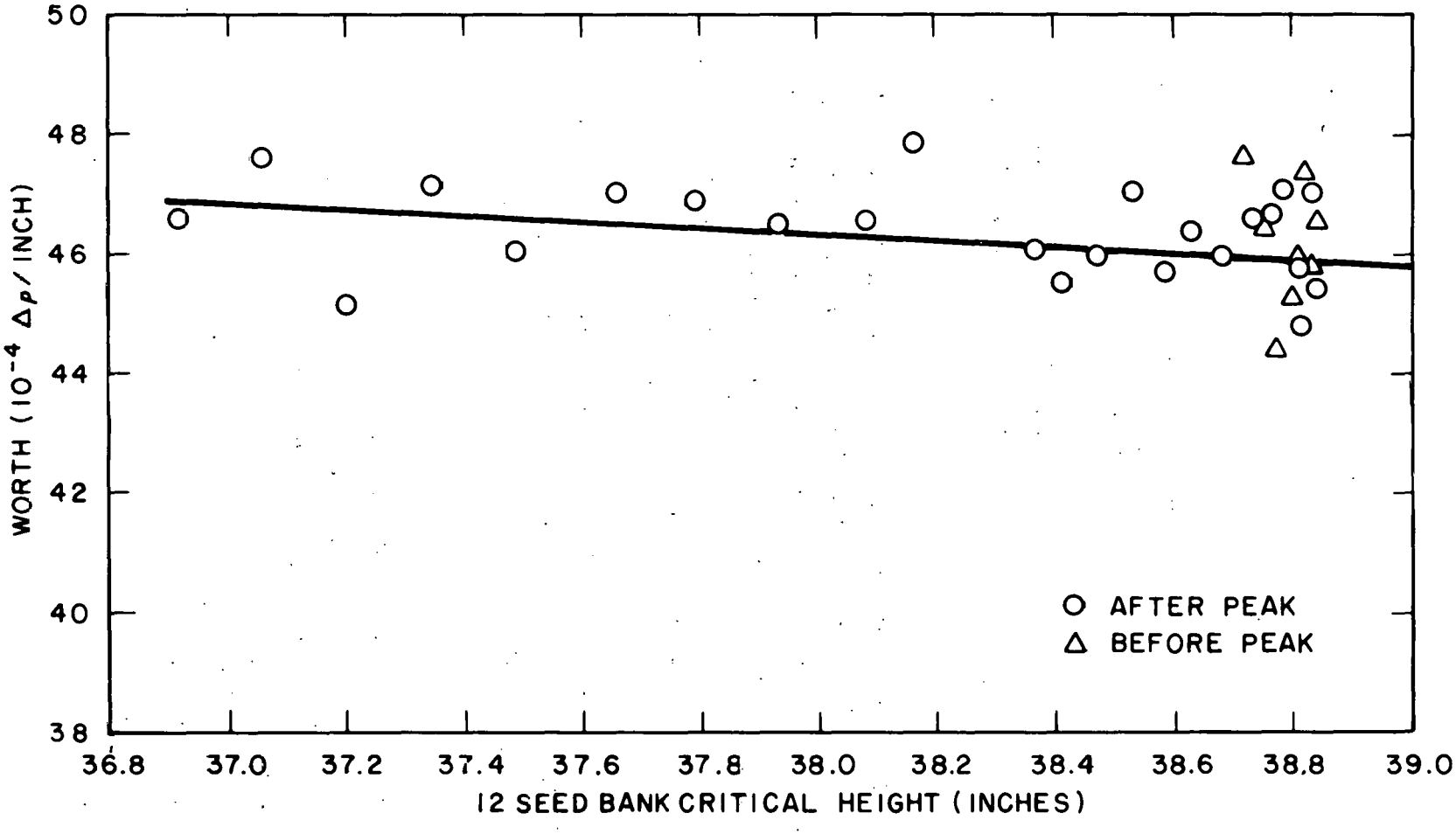

FIGURE V-35 - 12 SEED BANK WORTH VERSUS CRITICAL HEIGHT DURING XENON TRANSIENT

VI. CONCLUSIONS

In general, agreement between the measured test results and calculations using the as-built nuclear design model is good. The reactivity bias is within the off-nominal allowance of ±1% used in predicting the lifetime performance of LWBR. The basis for the ±1% off-nominal reactivity allowance is discussed in Reference 3. In addition, the measured test results confirm the adequacy of the ranges for the various nuclear design parameters assumed in the LWBR Safety Analysis Report (Reference 8).

The following comparisons may be made between the measured test results and predictions based on the as-built nuclear design model for the LWBR core at beginning-of-life.

A. The measured 12 seed bank height at 150°F and 325 psig was 0.55 inch lower than calculated, which implies that the cold core at beginning-of-life was 0.35% $\Delta\rho$ less reactive than predicted. The measured 12 seed bank height at 531°F and 1985 psig (normal operating temperature and pressure) was 0.1 inch lower than calculated, which implies that the hot core at beginning-of-life was 0.05% $\Delta\rho$ more reactive than predicted.

B. The measured 12 seed bank differential reactivity worth at 150°F and 325 psig was 1.07 times larger than calculated. The measured 12 seed bank differential reactivity worth at 531°F and 1985 psig was 1.119 times larger than calculated.

C. The measured value of the uniform temperature coefficient at cold plant conditions was $-0.31 \times 10^{-4} \Delta\rho/°F$ compared to the predicted value of $-0.66 \times 10^{-4} \Delta\rho/°F$. At hot plant conditions, the measured value of the uniform temperature coefficient was $-1.71 \times 10^{-4} \Delta\rho/°F$ compared to the predicted value of $-2.22 \times 10^{-4} \Delta\rho/°F$. The difference between the measured and the predicted values of the uniform temperature coefficient is relatively constant for both cold and hot conditions, varying from $0.35 \times 10^{-4} \Delta\rho/°F$ cold to $0.51 \times 10^{-4} \Delta\rho/°F$ hot.

D. Evaluation of core symmetry based on measured individual seed worths indicates symmetric core operation within ±1%.

E. Measurements of core shutdown reactivity indicate that the LWBR core was 1/2 to 1% $\Delta\rho$ more shutdown with a single Type III seed assembly 34.4 inches withdrawn above the 11 seed bank than calculations predict for beginning-of-life conditions.

F. Measurements of partial bank reactivity worths indicate that the LWBR core is tightly coupled; i.e., each partial bank worth was equal to the sum of the worths of its components, and the sum of the partial bank worths equaled the total bank worth.

G. The measured pressure coefficient of reactivity was 2.1×10^{-6} $\Delta\rho$/psi compared to the calculated value of 2.44×10^{-6} $\Delta\rho$/psi. This is good agreement considering that the reactivities measured were small compared to uncertainties in pressure, temperature, and bank height determination.

H. The measured flow induced reactivity change when switching from four pumps on FAST to three pumps on FAST was 0.43×10^{-4} $\Delta\rho$. The calculated value was 0.36×10^{-4} $\Delta\rho$ assuming that the only reactivity effect was a change in reactor pressure. This indicated that the reactivity change due to dimensional changes during a flow transient is small (less than 0.1×10^{-4} $\Delta\rho$).

I. Results from the zero power thorium and high power copper-nickel flux wire activations were in good agreement with calculated flux distributions in the core. The results indicated symmetric core operation within the experimental uncertainty of the measurements (1 to 2%).

J. The measured 12 seed bank critical position at full power equilibrium xenon at the end of the station startup test was 0.41 inch lower than calculated, which implies that the core was 0.18% $\Delta\rho$ more reactive than predicted for that core condition.

K. The measured power coefficient of reactivity is 1.06 times more negative than calculated and the measured negative temperature coefficient of reactivity at power is 0.95 times lower than the value calculated. The measured 12 seed bank reactivity worth near full power was 1.14 times larger than the calculated value. This result is consistent with the hot, xenon free worth measured at zero power.

L. The measured reactivity worths of equilibrium and peak xenon were higher than calculated by 1.03 and 1.09 times, respectively. The measured value of the power reactivity was 0.91 times lower than the calculated value. The total negative reactivity worth from zero power, xenon free to full power, equilibium xenon was measured as 3.51% $\Delta\rho$. The total negative reactivity worth of power reactivity and equilibrium xenon is smaller than calculated by 9×10^{-4} $\Delta\rho$ or 3%.

M. Explicit three-dimensional Monte Carlo predictions of the response of neutron detectors located in the neutron shield tank outside the Shippingport reactor vessel agreed in absolute value with measured results (within Monte Carlo statistical uncertainty) for the dry core before fill, the wet core after fill, and for full power conditions.

VII. REFERENCES

1. D.J. Miller and W.A. Shaughnessy, "An On-Line Solid-State Reactivity Computer for Reactor Physics Testing," WAPD-TM-896, August 1970.

2. L.B. Freeman, et al, "The Calculational Model Used in the Analysis of Nuclear Performance of the Light Water Breeder Reactor (LWBR)," WAPD-TM-1314, August 1978.

3. H.C. Hecker, Jr., "Summary of the Nuclear Design and Performance of the Light Water Breeder Reactor (LWBR)," WAPD-TM-1326, June 1979.

4. C.J. Pfeifer, C.J. Spitz, PDQ-8 Reference Manual, WAPD-TM-1266, May, 1978.

5. H.J. Amster and J.B. Callaghan, "KATE-1, A Program for Calculating Wigner-Wilkins and Maxwellian Averaged Thermal Constants on the Philco-2000," WAPD-TM-232, October 1960.

6. H. Bohl, Jr. and A.P. Hemphull, "MUFT-5, A Fast Neutron Spectrum Program for the Philco-2000," WAPD-TM-218, February 1961. Updated versions of MUFT and KATE are contained in the PAX program for the CDC-6600 and 7600 computers.

7. N.R. Candelore, R.C. Gast, L.A. Ondis II, "RCP01 - A Monte Carlo Program for Solving Neutron and Photon Transport Problems in Three-Dimensional Geometry with Detailed Energy Description," WAPD-TM-1267, August 1978.

8. Safety Analysis Report for the Light Water Breeder Reactor.

9. G.I. Bell and S. Glasstone, "Nuclear Reactor Theory", page 283, Van Nostrand Reinhold Company, New York, 1970.

APPENDIX A
FLUX WIRE ACTIVATION PROFILES

Table 1
List of Flux Wire Irradiations Performed Near Beginning of Life

Test Performance Sequence No.	Activation Number	Irradiation Date and Time	Type of Wire	Irradiation Time (Minutes)	Indicated Power Level (%)	12 Seed Bank Position (Inches)	No. of Wires Counted
1	1	9/3/77, 16:40	Thorium	150	1	32.73	6
1	2	9/4/77, 06:16	Thorium	150	1	32.73	4
3	1	9/14/77, 11:18	Copper-Nickel	15	68	36.71	5
4	1	9/15/77, 11:35	Copper-Nickel	15	71	38.96	4
5	1	9/22/77, 01:59	Copper-Nickel	10	97	41.80	5
5	2	9/22/77, 12:47	Copper-Nickel	10	97	41.89	4

LEGEND

▲-SEED OUTLET T/C LOCATION (21)
△-SEED INLET T/C LOCATION (7)
■-BLANKET OUTLET T/C LOCATION (12)
□-BLANKET FLOWMETER LOCATION (6)
●-FLUX THIMBLE LOCATION (8)
○-SEED FLOWMETER LOCATION (10)

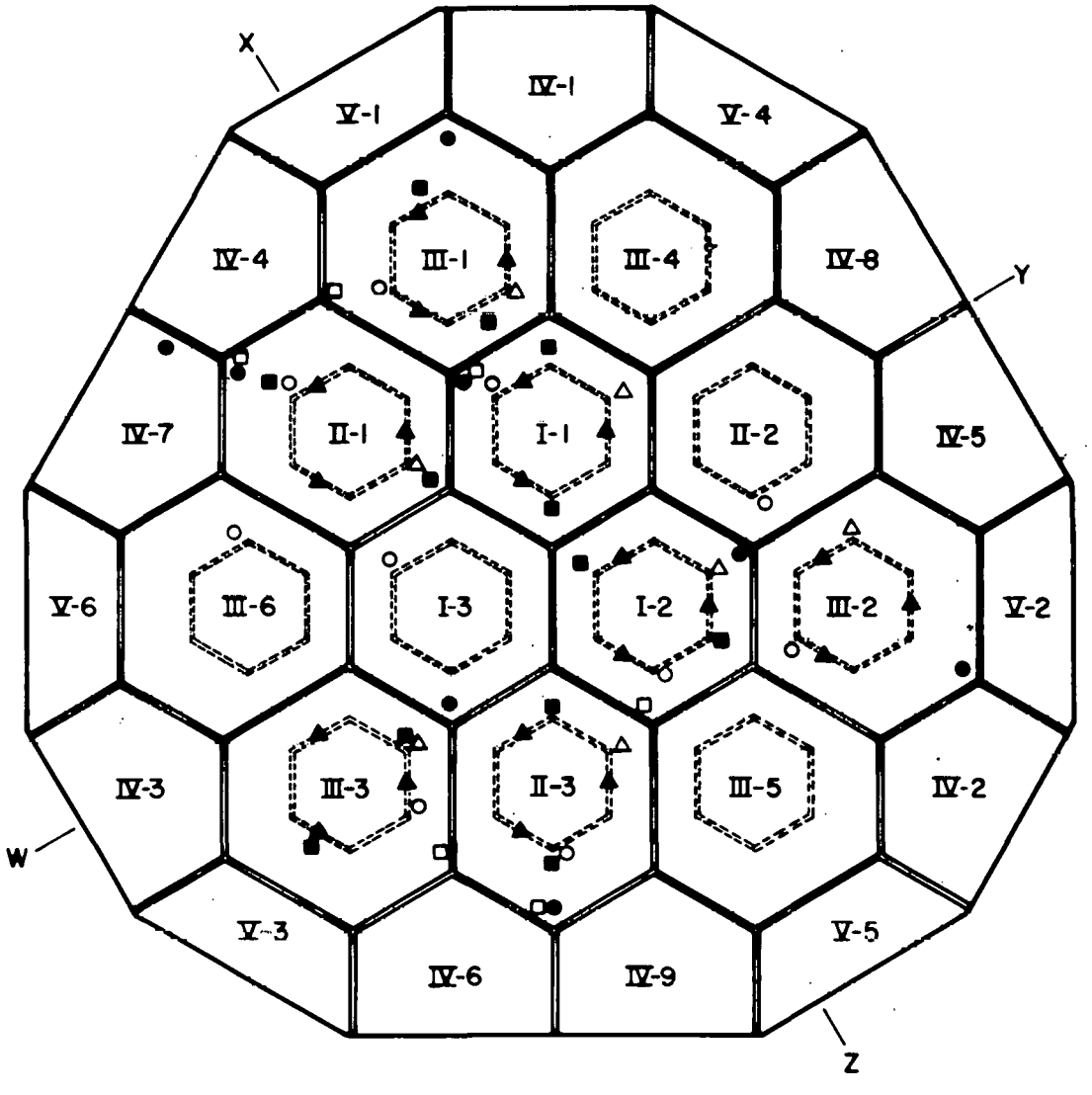

FIGURE I - IN-CORE INSTRUMENTATION LOCATIONS

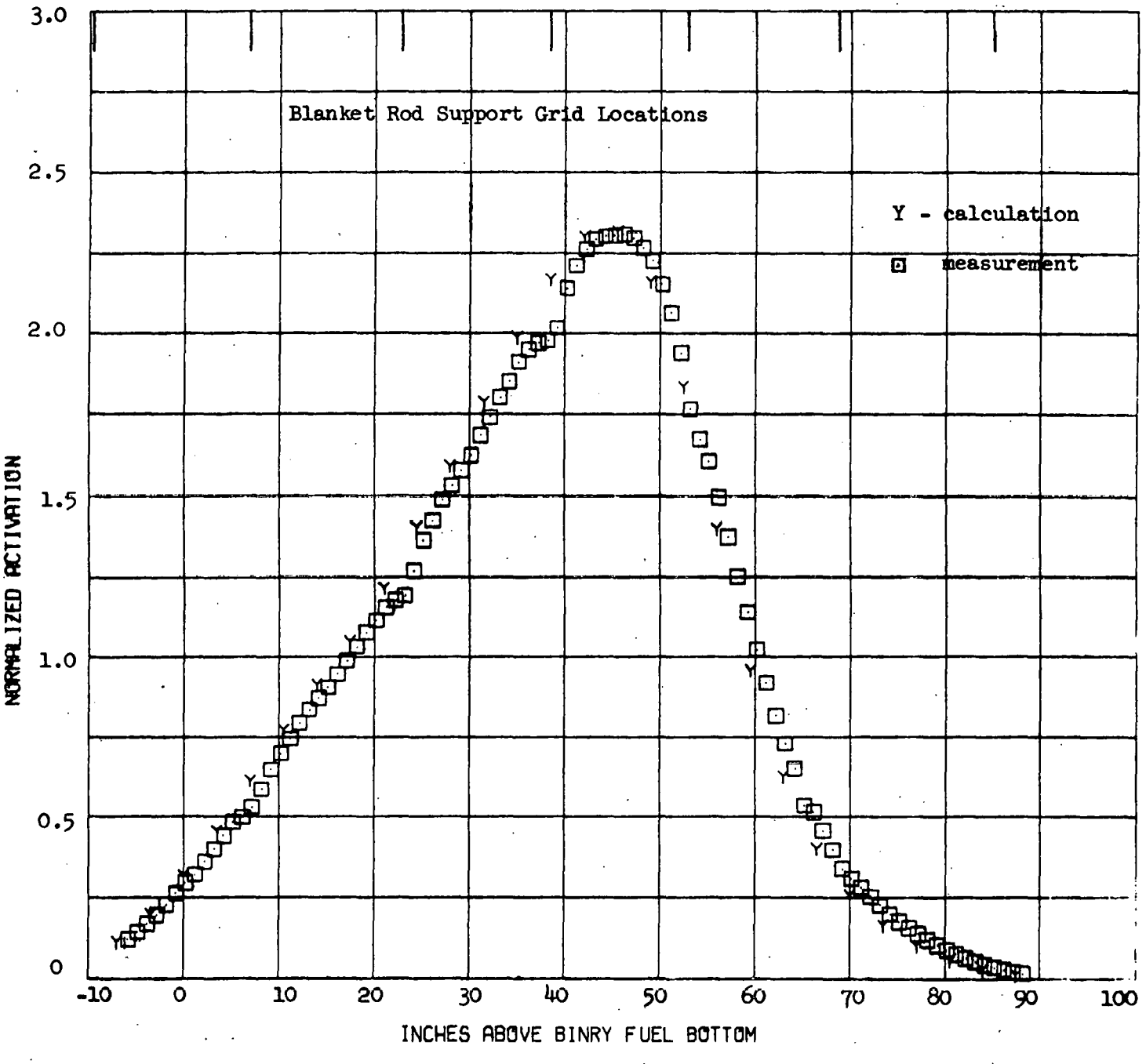

Thorium Activation Profile Near Zero Power For Module I-1

FIGURE 2

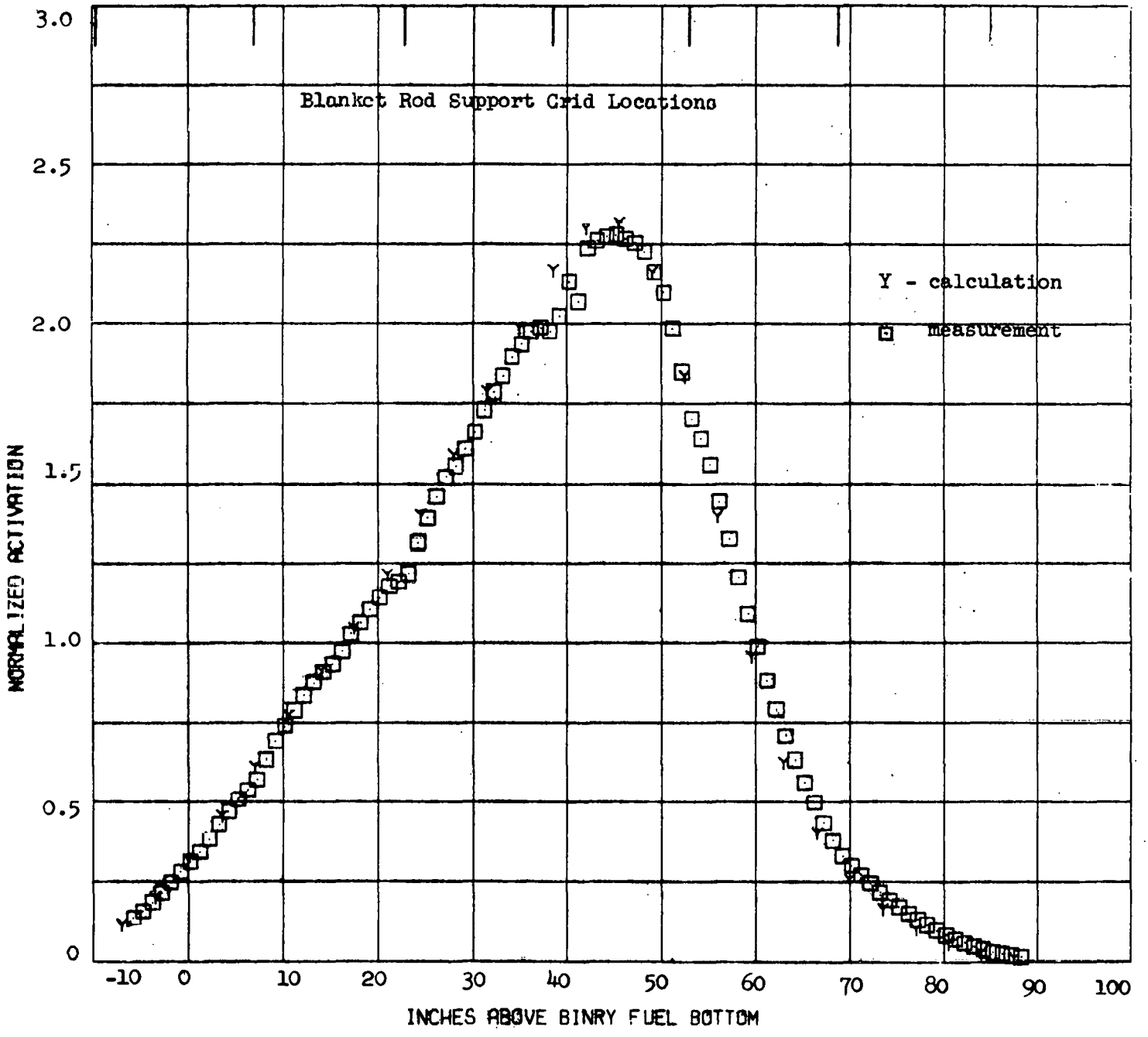

Thorium Activation Profile Near Zero Power for Module I-2

FIGURE 3

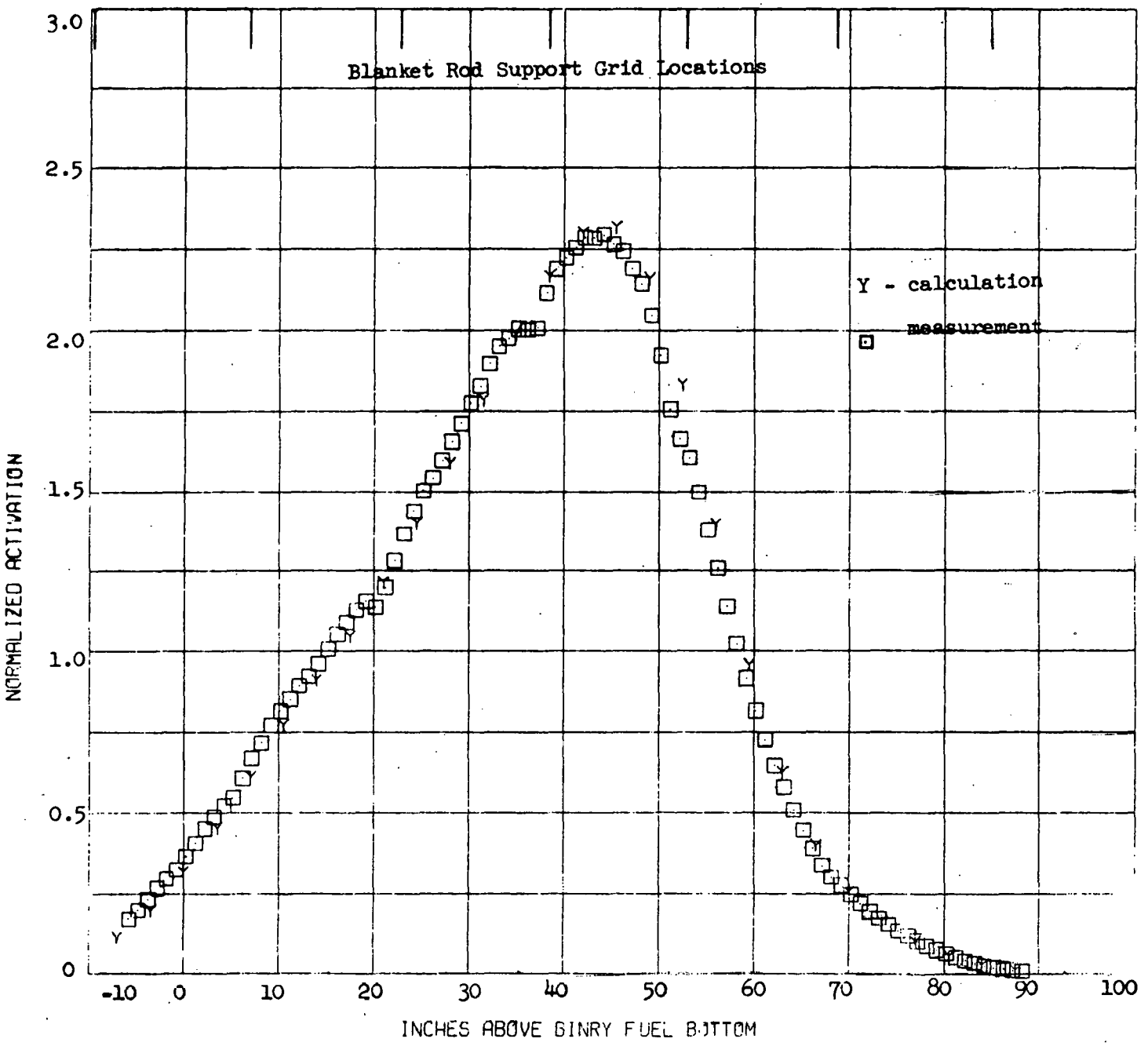

Thorium Activation Profile Near Zero Power for Module I-3

FIGURE 4

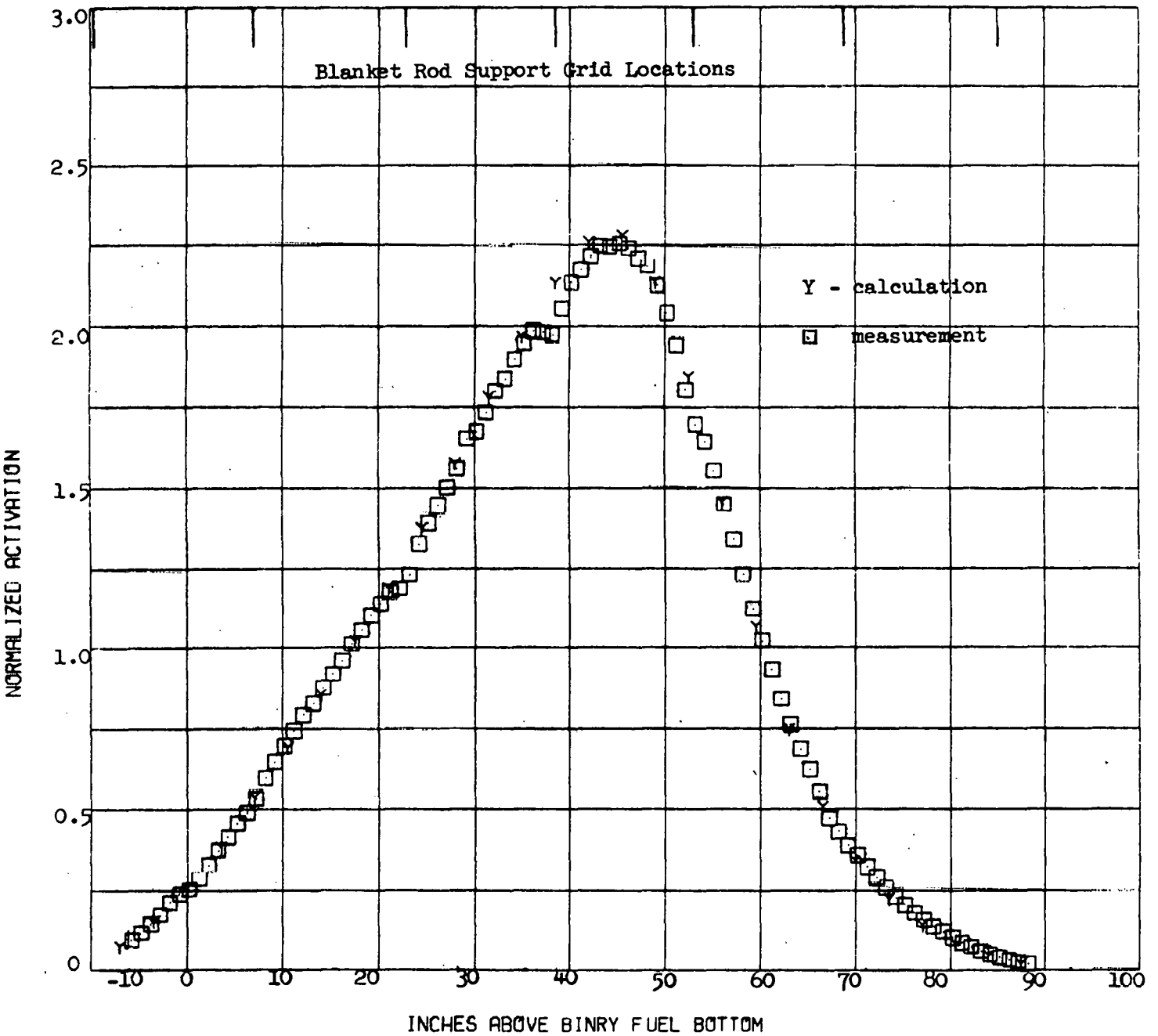

Thorium Activation Profile Near Zero Power for Module II-1

FIGURE 5

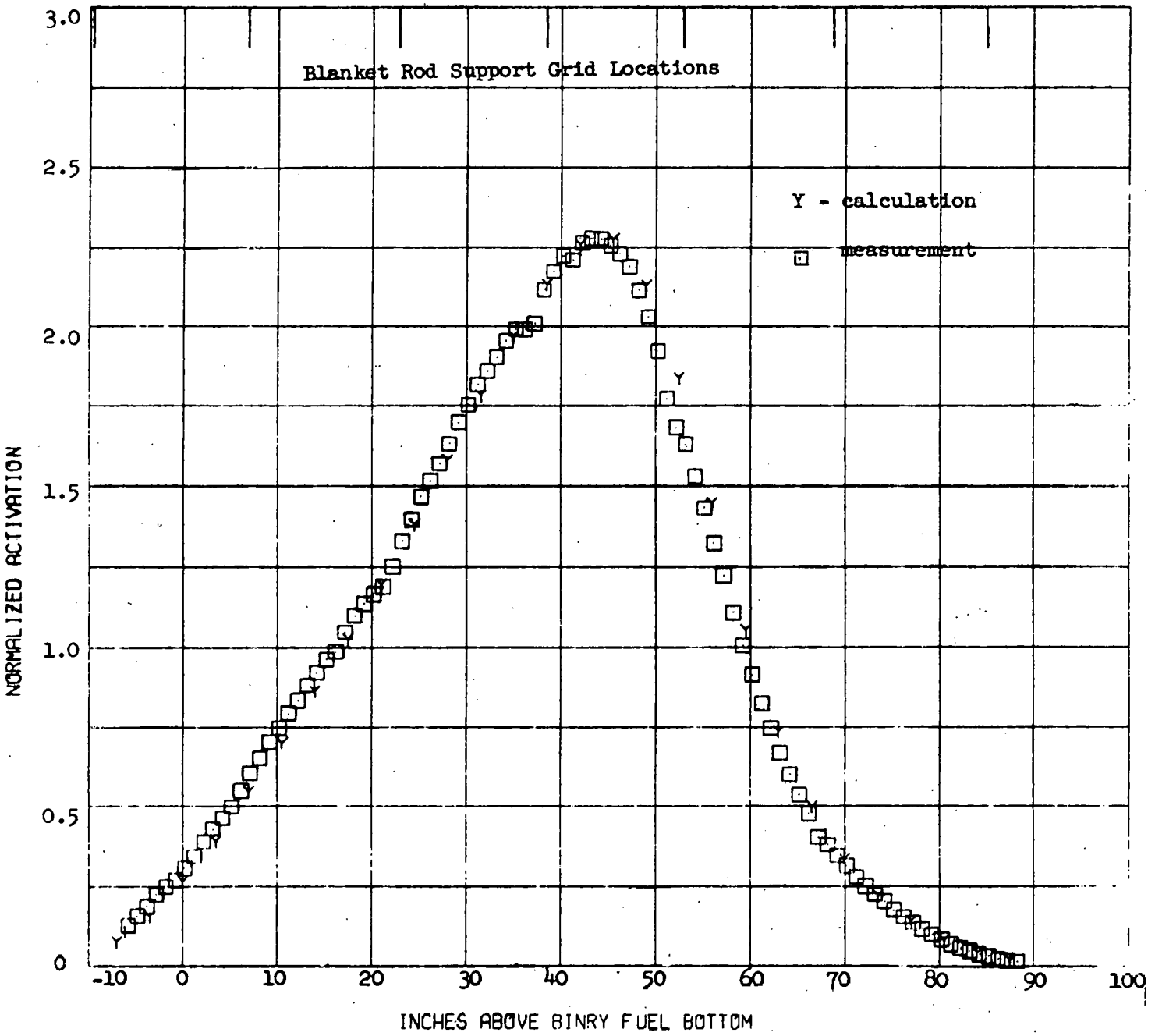

Thorium Activation Profile Near Zero Power for Module III-1

FIGURE 6

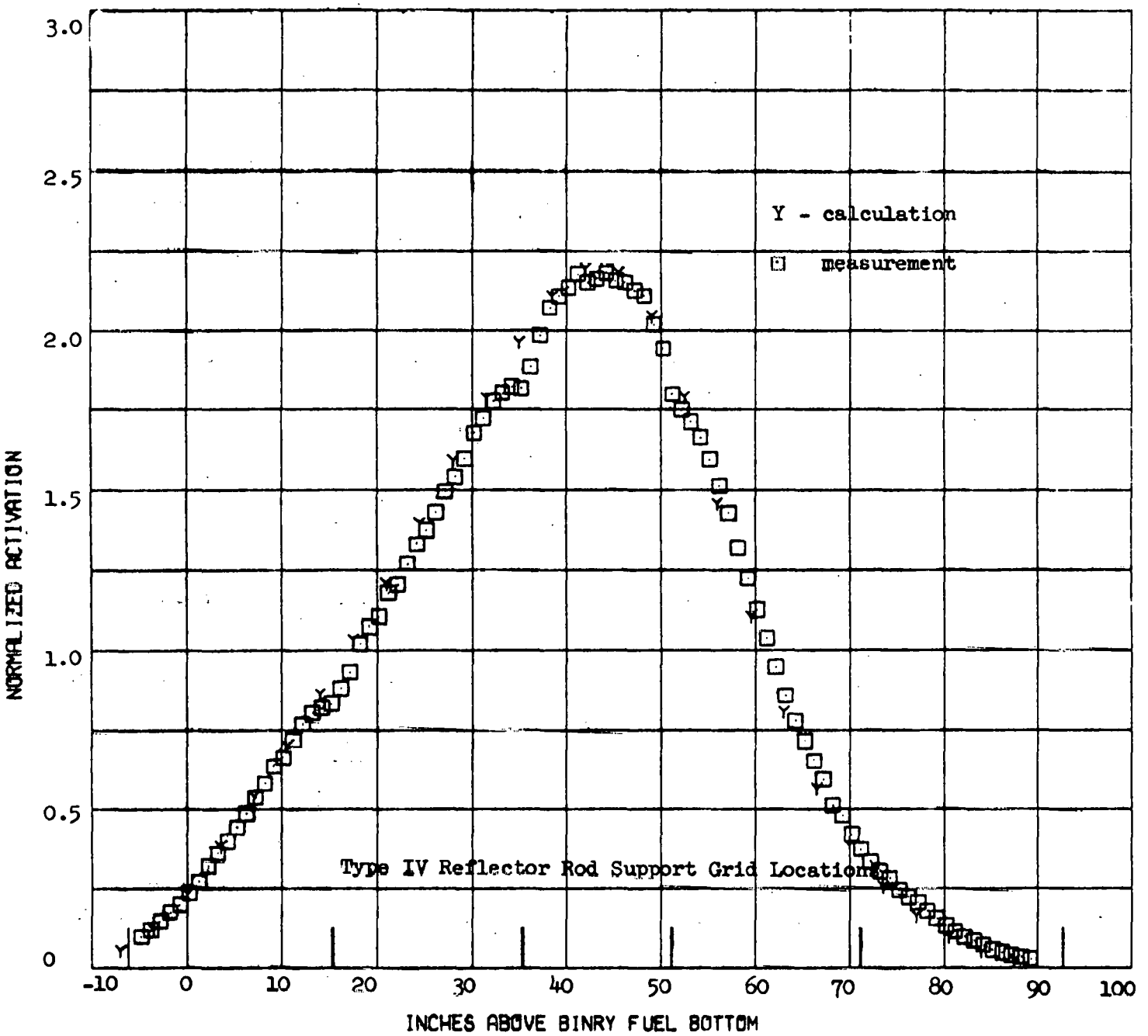

Thorium Activation Profile Near Zero Power for Module IV-7

FIGURE 7

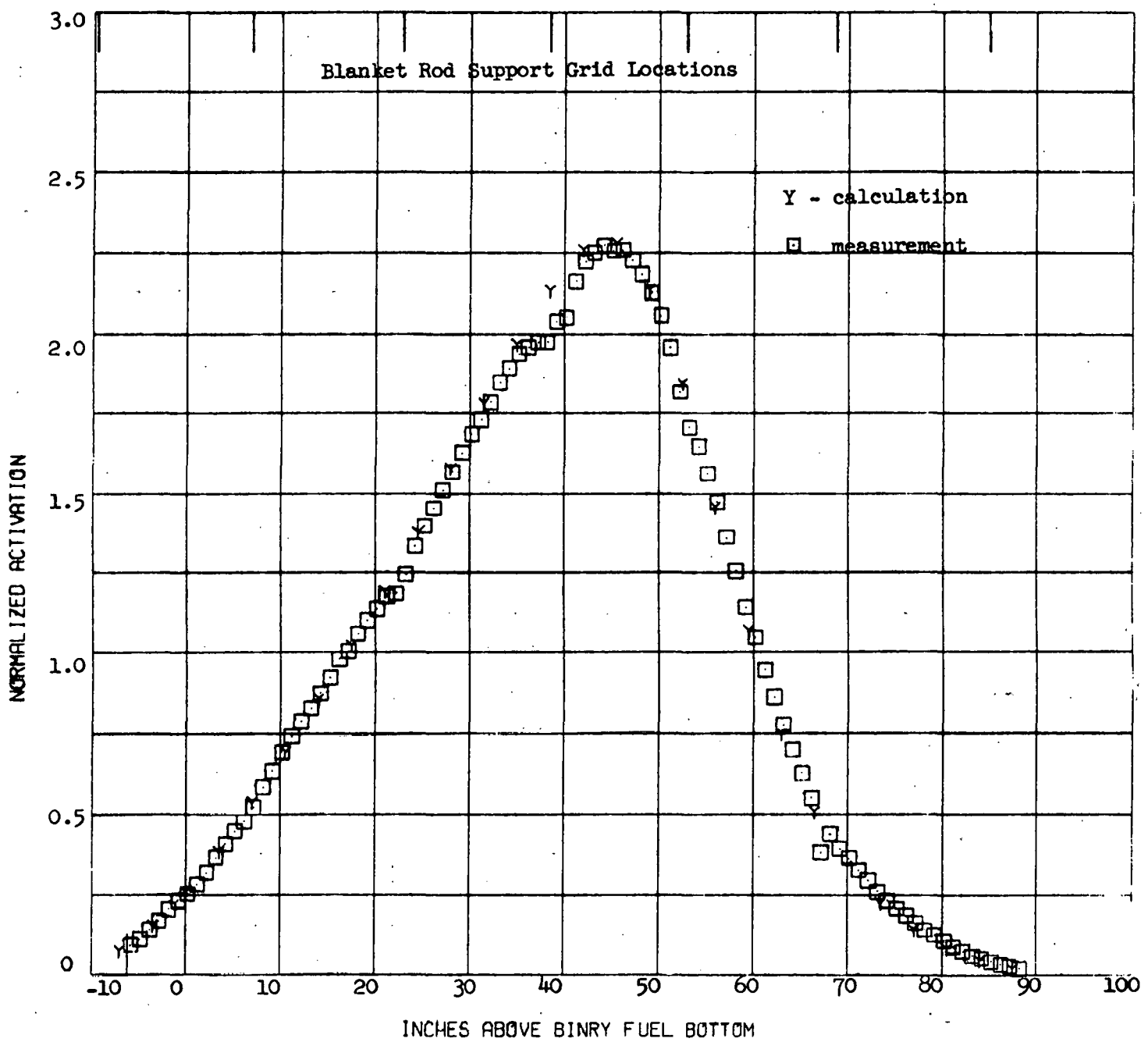

Thorium Activation Profile Near Zero Power for Module II-1

FIGURE 8

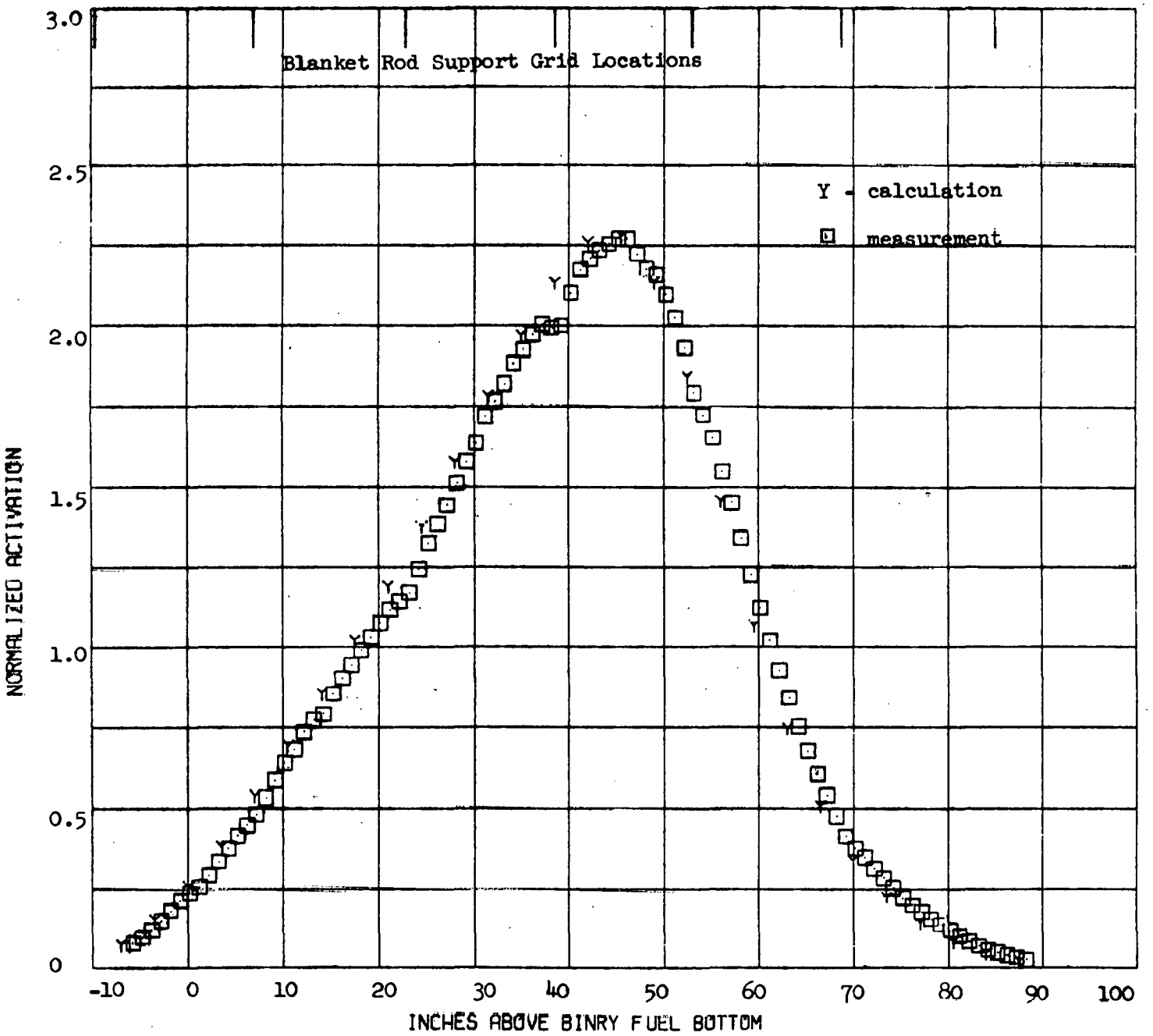

Thorium Activation Profile Near Zero Power for Module II-3

FIGURE 9

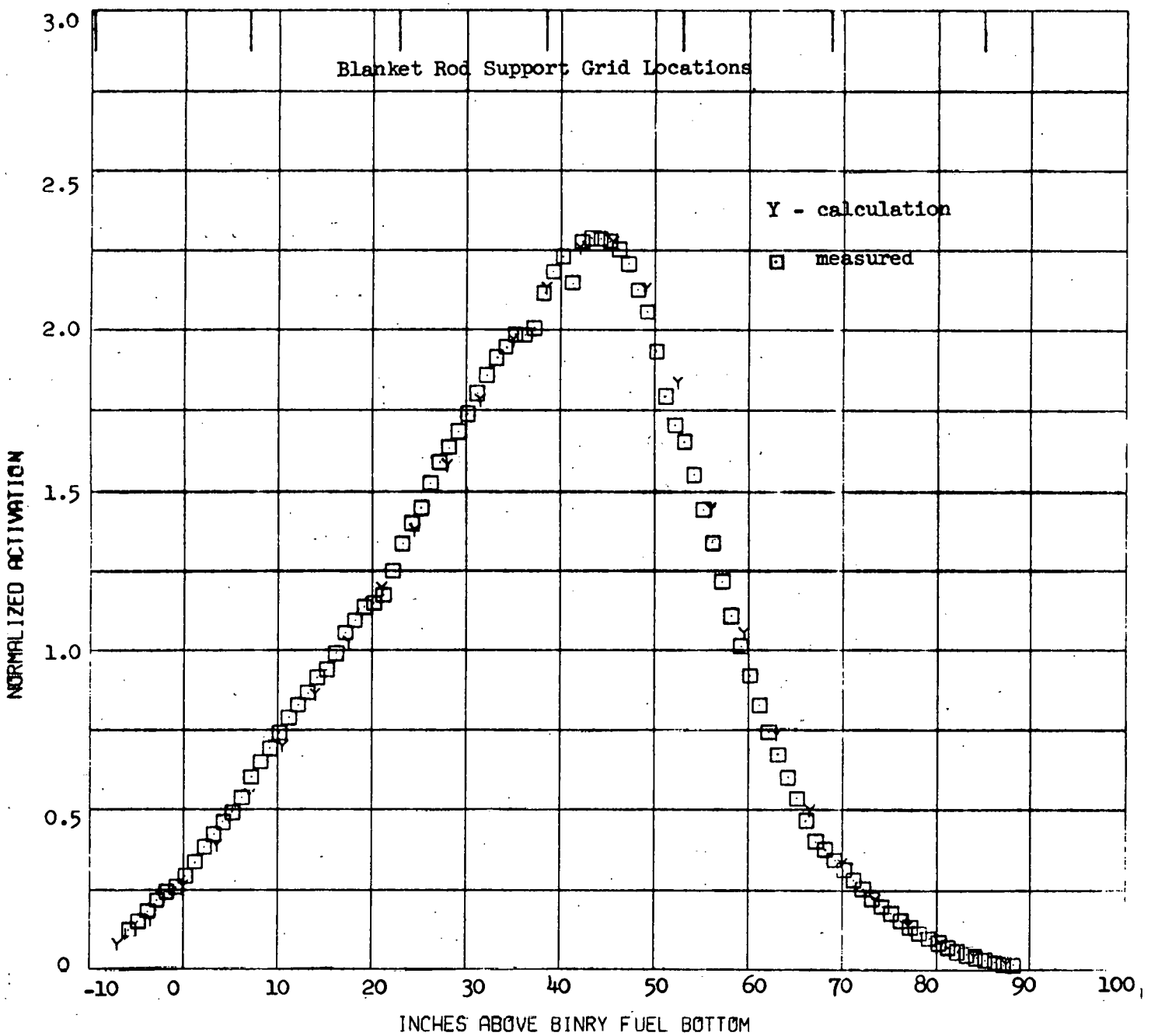

Thorium Activation Profile Near Zero Power for Module III-1

FIGURE 10

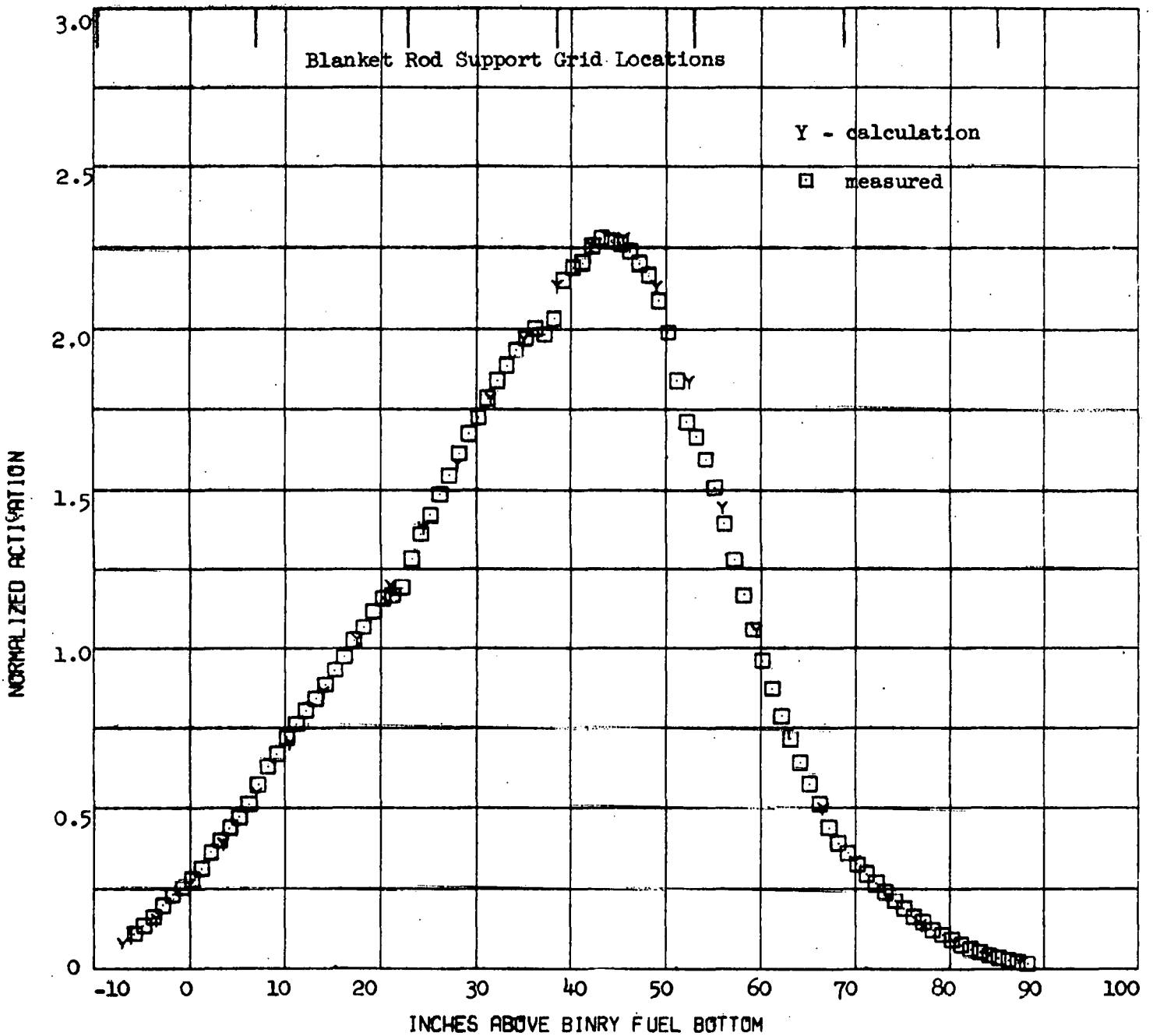

Thorium Activation Profile Near Zero Power for Module III-2

FIGURE 11

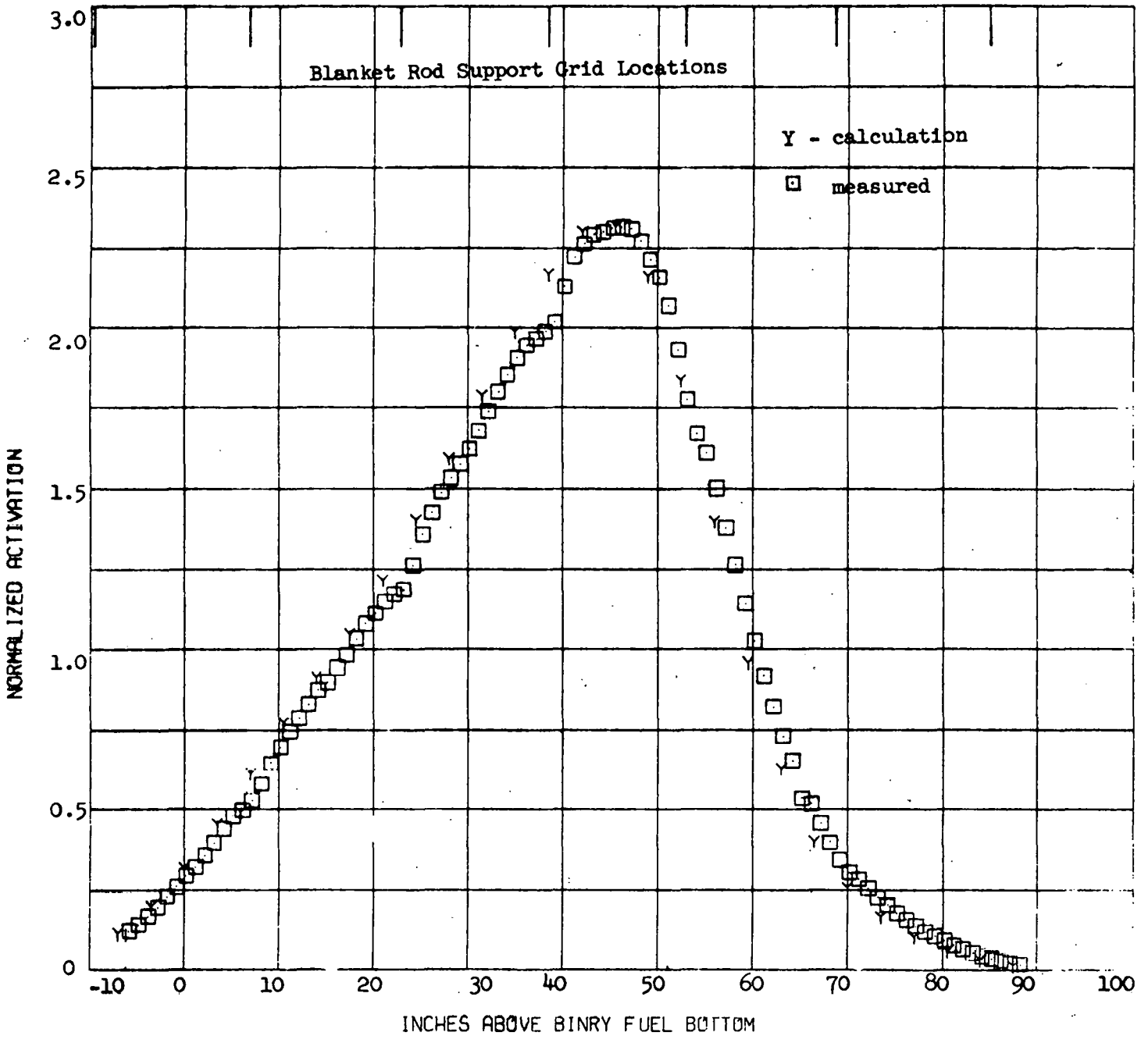

Thorium Activation Profile Near Zero Power for Module I-1 (Repeat Count)

FIGURE 12

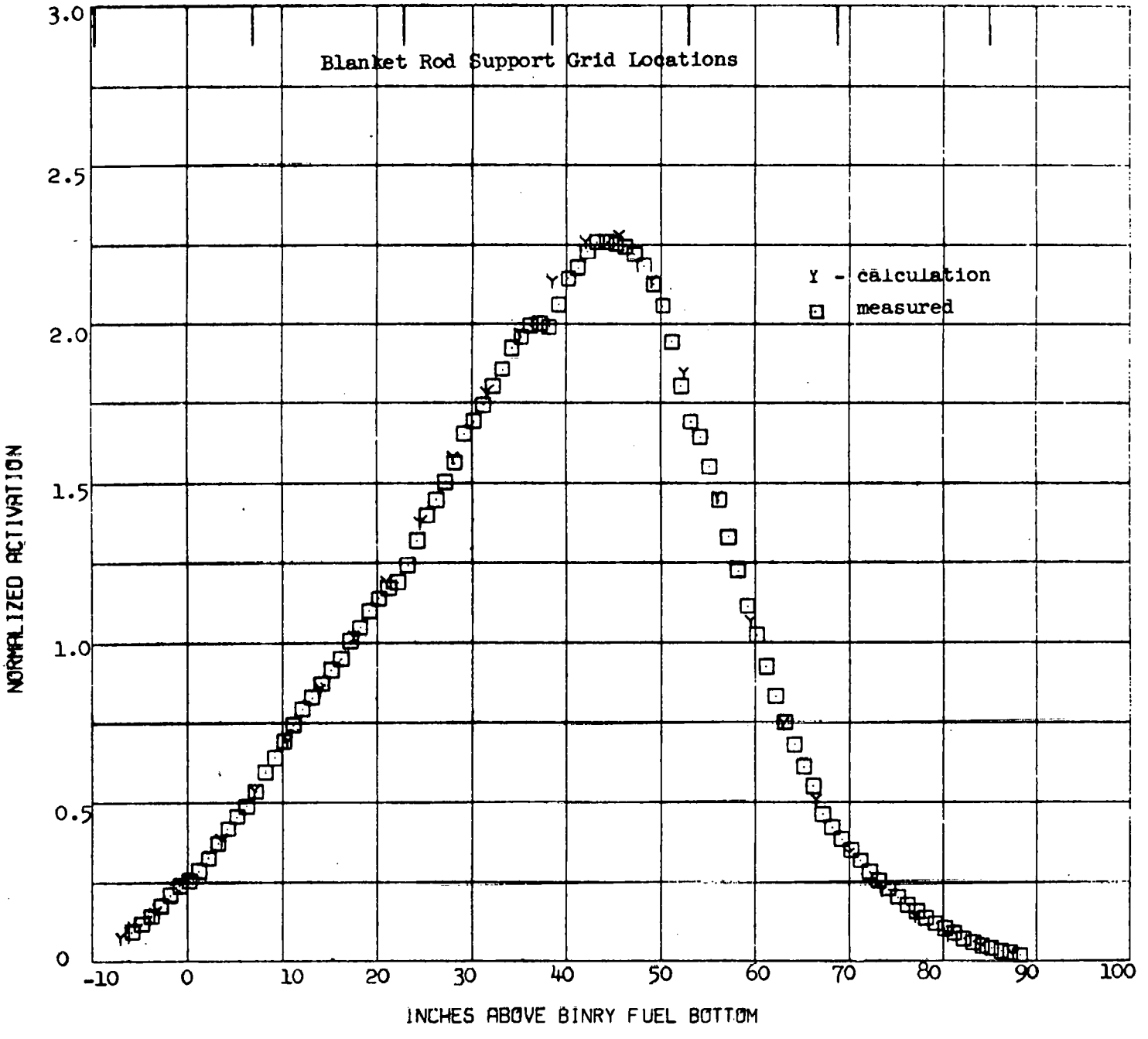

Thorium Activation Profile Near Zero Power for Module II-1 (Repeat Count)

FIGURE 13

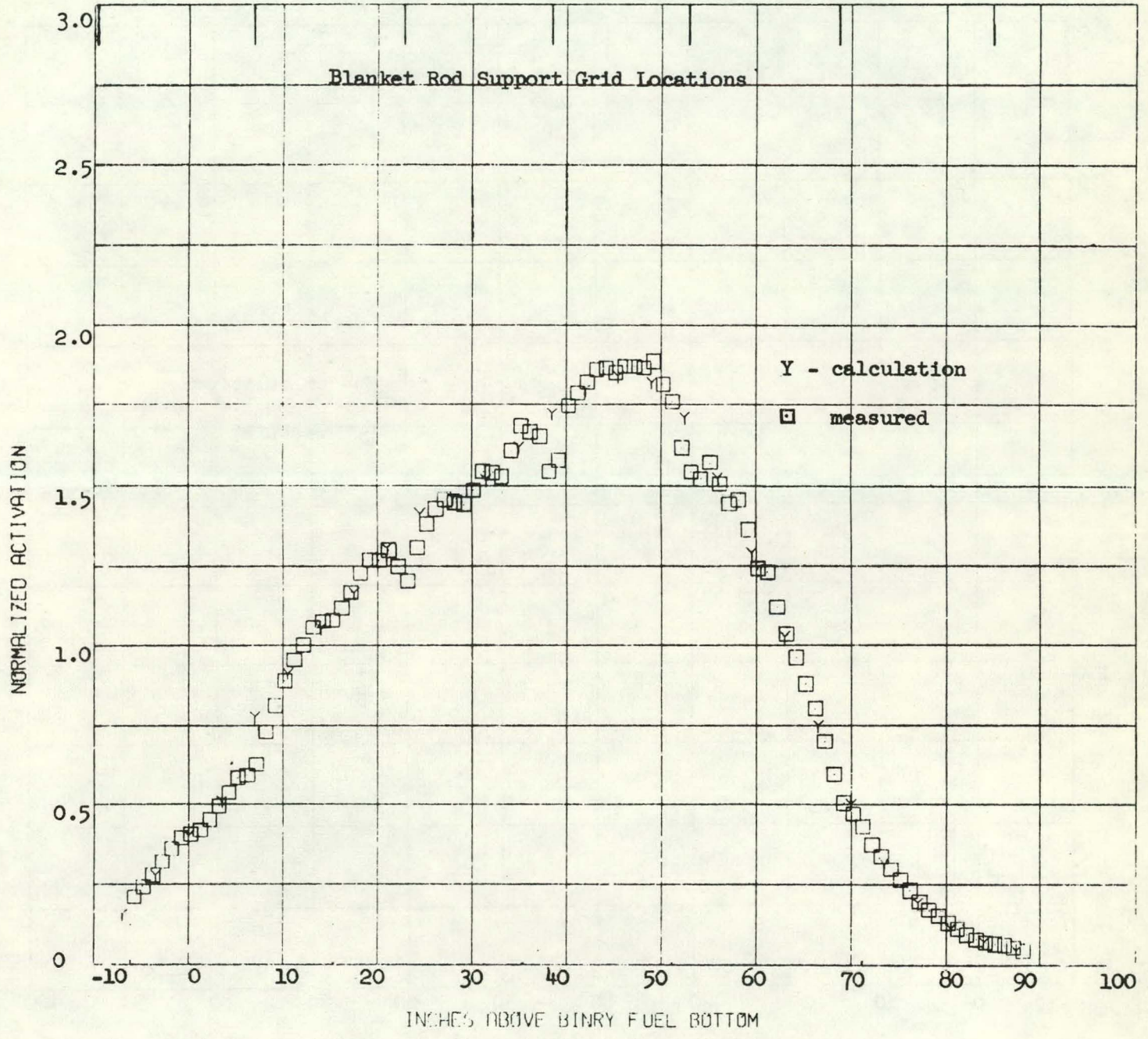

Copper Activation Profile at Full Power, Equilibrium Xenon for Module I-1

FIGURE 14

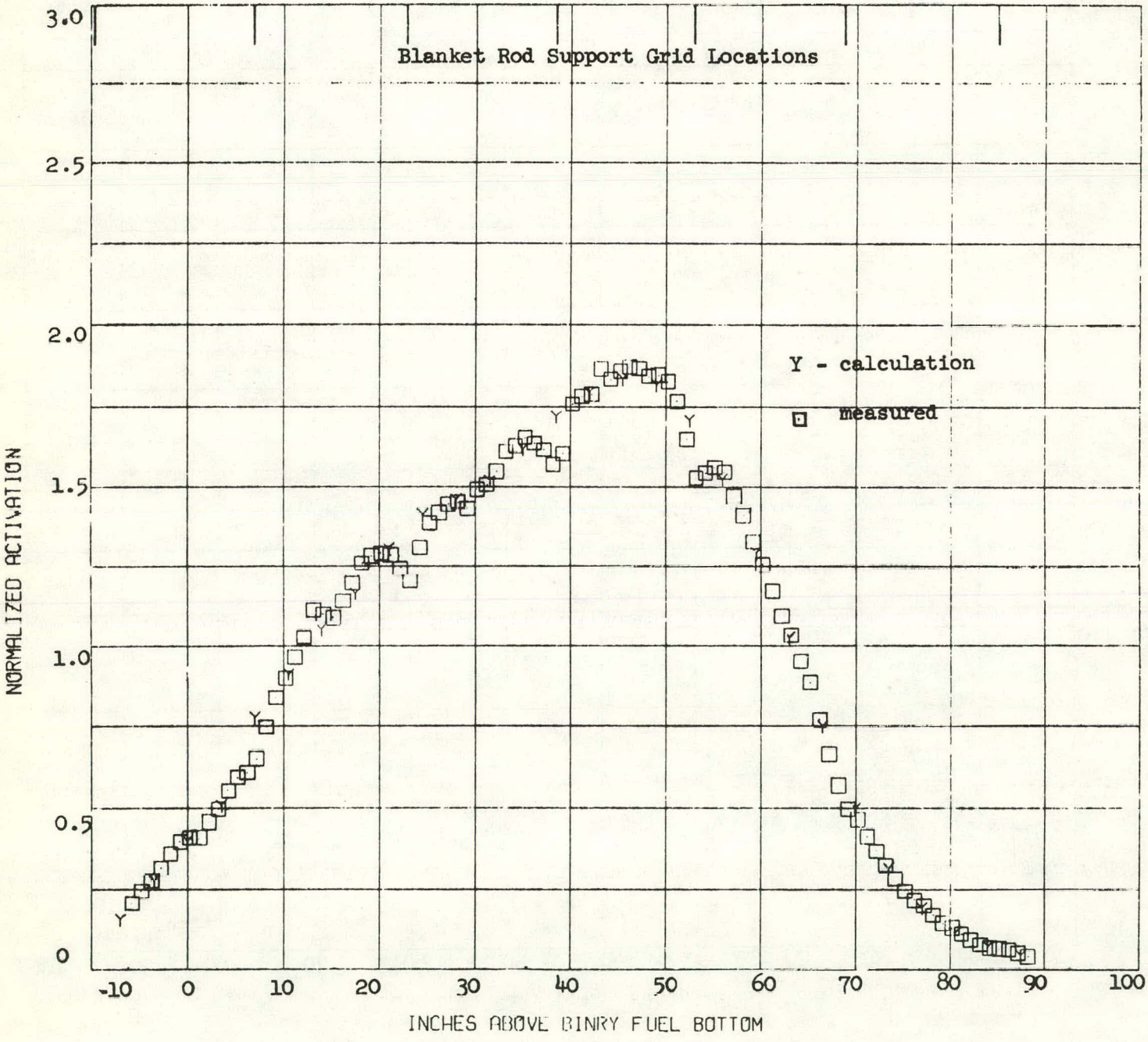

Copper Activation Profile at Full Power, Equilibrium Xenon for Module I-2

FIGURE 15

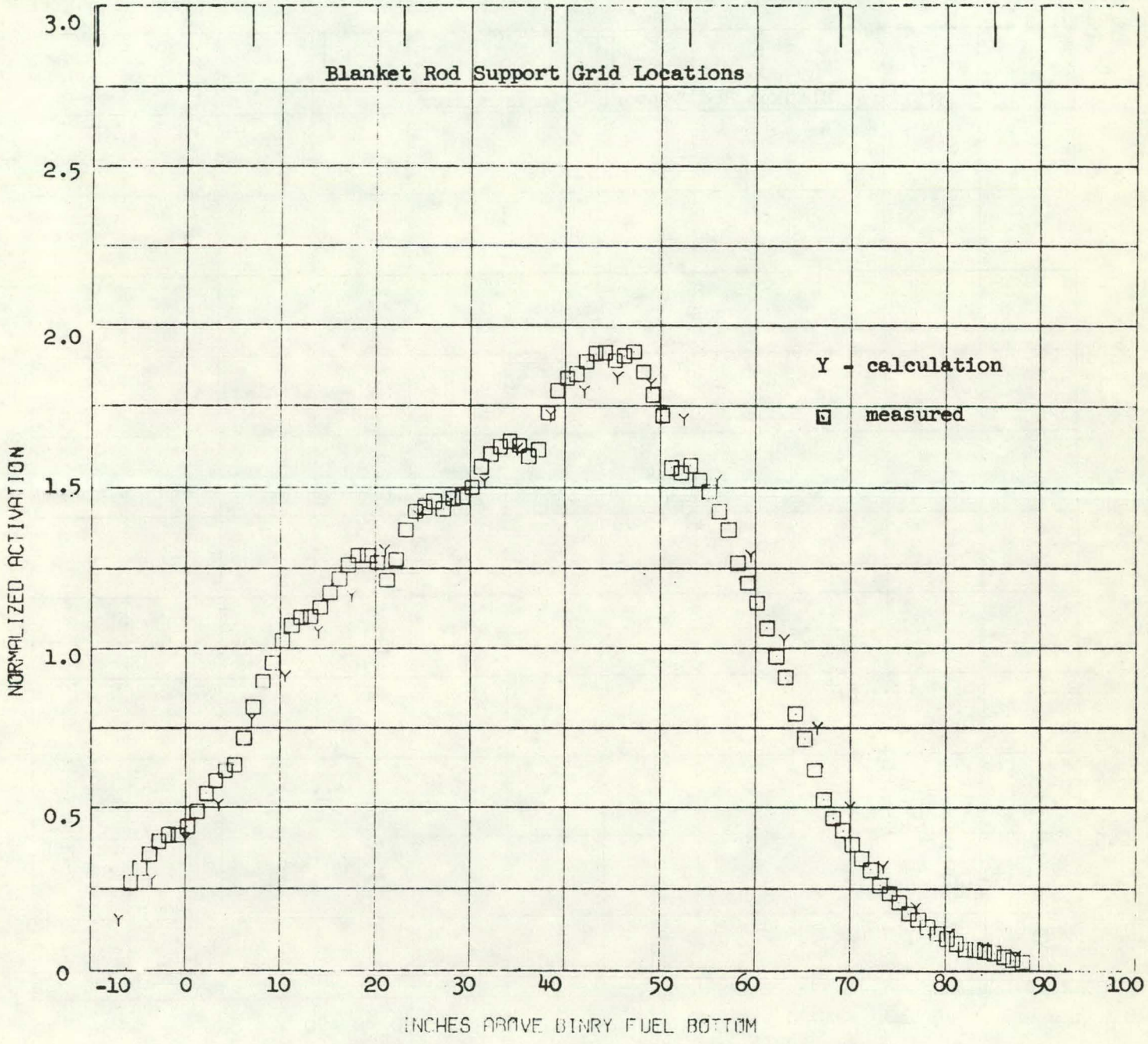

Copper Activation Profile at Full Power, Equilibrium Xenon for Module I-3

FIGURE 16

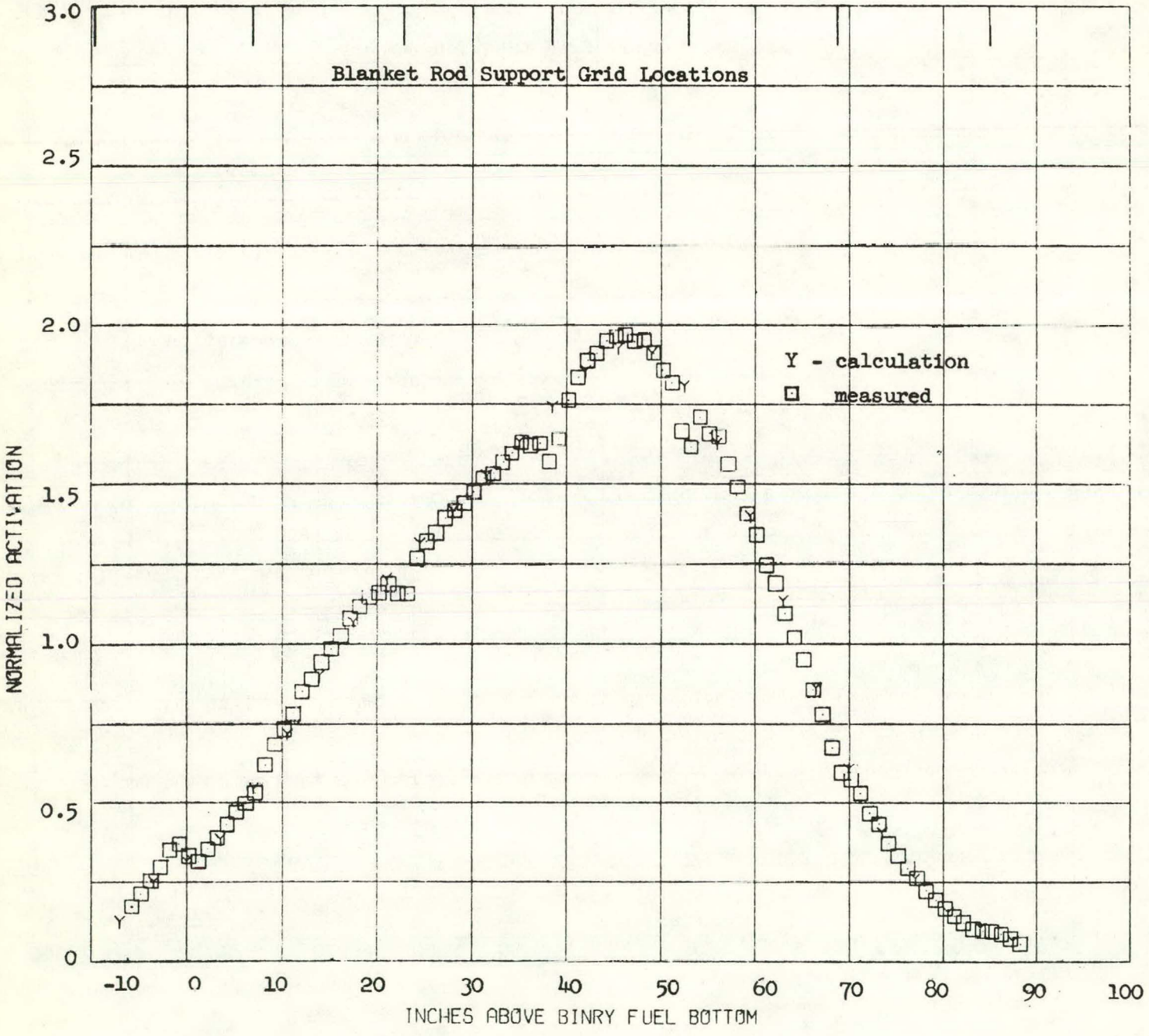

Copper Activation Profile at Full Power, Equilibrium Xenon for Module II-1

FIGURE 17

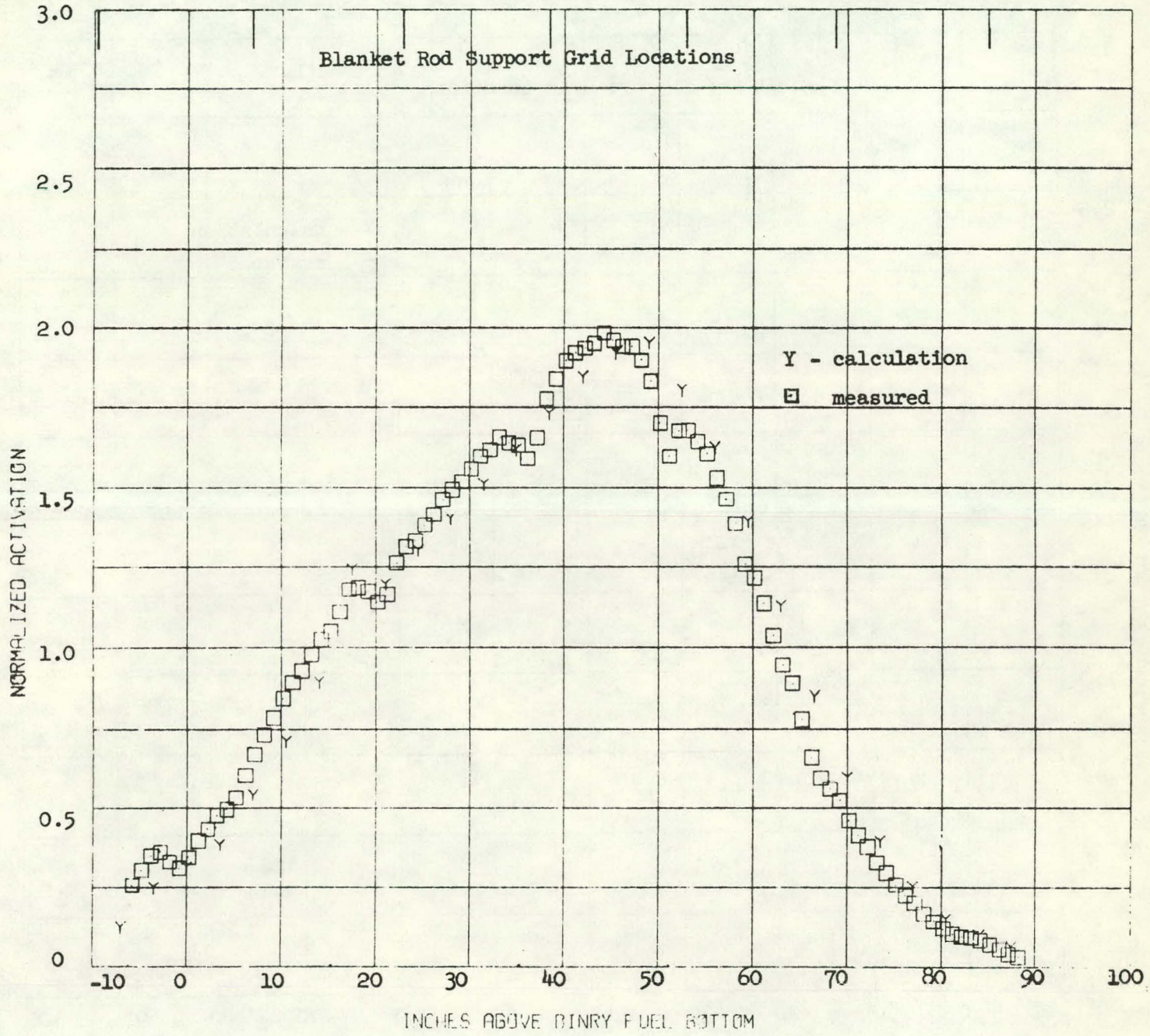

Copper Activation Profile at Full Power, Equilibrium Xenon for Module III-1

FIGURE 18

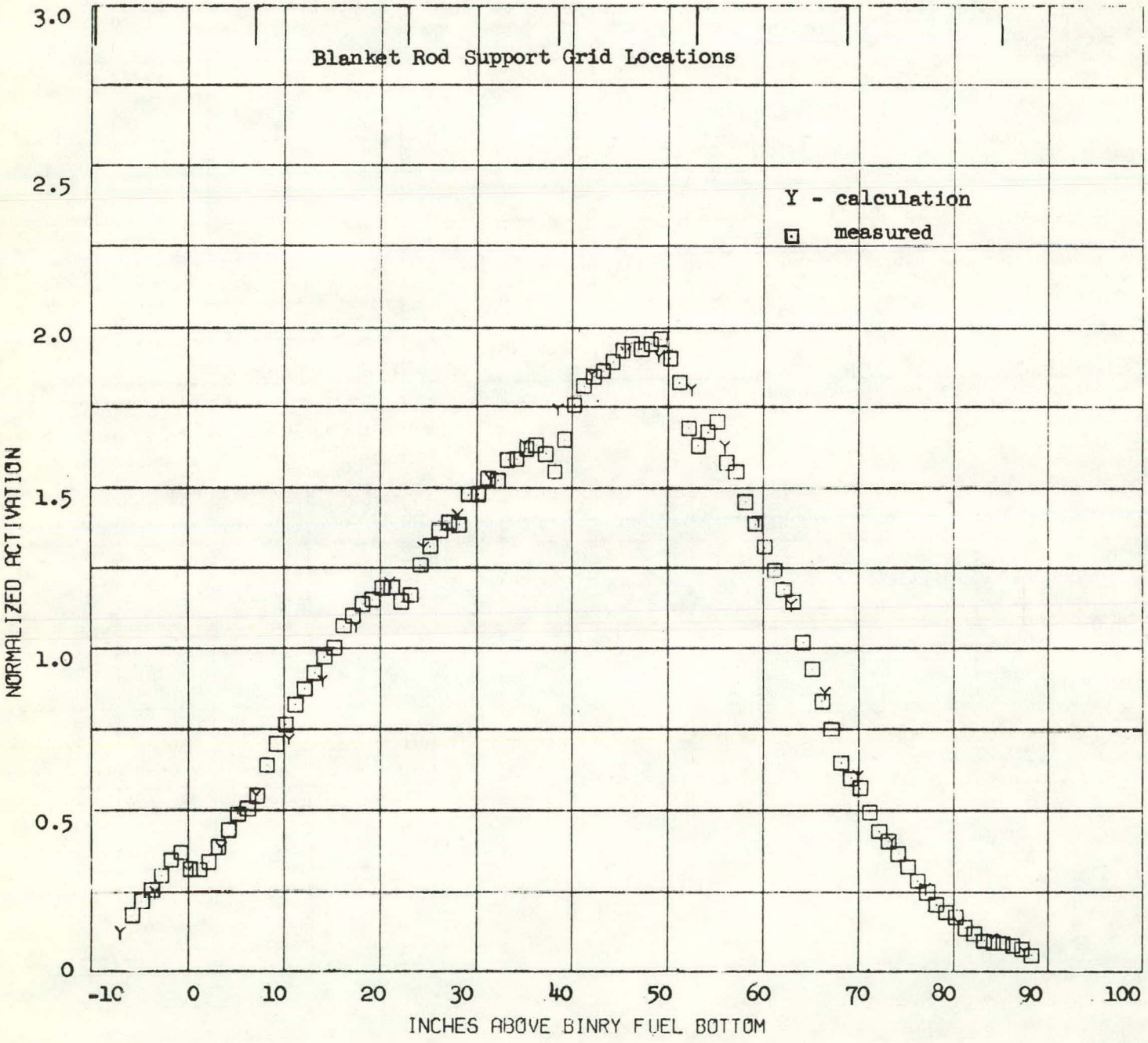

Copper Activation Profile at Full Power, Equilibrium Xenon for Module II-1

FIGURE 19

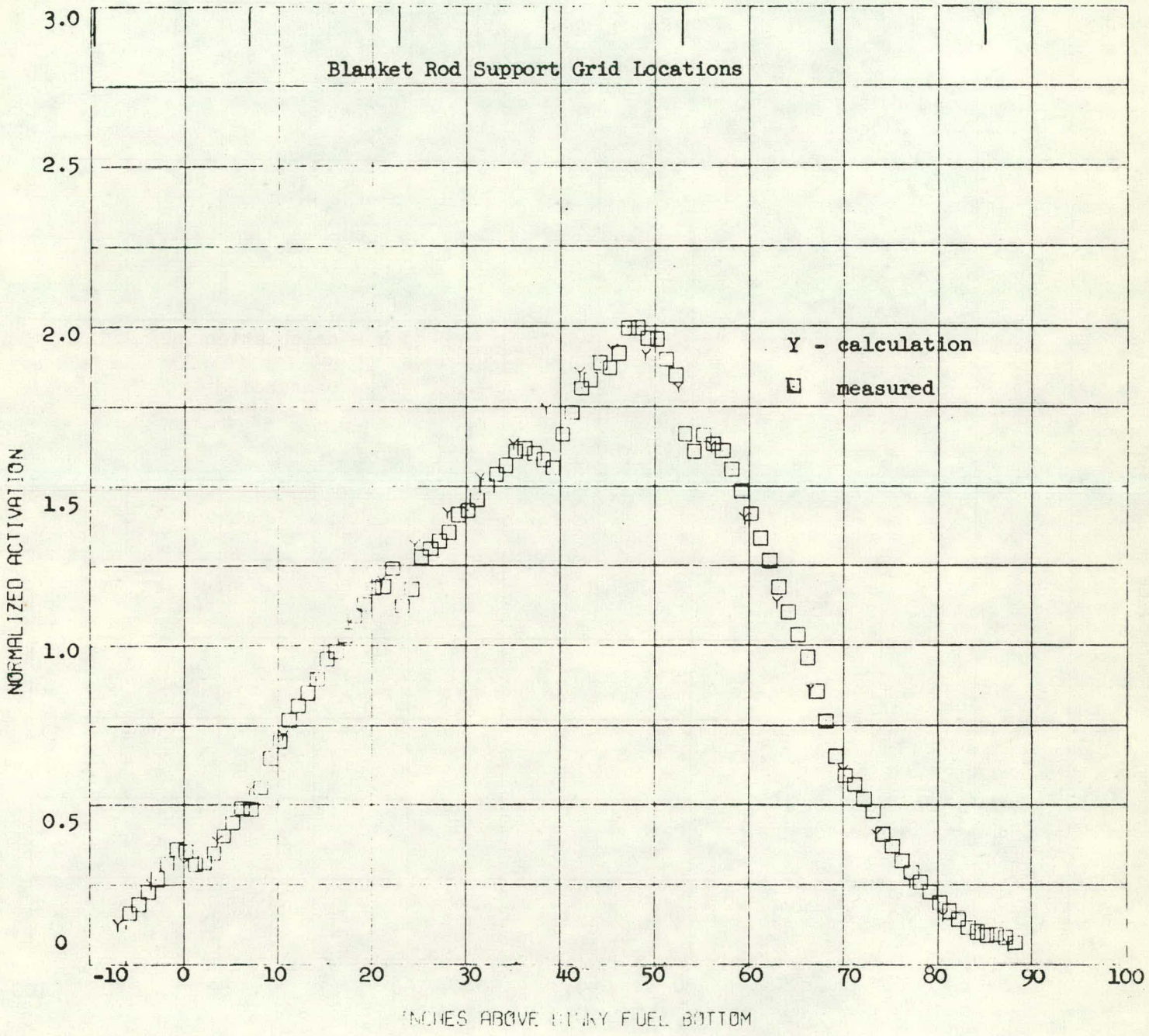

Copper Activation Profile at Full Power, Equilibrium Xenon for Module II-3

FIGURE 20

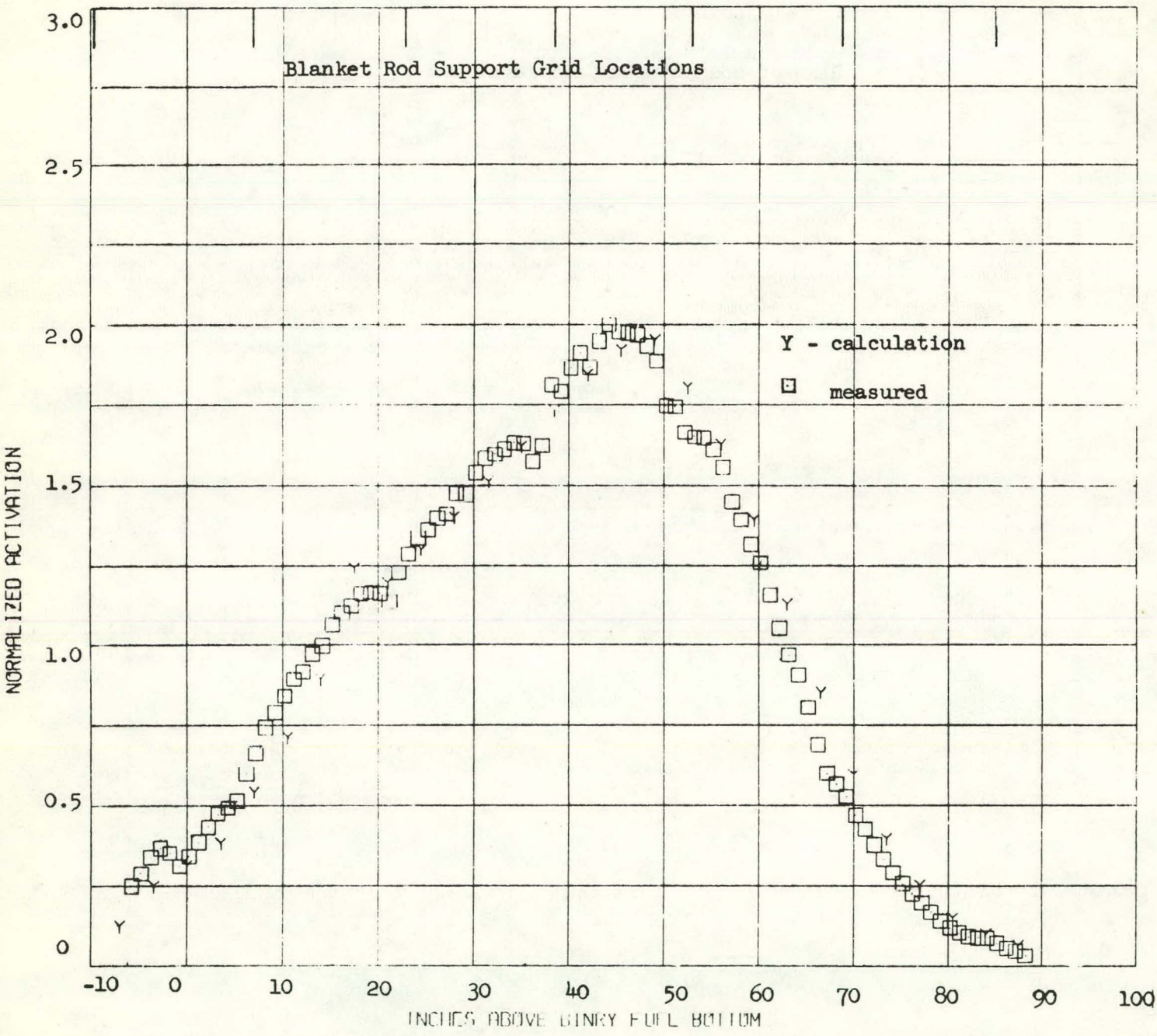

Copper Activation Profile at Full Power, Equilibrium Xenon for Module III-1

FIGURE 21

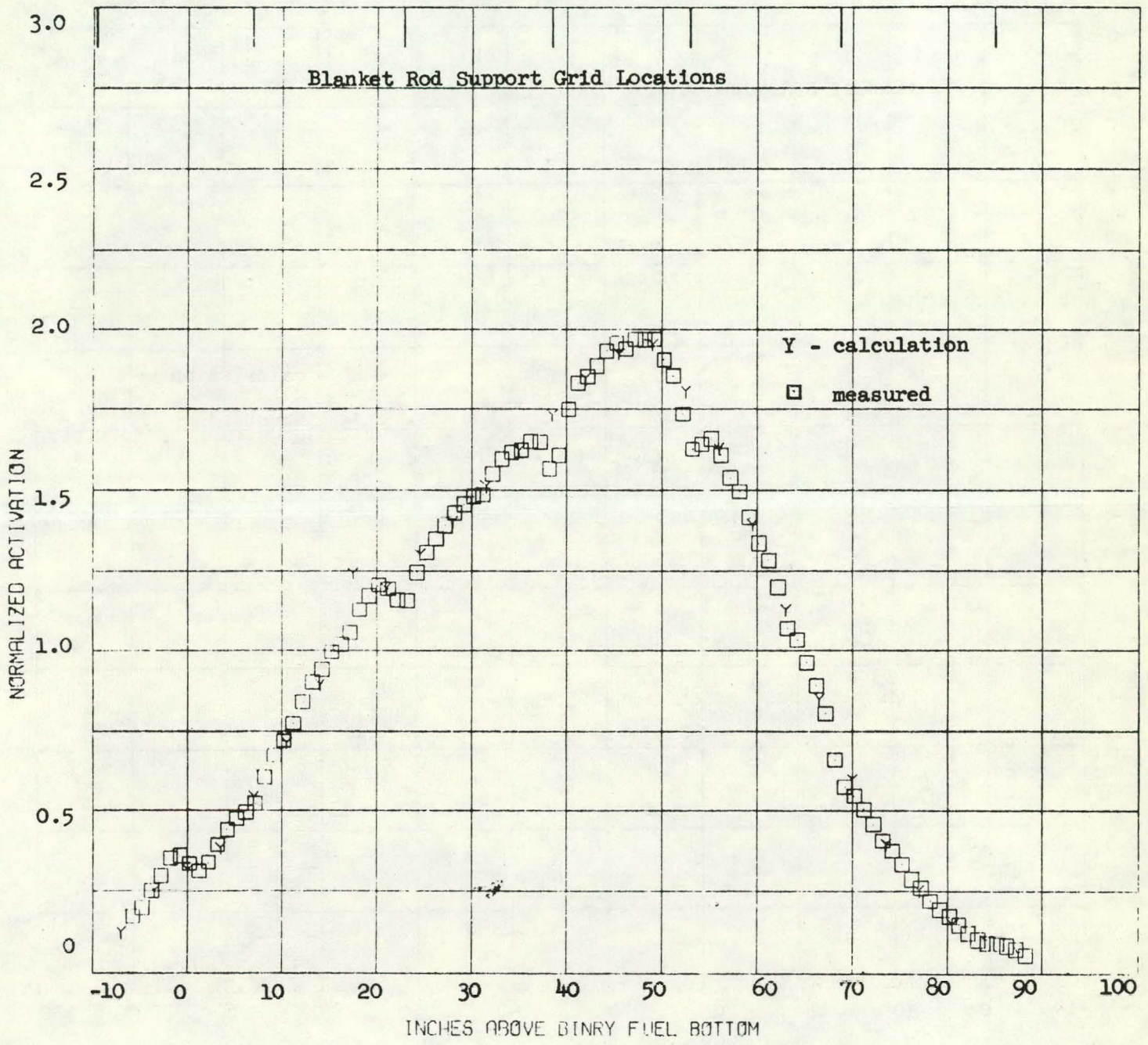

Copper Activation Profile at Full Power, Equilibrium Xenon for Module III-2

FIGURE 22

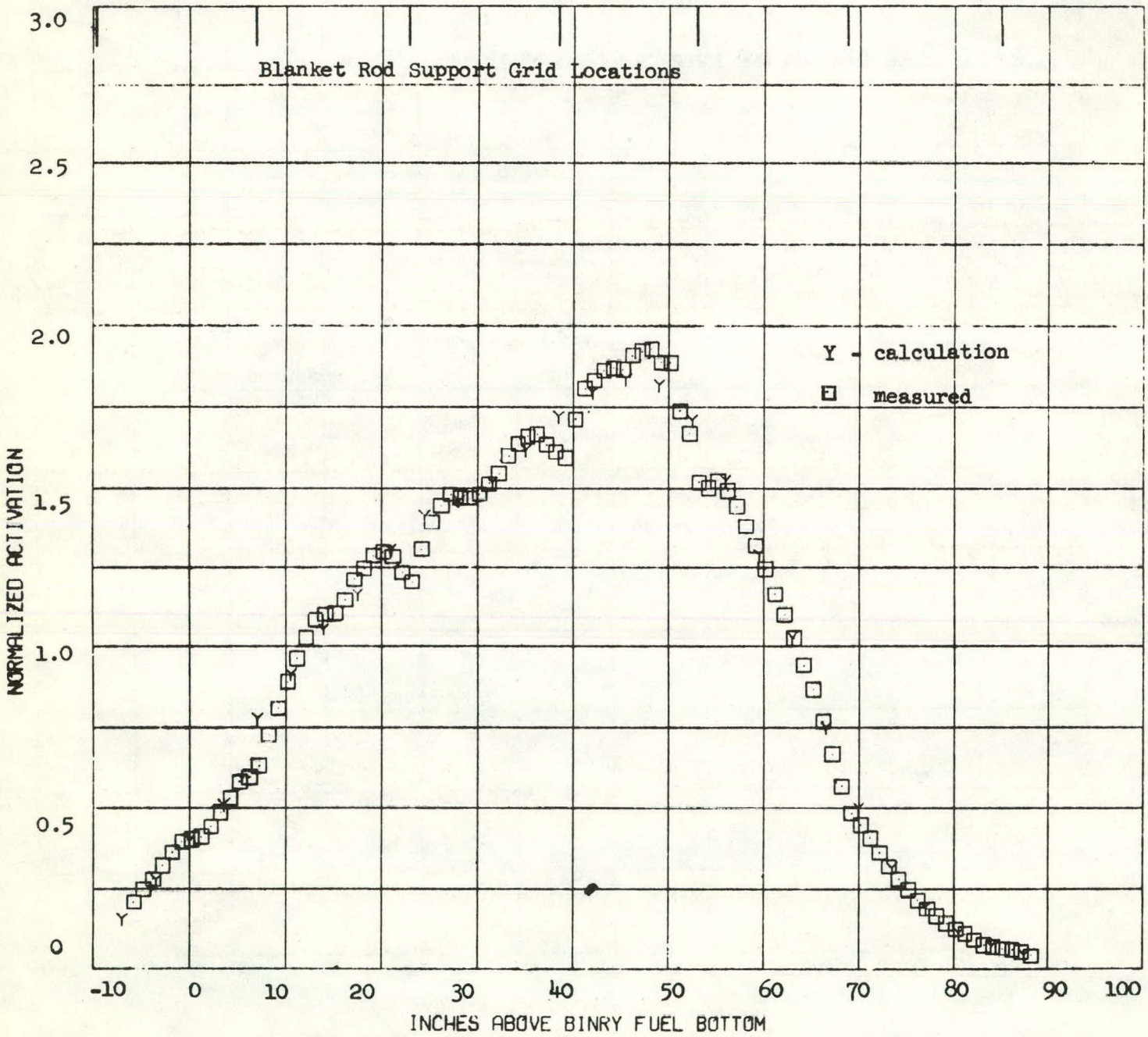

Copper Activation Profile at Full Power, Equilibrium Xenon for Module I-1

(Repeat Count)

FIGURE 23

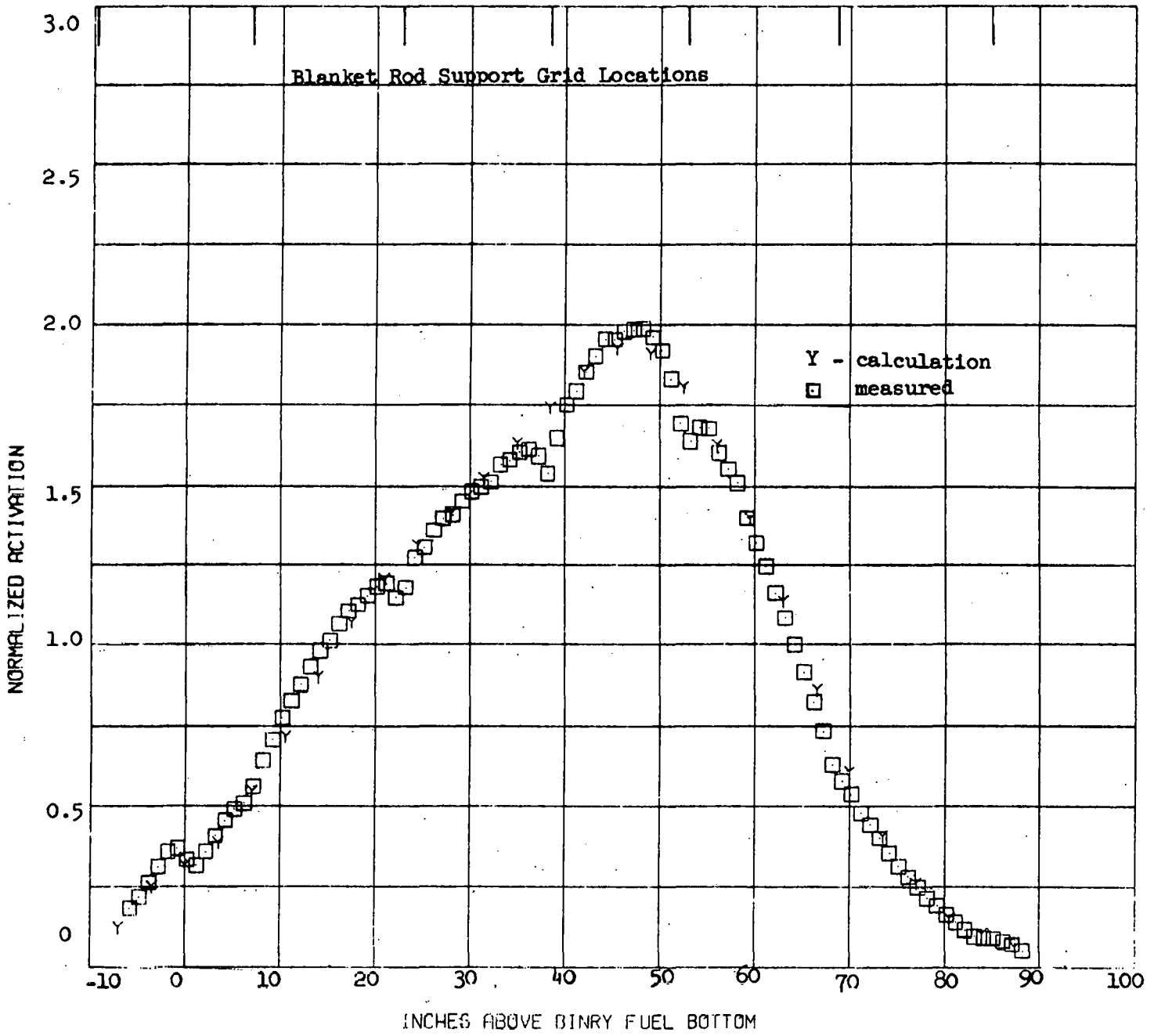

Copper Aetivation Profile at Full Power, Equilibrium Xenon for Module II-1
(Repeat Count)

FIGURE 24

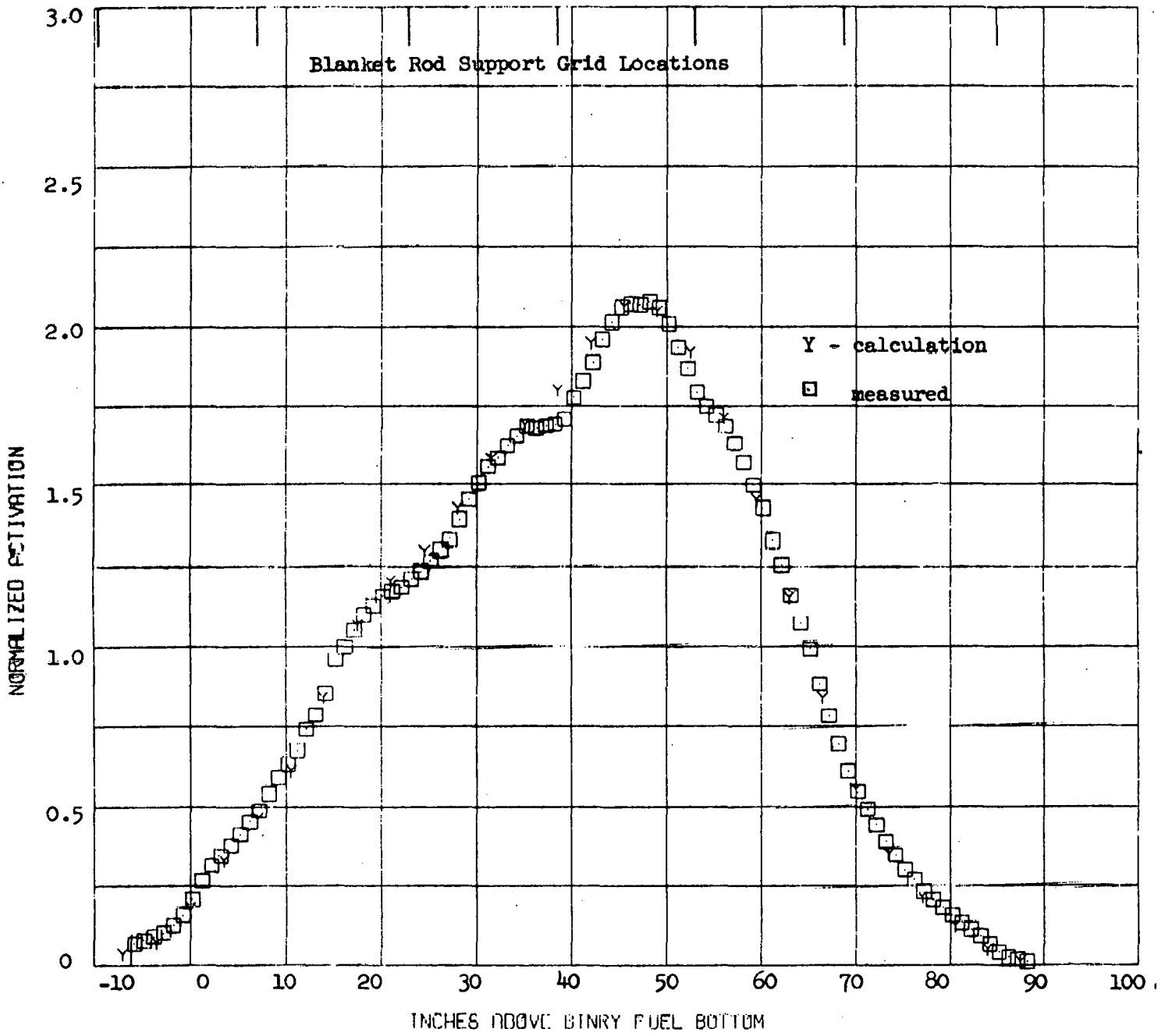

Nickel Activation Profile at Full Power, Equilibrium Xenon for Module I-1

FIGURE 25

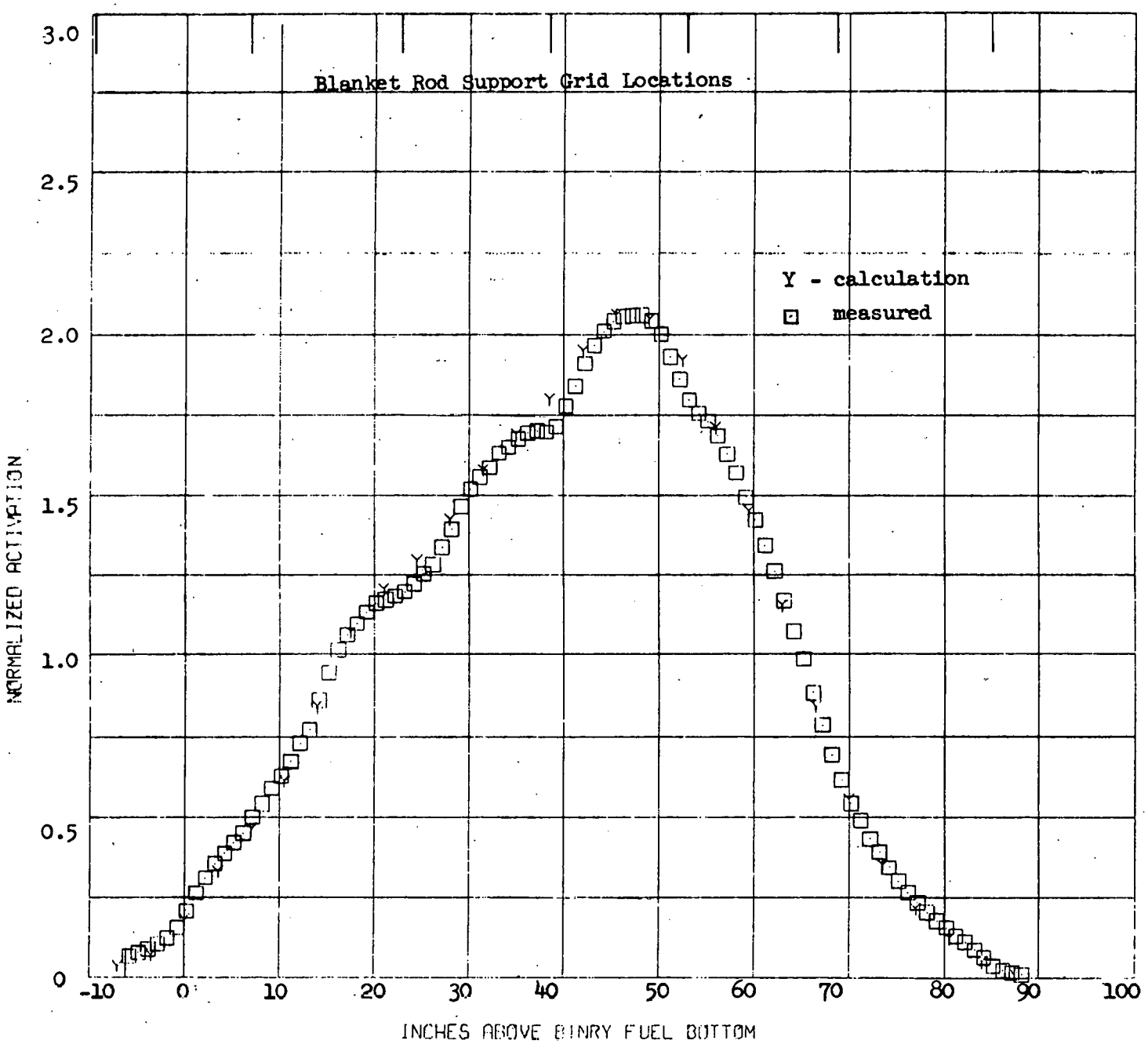

Nickel Activation Profile at Full Power, Equilibrium Xenon for Module I-2

FIGURE 26

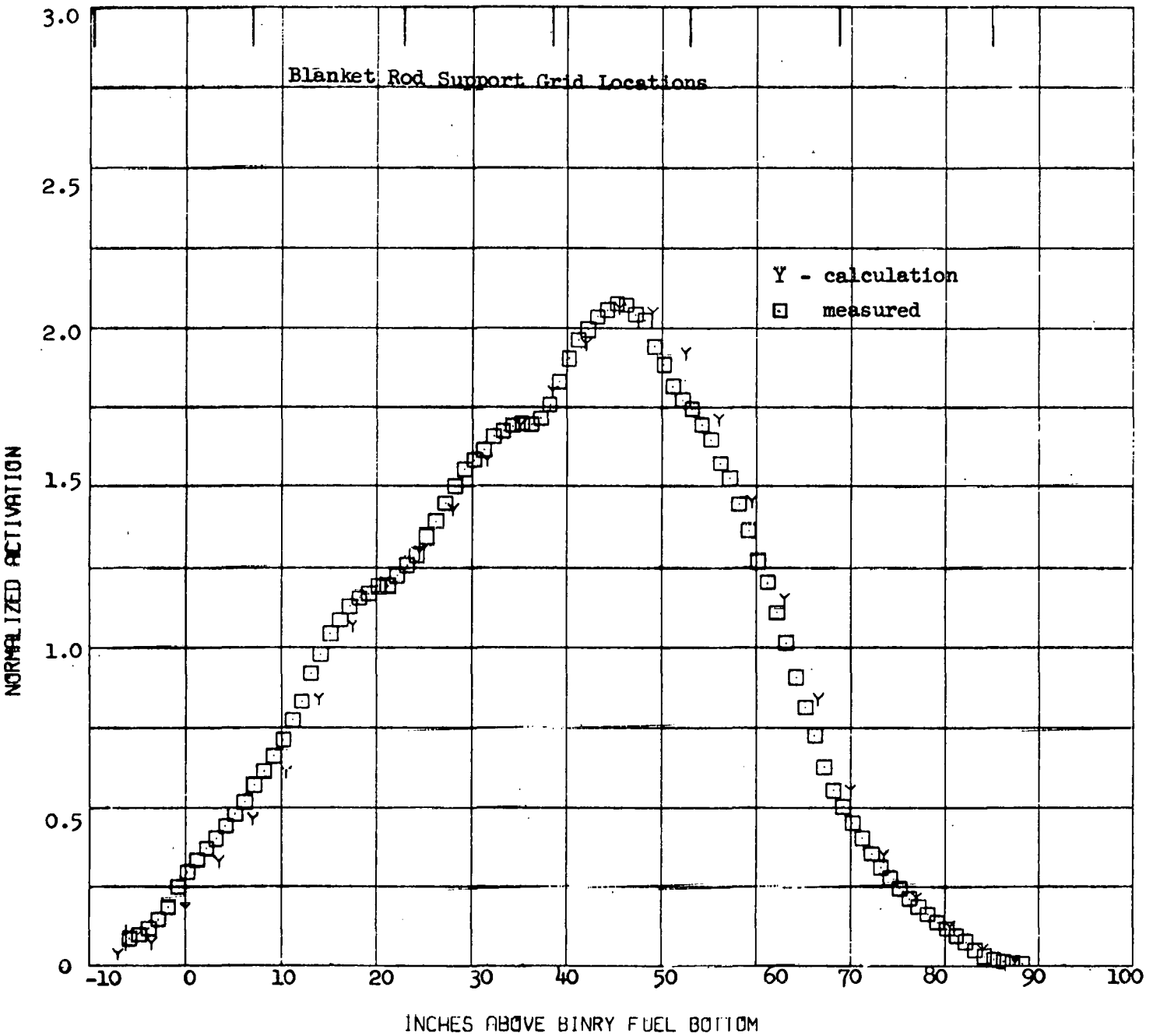

Nickel Activation Profile at Full Power, Equilibrium Xenon for Module I-3

FIGURE 27

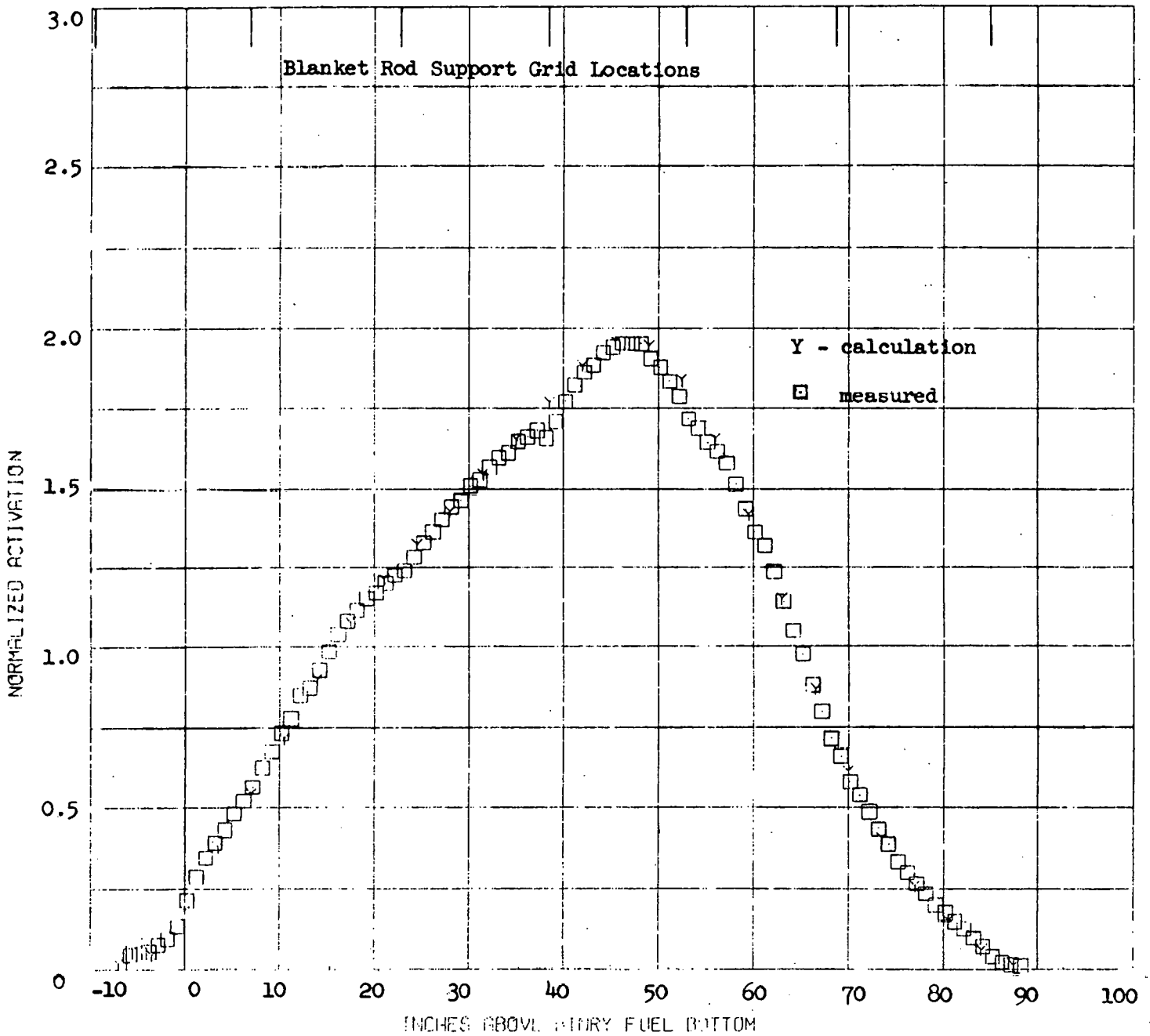

Nickel Activation Profile at Full Power, Equilibrium Xenon for Module II-1

FIGURE 20

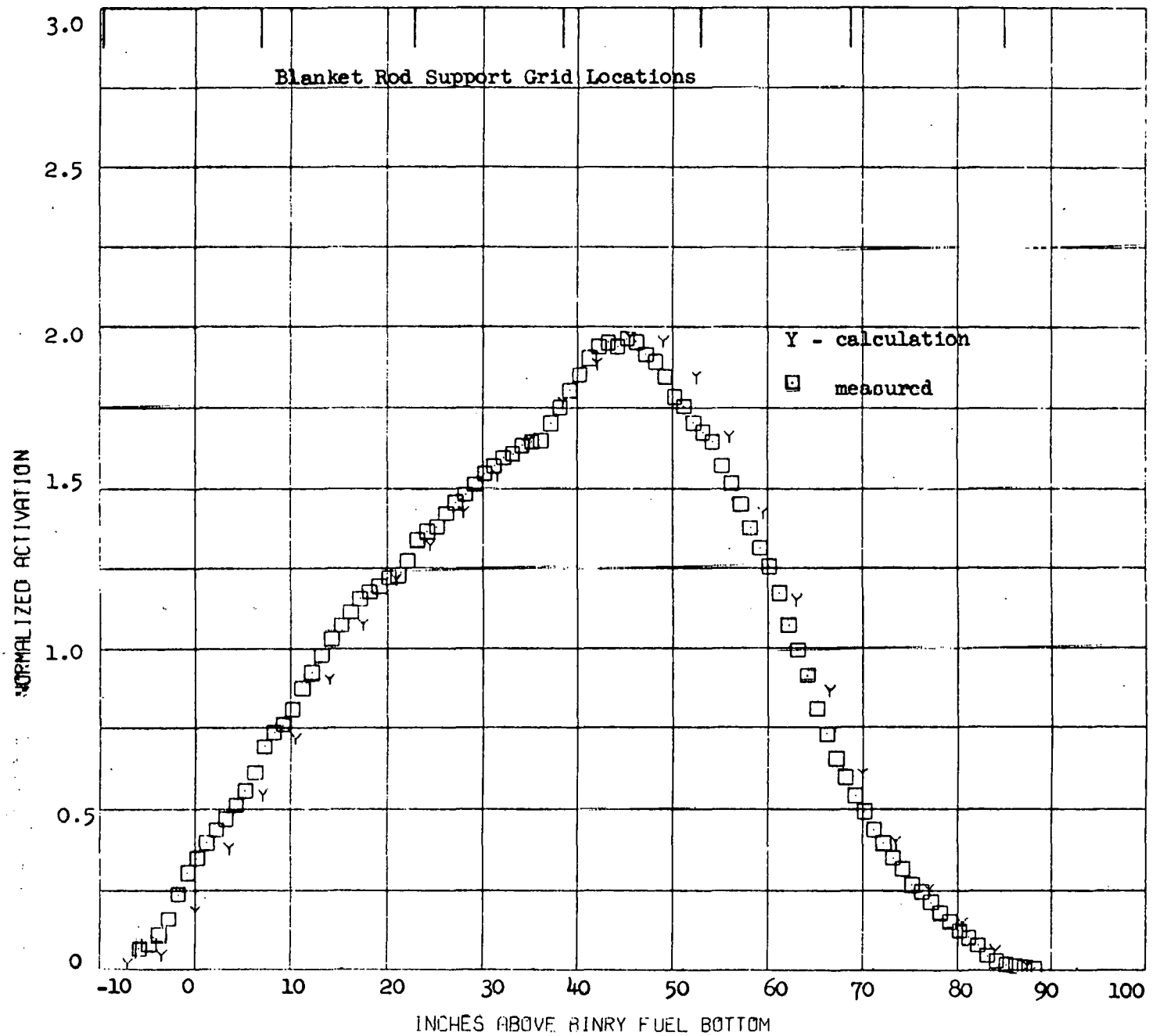

Nickel Activation Profile at Full Power, Equilibrium Xenon for Module III-1

FIGURE 29

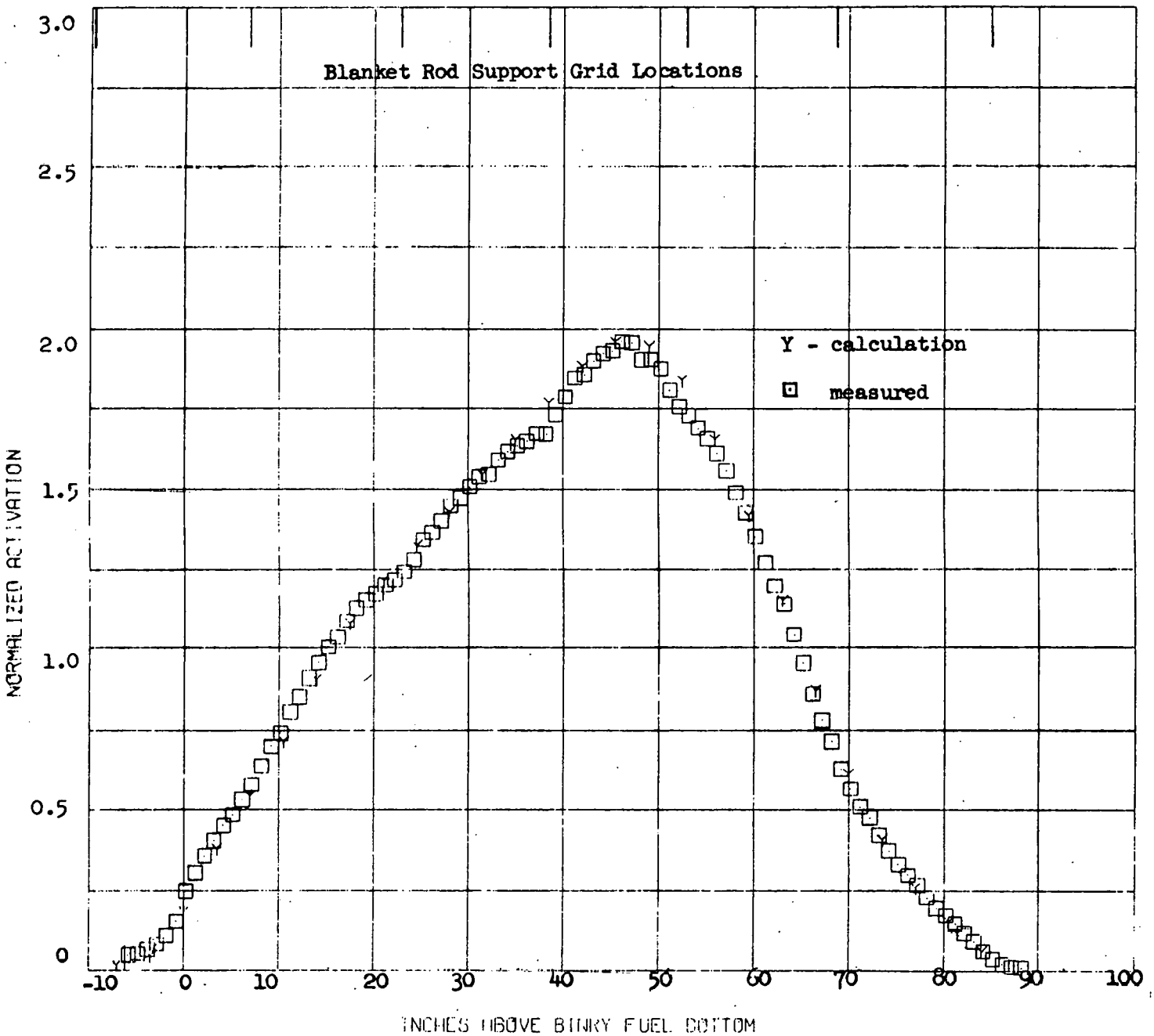

Nickel Activation Profile at Full Power, Equilibrium Xenon for Module II-1

FIGURE 30

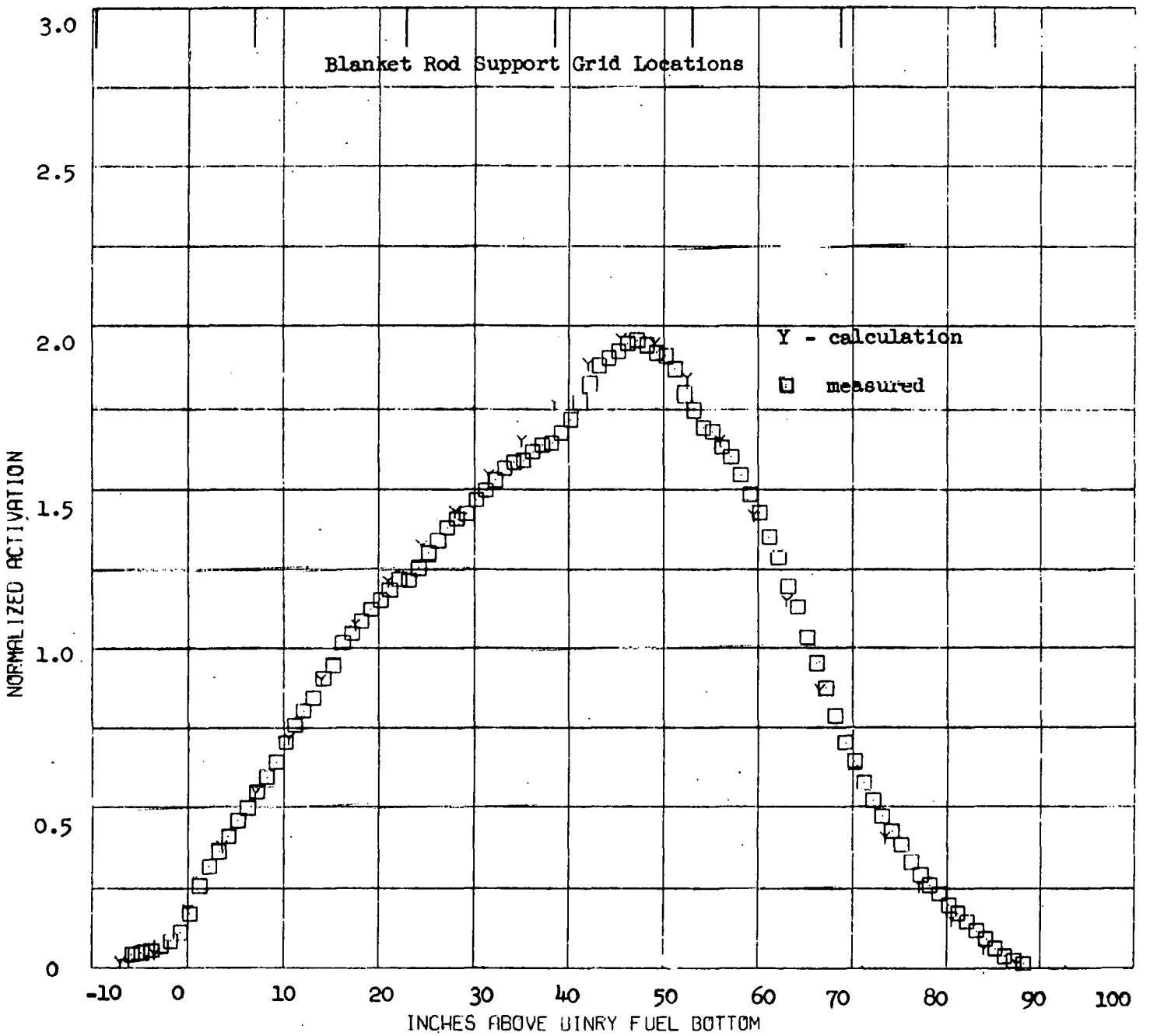

Nickel Activation Profile at Full Power, Equilibrium Xenon for Module II-3

FIGURE 31

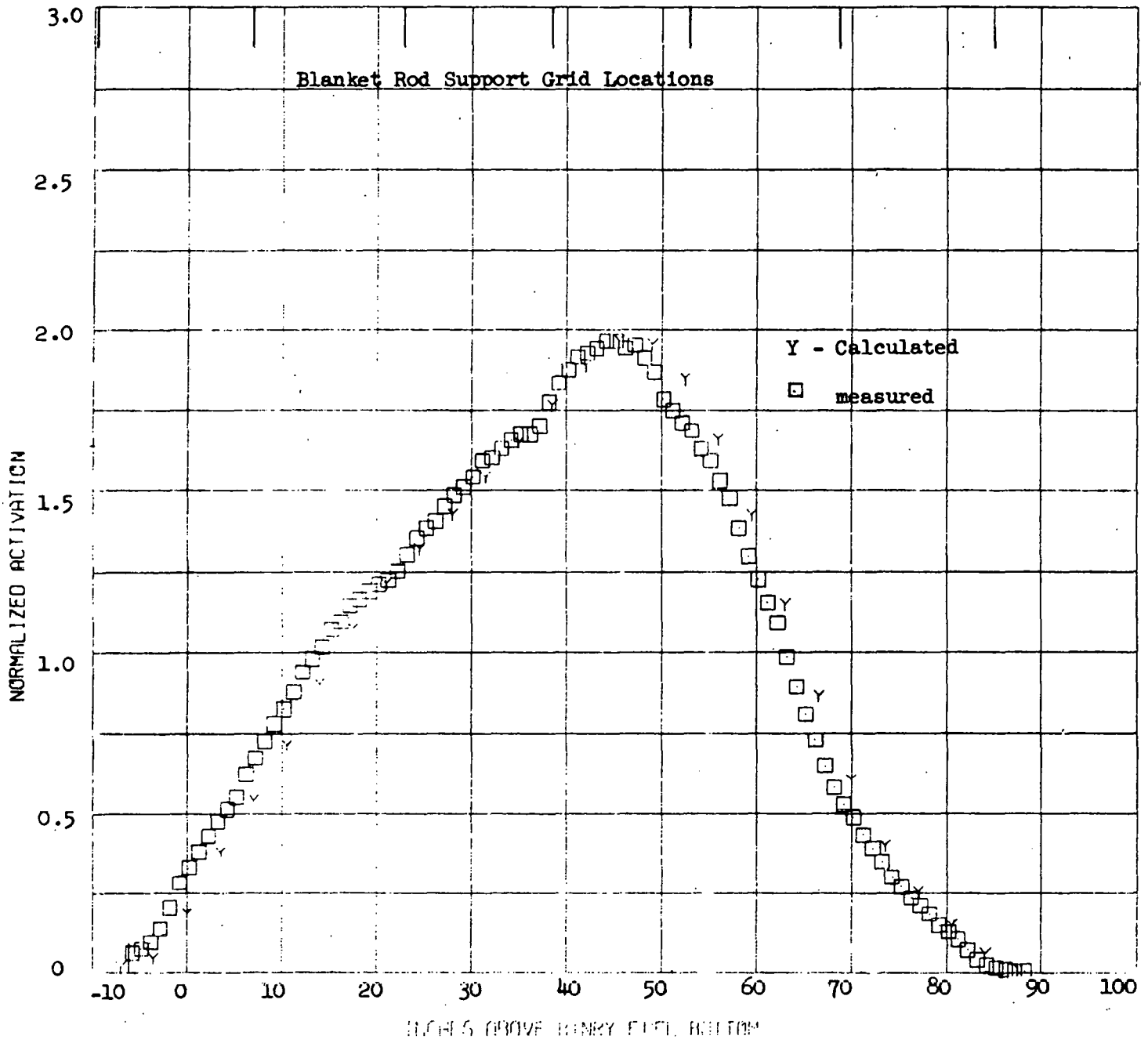

Nickel Activation Profile at Full Power, Equilibrium Xenon for Module III-1

FIGURE 32

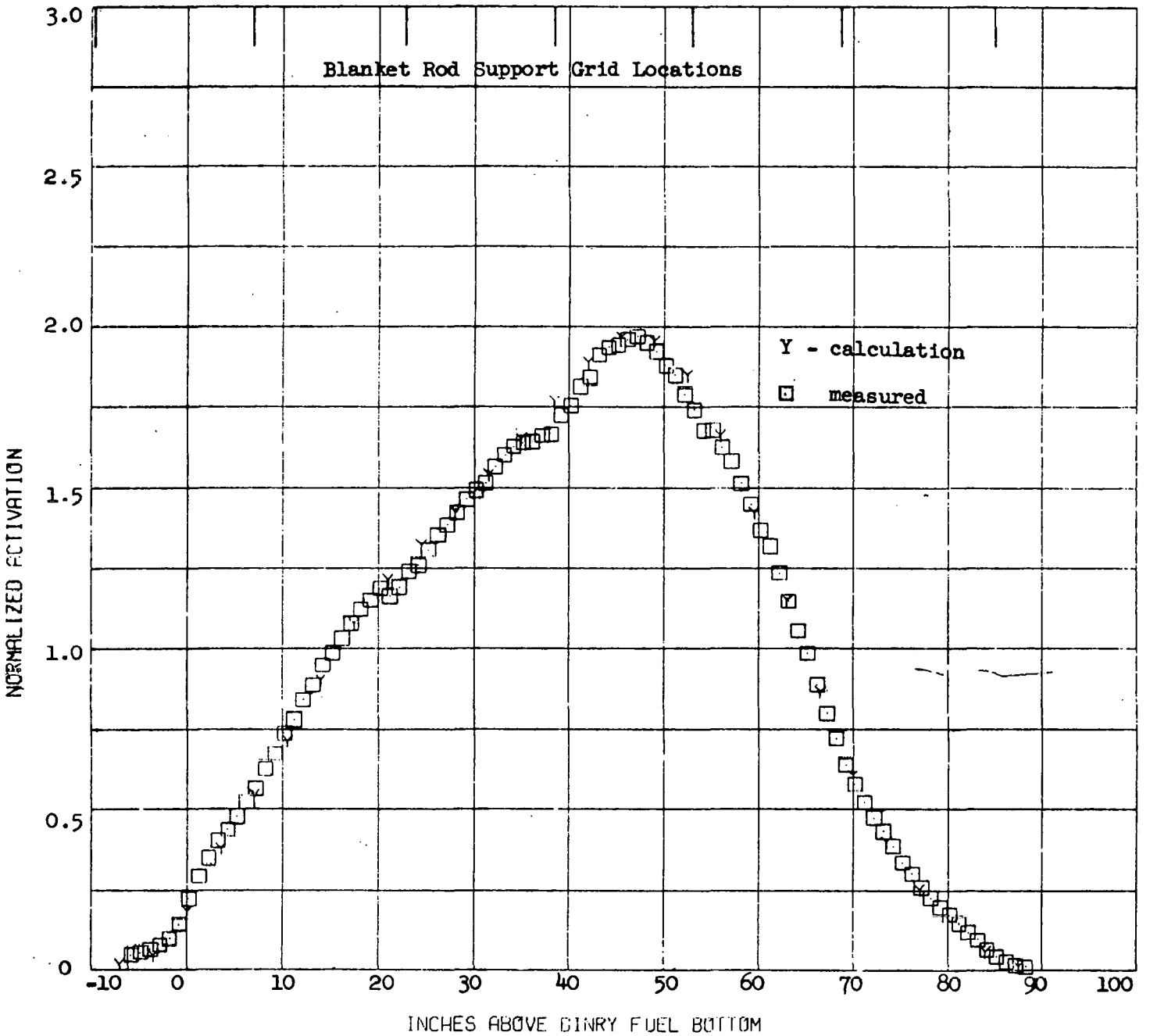

Nickel Activation Profile at Full Power, Equilibrium Xenon for Module III-2

FIGURE 33

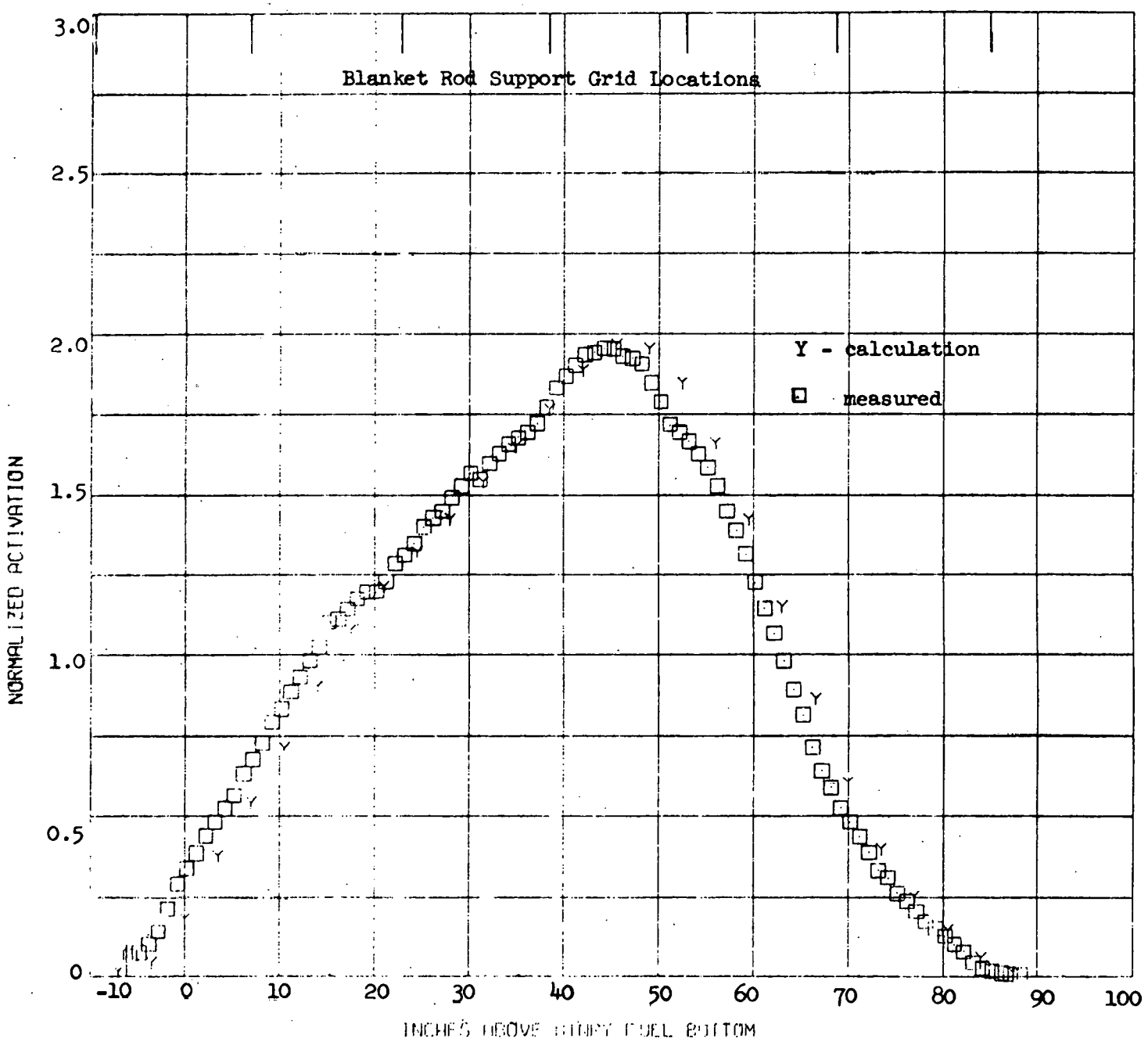

Nickel Activation Profile at Full Power, Equilibrium Xenon for Module III-1

FIGURE 34

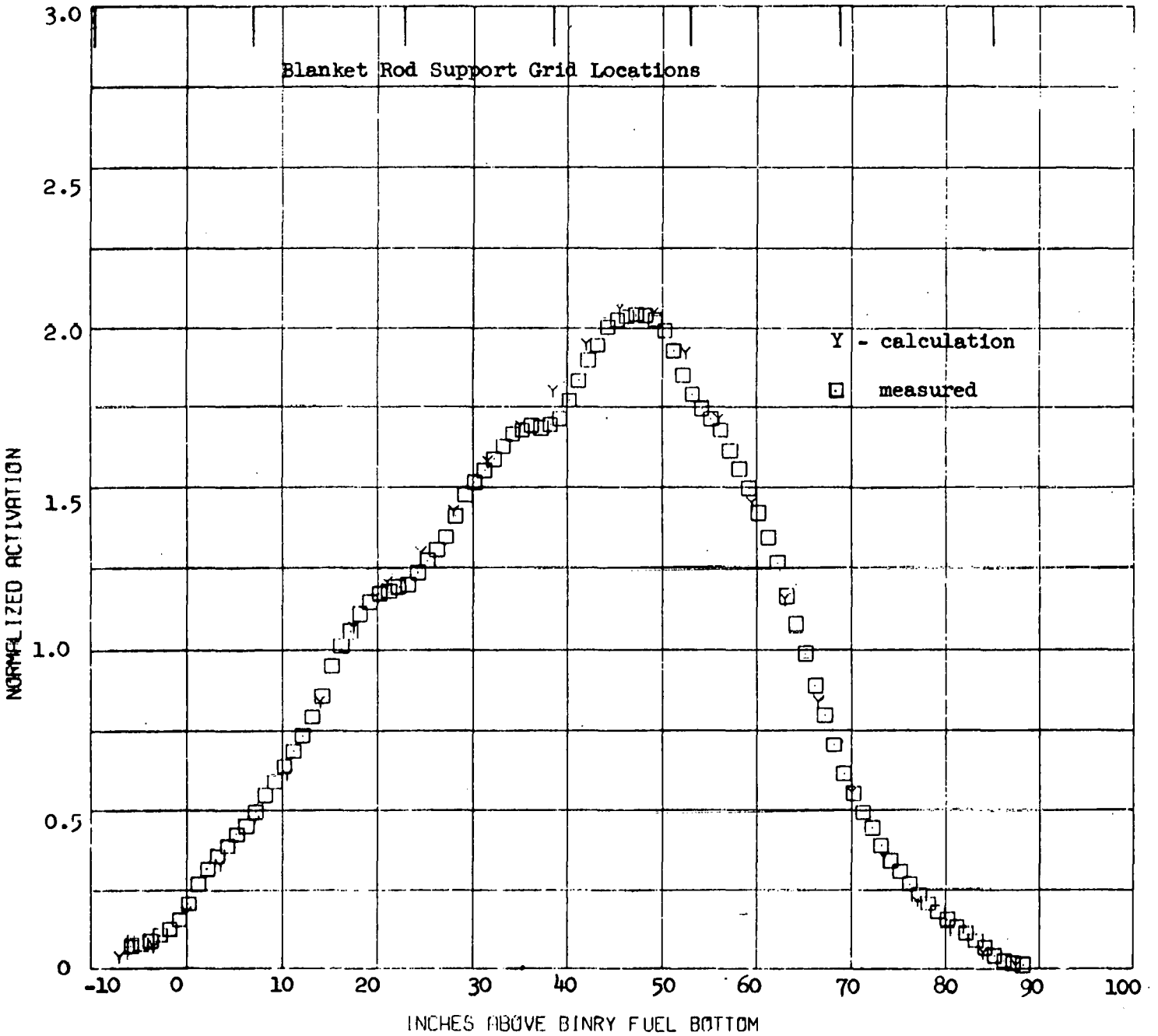

Nickel Activation Profile at Full Power, Equilibrium Xenon for Module I-1

FIGURE 35

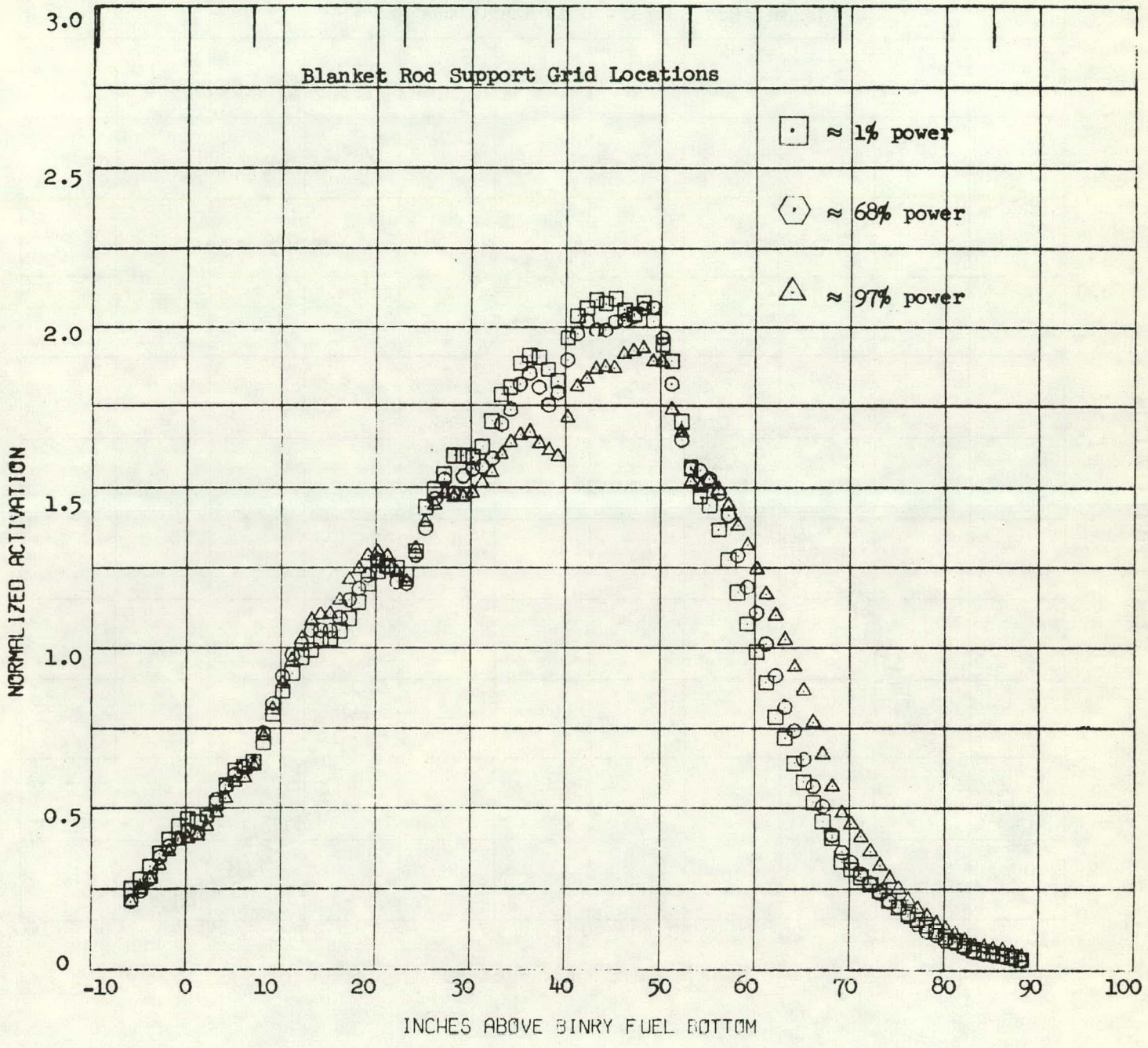

Copper Activation Profiles for Module I-1

FIGURE 36

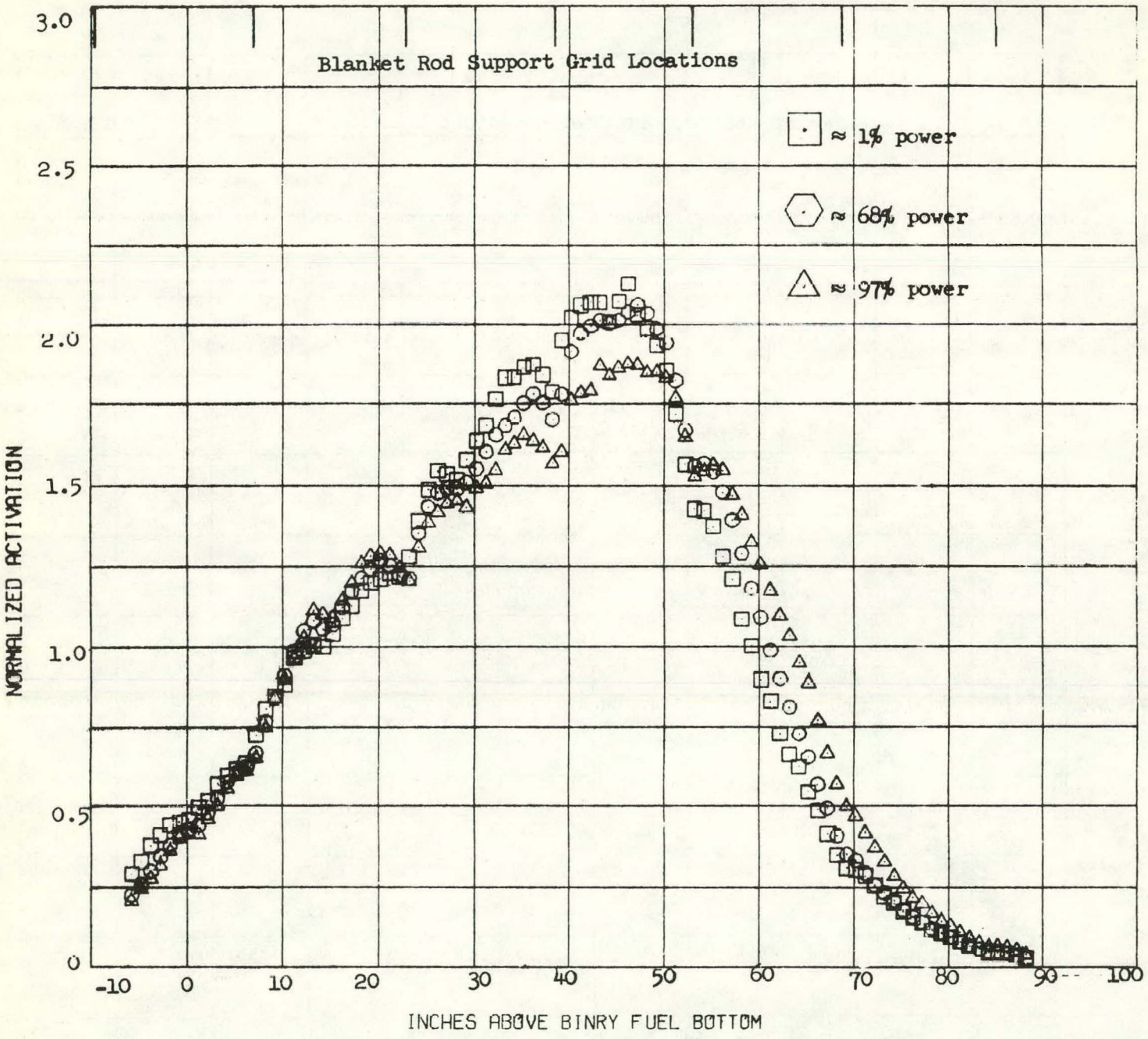

Copper Activation Profiles for Module I-2

FIGURE 37

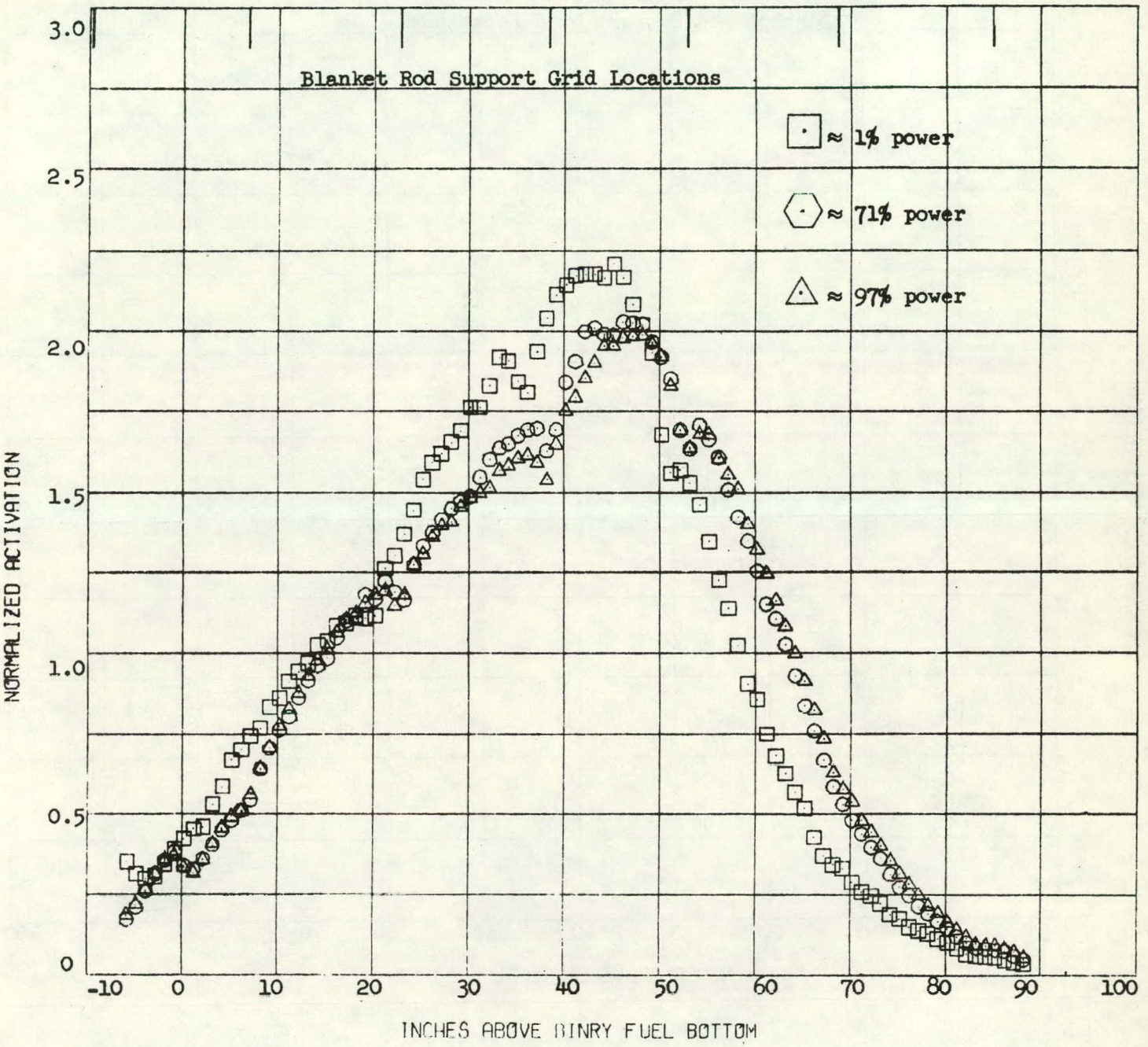

Copper Activation Profiles for Module II-1

FIGURE 38

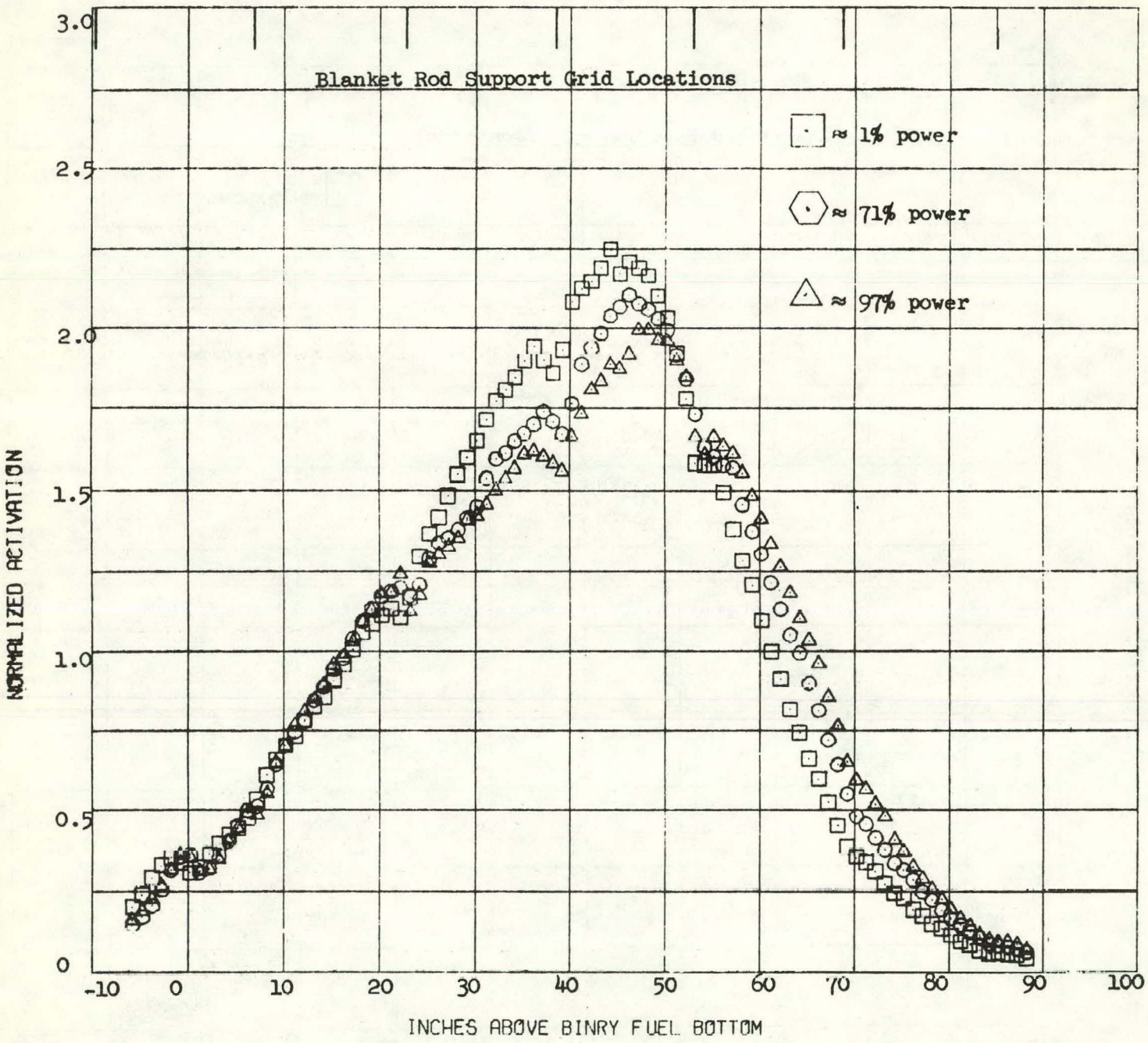

Copper Activation Profiles for Module II-3

FIGURE 39

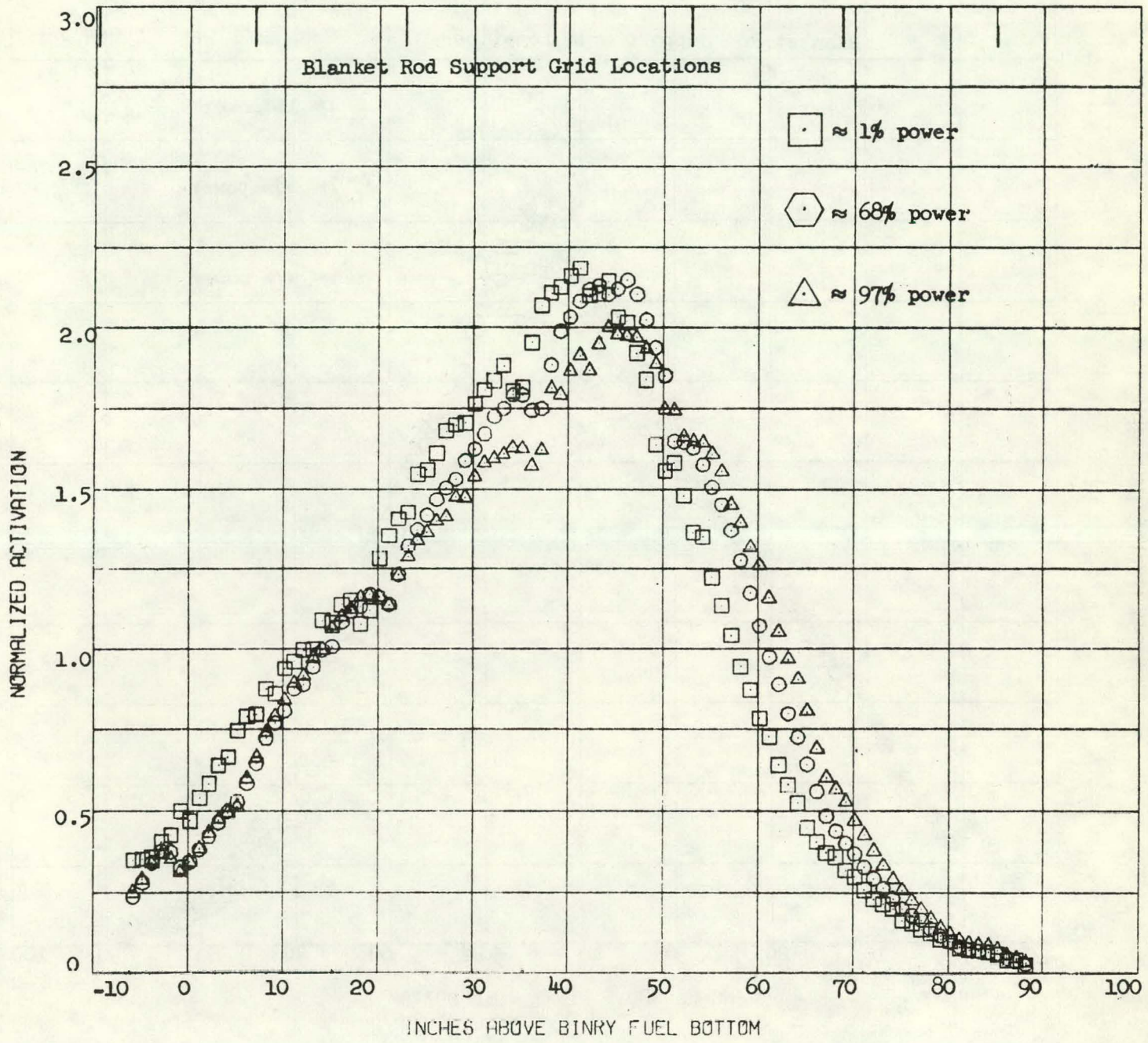

Copper Activation Profiles for Module III-1

FIGURE 40

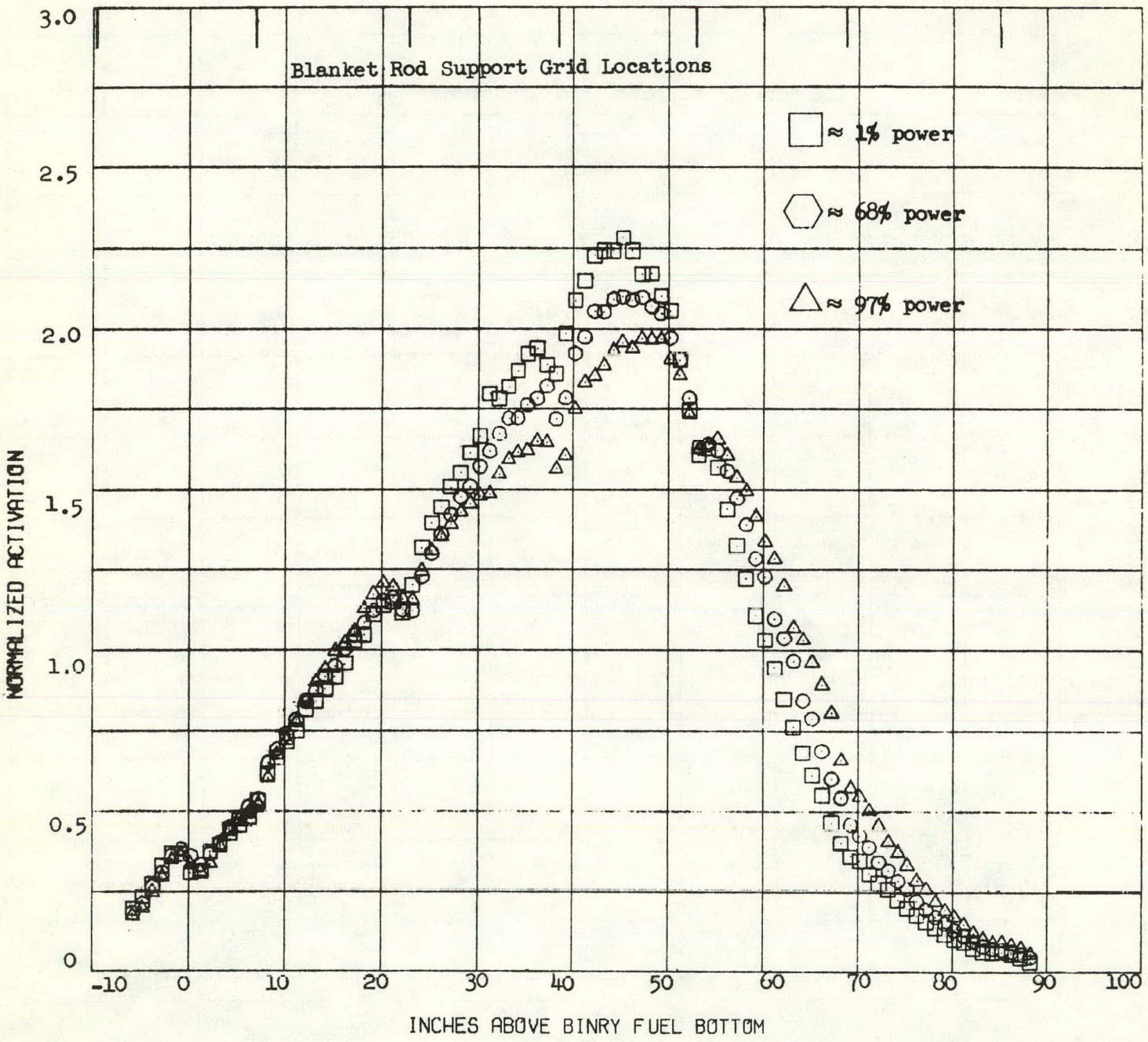

Copper Activation Profiles for Module III-2

FIGURE 41

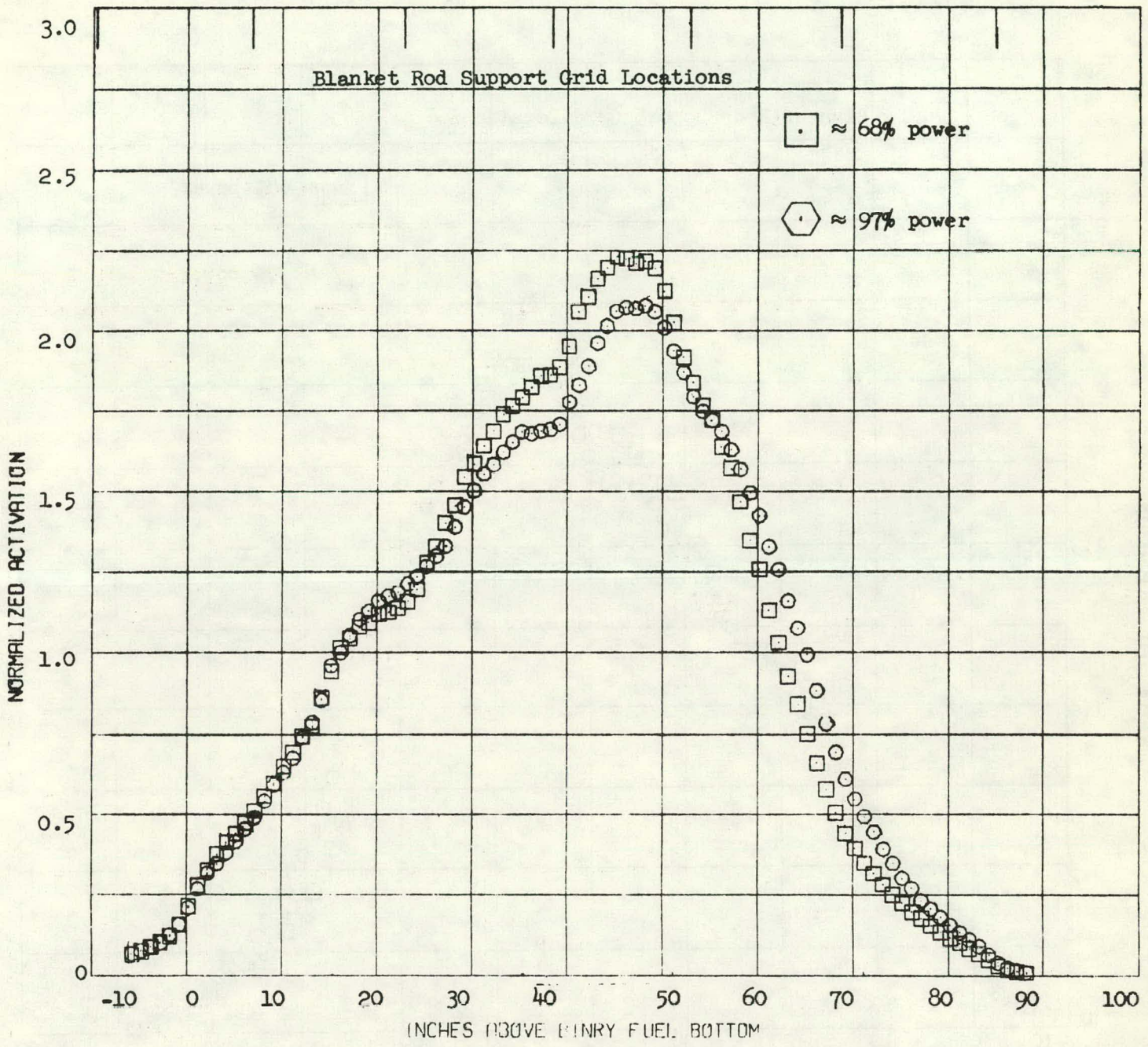

Nickel Activation Profiles for Module I-1

FIGURE 42

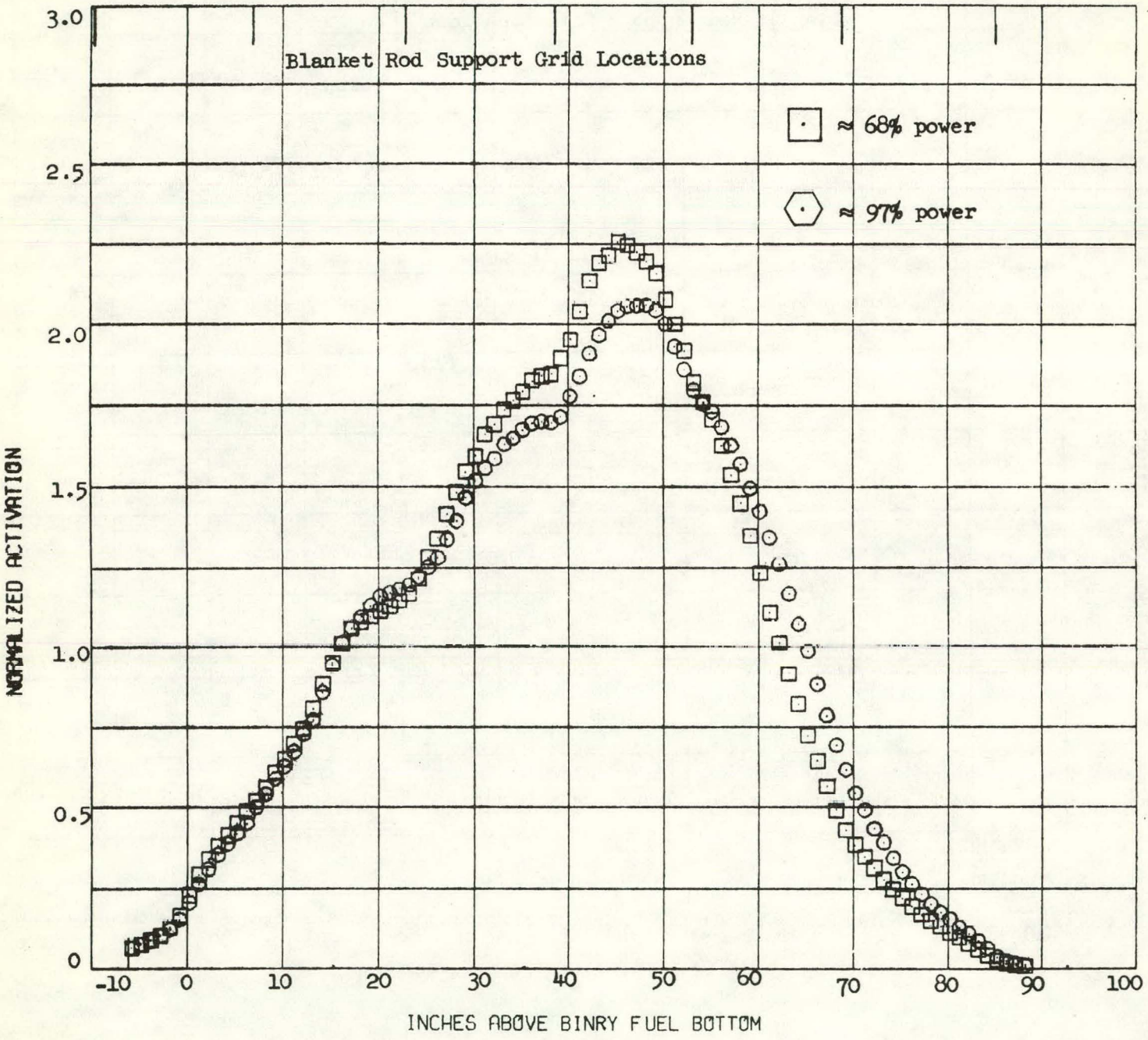

Nickel Activation Profiles for Module I-2

FIGURE 43

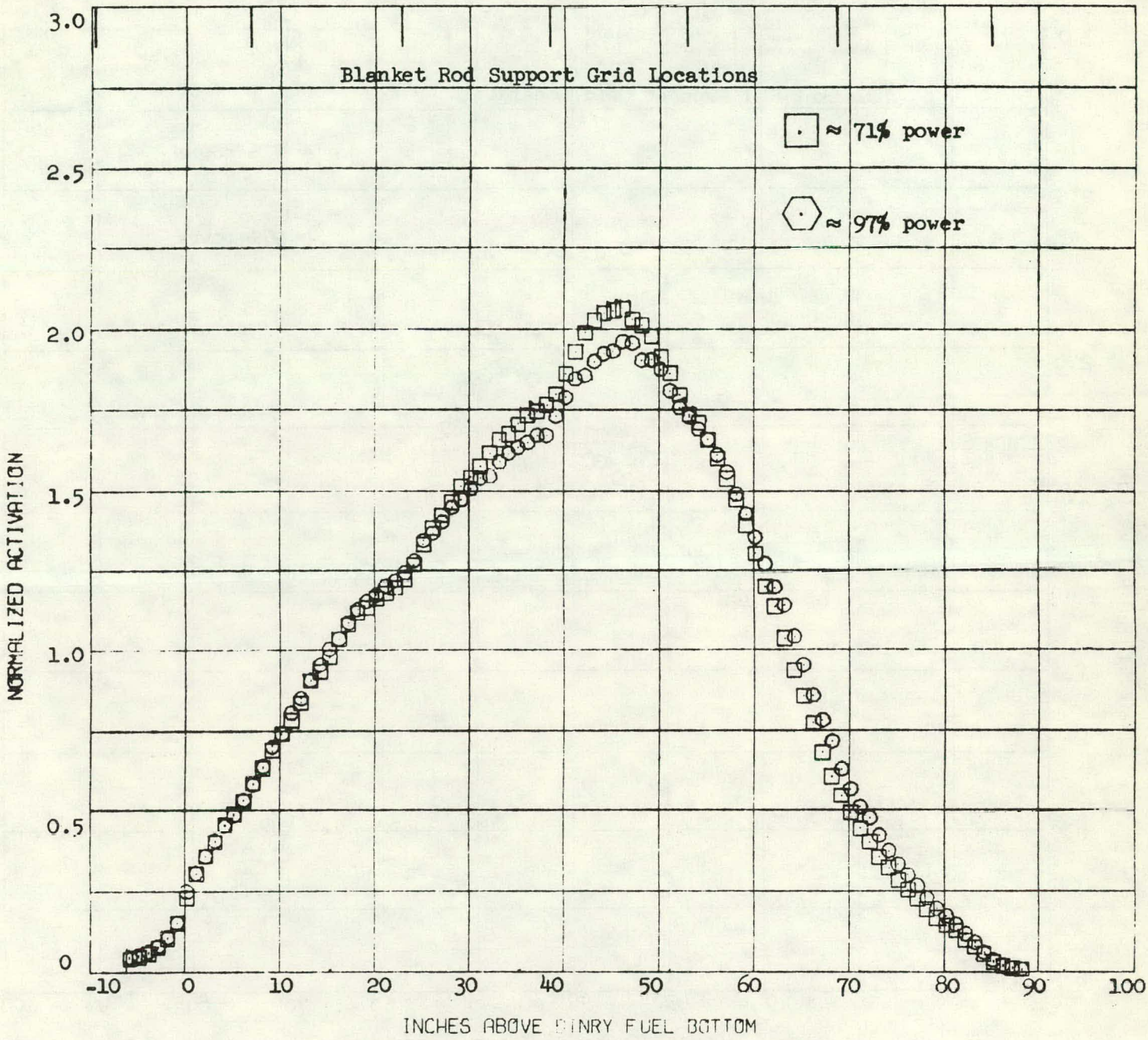

Nickel Activation Profiles for Module II-1

FIGURE 44

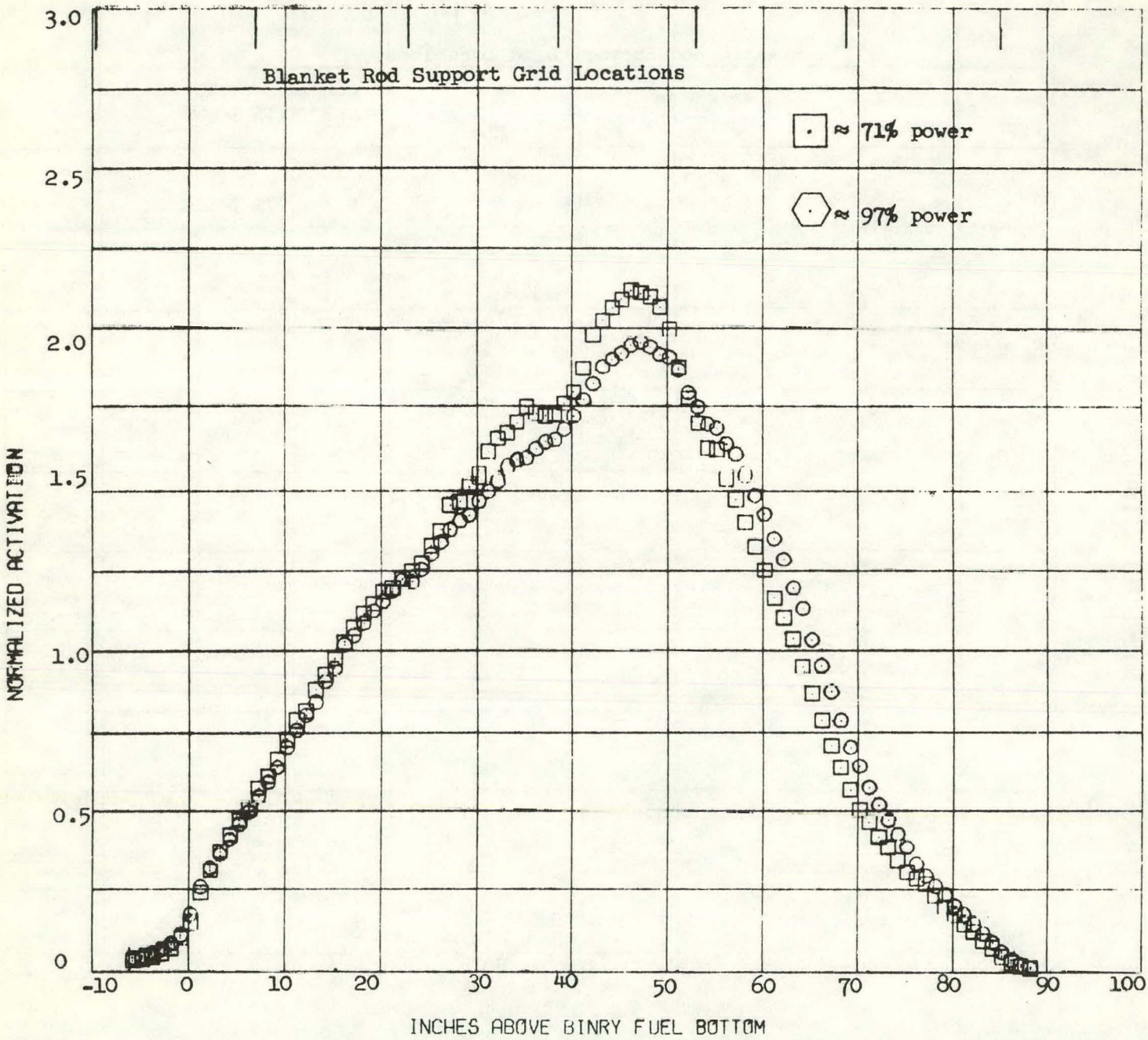

Nickel Activation Profiles for Module II-3

FIGURE 45

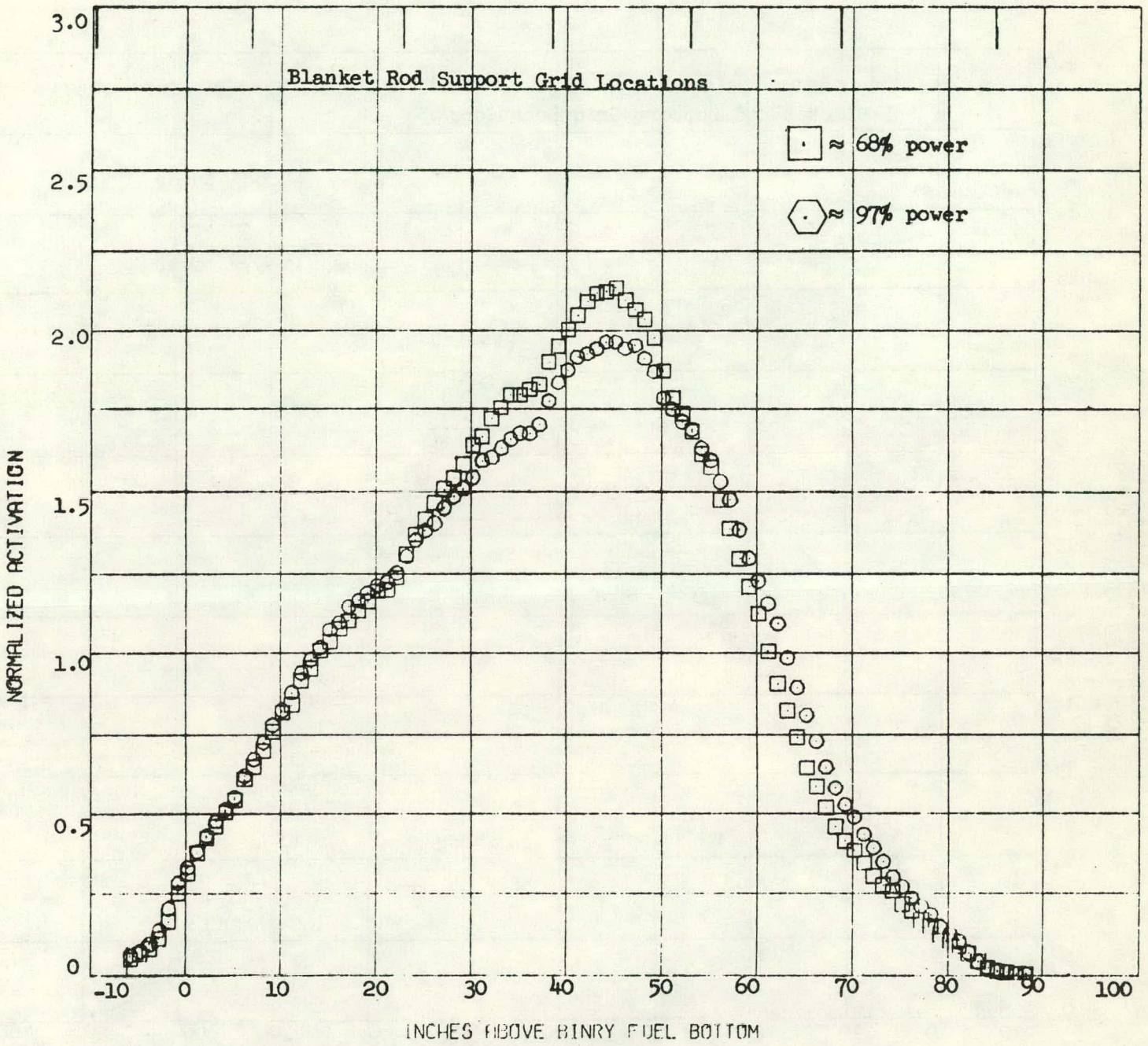

Nickel Activation Profiles for Module III-1

FIGURE 46

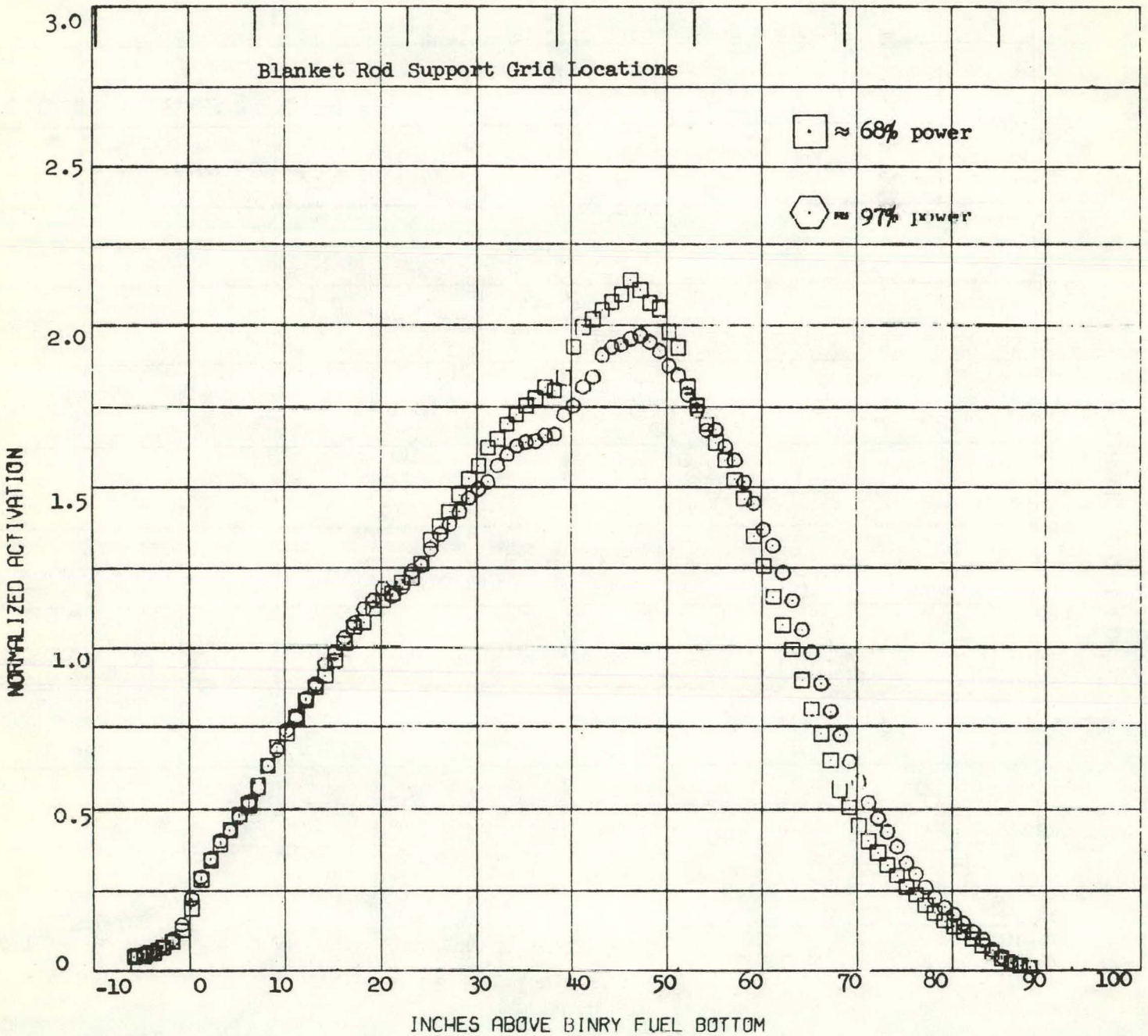

Nickel Activation Profiles for Module III-2

FIGURE 47

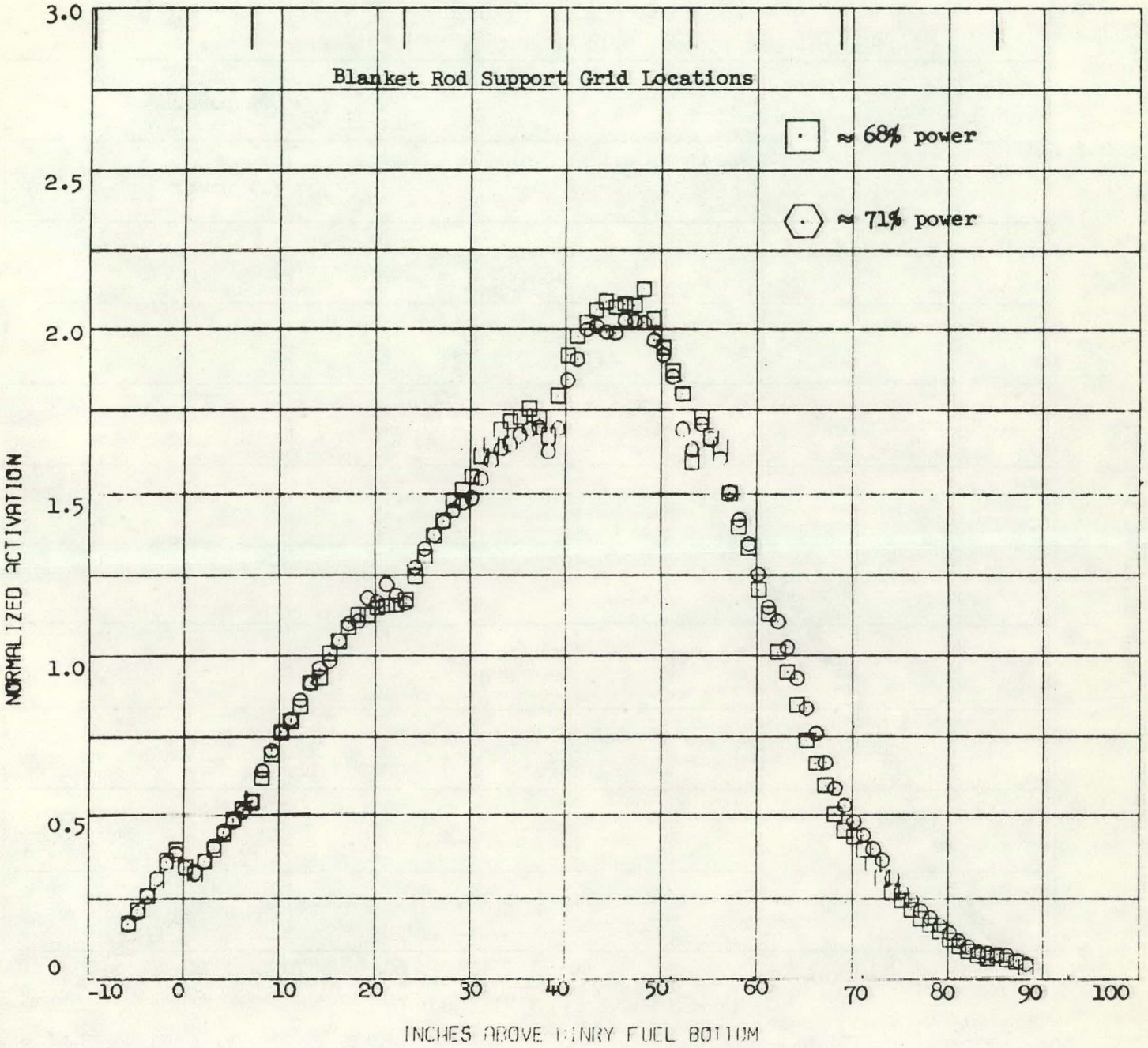

Copper-Activation Profiles for Module II-1

FIGURE 48

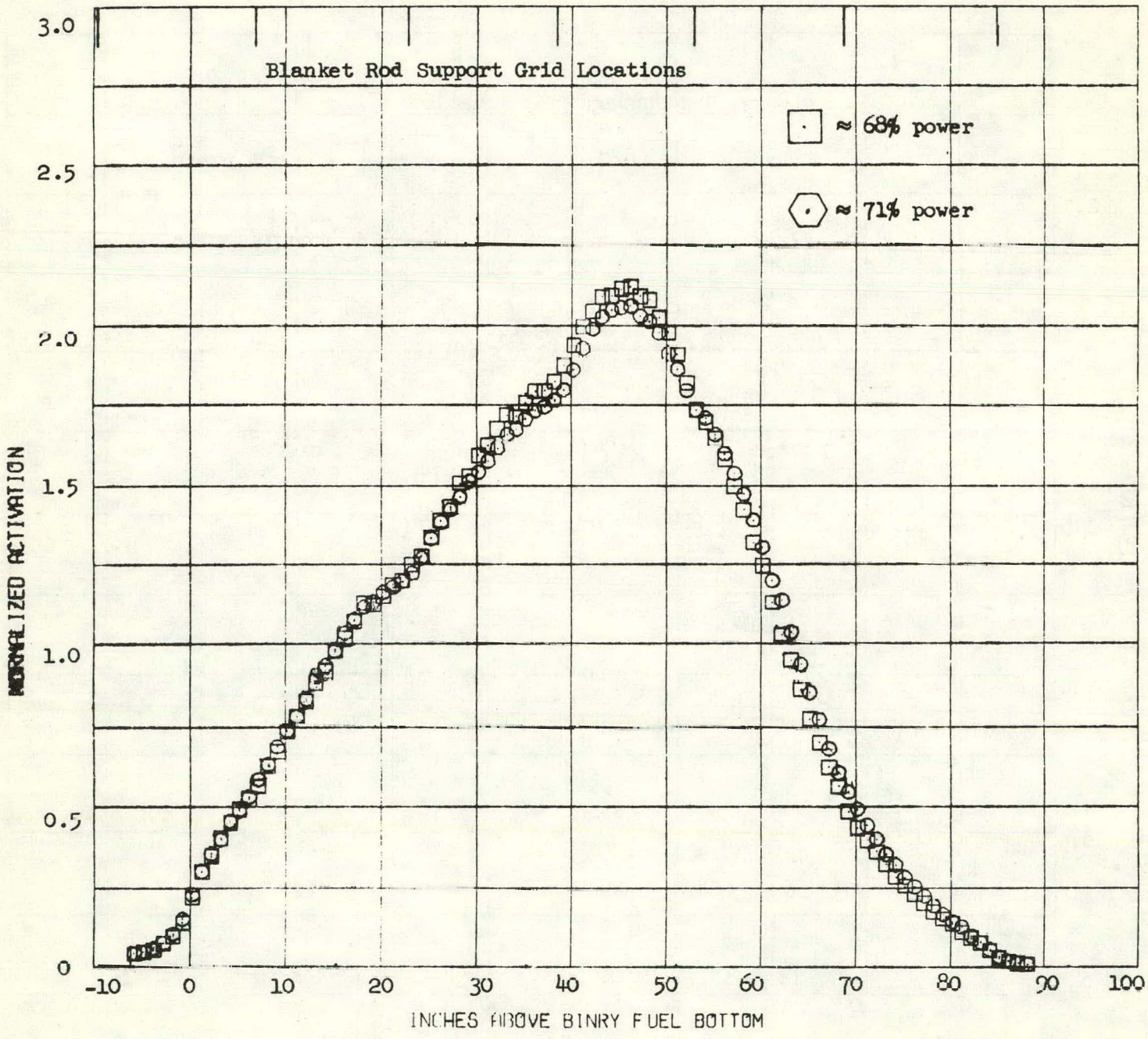

*U.S. GOVERNMENT PRINTING OFFICE: 1980/603-113/182

Nickel Activation Profiles for Module II-1

FIGURE 49